الجمهورية الجزائرية الديمقراطية الشعبية
وزارة التعليم العالي و البحث العلمي
People's Democratic Republic of Algeria
The Minister of Higher Education and Scientific Research
ⵜⴰⴳⵍⴷⵉⵜ ⵜⴰⵎⴰⵡⴰⵙⵜ ⵏ ⵜⵣⵣⵓⵖⵜ ⵜⴰⵎⴰⵡⴰⵙⵜ ⵏ ⵜⵙⴷⴰⵡⵉⵏ ⵉⵜⵎⵄⵔⴰⵏ

ABOU BEKR BELKAID UNIVERSITY
TLEMCEN
FACULTY OF MEDICINE- Dr. B. BENZERDJEB
PHARMACY DEPARTMENT

جامعة أبو بكر بلقا يد - تلمسان
كلية الطب - د. ب. بن زرجب
قسم الصيدلة

MEMOIRE DE FIN D'ETUDES POUR
L'OBTENTION DU DIPLOME DE DOCTEUR EN PHARMACIE

THÈME :

Contribution of Monte Carlo simulation to the assessment of low-dose radiation effects on non-target organs during hyperthyroidism and thyroid cancer treatment.

Présenté par :
DAOUD Zakaria

Soutenu le
02/06/2022

Jury

Président :
Dr. BRIKCI NIGASSA Nawal — Maitre assistante en Biophysique

Membres :
Dr. KRIM Latefa — Maitre assistante en Biophysique
Dr. MILOUD ABID Dalila — Maitre assistante en Toxicologie

Encadrant :
Dr. BENALLAL Bouchra — Maitre assistante en Biophysique
Co-Encadrant
Dr. KHERBOUCHE Fatima Zohra — Assistante en Médecine nucléaire

Année universitaire : 2021-2022

Acknowledgment

First and foremost, I would like to praise and thank Allah, the almighty, who has granted me countless blessings, the knowledge, and the patience to start writing this dissertation and see it to fruition.

I would like to express my deepest gratitude to the people without whom this project would be impossible. First of all, **Dr. BENALLAL Bouchra**, words cannot express my gratitude for agreeing to be my academic advisor, thank you for coming up with the topic of this dissertation, and for your patience, guidance, availability, and feedback. You always believed that we can overcome every hurdle even when I could not see a way out, you believed in me without a shred of doubt, I wouldn't have and couldn't have undertaken this journey with anyone but you.

I am deeply grateful to my co-advisor **Dr. KHERBOUCHE Fatima Zohra**, you had the kindness to agree on taking this journey with us, your knowledge and expertise were much needed and appreciated.

My greatest gratitude goes to **Dr. Joseph Perl,** project leader for TOPAS, who had the kindness to be my guide in everything TOPAS-related and took effort in correcting my work, this endeavor wouldn't have been possible without him.

I would also like to express my deepest appreciation to **Dr. BRIKCI NIGASSA Nawal** our committee chairwoman who did us the honor to be our jury president.

I am also grateful to the jury members **Dr. KRIM Latefa** and **Dr. MILOUD ABID Dalila** for granting us their precious time and expertise in order to read and evaluate our work.

I would like to extend my sincere thanks to **BELKHIRI Youcef**, computer savvy, software engineer, and above all, my friend, for his help in everything computer-related, you and I both know that you did most of the heavy lifting in this work, thank you.

I'd like to acknowledge **Dr. BENABED Fatima Zohra** and **Dr. GUENDOUZ Abdou**, for their advice, suggestions, and moral support.

Dedication

To the woman who gave me everything, and then some; my mother.

To the man who built me up from nothing to what I am today; my father.

To the sister who endured listening to me complain about how hard my life is.

To the sister who suggested that I take this journey saying: “go for it, how hard can it be?”

To the sister whose interruptions were a welcomed study break even if I didn’t show it.

To my brother, YOUCEF, you were the one who enrolled me at the university and you have been a constant help ever since.

To my cousin and brother-in-law TOUR LAKHDAR, a promise is a promise so here you go your name is in all caps, I can’t even start to recount all that you’ve done and continue to do for me.

To my brother-in-law for his encouragement.

To my nieces and nephews, our constant bickering was a much-needed stress relief.

To my grandmother whose prayers and good wishes are always with me.

To the memory of my late grandparents.

To the friend who was instrumental to this journey.

To all my friends, you know I don’t use this word lightly and I am very honored by your friendship, you have shown throughout the years that I have known you an unwavering belief in me.

Looking back, I can say with certainty that all that I am and all that I will ever be is thanks to you.

All that I will ever achieve is as much yours as it is mine.
So let me start thanking you by dedicating this humble work to all of you.

THANK YOU ALL.

TABLE OF CONTENTS

1. Introduction 1
2. History 1
3. Iodine: 1
   3.1. Pharmacokinetics of iodine: 1
      3.1.1. Absorption: 1
      3.1.2. Distribution: 2
      3.1.3. Metabolism: 2
      3.1.4. Elimination: 3
   3.2. Radioactive iodine: 4
      3.2.1. Production of radioiodine: 4
      3.2.2. Radioactive decay of Iodine 131: 5
   3.3. Medical use of Iodine: 7
4. Thyroid: 8
   4.1. Anatomy 8
   4.2. Histology: 11
   4.3. Physiology: 12
   4.4. Hyperthyroidism 15
   4.5. Thyroid Carcinoma 16
5. Treatment with ^{131}I: 17
   5.1. For hyperthyroidism: 17
   5.2. For Thyroid carcinoma: 18
   5.3. NaI Capsule: 18
      5.3.1. Mode of administration: 19
      5.3.2. Pharmacokinetics: 19
      5.3.3. Protocol of use: 20
1. Fundamentals of nuclear medicine dosimetry: 21
2. Radioactivity: 21
   2.1. Definition: 21
   2.2. Radioactive decay: 21
      2.2.1. Law of radioactive decay: 21
      2.2.2. Half-lives: 22
   2.3. Types of radiation: 23
      2.2.3. Directly ionizing radiation: 23
      2.2.4. Indirectly ionizing radiation: 24

2.4. Interaction between ionizing radiation and matter: 25
2.4.1. Photon interactions: 25
2.4.2. Electron interactions: 27
2.5. Biological effects of radiation: 28
2.5.1. Deterministic effects: 29
2.5.2. Stochastic effects: 29
3. Dosimetry: 30
3.1. External dosimetry: 30
3.2. Internal radiation dosimetry 31
3.2.1. Absorbed dose: 31
3.2.2. Radiation dose rate: 31
3.2.3. Equivalent dose 31
3.2.4. Effective dose 32
3.2.5. Linear energy transfer: 34
3.2.6. Source and target organs: 35
3.2.7. Absorbed fraction: 35
3.2.8. Activity and Cumulated activity: 36
3.2.9. Absorbed dose per unit cumulative activity (S-value): 38
1. State of the art: 40
2. History: 40
3. Monte Carlo Method: 40
4. Monte Carlo software: 41
4.1. MCNP: 41
4.2. EGS: 41
4.3. FLUKA: 42
4.4. PENELOPE: 42
4.5. Geant4: 42
5. Anthropomorphic computational phantoms: 43
5.1. First-Generation Stylized Phantoms: 43
5.2. Second-Generation Voxelized Phantoms: 44
5.3. Third-Generation Hybrid Phantoms: 46
1. Problematic: 50
2. Aim of the study: 50
3. Material and methods: 51
3.1. Epidemiological study: 51

3.2. Simulation:..... 52
3.2.1. Creating the Anthropomorphic phantom using TOPAS MC:..... 53
3.2.2. Particle sources..... 79
3.2.3. Scoring 83
3.2.4. Physics..... 84
3.2.5. The TOPAS Graphical User Interface 84
4. Results..... 85
4.1. Epidemiology results:..... 85
4.2. Simulation results 91
4.2.1. Hyperthyroidism: 91
4.2.2. Thyroid cancer: 103
4.2.3. Comparison between hyperthyroidism and thyroid cancer:..... 115
5. Discussion..... 117
6. Conclusion 125

LIST OF ABBREVIATIONS

A	Radioactive Activity
Ã	Cumulated Activity
A_0	Radioactive Activity at time t=0
A(t)	Radioactive Activity at time t
ATP	Adenosine Triphosphate
BREP	Boundary REPresentation
c	Speed of light in vacuum
CLO^{4-}	Perchlorate
CSG	Constructive Solid Geometry
CT	Computed Tomography
C-Cell	Parafollicular cells
$\dot{D}$	Radiation Dose Rate
DIT	Diiodotyrosine
DNA	Deoxyribonucleic acid
D_T	Absorbed Dose
$D_{T,R}$	Mean Absorbed Dose in Organ or Tissue (T) from Radiation (R)
E_{el}	Energy of the electron
E_0	Original energy
EGS	Electron–Gamma–Shower
fT4	Free Thyroxine
FNAB	Fine-Needle Aspiration Biopsy
FLUKA	FLUktuierende KAskade
GD	Graves' Disease
Geant4	GEometry ANd Tracking
H2	Histamine Type-2 Receptor
H_2O_2	Hydrogen peroxide
He	Helium
$HO^{\bullet}$	Hydroxyl radical
HNO_3	Nitric acid
H_T	Equivalent Dose
^{131}I	Iodine 131
IDD	Iodine Deficiency Disorders
ICRP	International Commission on Radiological Protection
ICRU	International Commission on Radiation Units and Measurements
KI	Potassium iodide
KIO_3	Potassium iodate
Kr	Krypton
LET	Linear Energy Transfer
MC	Monte Carlo
MCNP	Monte Carlo N–Particle
MCT8	Monocarboxylate transporter 8
m_e	Mass of electron
MIT	Monoiodotyrosine
MIRD	Medical Internal Radiation Dose
^{99}Mo	Molybdenum 99
MRI	Magnetic Resonance Imaging
N	Number of Nuclei

N_0	the number of radioactive atoms at time t = 0
N(t)	the number of radioactive atoms at time t
Na	Sodium
NaOH	Sodium hydroxide
NCA	Non-Carrier Added
NIS	Sodium/Iodide Symporter
NURBS	Non-Uniform Rational B-Spline
ORNL	Oak Ridge National Laboratory
PENELOPE	PENetration and Energy LOss of Positrons and Electrons
PENGEOM	PENelope GEOMetry
$RO_2^{\bullet}$	Peroxy radical
RNT	Radionuclide therapy
r_T	Target region
rT3	reverse Triiodothyronine
r_S	Source region
S-value	Absorbed dose per unit cumulative activity
SCN^-	Thiocyanate
SNM	Society of Nuclear Medicine
$T_{\frac{1}{2}b}$	Biological half-life
$T_{\frac{1}{2}e}$	Effective half-life
$T_{\frac{1}{2}p}$	Physical half-life
T3	Triiodothyronine
T4	Thyroxine
TBG	Thyroxine-Binding Globulin
^{130}Te	Tellurium 130
^{131g}Te	Tellurium 131m
^{131m}Te	Tellurium 131g
TeO_2	Tellurium dioxide
Tg	Thyroglobulin
TOPAS	TOolkit for PArticle Simulation
TPO	Thyroid peroxidase
TSH	Thyroid Stimulating Hormone
TSHR-Ab	Thyrotropin Receptor Blocking Antibodies
^{235}U	Uranium 235
UAl_3	Uranium aluminide
W_R	Radiation weighting factor
W_T	Tissue weighting factor
Xe	Xenon
λ	Decay constant
λ_b	Biological decay constant
λ_e	Effective decay constant
λ_p	Physical decay constant
Φ_i	Absorbed Fraction

LIST OF TABLES

Table 1 : Radiation Weighting Factors [Summarized from ICRP (1991)] 32
Table 2 : Tissue Weighting Factors 33
Table 3 : ^{131}I β^- Transitions 79
Table 4 : ^{131}I γ Transitions 79

LIST OF FIGURES

***Figure 1**: (n, γ) reaction on ^{130}Te which leads to ^{131}I. 4*
***Figure 2:** Decay scheme of ^{131}I 5*
***Figure 3:** The shape and localization of the thyroid 8*
***Figure 4:** Vasculature of the thyroid 9*
***Figure 5:** Innervation of the thyroid 10*
***Figure 6:** Microscopic appearance of the thyroid 11*
***Figure 7:** Main factors for thyroid hormones synthesis 12*
***Figure 8:** Chemistry of thyroxine and triiodothyronine formation 13*
***Figure 9:** Synthesis of thyroid hormones 14*
***Figure 10:** 99mTc-Pertechnetate scintigraphy of the thyroid gland. (a) Graves' disease. (b) Toxic multinodular goitre. (c) Toxic adenoma 15*
***Figure 11:** Micrographs of the most common thyroid cancers (a) Papillary carcinoma. (b) Follicular carcinoma. (c) Medullary carcinoma. (d) Anaplastic carcinoma 17*
***Figure 12:** Sodium Iodide I-131 diagnostic product label 18*
***Figure 13 :** Types of radiation 23*
***Figure 14 :** Photoelectric effect 26*
***Figure 15 :** Compton effect 26*
***Figure 16 :** Pair production 27*
***Figure 17 :** Deterministic and stochastic effects 29*
***Figure 18** : Personal dosimeter (Polimaster) 30*
***Figure 19 :** Difference between equivalent and effective dose 33*
***Figure 20 :** Absorbed dose, equivalent dose and effective dose 34*
***Figure 21 :** Source and target organs. (Created with BioRender). 35*
***Figure 22 :** Difference between beta and gamma energy deposition. (Created with BioRender) 36*
***Figure 23 :** Time-activity curve 37*
***Figure 24 :** Stylized computational phantom (a) external view of male phantom (b) internal view of female phantom. 44*
***Figure 25 :** Voxelized phantoms 46*
***Figure 26 :** Construction of a hybrid phantom 46*
***Figure 27 :** Hybrid phantoms. 47*
***Figure 28 :** Three phantom generations; (a) stylized phantom; (b) voxel phantom (but displayed in smooth surfaces); (c) BREP phantom. 48*
***Figure 29 :** The algorithm for the soft tissue. 53*
***Figure 30 :** The algorithm for the skeleton. 53*
***Figure 31 :** The algorithm for the lung material. 54*
***Figure 32 :** The algorithm for the head volume. 55*
***Figure 33 :** The algorithm for the skull volume. 56*
***Figure 34 :** The algorithm for the brain volume. 56*
***Figure 35 :** the algorithm for the upper spine volume. 57*
***Figure 36 :** The algorithm for the thyroid volume. 58*

Figure 37: *TOPAS MC representation of the head volume and its constituents (red: head, yellow: thyroid, grey ellipsoid: skull and grey elliptical tube: upper spine). 59*
Figure 38 : *The algorithm for the trunk volume. 59*
Figure 39 : *The algorithm for the left lung volume. 60*
Figure 40 : *The algorithm for the heart volume. 61*
Figure 41 : *TOPAS MC representation of the heart and the lungs. 62*
Figure 42 : *The algorithm for the left kidney volume. 63*
Figure 43 : *TOPAS MC representation of the left and right kidney. 63*
Figure 44 : *The algorithm for the liver volume. 64*
Figure 45 : *TOPAS MC representation of the liver volume (left: front view, right: top view). . 65*
Figure 46 : *The algorithm of the stomach volume. 65*
Figure 47 : *the algorithm to create the stomach's cavity volume. 66*
Figure 48: *TOPAS MC representation of the stomach volume (yellow) and the stomach's cavity (white). 66*
Figure 49 : *The algorithm for the pancreas volume. 67*
Figure 50 : *TOPAS MC representation of the pancreas volume. 68*
Figure 51 : *The algorithm of the spleen volume. 68*
Figure 52 : *TOPAS MC representation of the spleen volume. 69*
Figure 53 : *The algorithm of the thymus volume. 69*
Figure 54 : *The algorithm for the small intestine volume. 70*
Figure 55 : *TOPAS MC representation of the small intestine volume (up: front view, down: bottom view). 71*
Figure 56 : *The algorithm for the urinary bladder volume. 72*
Figure 57 : *TOPAS MC representation of the urinary bladder volume. 72*
Figure 58 : *The algorithm for the left leg. 73*
Figure 59 : *The algorithm for the left leg bone. 73*
Figure 60 : *The algorithm for the left ovary volume. 74*
Figure 61 : *The algorithm for the uterus volume. 75*
Figure 62 : *TOPAS MC representation of the uterus and the two ovaries' volumes (up: front view; down: upper view). 76*
Figure 63 : *The algorithm for the left breast. 77*
Figure 64 : *TOPAS MC representation of the breasts and rib cage volumes. 77*
Figure 65 : *The algorithm for the male genitalia. 78*
Figure 66 : *The algorithm for the left testicle volume. 79*
Figure 67 : *The algorithm for the stomach's cavity as a source. 80*
Figure 68 : *The algorithm for the small intestine as a source. 81*
Figure 69 : *The algorithm for the thyroid as a source. 81*
Figure 70 : *The algorithm for the right and left kidneys as a source. 82*
Figure 71 : *The algorithm for the urinary bladder as a source. 83*
Figure 72 : *The algorithm for the stomach as a scorer for absorbed dose. 83*
Figure 73 : *Pie of pathology distribution. 85*
Figure 74 : *Pie of sex distribution for hyperthyroidism. 86*
Figure 75 : *Chart of female age distribution for hyperthyroidism. 86*
Figure 76 : *Chart of male age distribution for hyperthyroidism. 87*

Figure 77 : *Pie of female dose distribution in hyperthyroidism. 87*
Figure 78 : *Pie of male dose distribution in hyperthyroidism. 88*
Figure 79 : *Pie of sex distribution for thyroid cancer. 88*
Figure 80 : *Chart of female age distribution for thyroid cancer. 89*
Figure 81 : *Chart of male age distribution for thyroid cancer. 89*
Figure 82 : *Pie of female dose distribution in thyroid cancer. 90*
Figure 83 : *Pie of male dose distribution in thyroid cancer. 90*
Figure 84 : *Equivalent dose at 1 and 30 min for a male afflicted with hyperthyroidism. 91*
Figure 85 : *Equivalent dose at 1 and 30 min for a male afflicted with hyperthyroidism (HT<1.8E-03 Sv). 91*
Figure 86 : *Equivalent dose after 1 and 30 min for a female afflicted with hyperthyroidism (sex-specific organs). 92*
Figure 87 : *Equivalent dose after 90 min residence in the small intestine for a male afflicted with hyperthyroidism. 92*
Figure 88 : *Equivalent dose after 90 min residence in the small intestine for a male afflicted with hyperthyroidism (H_T<2.5E-03 Sv) 93*
Figure 89 : *Equivalent dose after 90 min residence in small intestine for a female afflicted with hyperthyroidism (sex-specific organs). 93*
Figure 90 : *Equivalent dose to the thyroid after 24H, 5 and 10 days residence in the thyroid for a male afflicted with hyperthyroidism. 94*
Figure 91 : *Equivalent dose to the head after 24H, 5 and 10 days residence in the thyroid for a male afflicted with hyperthyroidism. 94*
Figure 92 : *Equivalent dose after 24H, 5 and 10 days residence in the thyroid for a male afflicted with hyperthyroidism (H_T<0.8E-04 Sv) 95*
Figure 93 : *Equivalent dose after 24H, 5 and 10 days residence in the thyroid for a female afflicted with hyperthyroidism (sex-specific organs) 95*
Figure 94 : *Equivalent dose to the kidneys after 24H and 5 days residence in the kidneys for a male afflicted with hyperthyroidism. 96*
Figure 95 : *Equivalent dose after 24H and 5 days residence in the kidneys for a male afflicted with hyperthyroidism (H_T<0.3E-01 Sv) 96*
Figure 96 : *Equivalent dose after 24H and 5 days residence in the kidneys for a female afflicted with hyperthyroidism (sex-specific organs) 97*
Figure 97 : *Equivalent dose to the urinary bladder after 24H and 5 days residence in the urinary bladder for a male afflicted with hyperthyroidism. 97*
Figure 98 : *Equivalent dose after 24H and 5 days residence in the urinary bladder for a male afflicted with hyperthyroidism (H_T<1.4E-01 Sv) 98*
Figure 99 : *Equivalent dose after 24H and 5 days residence in the urinary bladder for a male afflicted with hyperthyroidism (H_T<0.2E-02 Sv) 98*
Figure 100 : *Equivalent dose after 24H and 5 days residence in the urinary bladder for a female afflicted with hyperthyroidism (sex-specific organs) 99*
Figure 101 : *Equivalent dose 2H after the ingestion of NaI capsule for a male afflicted with hyperthyroidism 99*
Figure 102 *: Equivalent dose 2H after ingestion of capsule for a male afflicted with hyperthyroidism (H_T<0.2E-02 Sv) 100*

Figure 103 : *Equivalent dose 24H after ingestion of capsule for male afflicted with hyperthyroidism..... 100*
Figure 104 : *Equivalent dose 24H after ingestion of capsule for male afflicted with hyperthyroidism (H_T<1.2 Sv)..... 101*
Figure 105 : *Equivalent dose 24H after ingestion of capsule for male afflicted with hyperthyroidism (H_T<0.04 Sv)..... 101*
Figure 106 : *Equivalent dose 5d after ingestion of capsule for male afflicted with hyperthyroidism (H_T<0.3E-1 Sv)..... 102*
Figure 107 : *Equivalent dose at 1 and 30 min for a male afflicted with thyroid cancer..... 103*
Figure 108 : *Equivalent dose at 1 and 30 min for a male afflicted with thyroid cancer (H_T<0.35E-01 Sv)..... 103*
Figure 109 : *Equivalent dose at 1 and 30 min for a female afflicted with thyroid cancer (sex-specific organs)..... 104*
Figure 110 : *Equivalent dose after 90 min residence in the small intestine for a male afflicted with thyroid cancer..... 104*
Figure 111 : *Equivalent dose after 90 min residence in the small intestine for a female afflicted with thyroid cancer (sex-specific organs)..... 105*
Figure 112 : *Equivalent dose to the thyroid after 24H, 5 and 10 days residence in the thyroid for a male afflicted with thyroid cancer..... 105*
Figure 113 : *Equivalent dose to the head after 24H, 5 and 10 days residence in the thyroid for a male afflicted with thyroid cancer. 106*
Figure 114 : *Equivalent dose after 24H, 5 and 10 days residence in the thyroid for a male afflicted with thyroid cancer (H_T<2.5E-04 Sv). 106*
Figure 115 : *Equivalent dose after 24H, 5 and 10 days residence in the thyroid for a female afflicted with thyroid cancer (sex-specific organs)..... 107*
Figure 116 : *Equivalent dose in kidneys after 24H and 5 days residence in the kidneys for a male afflicted with thyroid cancer 107*
Figure 117 : *Equivalent dose after 24H and 5 days residence in the kidneys for a male afflicted with thyroid cancer (H_T<0.7 Sv)..... 108*
Figure 118 : *Equivalent dose after 24H and 5 days residence in the kidneys for a female afflicted with thyroid cancer (sex-specific organs)..... 108*
Figure 119 : *Equivalent dose to the urinary bladder after 24H and 5 days residence in the urinary bladder for a male afflicted with thyroid cancer 109*
Figure 120 : *Equivalent dose after 24H and 5 days residence in the urinary bladder for a male afflicted with thyroid cancer (H_T<0.9 Sv)..... 109*
Figure 121 : *Equivalent dose after 24H and 5 days residence in the urinary bladder for a female afflicted with thyroid cancer (sex-specific organs)..... 110*
Figure 122 : *Equivalent dose 2H after the ingestion of the capsule for a male afflicted with thyroid cancer..... 110*
Figure 123 : *Equivalent dose 2H after ingestion of the capsule for a male afflicted with thyroid cancer (H_T<0.4E-01 Sv)..... 111*
Figure 124 : *Equivalent dose 2H after ingestion of the capsule for a female afflicted with thyroid cancer (sex-specific organs)..... 111*

Figure 125 : *Equivalent dose 24H after ingestion of capsule for male afflicted with thyroid cancer (H_T<2.5 Sv)..... 112*
Figure 126 : *Equivalent dose 24H after ingestion of capsule for a female afflicted with thyroid cancer (sex-specific organs). 112*
Figure 127 : *Equivalent dose 5d after ingestion of the capsule for male afflicted with thyroid cancer. 113*
Figure 128 : *Equivalent dose 5d after ingestion of the capsule for male afflicted with thyroid cancer (H_T<25 Sv)..... 113*
Figure 129 : *Equivalent dose 5d after ingestion of the capsule for male afflicted with thyroid cancer (H_T<0.2 Sv)..... 114*
Figure 130 : *Equivalent dose 5d after ingestion of the capsule for a female afflicted with thyroid cancer (sex-specific organs). 114*
Figure 131 : *A comparison between equivalent dose in the thyroid in male after 24H, 5 and 10 days residence in thyroid..... 115*
Figure 132 : *A comparison between equivalent dose in the head in male after 24H, 5 and 10 days residence in thyroid..... 115*
Figure 133 : *A comparison between equivalent dose in the heart, left & right lung in a male after 24H, 5 and 10 days residence in thyroid..... 116*
Figure 134 : *A comparison between equivalent dose in the left & right lung in a female after 24H, 5 and 10 days residence in thyroid 116*

Introduction

Introduction

Unsealed source radiotherapy has been used for over 70 years. These sources are administered orally or intravenously; capsules containing radioactive iodine are the most common RNT, so, while it has been in clinical use for over 50 years, constant debate is being held over the amount of recommended activity used for the treatment of hyperthyroidism and thyroid cancer.

Being a non-targeted radiotherapy, ^{131}I is bound to irradiate tissues and organs other than its therapeutic target. The treatment strategy must deliver the right dose to the thyroid gland without harming other organs, hence the importance of internal dosimetry.

To this day, the health effects of ionizing radiation are still not fully understood and their prediction is a major issue in radiobiology. The diversity of the molecules involved, (DNA and radical species), and physical, chemical, and biological mechanisms at different scales of size and time make the problem very complex.

In order to optimize treatment, it is important to assess the accurate level of doses absorbed by each critical organ.

Most radio epidemiological data relate only to high doses. The usual method of assessing risk at low doses is to determine a dose-response relationship by extending the linear segment in the region of low doses for which no data is available.

For the estimation of the radiation absorbed dose to target and non-target organs, the medical internal radiation dose committee (MIRD) has published a series of pamphlets and methods detailing the accurate way to calculate the absorbed dose. Furthermore, a decent number of Monte Carlo codes are available to simplify this task for health professionals.

Our work will focus on iodine 131, the emitter of beta and gamma radiation. It is a radionuclide frequently used in nuclear medicine. Its β-emission damages both normal and abnormal thyroid tissue, hence its use in this practice. On the other hand, the emission of γ radiation associated with its disintegration leads to exposure of other non-target tissues, as well as the irradiation of personnel and the public.

In this context, the numerical simulation of material or biophysical phenomena is a powerful tool that describes the physical interactions of radiation with biological matter, using TOPAS MC and a stylized anthropomorphic phantom, simulations were performed to determine the absorbed dose per disintegration, thus an effort is made to quantify a value that is otherwise unquantifiable. These results will be the stepping stone to predicting radiobiological effects.

Part One: Literature Review

Chapter One: Iodine and Thyroid

1. Introduction

A look at the history of medicine will show that the advanced practice of nuclear medicine is the product of an endless stream of ideas and inventions. Many clinical fields have had a substantial impact on the inception of this discipline; first and foremost was thyroidology, which has immensely benefited from nuclear medicine research (1). No organ of the human body has been more crucial in the development of nuclear medicine than the thyroid gland (2).

2. History

Between 1891 and 1892, a series of publications appeared in the British Medical Journal, documenting for the first time the effective use of thyroid extracts both orally and parentally in subjects with hypothyroidism (3–5). In 1895, Bauman detected high concentrations of iodine in the thyroid gland and suggested that the active ingredient in the thyroid extracts contains iodine (6).

The remarkable growth of iodine-containing products, from 10 preparations listed in the pharmacopeias in 1851 to 1,700 names assigned to iodine-containing products in 1956, is compelling evidence for the widespread applications of iodine in medicine (7).

Applying iodine alone to patients with hyperthyroidism, Thompson et al. (8) declared in 1930 a success rate of 88%, and Starr et al. (9) reported in 1924 a success rate of 92% with Lugol solution at daily doses of 6 to 90 mg.

During the first 100 years following the discovery of iodine, its clinical use was entirely empirical and the effective dose was reached through trial and error (10).

3. Iodine:

3.1. Pharmacokinetics of iodine:

3.1.1. Absorption:

Iodine occurs in foods mainly as inorganic iodide. A major amount of iodine enters the human organism via the food chain (11). Lack of iodine leads to iodine deficiency disorders (IDD), while excessive iodine dietary intake can result in pathological problems, namely the goitrogenic effect (12,13). Low iodine intake resulting in IDD is recognized as a global concern, while excessive iodine intake is not so frequent. In general, iodine content in foodstuffs is low, usually in the range of 10–200 (g/kg) fresh mass, except for in seafood (14).

Dietary iodine is absorbed efficiently in the gastrointestinal tract, yet other forms are reduced to iodide in the alimentary tract before absorption (15,16).

Gastrointestinal absorption of iodine is rapid and generally thought to be approximately 100% after an ingested dose of water-soluble iodide salts, such as potassium or sodium iodide (17). It appears to be similar in children, adolescents, and adults, however, it may be lower in infants (18–20). The absorption rate in fasting subjects was about 5% min^{-1} and it was slower when iodide was ingested with foodstuff but was virtually complete after about 3 h. More than

99% of iodine administered orally as potassium iodide was absorbed into the blood in normal subjects (21).

In general, injection of the radioiodine intramuscularly or intravenously results in higher thyroid uptakes than when the radioiodine was administered orally, suggesting incomplete absorption of the oral dose. The ratio of the thyroid uptakes after the oral and injected iodine doses suggests a fractional oral absorption of approximately 70% (22,23).

Iodine secreted into saliva and gastric juice is reabsorbed in the small intestine. This represents the enteric phase of iodine's absorption (24).

3.1.2. Distribution:

The human body contains approximately 10–15 mg of iodine, of which almost 70–90% is trapped and concentrated in the thyroid gland, which accumulates iodine to produce thyroid hormones for export to the blood and other tissues whereas iodide circulating in plasma is exchanged rapidly with iodide in red blood cells and with both rapid and slow extracellular compartments (25,26).

Iodide concentrations in the thyroid are usually 20–50 times that of serum (0.2–0.4 mg/dl); however, concentrations exceeding 100 times that of blood occur when the gland is stimulated by thyrotrophin (TSH) (27).

In the serum, approximately 5% of the absorbed dose is represented by the inorganic form of iodide; the remaining 95% consists of various organic forms of iodine, principally protein complexes of the thyroid hormones T4 and T3 (17,28).

Iodide is mostly confined to the extracellular fluid compartment except for the tissues that possess particular transport mechanisms for accumulating iodide; these include the thyroid, salivary glands, gastric mucosa, mammary glands, placenta, choroid plexus, and sweat glands (29).

Iodine uptake into the thyroid gland is highly sensitive to iodide intake. At very low intakes, i.e., iodine deficiency (e.g., 20 µg/day), uptake of iodide into the thyroid gland is increased. TSH is the one responsible for mediating this response, by stimulating iodide transport and iodothyronine production in the thyroid gland (30). At very high intakes of iodine, representing an intake excess (e.g., > 1 mg/day), iodine uptake into the thyroid gland decreases, primarily as a result of decreased iodothyronine synthesis and iodide transport into the gland (31).

The biological half-lives of iodine are: blood, 0.25 days; thyroid, 80 days; rest of the body, 12 days (32).

3.1.3. Metabolism:

In the thyroid gland, iodide is incorporated into a protein, thyroglobulin, forming covalent complexes with tyrosine residues.

Uptake of thyroglobulin occurs by endocytosis at the apical membrane, which is followed by fusion of endocytotic vesicles with lysosomes. Proteolytic enzymes in the lysosomes break down the thyroglobulin into constituent amino acid residues, including T4, T3,

monoiodotyrosine, and diiodotyrosine. T4 and T3 are exported to the blood, while monoiodotyrosine and diiodotyrosine residues are retained in the cell and deiodinated, and the iodide is recycled into the follicular lumen where it is reincorporated into thyroglobulin (33).

The most important pathways of metabolism of iodine taking place outside the thyroid gland represent the catabolism of T4 and T3, this includes:

a) Deiodination reactions:

The monodeiodination of T4 to T3 is the principal source of production of peripheral T3 which is the more potent form, and together with the production of rT3 accounts for approximately 80% of total T4 turnover in humans (34,35).

The production of circulating T3 takes place predominantly in the liver and kidneys (36).

Iodothyronine deiodinase also catalyzes the inactivation of T4 and T3, hence deactivating the thyroid hormones with the released iodide being either taken up by the thyroid or excreted (37).

Enzymes responsible for deiodination are selenium-dependent (selenodiodinases) (38,39).

1. Oxidative deamination and decarboxylation of the side chain of thyronine:

It represents approximately 2 and 14% of the total T4 and T3 turnover, respectively (40).

The acetic acid analogs of the iodothyronines undergo deiodination and conjugation with glucuronic acid and sulfate (34,41).

2. Conjugation of the phenolic hydroxyl group on thyronine with glucuronic acid and sulfate:

Both conjugations of the phenolic group of iodothyronines occur in the liver and probably in other tissues (42).

Sulfate conjugation is catalyzed by phenolic arylsulfotransferase. Its products undergo deiodination.

Glucuronide conjugation is catalyzed by glucuronosyltransferase (43).

3. Ether bond cleavage of thyronine:

This is a minor pathway of the metabolism of iodotyrosines under normal conditions (43).

3.1.4. Elimination:

The human body has different routes for eliminating iodine; the kidneys and urinary bladder account for about two-thirds of the iodide cleared from the plasma and at least 90% of iodide excreted from the organism (26); breast milk and perspiration account for various fractions of iodide elimination; however, the fecal route barely contributes to 1% of total body iodide clearance (25,44).

The whole-body elimination half-time of absorbed iodine has been estimated to be generally 31 days in healthy adult males; however, there is significant inter-individual variability in the half-time (20,26).

The glucuronide and sulfate conjugates of T4, T3, and the other metabolites are secreted into bile (45).

The quantity of iodide excreted in breast milk differs depending on the functional status of the thyroid gland and iodine intake. A larger fraction of the absorbed dose is excreted in breast milk in the hypothyroid state compared to the hyperthyroid state (46)

In cases of strenuous physical activity, significant amounts of iodine can be eliminated in sweat (47).

Studies have proved that iodide can be excreted in human tears (48).

3.2. Radioactive iodine:

3.2.1. Production of radioiodine:

Iodine-131 is a reactor-produced radionuclide and is commercially available in considerable quantities (49).
There are two routes for its production:

a) Fission of ^{235}U:

Since the chain yield of mass ^{131}I is fairly high (2.885%) and the radioiodines with a mass higher than 131 are short-lived, ^{131}I is effortlessly obtained in a pure form. The irradiated $^{235}UAl_3$ is first stored for 24 h to recognize the disintegration of short-lived products. Thereafter, it is treated with NaOH through which radioactive inert gases (Xe and Kr) are emitted; on filtration, uranium and some fission products are eliminated. The filtrate is then acidified with HNO_3. On heating, radioiodine is distilled and collected in a trap. The rest of the reaction mixture is treated further for separation of ^{99}Mo and other fission products (50).

b) (n, γ) reaction:

The (n, γ) reaction on ^{130}Te leads to the creation of ^{131m}Te and ^{131g}Te, both of which ultimately decay to ^{131}I. The reaction sequence is thus:

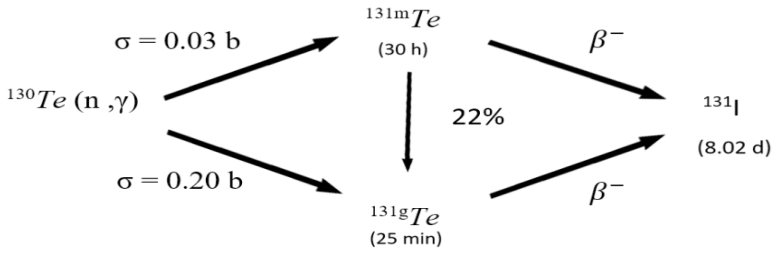

***Figure 1**: (n, γ) reaction on ^{130}Te which leads to ^{131}I.*

The target material for irradiation is either TeO_2 or Te-metal, depending on whether a wet chemical separation procedure is employed or a dry distillation method is used. In general,

the latter is preferred. The irradiated TeO_2 is allowed to disintegrate for about 3 days so that a larger part of ^{131m}Te is transformed into ^{131}I. The distillation of radioiodine is then completed in a stream of air at 750°C, i.e., just above the melting point of TeO_2, and it is collected in a trap. The cross-sections for the formation of both ground and metastable states of ^{131}Te are rather low, so the expected overall yield of ^{131}I via the (n, γ) reaction is much lower than that via the fission process (51).

3.2.2. Radioactive decay of Iodine 131:

With 53 protons and 78 neutrons in its nucleus and a half-life of 8.0197 days, ^{131}I decays with beta and gamma emissions. The only stable isotope, ^{127}I, has only 74 neutrons (52).

When it decays, ^{131}I usually (89% of the time) expends its 971 KeV of decay energy by transforming into the stable ^{131}Xe in two steps, with gamma decay succeeding rapidly the beta decay as shown in equations 1.1 and 1.2:

$$^{131}_{53}I \longrightarrow {}^{131}_{54}Xe^{*} + \beta^{-} + \bar{\nu}_e + 606\ \text{keV} \qquad \textbf{(1.1)}$$

$$^{131}_{54}Xe^{*} \longrightarrow {}^{131}_{53}Xe + \gamma\text{-rays} + 364\ \text{keV} \qquad \textbf{(1.2)}$$

The primary emissions of ^{131}I decay are thus beta particles with a maximal energy of 606 KeV with 89.6% abundance and 364 KeV gamma rays with 81.5% abundance as illustrated in figure 2. β-decay also produces an antineutrino, which carries off various amounts of energy.

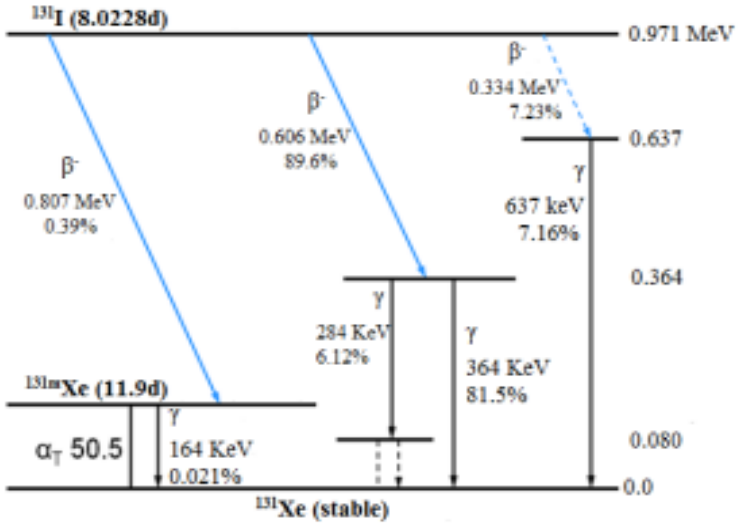

Figure 2: *Decay scheme of ^{131}I (53).*

^{131}I is characterized by the emission of several β-particles with different energies. A direct transition to the ground state of the daughter nuclide ^{131}Xe has not been discovered. Transitions occur through the excited states of the daughter nuclide and with a very small (0.39%) probability through the metastable ^{131m}Xe that has a half-life of 11.9 days. This

metastable state has an energy difference from the ground state of 164 KeV. The dots in the ^{131}I scheme indicate further weak transitions (53).

There is widespread awareness of the application of radiation and radioisotopes in medicine, particularly for diagnosis (identification) and therapy (treatment) of different medical conditions (54).

In the case of iodine, there are more than 20 recognized radioactive isotopes in addition to the stable isotope, ^{127}I. Only 2 are currently used in clinical practice, ^{131}I for treatment and ^{123}I for imaging. Both are typically administered as sodium iodide (55).

Using a radioisotope for diagnosis means that it must emit gamma rays of sufficient energy to escape from the body and it must have a short enough half-life for it to decay away soon after imaging is completed. Consequently, ^{123}I is excellent for thyroid imaging since it delivers far less radiation to the thyroid than ^{131}I, has a short half-life (13 h), and does not emit destructive beta radiation. Furthermore, its gamma radiation emission energy (159 keV) is ideally suited to thyroid scanning (56). Its use has been superseded for most routine thyroid imaging by Technetium-99m, an isotope that is actively transported by the sodium iodide symporter, with radiation characteristics similar to those of ^{123}I but with the advantages of minimal cost and ready availability due to its widespread use in nuclear medicine (57).

Most therapeutic radioisotopes are either alpha or beta emitters. Alpha emitters release large helium nuclei into the surrounding tissues while beta emitters release highly energetic electrons that can penetrate several millimeters of tissues depending on their maximal energy emission (58). In this manner, ^{131}I is ideal for ablative thyroid therapy by its large beta particle emissions of moderate energy (364 keV) and is associated with a moderate but sufficiently long half-life of 8.1 days. The beta particles of ^{131}I are essentially nonpenetrating and so act locally, delivering 90% of the radiation dose within a 1 to 2 mm zone to the thyroid follicular cells (56).

Emitted beta particles tend to have a high LET and are deposited in the nearby cells. This means that most of the damage is registered in the organs where ^{131}I is concentrated. On the other hand, gamma emissions tend to travel far from their source, therefore they increase the total body dose (59).

The human body does not differentiate between stable and radioactive iodine. As a result, ^{131}I behaves just as stable iodine (60). That's to say that a large part of the intake will be concentrated in the thyroid within 24 to 48 hours. The radioactive iodine will irradiate the thyroid tissue, resulting in the death of tumor cells or a substantial amount of normal thyroid cells. Those damaged cells lose their capacity to organify iodine and, consequently, the iodine is released back to the bloodstream, resulting in its elimination.

The total amount of radioactive iodine reduced to half its original value at a rate that depends on the state of disease: one day, in the case of thyroid cancer and total ablation of thyroid tissue, and seven days for patients with euthyroid goitre. In the case of hyperthyroidism, the effective half-life, which is based on the physical and biological half-lives, is about four to five days (61).

3.3. Medical use of Iodine:

a) Iodinated X-Ray contrast agents:

Iodinated contrast media are contrast agents that contain iodine atoms used for X-Ray-based imaging methods such as computed tomography (CT). They can also be used in fluoroscopy, angiography and venography, and even occasionally, simple radiography. Iodine has maintained its dominating role as a contrast-providing element for many reasons, above all for its high absorption coefficient, its easy chemistry, and its relative inertness (62).

b) Iodine as a disinfectant:

Iodine is a very effective topical antimicrobial that has been used clinically in the treatment of wounds for over 170 years (63). It has a vast spectrum of antimicrobial activity with efficacy against bacteria, fungi, mycobacteria, protozoa, and viruses and can be used to cure both acute and chronic wounds (64). As far as is known, the first use of iodine in medical practice was as a remedy for bronchocele (65). Soon afterward, Lugol treated scrofuloderma (tuberculous lesions of the skin) with an iodine/iodide solution bearing his name, which is still in use untill now (66). It is also relatively cheap and easy to use but is often underused as a topical antiseptic due to its recognized toxicity (67).

c) Synthetic thyroid hormone:

Iodide is a micronutrient required for humans and other mammals solely to produce thyroxine (T4) and triiodothyronine (T3) (68).

d) Iodine deficiency disorders and their correction using iodized salt and/or iodine supplements:

There are two approaches commonly used to rectify iodine deficiency in a population: iodized oil and iodized salt. In almost all countries affected by iodine deficiency, the most appropriate way to control iodine deficiency is through salt iodization. All salt for human consumption, including salt used in the food industry, should be continuously iodized. Iodine can be incorporated into the salt in the form of potassium iodide (KI) or potassium iodate (KIO_3). KIO_3 is the recommended form because it has higher stability in the presence of salt impurities, humidity, and porous packaging (69).

e) Pharmaceuticals:

Some examples are: Amiodarone which is an antiarrhythmic agent and Iodoxuridine an anti-herpes virus antiviral agent (68).

4. Thyroid:

The thyroid gland is a highly vascular endocrine organ and plays a key role in the energy metabolism, growth, and maturation of the human body. These effects are mediated by the thyroid hormones, thyroxine (T4) and triiodothyronine (T3). Thyroid hormones stimulate diverse metabolic activities,leading to an increase in basal metabolic rate (70).

4.1. Anatomy

The thyroid gland is a butterfly-shaped, vascular, red-brown endocrine gland situated in the midline of the anterior neck. Typically, the gland weighs between 15 and 25 g and is the largest of the endocrine glands.

The gland is formed by 2 elongated lateral lobes with superior and inferior poles connected by a median isthmus, with an average height of 12-15 mm, overlying the second to fourth tracheal rings (70,71).

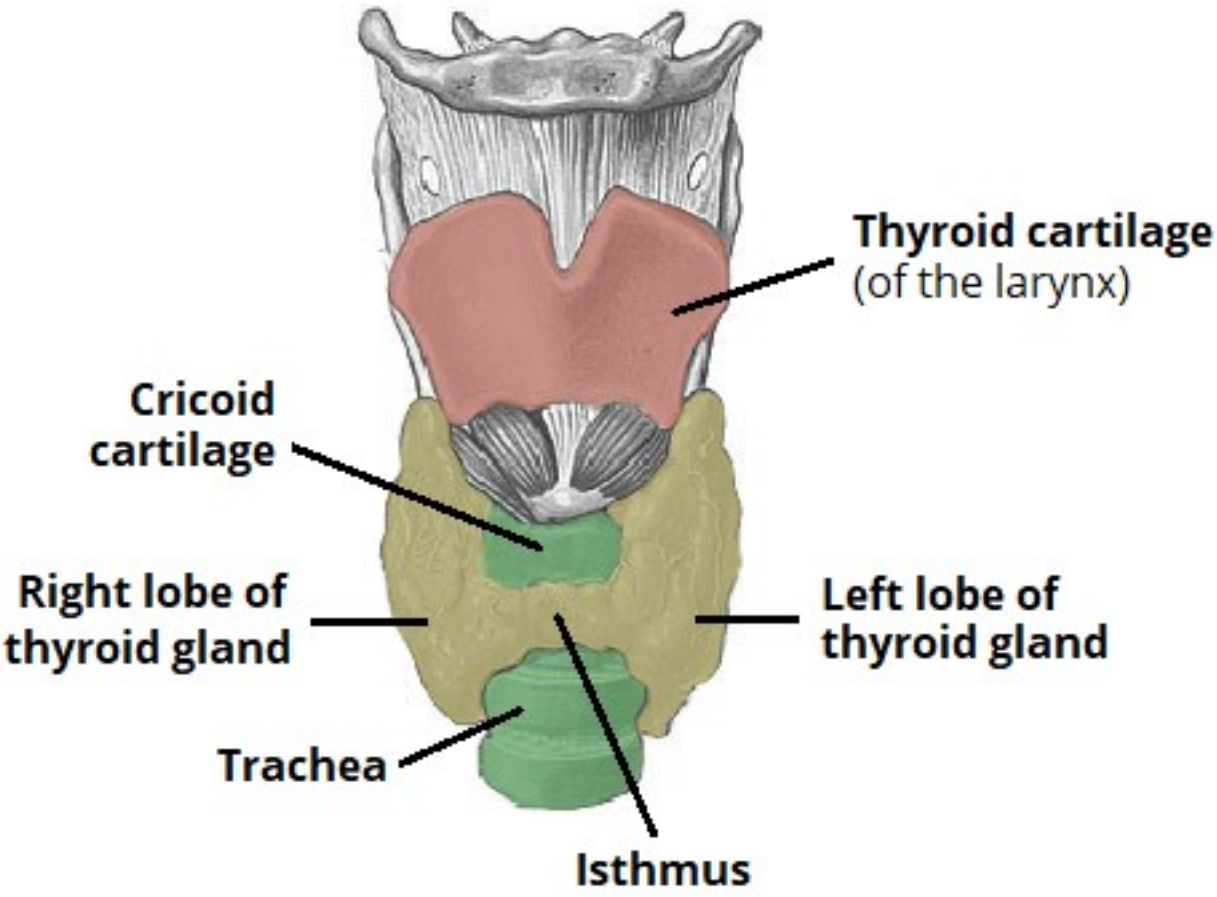

Figure 3: *The shape and localization of the thyroid (72).*

The arterial vascularization of the thyroid is very rich and important, three times that of the brain and six times that of the kidney.

It is ensured by the two upper thyroid arteries, the two lower thyroid arteries, and an accessory medium thyroid artery.

Thyroid veins form the thyroid plexus on the surface of the thyroid. This plexus is made of irregular veins.

This network is drained by:

- The superior thyroid vein, which is parallel and posterior to the artery.
- The lower thyroid veins.
- The medium thyroid vein, formed by one or two more or less voluminous branches, depending on the case and especially the functional state of the lobe.

All the thyroid veins discharge into the internal jugular vein (72).

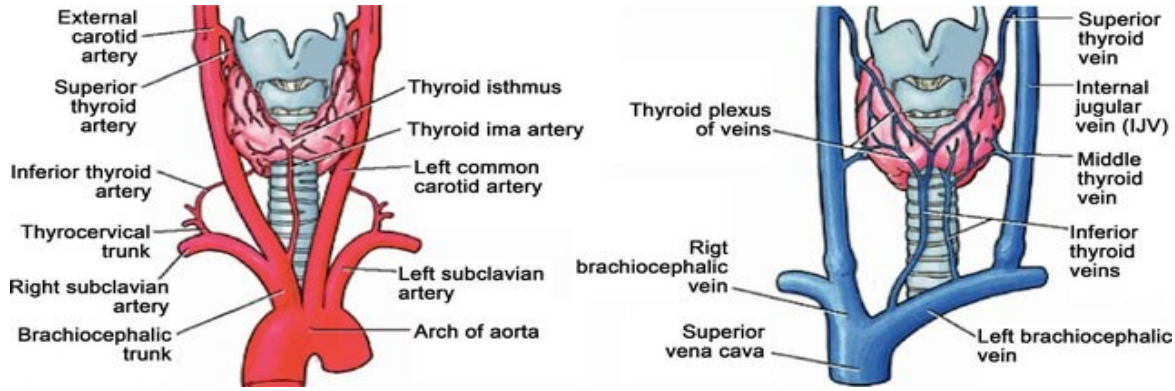

Figure 4: *Vasculature of the thyroid (74).*

The thyroid gland is innervated by branches derived from the sympathetic trunk.

These nerves only control the vasomotor function of the gland but not the secretory one; in fact, the release of thyroid hormones is regulated by the pituitary gland (73).

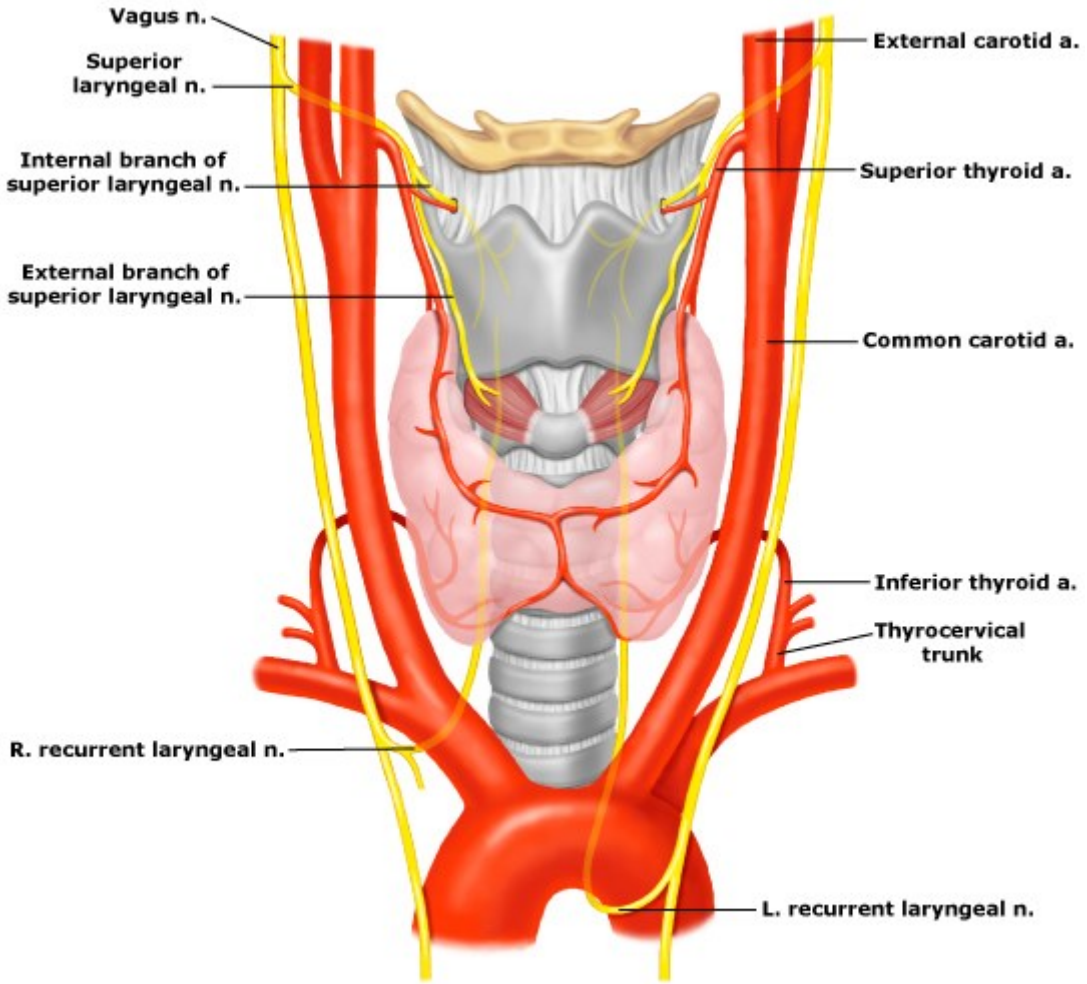

Figure 5: *Innervation of the thyroid (74).*

4.2. Histology:

The thyroid gland is divided into lobules. These lobules consist of many typical units called thyroid follicles. The thyroid follicles are the structural and functional units of the thyroid gland. They are spherical, and their walls are made up of a large number of cuboidal cells, the follicular cells which secrete thyroid hormone. They are filled with a substance called the colloid which is an inactive precursor of T3 and T4 and acts as storage compartments. This substance is made up of a glycoprotein called thyroglobulin and is made by epithelial cells. The iodine binds to the tyrosine residues of thyroglobulin.

Scattered within the gland are the small C-Cells, also known as Parafollicular cells. They secrete a polypeptide hormone known as calcitonin which is responsible for the regulation of blood calcium levels (74–76).

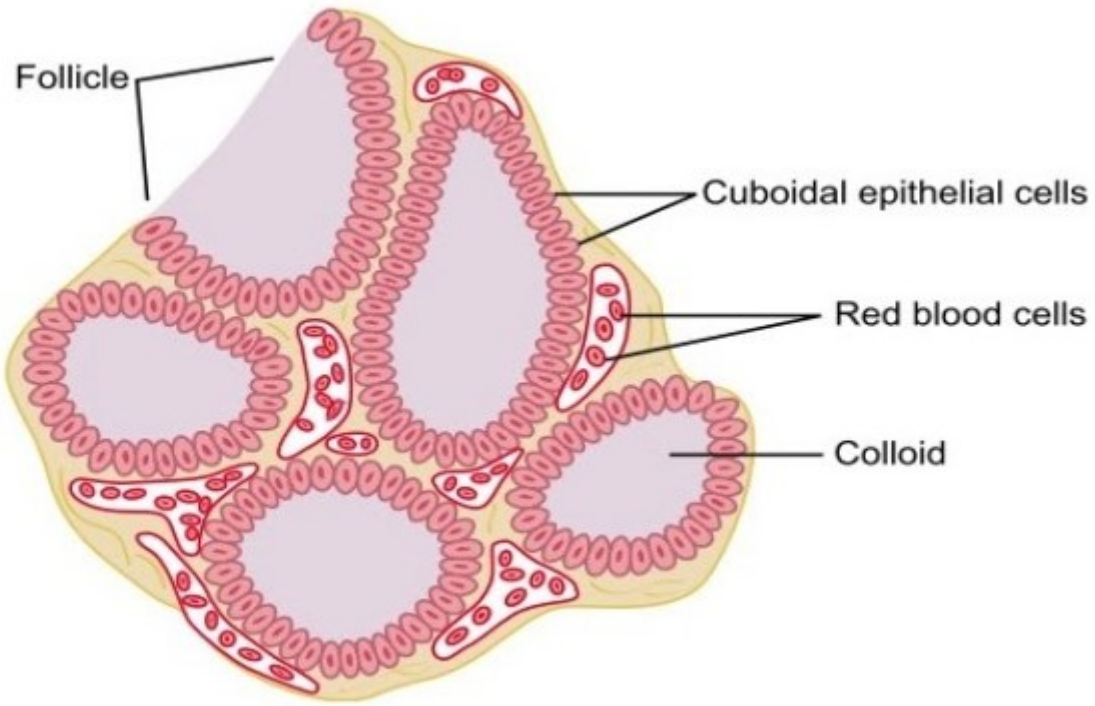

Figure 6: *Microscopic appearance of the thyroid* (77).

4.3. Physiology:

The thyroid is dependent on iodine to produce thyroxine and triiodothyronine.

Usually, about 90 µg of T4 is produced per day exclusively in the thyroid. The daily production of T3 is about 30 µg, of which a small part comes directly from the thyroid and the rest from enzymatic 5'-deiodination of T4 to T3 in extrathyroidal tissues.

Only about 0.1% of T4 and 0.3% of T3 occurs in a free form. The rest circulates bound to thyroxine-binding globulin (TBG), transthyretin (prealbumin), and albumin.

The following factors are basic elements for the synthesis of thyroid hormone:

- Iodide ions (I^-).
- Thyroglobulin (Tg).
- Thyroperoxidase (TPO).
- hydrogen peroxide (H_2O_2).

The structure and function of the follicle cell are critical in this process (78).

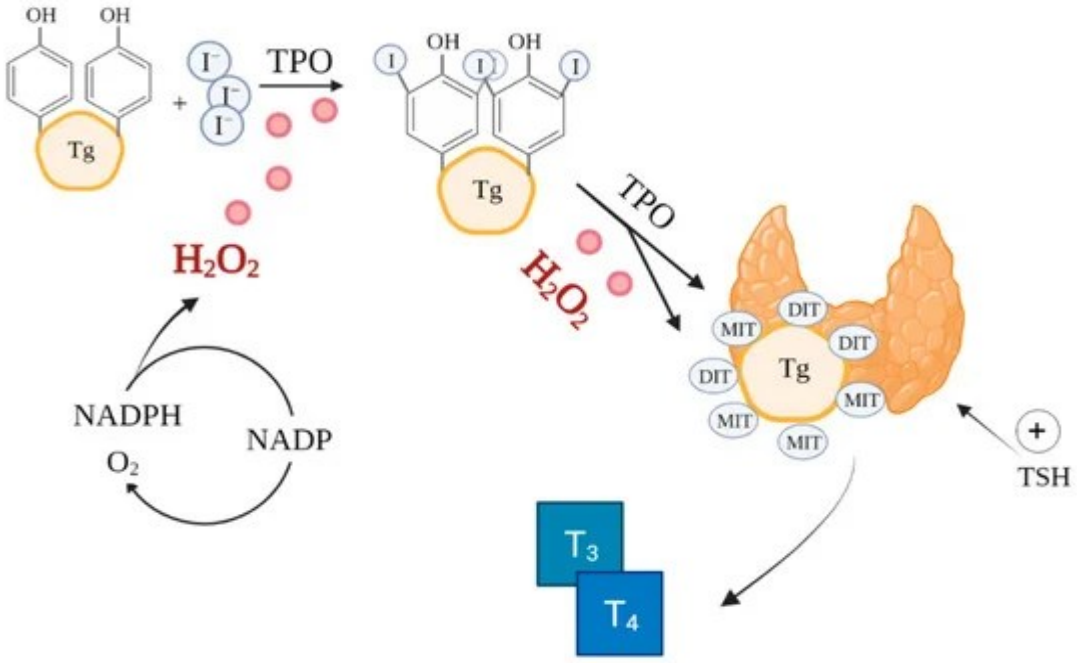

Figure 7: *Main factors for thyroid hormones synthesis (79).*

Thyroid hormones are the only iodine-containing human hormones and require an adequate dietary supply of this environmentally scarce element for their biosynthesis (79). Iodide (I^-) is the essential rate-limiting substrate for thyroid hormonogenesis (80).

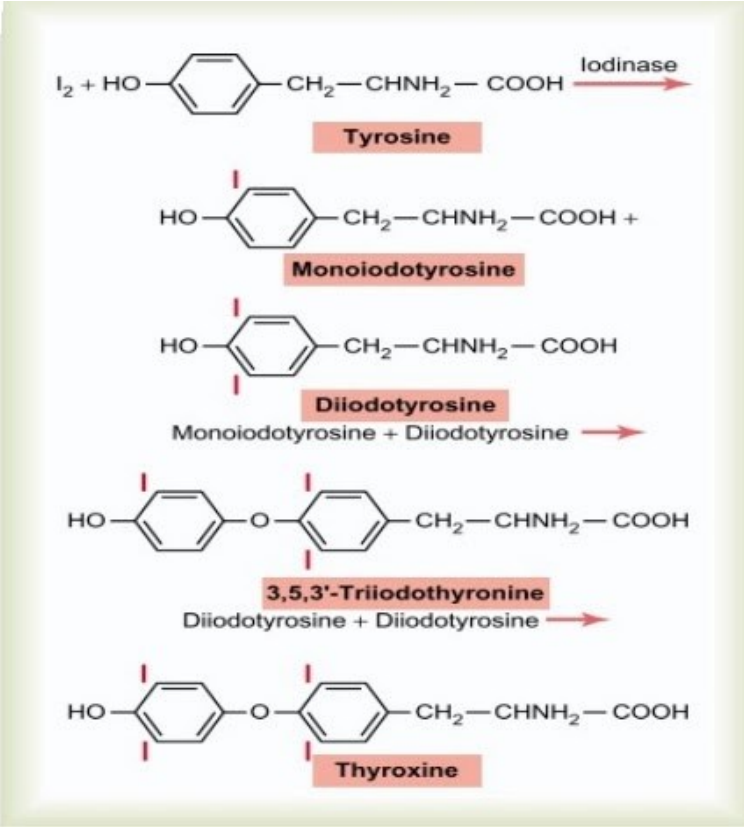

Figure 8: *Chemistry of thyroxine and triiodothyronine formation* (77).

The sodium (Na)/iodide symporter (NIS) is an integral plasma membrane glycoprotein localized at the basolateral plasma membrane of thyrocytes. (81) It is an adenosine triphosphate (ATP)-driven active transport protein that simultaneously transports Na^+ and I^- (in a 2:1 ratio) into the cytoplasm. This concentrates I^- against an electrochemical gradient and results in an intra- to extracellular I^- concentration ratio of up to 40:1 (82).

NIS activity is stimulated by thyrotropin-stimulating hormone (TSH) of pituitary origin and large anions such as thiocyanate (SCN^-) and perchlorate ($CLO^{4\ -}$) can inhibit the accumulation of iodide in the thyroid by competing with iodide.

In addition to thyroid follicular cells, NIS is expressed in several other tissues, including the salivary glands, gastric mucosa, and the lactating mammary gland, where it mediates active transport of iodide (83).

Before the iodization of tyrosine residues, there is an essential step which is the oxidation of iodide I^- to obtain an oxidized reactive species I+ and then its organification onto tyrosyl residues at their 3- and 5-phenyl ring positions within the colloid matrix. Both steps are catalyzed by thyroperoxidase (TPO) in the presence of hydrogen peroxide (H_2O_2), resulting in the formation of the biologically inactive MIT and DIT, TPO then further catalyzes the coupling of MIT and DIT by placing an ether bond between two phenyl rings, forming the active thyroid hormones T3 and T4, which are still attached to the thyroglobulin protein backbone.

TPO enzymatic activity is stimulated by TSH (84).

The iodothyronines (T3, T4, MIT, and DIT) remain stored within the thyroglobulin colloid reservoir until needed, then there is an uptake of thyroglobulin from the colloid into the follicular cell by endocytosis, the fusion of the thyroglobulin with a lysosome, and finally the proteolysis and release of T4, T3, DIT, and MIT which are secreted into the vasculature through the basolateral membrane by the active transmembrane monocarboxylate transporter 8 (MCT8) (85).

T4 and T3 are secreted by the thyroid in molar proportions as 17:1 (86). However, this direct thyroidal secretion accounts for only 20% (~ 6 µg) of the circulating T3, whereas the other 80% (~ 25 µg) is the result of peripheral conversion of T4 to T3 by 5′-deiodination of T4 (87).

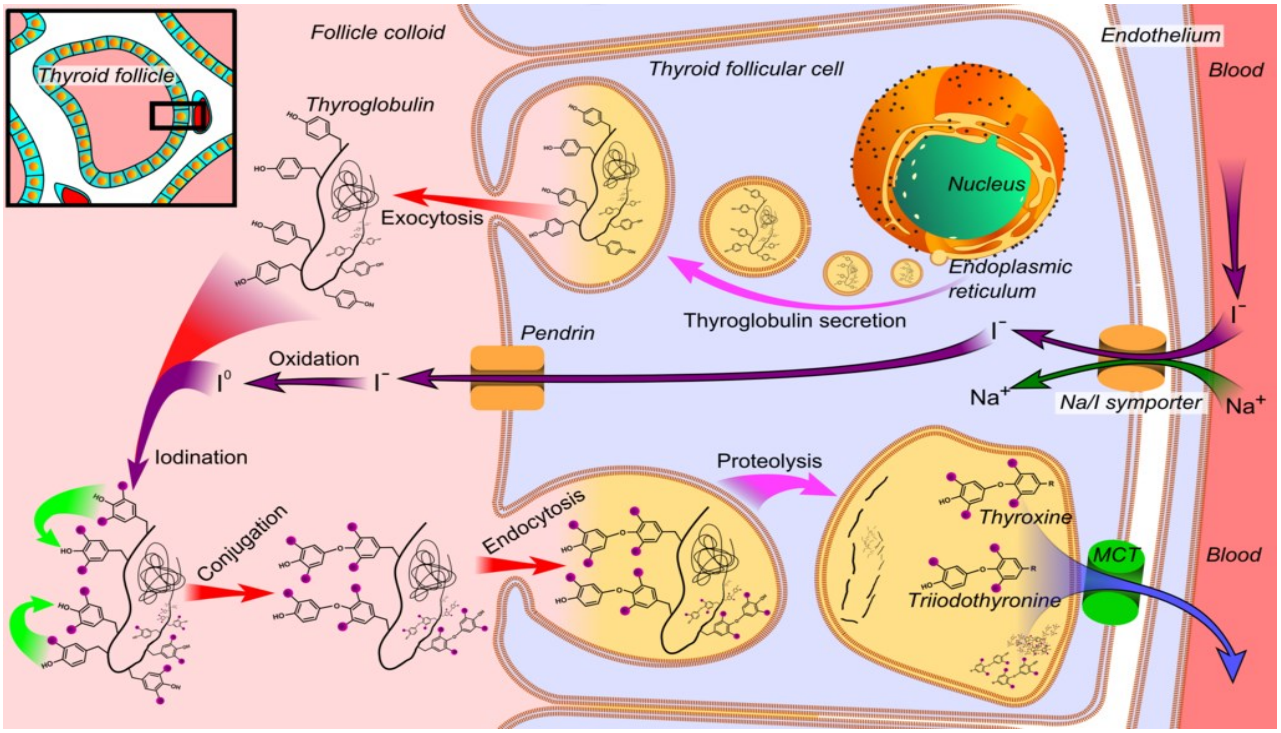

Figure 9: *Synthesis of thyroid hormones (89).*

4.4. Hyperthyroidism

Hyperthyroidism is characterized by increased thyroid hormone synthesis and secretion from the thyroid gland (88). It can either be due to a disorder of the thyroid gland, in which case it is called primary hyperthyroidism, or resulting from a pituitary disease in this case it is secondary hyperthyroidism (89).

Hyperthyroidism is a fairly common condition, with a prevalence rate of 2% in women and 0.2% in men in the general population. The annual incidence of hyperthyroidism in women is about 1 in 1000 in the general population. The incidence increases with age in both sexes.

The most common signs and symptoms of hyperthyroidism are: tiredness, heat intolerance, weight loss, palpitations, tremor, sweating, muscle weakness, loose bowel motions, anxiety, breathlessness, decreased exercise tolerance, and menstrual irregularities (90).

The most frequent causes of hyperthyroidism are:

- Graves' disease: GD as a thyroid autoimmunity is caused by stimulatory autoantibodies against the thyrotropin receptor (TSHR-Ab). These antibodies cause uncontrolled and continuous stimulation of the thyroid, leading to the excessive synthesis of the thyroid hormones and its hypertrophy. Measurements of serum TSH and free thyroxine (fT4) levels are essential for the evaluation of hyperthyroidism, and TSHR-Ab shows a high specificity of 99% and a sensitivity of 95% for confirmation of GD diagnosis (91).
- Toxic multinodular goitre: Multiple autonomous nodules secreting excess thyroid hormone.
- Toxic nodule: Single autonomous nodule secreting excess thyroid hormone (90).

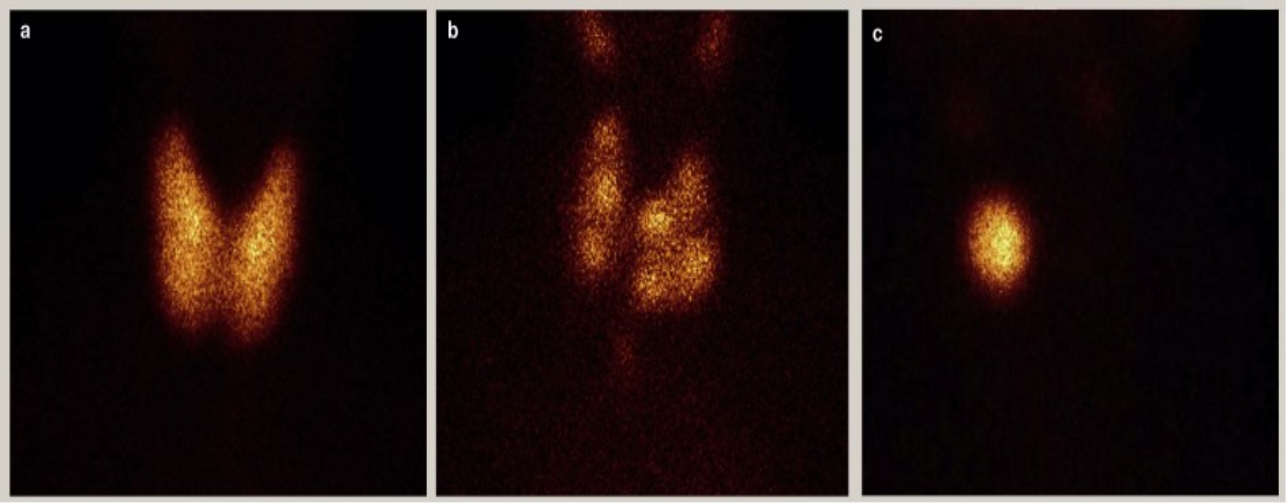

Figure 10: *99mTc-Pertechnetate scintigraphy of the thyroid gland. (a) Graves' disease. (b) Toxic multinodular goitre. (c) Toxic adenoma* (92).

4.5. Thyroid Carcinoma

Thyroid cancer is an abnormal, uncontrollable and permanent multiplication of thyroid cells, which ends up in the formation of a mass called a malignant tumor. It often occurs as a nodule; like all cancers, these harmful cells can migrate to other tissues and form other tumors; this is called a metastasis phase. This cancer can take many forms depending on the type of cells affected (93).

Thyroid cancer is rather rare, about 1% of all cancers combined. Nevertheless, it accounts for 88% of all cancers of the endocrine organs. Recently, the incidence of thyroid cancer has increased noticeably compared to other types of endocrine cancers.

The most common thyroid cancers (papillary and vesicular) are cured in about 90% of cases if the treatment is appropriate. Anaplastic and medullary cancers are rare and have a very unfavorable prognosis. Initial therapy for thyroid cancer is a total or near-total thyroidectomy (94).

Treatment with radioactive iodine is recommended in high-risk patients and requires a high thyroid-stimulating hormone (TSH) to be effective. Afterward, the patient must be placed on thyroid hormone replacement therapy for life.

a) Papillary Carcinoma:

Papillary carcinoma is the most common thyroid carcinoma since it accounts for 65 to 80% of thyroid cancers. It usually affects adults and young women. The histopathological diagnosis was originally based on microscopic detection of papillae. At the cytological level, the cells are more or less giant, and the nuclei are larger and wrinkled than those of normal cells.

b) Follicular Carcinoma:

Second in the frequency of occurrence is follicular carcinoma, which represents 20% of thyroid cancers. The diagnosis of follicular carcinoma isbased on the histopathological demonstration of infiltrative growth. There are two criteria:

1 true infiltration of the venous vessels outside the tumor capsule, and
2 fungus-like infiltration through the tumor capsule into the surrounding parenchyma.

c) Medullary (C-Cell) Carcinoma:

Characteristically the tumor is composed of solid nests and infiltrating formations of polygonal orspindle-shaped cells.

d) Anaplastic (Undifferentiated) Carcinoma:

Anaplastic carcinoma is mostly detected by the pathologist by fine-needle aspiration biopsy (FNAB) or tumor reduction specimen (95).

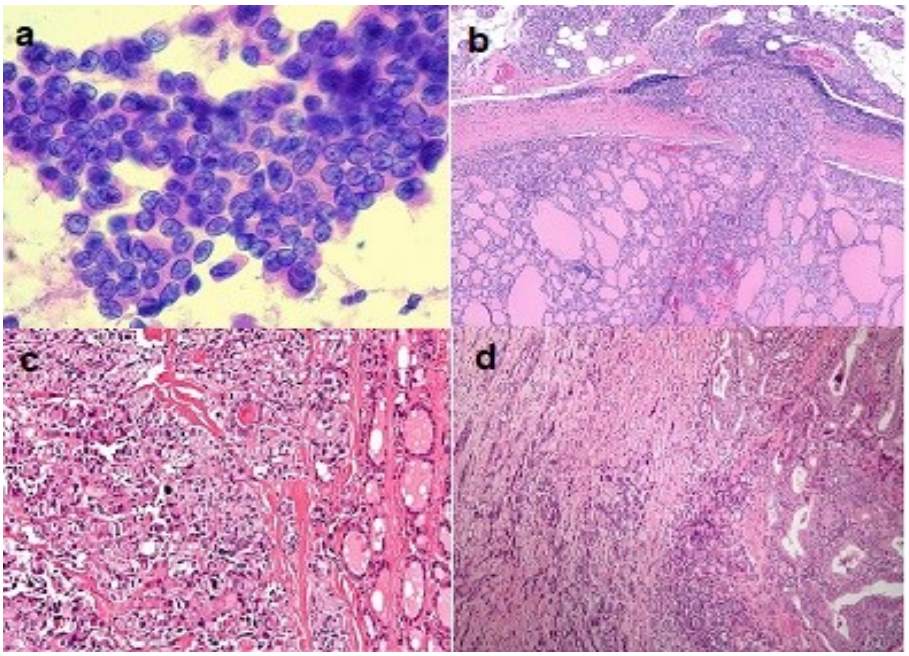

Figure 11: *Micrographs of the most common thyroid cancers (a) Papillary carcinoma. (b) Follicular carcinoma. (c) Medullary carcinoma. (d) Anaplastic carcinoma (97).*

5. Treatment with ^{131}I:

5.1. For hyperthyroidism:

Wherever possible, efforts should be made to obtain euthyroidism by pharmacological means. In case of failure or inability to continue medical treatment, radioactive iodine may be administered to treat hyperthyroidism.

The required activity depends on the cause of hyperthyroidism, thyroid size, thyroid fixation, and iodine clearance, it is generally between 200 and 800 MBq, but it may be necessary to repeat the treatment up to a maximum cumulative activity of 5000 MBq.

It is up to the clinician to decide which activity is best suited for the patient, this activity may be defined by fixed-dose protocols or may be calculated using the equation 1.3:

$$A\,(MBq) = \frac{Target\ dose\ (Gy) \times Target\ volume\ (ml)}{max.\ uptake\ I-131\% \times effictive\ T_{\frac{1}{2}}\ (days)} \times K \qquad \textbf{(1.3)}$$

With the following conditions:

- target dose: the target absorbed dose in the whole thyroid gland or in an adenoma.
- target volume: the volume of the whole thyroid gland.
- max. uptake I-131: the maximum uptake of ^{131}I in the thyroid gland or nodules in % of the administered activity as established in a test dose.
- effective T ½: the effective half-life of I-131 in the thyroid gland expressed in days.
- K is 24.67.

5.2. For Thyroid carcinoma:

Following partial or total thyroidectomy, the activity administered to remove residual thyroid tissue is between 1850 and 3700 MBq. This activity depends on the extent of the remaining tissue and its ability to fix ^{131}I. For further treatment of metastases, the administered activity ranges from 3700 to 11100 MBq (96).

5.3. NaI Capsule:

^{131}I-Sodium Iodide is an approved diagnostic and therapeutic agent for diseases of the thyroid. The dose depends on the application, either hyperthyroidism or thyroid carcinoma, it is supplied in either a capsule or a liquid form for oral administration with the most common being gelatin capsules. The first injection of ^{131}I-Sodium Iodide goes back to 1941, hence it was the first radiotherapeutic used in medicine. It became standard therapy as early as the beginning of the 1950s (97).

Capsules are prepared by evaporating an alcoholic solution of NCA ^{131}I-Sodium Iodide on the inner wall of a gelatin capsule. The activity remains firmly fixed, and capsules are convenient and safe to administer in both diagnostic and therapeutic dosages.

A capsule is preferred to a solution because it is safer from a radiation safety point.

Iodide (I) is oxidized to molecular iodine (I_2) due to the presence of air and free radicals (e.g.,$HO_2^{\bullet}$), which is potentially hazardous. To minimize air oxidation, sodium ascorbate or thiosulfate are added to the solution at alkaline pH, which is maintained between 7.5 and 9.0. A ^{131}I-NaI preparation has a shelf life of 4 weeks after calibration (98).

It should be noted that ^{131}I-Sodium Iodide can also be used in imaging to localize metastases associated with thyroid malignancies and for diagnosis of thyroid malfunction (hyperthyroidism, hypothyroidism). Doses for this purpose are in the range of 0.3–2 mCi (97).

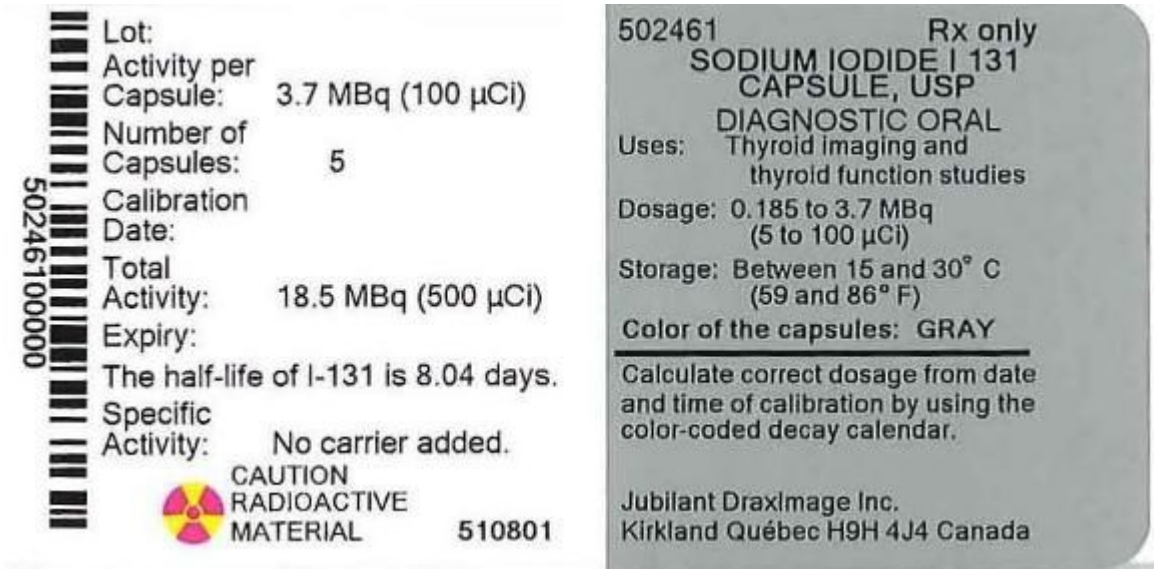

Figure 12: *Sodium Iodide I-131 diagnostic product label (101).*

5.3.1. Mode of administration:

The capsule is administered orally. It should be taken on an empty stomach and must be swallowed whole with a large amount of liquid to guarantee its transit through the stomach and the upper part of the small intestine (99).

The patients are encouraged to drink heavily for the first 24 hours, especially the patients taking high doses for the treatment of thyroid carcinoma to limit bladder irradiation by frequent urination (100).

To boost the passage of the capsule in the oesophagus and create in the stomach a favorable medium for its dissolution, it is recommended that the patient drink a warm drink quickly after ingestion of the capsule. It is also recommended to combine treatment with H2 antihistamines or proton pump inhibitors.

In the case of administration to a child, in particular to a young child, it should be ensured that the capsule can be swallowed whole, without being chewed. It is recommended to give it with crushed food (99).

5.3.2. Pharmacokinetics:

a) Absorption:

Following oral administration, 90% of the administered radioactivity of ^{131}I is systemically absorbed in the first 60 minutes (101).

Studies on the dissolution of the capsules have revealed that it occurs within 5 to 12 minutes and that radioactivity is distributed homogeneously over the gastric mucosa.

Studies of the various levels of radioactivity in the serum have shown that after a first rapid increase time, lasting between 10 and 20 minutes, equilibrium is reached after about 40 minutes. The same results are obtained after oral administration of sodium iodide (^{131}I) solution (102).

b) Distribution:

The circulating iodide is distributed in the extra-thyroid compartment, from which it is essentially fixed by the thyroid which captures about 20% of the iodide in a single passage or is eliminated by the renal route.

Thyroid iodide fixation reaches a maximum after 24-48 hours and 50% of the peak is reached after 5 hours. Fixation is influenced by several factors: the patient's age, the volume of the thyroid gland, renal clearance, plasma iodide concentration, and other medications (102).

c) Metabolism:

Iodide fixed by the thyroid gland follows the known metabolism of thyroid hormones and is incorporated into the organic substances from which thyroid hormones are synthesized. Thyroid-bound iodide enters the known metabolic pathway of thyroid hormones and is incorporated into the organic substances used in the synthesis of thyroid hormones (103).

d) Elimination:

^{131}I is excreted in urine and feces. The normal range of urinary excretion is 37% to 75% of the administered dose, varying with the thyroid and renal function of the patient. Fecal excretion is about 10% (101).

5.3.3. Protocol of use:

Follow these steps to administer the product to the patient.

Step 1: Check the calibration activity and date on the shielded container label.

Step 2: Immediately before calibration or administration, unscrew the cap counter-clockwise.

Step 3: Remove the entire cap.

Step 4: Place the applicator at the opening of the shielded container. Turn clockwise until you feel a slight resistance.

The container containing the capsule is now attached to the applicator.

Step 5: Confirm the activity of the capsule by placing the applicator in a calibrated ionization chamber.

Step 6: Replace the capsule in the shielded container by repeating the previous steps in the opposite direction

Step 7: When the patient is ready for administration repeat steps 2, 3, and 4.

Step 8: Ask the patient to remove the plastic cap at the striated end of the applicator by lifting it up.

Step 9: The patient can now swallow the capsule by carrying the ridged end of the applicator to his mouth and gently tilting the applicator so that the capsule slides along the applicator and falls freely into his mouth.

Step 10: The patient will take a warm drink before or with the capsule (be sure not to chew the capsule) followed by another warm drink after swallowing (104).

Chapter Two: Radioactivity and Dosimetry

1. Fundamentals of nuclear medicine dosimetry:

Nuclear medicine and specifically radiation therapy is a state-of-the-art discipline that has revolutionized patient care (105), it is based on the interaction of radiation with matter; however, the energy deposition of these radiations must be quantified, thoroughly studied, and analyzed to get the desired results without causing any unnecessary side effects, hence the importance of dosimetry in radioprotection (106).

2. Radioactivity:

2.1. Definition:

Radioactivity (radioactive decay or nuclear decay), is the process of the spontaneous decay and disintegration of unstable nuclei through which they emit radiation and nuclear entities in order to reach more stable energy levels. These emissions include alpha particles, beta particles, and gamma particles (107,108).

There are two types of radioactivity: natural and artificial activity. Whenever a nucleus disintegrates spontaneously, it is natural decay.

When stable isotopes are bombarded with particles such as neutrons, artificial decay occurs (109).

2.2. Radioactive decay:

Even though the phenomenon of disintegration is random and unpredictable; the statistical evolution of a population of nuclei corresponds to a well-defined law of probability.

Any decay process is subject to the same basic law.

The rate of decay (number of disintegrations per unit time) is proportional to N.

$$dN / dt \propto -\lambda N \qquad \textbf{(2.1)}$$

The negative sign signifies that N is decreasing with time. N is the number of radioactive nuclei in the sample.

λ is called the decay constant, it is the probability per unit time that a given radioactive nucleus will decay (110).

2.2.1. Law of radioactive decay:

Let N_0 be the number of all identical radioactive nuclei initially present in the sample.

After a time (t), the core population has declined.

Let N(t) be the number of all identical radioactive nuclei present in the sample at time (t).

The mean number of disintegration (variation of population ΔN) is proportional to the existing population N(t) and the duration of measure Δt as illustrated in equation 2.2:

$$\Delta N = -\lambda N(t)\Delta t \qquad \textbf{(2.2)}$$

If the duration Δt tends to 0, equation 2.1 is simplified and gives the differential equation 2.3:

$$\frac{dN(t)}{dt} = -\lambda N(t) \qquad \textbf{(2.3)}$$

with λ in s^{-1}.

The solution of this differential equation gives the law of radioactive decay in equation 2.4 (111):

$$N(t) = N_0 e^{-\lambda t} \qquad \textbf{(2.4)}$$

2.2.2. Half-lives:

They are characteristic properties of the various unstable atomic nuclei and the particular way in which they decay (112). There are three half-lives that are important when considering the use of radioactive drugs for both diagnostic and therapeutic purposes (99).

a) Physical half-life:

The physical half-life of a radionuclide ($T_{1/2}p$) is the time in which the amount of radioactivity decreases to one-half of its original value. This value does not depend on the moment chosen: the amount of time taken for the nuclei to halve will always be the same (113,114).

b) Biological half-life:

If a radioisotope is ingested or taken in through different pathways, it will gradually be removed from the body via various elimination routes. This means that a radioactive atom can be excreted before it has had the chance to decay. The time elapsed before half of a compound has been removed by biological means is called the biological half-life and is usually denoted ($T_{1/2}b$) (115,116).

c) Effective half-life:

The time required for the activity of a particular radioisotope deposited in a living organism, such as a human or an animal, to be reduced by half as a result of the combined action of radioactive decay and biological elimination (117). An effective half-life of the radioactive substance will involve a decay constant that represents the sum of the biological and radioactive decay constants, as in the formula (2.5):

$$\lambda_e = \lambda_p + \lambda_b \qquad \textbf{(2.5)}$$

Or in terms of half-lives, we get the equation 2.6 and 2.7:

$$\frac{1}{T_{\frac{1}{2}}e} = \frac{1}{T_{\frac{1}{2}}p} + \frac{1}{T_{\frac{1}{2}}b} \qquad \textbf{(2.6)}$$

$$T_{\frac{1}{2}}e = \frac{T_{\frac{1}{2}}p \times T_{\frac{1}{2}}b}{T_{\frac{1}{2}}p + T_{\frac{1}{2}}b} c \qquad \textbf{(2.7)}$$

As a result, the biological mechanisms always decrease the overall dose from internal contamination.

Moreover, if $T_{1/2}p$ is large in comparison to $T_{1/2}b$, the effective half-life is approximately the same as $T_{1/2}b$. On the other hand, radionuclides with very short radioactive half-lives have also very short effective half-lives (118).

2.3. Types of radiation:

Radiation is classified into two main categories: non-ionizing and ionizing radiation, depending on its ability to ionize matter.

The energy of non-ionizing radiation is enough to move atoms in a molecule around or cause them to vibrate, but not enough to remove electrons from atoms because it is lower than the ionization potential of these atoms. Examples of this type of radiation are radio waves, visible light, and microwaves. On the other hand, ionizing radiation has so much energy it can snatch electrons out of atoms, a process known as ionization, which can be either direct or indirect (119,120).

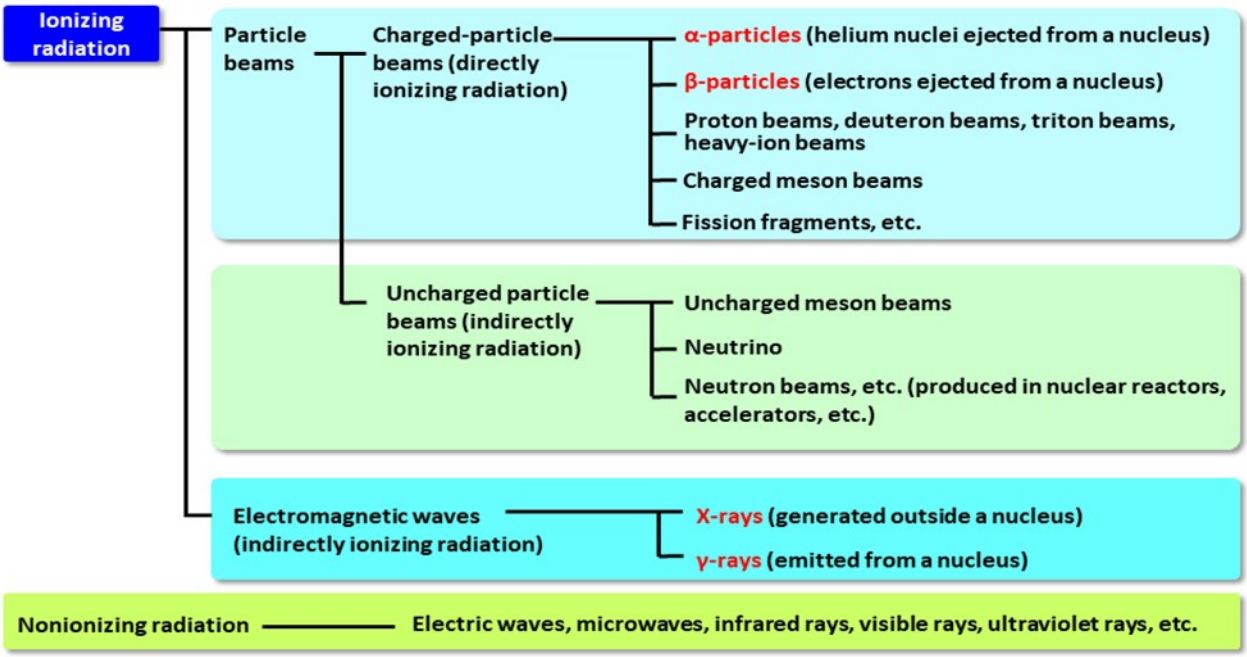

Figure 13 : *Types of radiation* (121).

2.2.3. Directly ionizing radiation:

- Alpha (α) particles:

In alpha decay, the parent atom ${}^{A}_{Z}P$ emits an alpha particle α and results in a daughter nuclide. The alpha ${}^{A-4}_{Z-2}D$ decay process is described by equation 2.8

$$ {}^{A}_{Z}P \rightarrow {}^{A-4}_{Z-2}D + {}^{4}_{2}\alpha \rightarrow {}^{A-4}_{A-2}D + {}^{4}_{2}He \qquad \textbf{(2.8)} $$

The process of alpha decay is encountered mainly in proton-rich, high atomic number nuclides since electrostatic repulsive forces increase more rapidly in heavy nuclides than the cohesive nuclear force (122).

Alpha decay is observed for the elements heavier than lead and a few nuclei as light as the lanthanide elements (123).

Due to their large mass and positive charge, alpha particles cannot go very far through the air or get very deep into a solid. Alpha particles only affect surfaces, so alpha decay is rarely used in external medical radiation therapy (124). However, if they are taken internally, they are very toxic because of the large amount of energy released in a short distance within living tissue. This property can be used for killing cancer cells in such processes as alpha-immunotherapy (122).

- Beta (β) particles:

Beta decay is the spontaneous emission of an electron or a positron.

The β^- decay is possible in neutron-rich nucleons if the energy difference between the initial and final states exceeds $2m_ec^2$, where m_e is the mass of electron and c is the speed of light.

A neutron converts to a proton and the electron is emitted with the creation of an antineutrino according to the reaction 2.9

$$ {}^{1}_{0}n \rightarrow {}^{1}_{1}p + {}^{0}_{-1}e + {}^{0}_{0}\bar{\nu} \qquad \textbf{(2.9)} $$

The β^+ decay is possible in proton-rich nucleons if the energy difference between the initial and final states exceeds $2m_ec^2$.

A proton converts to a neutron and the positron is emitted with the creation of a neutrino according to the reaction 2.10 (125):

$$ {}^{1}_{1}p \rightarrow {}^{1}_{0}n + {}^{0}_{+1}e + {}^{0}_{0}\nu \qquad \textbf{(2.10)} $$

Elements that have beta decay can have useful medical applications such as radionuclide therapy or radiotherapy in cancer treatment. ^{131}I is a good example of this kind of therapy (126).

In both alpha and beta decay, the same amount of energy is released in every individual decay of a particular radionuclide. In the alpha decay of a particular radionuclide, every emitted alpha particle has the same kinetic energy. However, in beta decay, the disintegration energy is shared, in varying proportions, between the emitted electron/positron and antineutrino/neutrino all the while the sum of the energies of each pair is always constant. That's the reason why alpha emission has a discrete spectrum while beta decay gives a continuous spectrum (127).

2.2.4. Indirectly ionizing radiation:

- Gamma ray:

When a heavy nucleus disintegrates by either α-decay, β-decay, or by fission, the daughter nucleus is sometimes produced in an excited state. If this state is below the excitation energy for fission, it will de-excite, usually, by emitting a high-energy photon, it may emit one or more photons of discrete energies (128).

The emission of gamma rays does not alter the number of protons or neutrons in the nucleus but instead has the effect of converting the nucleus from a higher to a lower energy state (unstable to stable) (129).

Gamma rays are a radiation hazard for the entire body. They can easily penetrate barriers that can stop alpha and beta particles, such as skin and clothing (130). Gamma rays have so much penetrating power that several inches of a dense material like lead, or even a few feet of concrete may be required to stop them. Gamma rays can pass completely through the human body; as they pass through, they can cause ionizations that damage tissue and DNA (119).

2.4. Interaction between ionizing radiation and matter:

2.4.1. Photon interactions:

a) Photoelectric effect:

Light can be used to push electrons, freeing them from the surface of a solid. This can be explained by the photoelectric effect.

The photoelectric effect (photoelectric emission or photoemission) describes the process in which an incident photon interacts with a bound atomic electron. A material that can exhibit this phenomenon is said to be photoemissive, and the ejected electrons are called photoelectrons, but there is nothing that would distinguish them from other electrons (131).

The photon must have sufficient energy to overcome the binding energy of the electron, The latter is displaced from its orbit while the photon is completely absorbed, all excess energy is transferred to kinetic energy of the ejected electron (132).

It was observed that only certain frequencies of light can cause the ejection of electrons. If the frequency of the incident photon is too low, then no electrons were ejected even if the intensity of the light was very high or it was applied onto the surface for a long time. On the other hand, at a higher frequency, electrons get ejected from the surface even if the intensity of the light was very low or it was applied for only a short time. This minimum frequency needed to cause electron ejection is referred to as the threshold frequency (133).

The photoelectric effect is especially important for gamma rays of low energy (<0.2 MeV). It involves the inelastic collision of a photon and an electron in which all the energy of the photon is transferred to the electron (134). When the electron leaves its orbit, it results in a vacancy in the electron shell. Other electrons cascading down from outer orbital shells fill the vacancy left by this electron (132).

During the cascade process, characteristic X-rays are emitted. The energy of these X-ray photons may also be transferred to an atomic electron, which may be ejected as an Auger electron.

The photoelectric effect dominates interaction processes at low photon energies (up to ~50 keV in water or human tissues) (132).

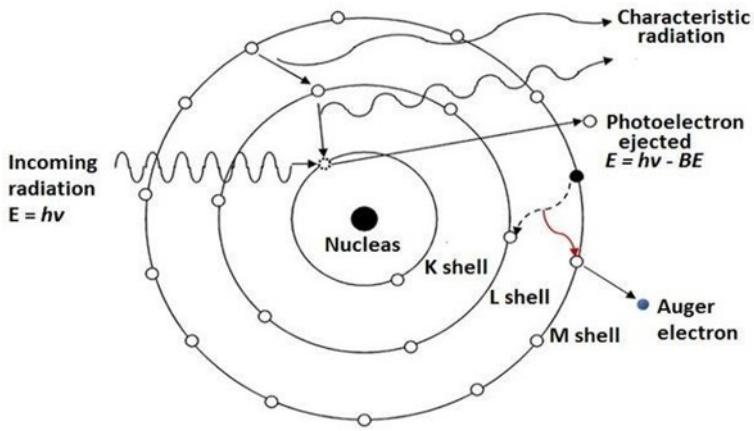

Figure 14 : *Photoelectric effect (135).*

b) Compton effect:

The Compton effect (also called Compton scattering or incoherent scattering) is the result of a high-energy photon colliding with a target, which releases loosely bound electrons from the outer shell of the atom or molecule (136).

The incident photon has energy and linear momentum. A fraction of the energy and momentum are transferred to the charged particle (recoil electron) and since the total energy and linear momentum must be conserved, the photon moves off with reduced energy and a change of momentum. As a result, the incident gamma-ray photon is deflected through an angle ϕ with respect to its original direction (136,137).

The transferred energy can vary from zero to a large fraction of the incident gamma-ray energy because all scattering angles are possible.

Compton scattering dominates at intermediate energies.

Photons undergo a wavelength shift called the Compton shift (138).

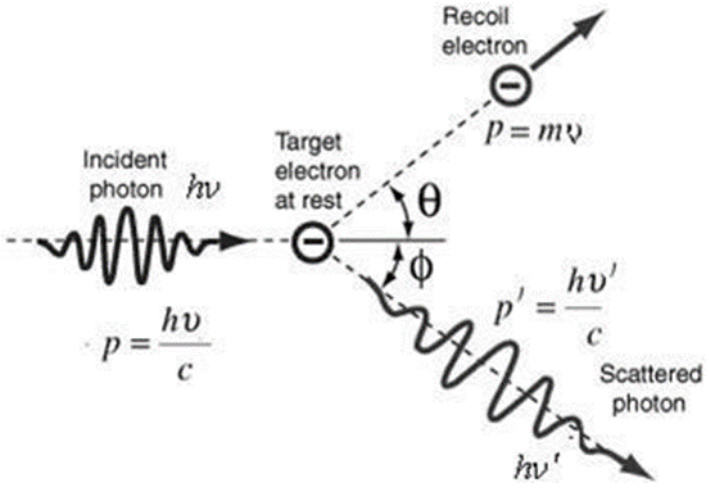

Figure 15 : *Compton effect (139).*

c) Pair production:

It is a process whereby a photon disappears, producing an electron and a positron. It occurs only in a field of a Coulombic force, either in the field of a nucleus or in the field of an electron (140). The photon is totally absorbed and its energy is used to produce an electron-positron pair.

The energy threshold for pair production in a nuclear field is $2m_ec^2 = 1.022$ MeV.

The energy threshold for pair production in an electron field, also called triplet production because the host electron also acquires significant kinetic energy due to the conservation of momentum, is $4m_ec^2 = 2.044$ MeV.

For energies larger than the threshold energy, the excess energy is divided between the electron-positron pair. As the positron is an anti-particle, it will recombine with an electron and two annihilation photons will be produced (141).

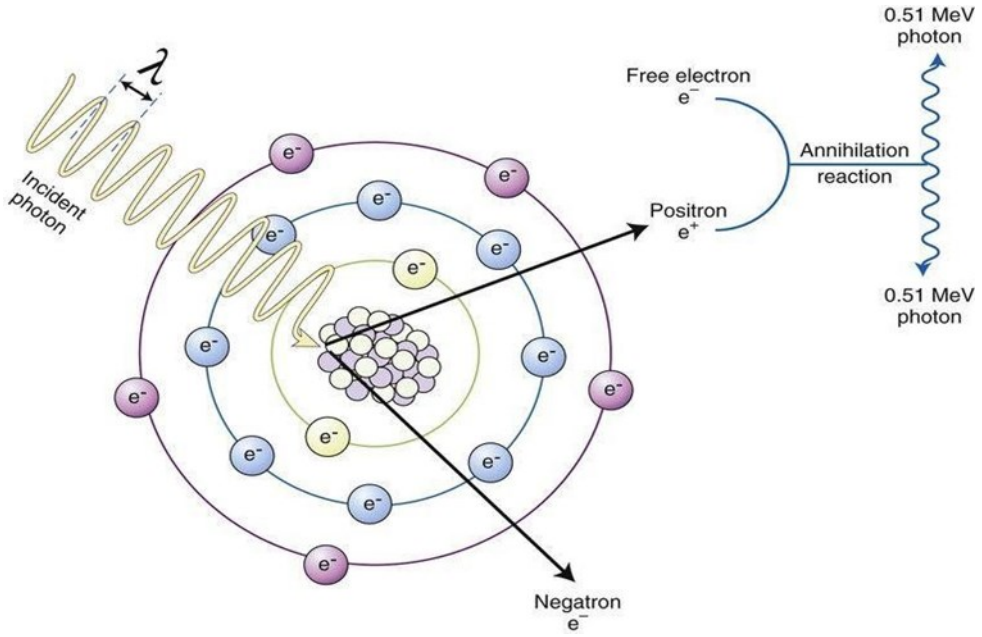

Figure 16 : *Pair production (142).*

2.4.2. Electron interactions:

When an electron hits a material, different interactions can occur. For systemization, the interactions are classified into two different types, namely elastic and inelastic interactions (143).

a) Elastic Interactions:

In this case, no energy is transferred from the electron to the sample. As a result, the electron leaving the sample still has its original energy E_0: $E_{el} = E_0$ (143).

Elastic collisions with the nucleus result in scattering of the electron with no loss of energy. The amount of scattering that occurs is dependent on the atomic number of the nucleus; higher atomic numbers cause more scattering.

Elastic collisions with the orbital electrons of an atom, also lead to scattering of the incident electron but no transfer of energy (144).

b) Inelastic Interactions:

If energy is transferred from the incident electrons to the sample, then the electron energy of the electron after interaction with the sample is consequently reduced: $E_{el} < E_0$ (143).

Inelastic collisions with orbital electrons result in loss of energy from the incident electron to the orbital electron. If this energy is sufficient for the electron to ascend to a higher shell it is known as excitation. The space in the lower shell is rapidly filled by another orbital electron, which releases a photon. This photon may generate characteristic X-rays if the binding energy of the shell is sufficiently large (seen with heavier elements such as lead or tungsten), or visible light for less tightly bound electrons.

If sufficient energy is transferred to an orbital electron, it may be able to escape the atom, leaving the atom ionized. This atom is often highly reactive and quickly reacts with a neighboring atom to achieve a stable state. The freed electron may cause further ionizations before it loses its energy and is captured by an atom.

Inelastic collisions with the nucleus result in bremsstrahlung. Bremsstrahlung is German for "braking radiation". As the electron interacts with the nucleus, it slows down and changes direction. The energy that is lost by the electron is released as a photon (144).

2.5. Biological effects of radiation:

Whether the source of radiation is natural or man-made, be it a small or a large dose of radiation, there will be some radiation damages resulting in biological effects (145).

Radiation damage to the cell can be caused either by the direct or indirect action of radiation on the DNA molecules.

In direct action, the radiation hits the DNA molecule directly, disturbing the molecular structure. Such structural change leads to cell damage or even cell death. Damaged cells that survive may later induce carcinogenesis or other abnormalities.

In the indirect action, the radiation hits the water molecules and other organic molecules in the cell, whereby free radicals such as hydroxyl ($HO^{\bullet}$) and alkoxy ($RO_2^{\bullet}$) are produced.

Free radicals are characterized by an unpaired electron in the structure, which is very reactive and therefore reacts with DNA molecules to cause molecular structural damage.

Hydrogen peroxide, H_2O_2, is also toxic to the DNA molecule.

The result of indirect action of radiation on DNA molecules is the impairment of function or death of the cell (146).

The biological effects of radiation can be grouped into two broad categories according to how the responses relate to dose:

2.5.1. Deterministic effects:

One of the characteristics of the deterministic effects is the existence of the threshold dose below which no detectable clinical effects occur, but exposure to radiation above this level causes effects with a severity that increases with radiation dose (147).

Deterministic effects are short-term, adverse tissue reactions resulting from a dose that is significantly high enough to damage living tissues.

This type of effect is predictable and reproducible (148).

2.5.2. Stochastic effects:

Effects that occur by chance, generally without a threshold level of dose; These effects have an increase probability of occurrence with increase dose and their severity does not depend on magnitude of absorbed doses (149,150).

Stochastic effects are of two types:

a) Somatic stochastic effect

These effects of radiation are limited to exposed individuals and they are distinguished from genetic effect. The exposed individuals suffer from these effects during their lifetime.

b) Genetic effect

The ionizing radiation damage the genetic material in reproductive cells and as a result these effects are transmitted from generation to generation. Radiation induced aberrations to an individual gene and DNA can contribute to the birth of defective descendants (150).

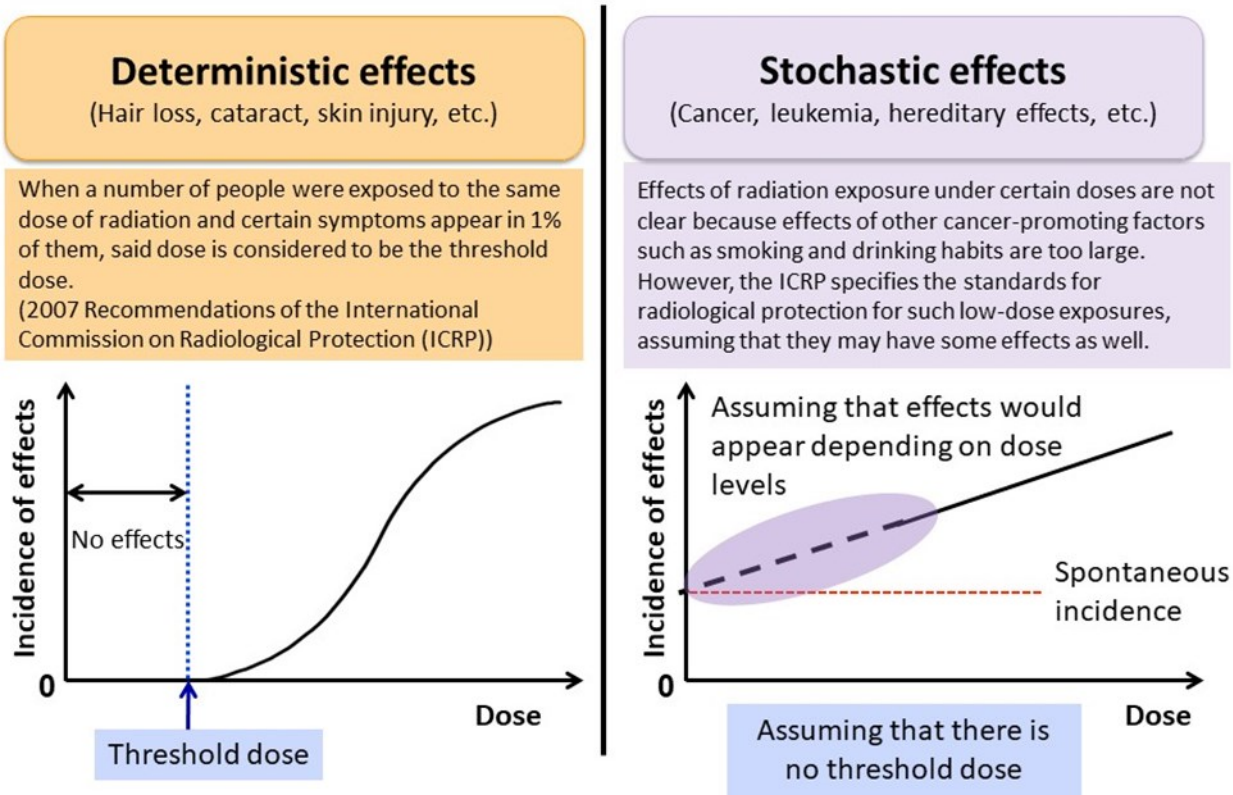

Figure 17 : *Deterministic and stochastic effects. (147)*

3. Dosimetry:

Accurate measurements are important in physics and when it comes to medical treatment for diseases, it is certainly necessary to be precise. In this regard, ionizing radiation requires the utmost care in ensuring that it is accurately measured. Otherwise, too much radiation can be harmful for cancer patients, medical personnel or even the patient's family members (151).

3.1. External dosimetry:

External dosimetry is the application of principles and techniques involved in the measurement and documentation of personnel dose from external sources of radiation, such as exposure from gamma rays and beta particles (152). Since photons and beta particles interact through electromagnetic forces, their detection methods and dosimetry are substantially different from that of neutrons that interact through nuclear forces (153).

The objective of external dosimetry is the detailed assessment of personnel exposure to radiation outside the body (152).

One of the key parts of external radiation dosimetry is personal dosimetry. It is used primarily to determine doses for individuals who are exposed to radiation related to their work activities. These doses are usually measured by devices known as dosimeters. Dosimeters usually record the dose. A personal dosimeter is a dosimeter that is worn at the surface of the body by the person being monitored, and it records the radiation dose received. Personal dosimetry techniques vary and depend partly on whether the source of radiation is outside the body (external) or taken into the body (internal).

Personal dosimeters are used to measure external radiation exposures (153).

Figure 18 *: Personal dosimeter (Polimaster) (154).*

3.2. Internal radiation dosimetry

Obviously, to calculate the radiation dose, one should know the meaning of radiation dose and radiation dose rate and their units of measurement as well as the protection quantities.

3.2.1. Absorbed dose:

The absorbed dose is the amount of energy deposited by ionizing radiation in a mass of tissue or an organ (155). The absorbed dose describes the intensity of the energy deposited in any small amount of tissue located anywhere in the body, and is used to assess the potential for damage to a particular organ or tissue. It is expressed in units of joule per kilogram (J/kg) and called "gray" (Gy), thus replacing the units of "rad" (short for "radiation absorbed dose"). One hundred rad equals 1 Gy (156).

The formula for the absorbed dose is given by equation (2.11) (155).

$$D_T = \frac{\Delta ED}{\Delta m}\left[\frac{J}{kg}\right] \qquad \textbf{(2.11)}$$

3.2.2. Radiation dose rate:

Radiation dose rate is defined as the amount of energy absorbed per unit time per unit of mass of tissue, as illustrated in equation 2.12.

Its unit may be expressed in various ways, such as mGy per minute, cGy (rad) per hour, or Gy per day.

$$\dot{D} = \frac{\Delta D}{\Delta t}\left[\frac{J}{kg.sec}\right] \qquad \textbf{(2.12)}$$

Since the amount of radiation exposure depends directly on the time people spend near the source of radiation, the absorbed dose is equal to the strength of the radiation field (dose rate) multiplied by the length of time spent in that field.

The absorbed dose is a measure of the actual energy deposited in the irradiated tissue and can be used to compare against deterministic effects, but it is not suitable for comparing the stochastic radiological risk. To estimate the stochastic risk, the type of radiation and the sensitivity of the irradiated tissues must be considered. The equivalent dose and effective dose were created to calculate the biological effect of an absorbed dose (156).

3.2.3. Equivalent dose

The equivalent dose (H_T) is a quantity that considers the relative biologic damage caused by radiation interacting with a distinct tissue or organ. Tissue damage depends on the type and energy of the radiation, and how exactly the radiation deposits its energy in the tissue (157). Thus, radiation that has a high LET is more damaging to tissue than radiation with low LET.

The relative biologic effectiveness of various types of radiation is called the radiation weighting factor (W_R).

For instance, deposition of 1 Gy of high-energy protons causes five times as much damage as 1 Gy of X-ray photons.

To account for this difference, the equivalent dose is computed as the product of the absorbed dose (D_T) averaged over a tissue or organ and the W_R as shown in equation (2.12) (158):

$$H_T = \sum W_R \times D_{T,R} \qquad \textbf{(2.12)}$$

The W_R is the radiation weighting factor for radiation (R) and $D_{T,R}$ is the mean absorbed dose in organ or tissue (T) from radiation (R).

The unit for the equivalent dose is the Sievert (Sv) and the dimensions are the same as the gray, joules per kilogram whereas, the traditional unit of equivalent dose is the rem (roentgen equivalent man); 1 Sv equals 100 rem (159).

Type and Energy Range	Radiation Weighting Factors
X and Gamma rays	1
Electrons	1
Neutrons (energy dependent)	5 – 20
Protons	5
Alpha Particles	20

Table 1 : *Radiation Weighting Factors [Summarized from ICRP (1991)] (160).*

For radiations of interest in nuclear medicine γ-rays, X-rays, electrons, and positrons, the radiation weighting factor is equal to 1. Therefore, the equivalent dose or dose equivalent in Sv (or rem) is numerically equal to the absorbed dose in Gy (or rads) (157).

3.2.4. Effective dose

Since body tissues react differently to radiation and cancer induction occurs at a different rate of dose in different tissues, which illustrates perfectly the characteristic of radio-sensitivity of tissues and organs, equivalent doses are not adequate to represent overall exposure, thus, in order to obtain an indication of how exposure can affect the human body, the equivalent dose is multiplied by a tissue weighting factor (W_T) related to the risk for a particular tissue or organ. The result is the effective dose absorbed by the body. This parameter is given by the expression (2.13):

$$E = \sum_T W_T \sum_R W_R D_{T,R} \quad \text{or} \quad E = \sum_T W_T H_T \qquad \textbf{(2.13)}$$

The unit used for effective dose is the same as for the equivalent dose: sievert (161).

ICRP has created the effective dose to provide a dose quantity related to the probability of health detriment due to stochastic effects from exposure to low doses of ionizing radiation (162); it has also proposed the tissue weighting factors which are derived from epidemiological evidence

This quantity can be related to the increases in cancer and hereditary effects for standard persons (163).

The following tissue weighting factors have been proposed by the ICRP:

Organ or tissue	*W_T ICRP 30 (1979)* [a]	*WT ICRP 30 (1991)*	*W_T ICRP 103 (2007)*
Gonads	0.25	0.20	0.08
Red bone marrow	0.12	0.12	0.12
Large intestine		0.12	0.12
Lung	0.12	0.12	0.12
Stomach		0.12	0.12
Bladder		0.05	0.04
Breast	0.15	0.05	0.12
Liver		0.05	0.04
Oesophagus		0.05	0.04
Thyroid	0.03	0.05	0.04
Skin		0.01	0.01
Bone surface	0.03	0.01	0.01
Rest [b]	0.30	0.05	0.12
Brain			0.01
Total	1.00	1.00	1.00

[a] ICRP 30 W_T are used to calculate EDE, whereas ICRP 60 W_T and ICRP 103 W_T give E values.
b 'Rest' includes adrenals, small intestine, kidney, muscle, brain (except ICRP 103 W_T), pancreas, spleen, thymus and uterus.

Table 2 : *Tissue Weighting Factors (164).*

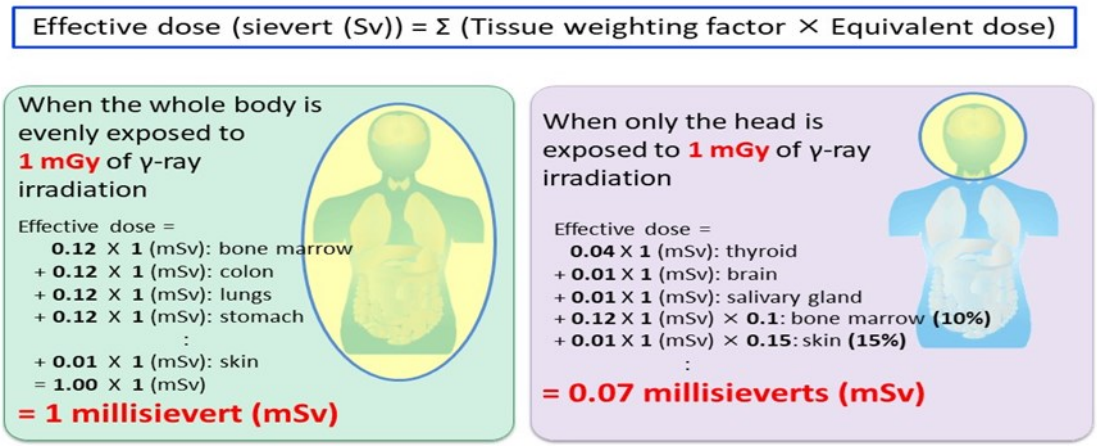

Figure 19 : *Difference between equivalent and effective dose (165).*

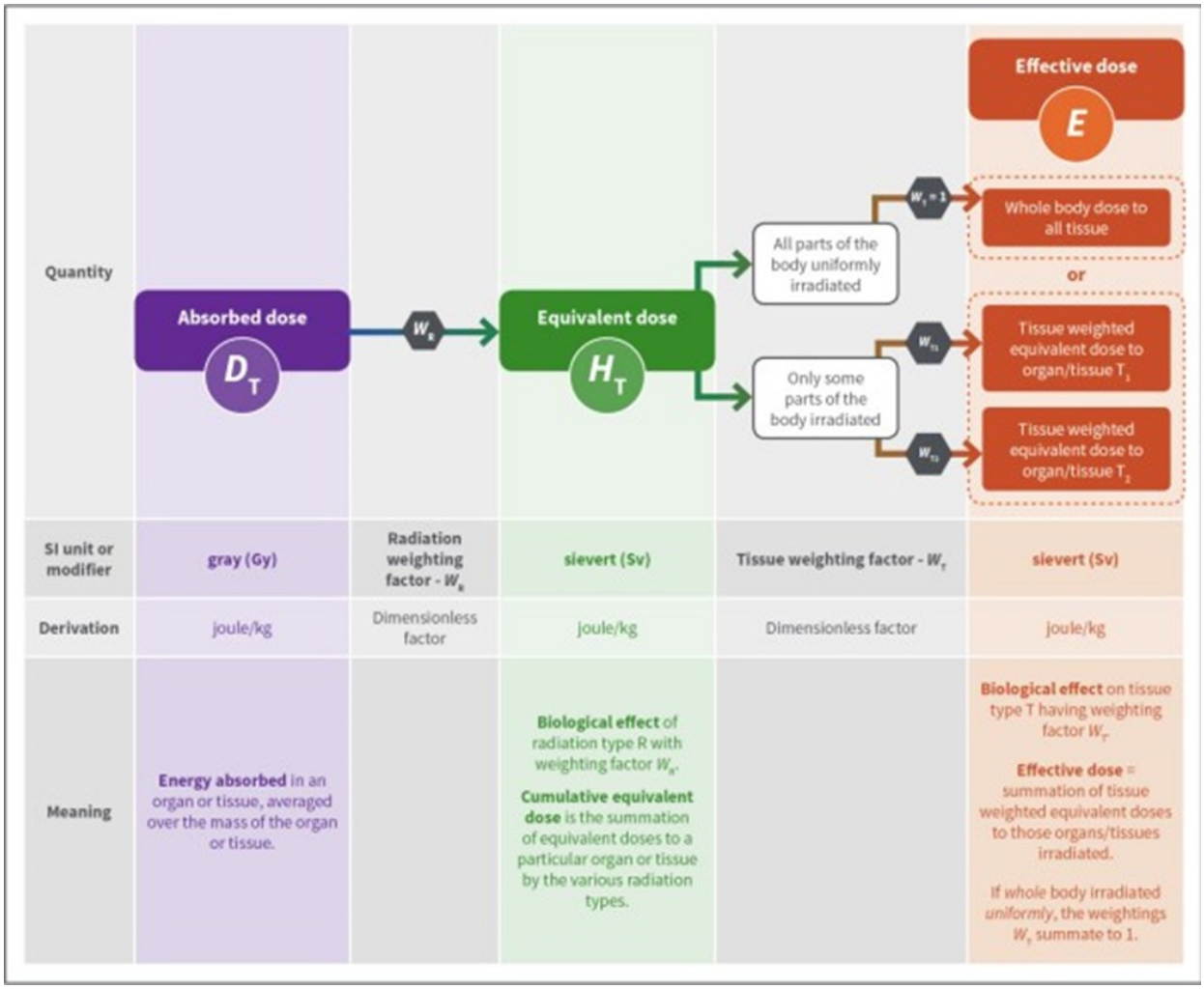

Figure 20 : *Absorbed dose, equivalent dose and effective dose (166).*

3.2.5. Linear energy transfer:

It is a measure of the linear rate at which radiation is absorbed in the absorbing medium by the secondary particles and is defined by the International Commission on Radiation Units and Measurements (ICRU) in expression 2.14:

$$LET = \frac{dE}{dl} \qquad \textbf{(2.14)}$$

Where dE is the average energy locally imparted to the medium by a charged particle of specified energy in traversing a distance dl.

The unit usually employed for LET is kiloelectronvolt per micrometre (keV/µm) (167).

According to the density of ionization produced in the absorber there are two distinct categories of ionizing radiation:

Low LET (also referred to as sparsely ionizing) radiation for example: beta particles and photons.

High LET (also referred to as densely ionizing) radiation for example: alpha particles (168).

3.2.6. Source and target organs:

Source organ is the organ with a significant uptake of isotope whereby the radiopharmaceutical in question may reside for an extended period of time.

Target organ is the organ of interest receiving absorbed radiation during dosimetric calculation (169).

Self-absorbed dose: refers to when the source and target regions are identical and it commonly gives the largest fractional contribution to the total absorbed dose in a target region.

Cross-absorbed dose: refers to when source and the target regions are different (167).

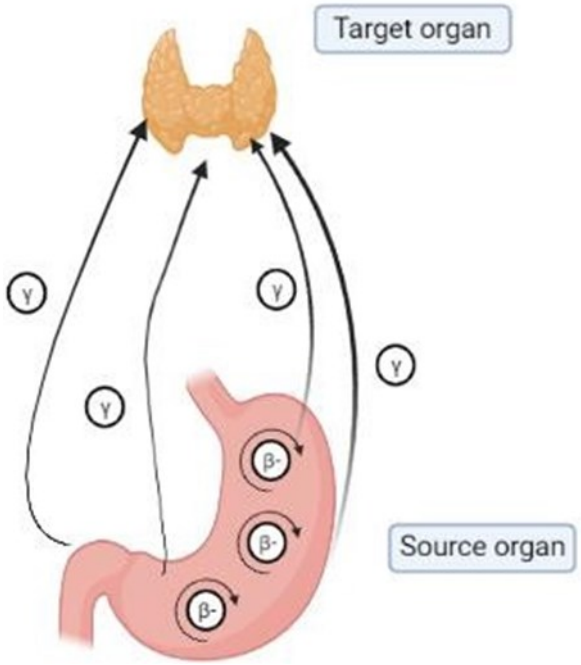

Figure 21 : *Source and target organs. (Created with BioRender).*

3.2.7. Absorbed fraction:

The absorbed fraction ϕ_i represents the fraction of the energy emitted by the radionuclide in the source organ that is deposited in the target tissue for which the absorbed dose is being calculated. The absorbed dose must be measured for each of the radiation emitted by the radionuclide since the absorbed fraction is a function both of the energy and the type of radiation (170).

The absorbed fraction ϕ_i for the i_{th} type of radiation is expressed by:

$$\phi_i = \frac{\text{energy deposited in the target tissue by the } i_{th} \text{type of radiation emitted by the radionuclide in the source tissue}}{energy\ of\ the\ ith\ type\ of\ radiation\ emitted\ by\ the\ radionuclide\ in\ the\ source\ tissue}$$

If 95% or more of the energy associated with a given radiation of a radionuclide is absorbed within the tissue in which it originates, then the radiation is called nonpenetrating. Here, the absorbed fraction is conventionally taken as unity since almost the total energy emitted by the

radionuclide in the source tissue is absorbed in the target tissue. Such is the case of electrons and alpha particles; they are absorbed almost entirely in the region where they originated.

If the source tissue is not identical to the target tissue, then the absorbed fraction of nonpenetrating radiation is taken as zero (170).

Unlike alpha particles and electrons, photons do not have a fixed range in tissue. They are a form of penetrating radiation; As a result, there are many probabilities for the deposition of energy at any location in the body (171).

The absorbed fraction of photons is estimated by Monte Carlo methods (172).

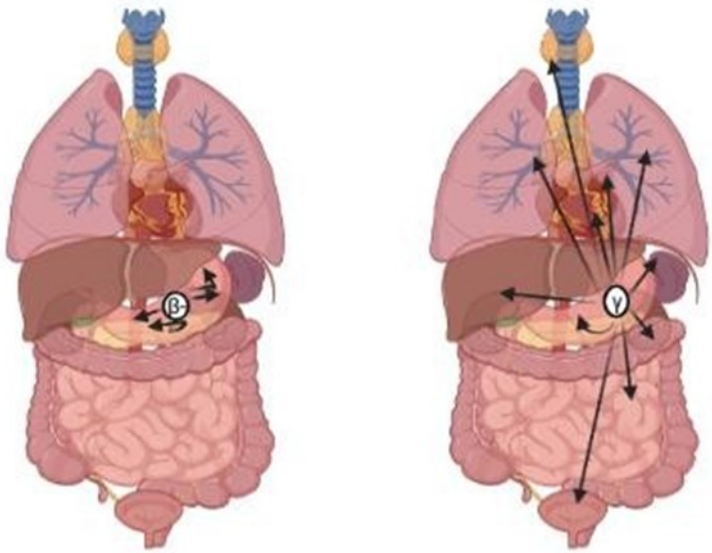

Figure 22 : *Difference between beta and gamma energy deposition. (Created with BioRender)*

3.2.8. Activity and Cumulated activity:

The activity A(t) is the total number of nuclei that are decaying per second, in other words, the number of radioactive disintegrations per second (173).

It represents the probability that any individual atom will undergo decay during the same period, as expressed in equation 2.15

$$A = \lambda N \qquad \textbf{(2.15)}$$

where A = activity, N = the number nuclei in the sample and λ = decay constant.

Its unit in the SI is the becquerel (Bq) with 1 Bq = 1 transition/s although the earlier unit of activity is the curie (Ci) with 1 Ci = 10^{10} Bq

Exponential decay is characterized by disappearance of a constant function of activity or number of atoms prevented per unit time interval; this can be expressed by eqution 2.16:

$$A(t) = A_0 e^{-\lambda t} \qquad \textbf{(2.16)}$$

where A (t) is the activity of radionuclide at a given time t; A_0 is the activity of radionuclide at time t = 0 (174);

decay constant (λ) is the proportionality between the size of a population of radioactive atoms and the rate at which the population decreases because of radioactive decay, its unit is s^{-1} (175).

The cumulated activity ($\tilde{A}$) depends on the amount of activity present in the source organ and on the period of time for which this activity is present, its SI unit is the Bq.sec, and its corresponding traditional unit is the μCi.hr (176).

Cumulated activity is essentially the number of decays in the source region during the relevant time period (177).

The amount of activity contained in a source organ therefore generally changes with time. If the time-activity curve is known, the cumulated activity for a source organ is obtained by measuring the area under this curve.

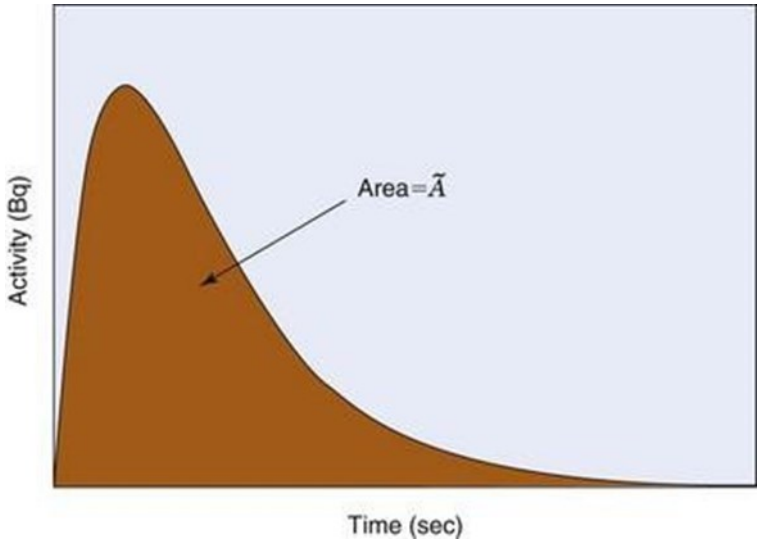

Figure 23 : *Time-activity curve (157).*

Mathematically, if the time-activity curve is described by a function A(t), then:

$$\tilde{A} \approx \int A(t)\, dt \qquad \textbf{(2.17)}$$

Time-activity curves can be quite complex, and thus equation 2.17 may be difficult to analyze. Frequently, however, certain assumptions can be made to simplify this calculation.

For example: Uptake is considered instantaneous and both physical decay and biologic excretion is significant, the total clearance is described by a single-component exponential curve with an effective half-life $T_{1/2}e$ given by equations 2.5 and 2.6 (157).

Cumulated activity is given by equation 2.18:

$$\tilde{A} \approx 1.44 T_{\frac{1}{2}e} A_0 \qquad \textbf{(2.18)}$$

3.2.9. Absorbed dose per unit cumulative activity (S-value):

The S-value states the mean absorbed dose to the target region r_T per radioactive decay in the source region r_S, it is given by equation 2.19:

$$S\,(r_T \leftarrow r_S) = \frac{1}{M}\sum_i E_i \bullet Y_i \bullet \phi(r_T \leftarrow r_S, E_i) \qquad \textbf{(2.19)}$$

Where:

E_i: mean energy of the i_{th} nuclear transition.

Y_i: the yield, i.e., the number of the i_{th} nuclear transitions per nuclear transformation (number of emitted particles or photons per decay).

$\phi(r_T \leftarrow r_S, E_i)$: absorbed fraction of the energy emitted from the source region r_S that is absorbed in the target region r_T.

M: mass of the target region (178).

The quantity S is specific to the radionuclide and to the computational phantom defining the spatial relationship and tissue compositions of r_S and r_T and their intervening tissues in the reference individual or tissue model (179).

Another definition to S-value can be given through the absorbed dose $D(r_T)$ which is defined as the mean energy imparted to target tissue (or region) r_T per unit tissue mass. The time-dependent rate at which the absorbed dose is delivered $\dot{D}\,(r_T,\, t)$ to target tissue r_T within a patient from a radioactive material distributed uniformly within source tissue r_S at time t after administration is given by equation 2.20 or 2.21:

$$\dot{D}(r_T, t) = \sum_{r_s} A(r_s, t) \bullet S(r_T \leftarrow r_s, t\,) \qquad \textbf{(2.20)}$$

$$D(r_T) = \sum_s \tilde{A}\,(r_s) \bullet S(r_T \leftarrow r_s\,) \qquad \textbf{(2.21)}$$

where $A\,(r_S,\, t)$ is the time-dependent activity of the radiopharmaceutical in source tissue r_S, and

$S\,(r_T \leftarrow r_S,\, t)$ is the radionuclide-specific quantity representing the mean absorbed dose rate to target tissue r_T at time t after administration per unit activity present in source tissue r_S (157).

The value of S may be based on preconstructed whole-body computational phantoms representing reference individuals of a given age, sex, total-body mass, and standing height (179).

Absorbed fractions and S values and are calculated by Monte Carlo radiation energy transport calculations (180).

Chapter Three: Monte Carlo Simulation

1. State of the art:

A lot of the progress achieved in medical physics would not have been possible without the contribution of information technology.

Computer simulations are divided into two major categories: analytical simulations and Monte Carlo simulations (181).

Monte Carlo simulation uses random sampling and statistical modeling to estimate mathematical functions and simulate the operations of complex systems (182). This simulation method is very closely related to random experiments, for which the specific result is not known in advance (183).

2. History:

The Monte Carlo Method was invented by John von Neumann and Stanislaw Ulam during World War II. It was named after a well-known casino town, called Monaco since the element of chance is core to the modeling approach, similar to a game of roulette (184).

The earliest published work on Monte Carlo is perhaps the paper of Metropolis and Ulam in the year 1949 (185).

As for the medical field, Snyder at Oak Ridge National Laboratory was the first to introduce the Monte Carlo method in order to assess the fraction of photon and electron energy emitted from radionuclides in source tissues, deposited in various target tissues (186).

3. Monte Carlo Method:

Monte Carlo is a statistical method of understanding complex physical or mathematical systems by using randomly generated numbers as input into those systems to generate a range of solutions. The more trials it produced the more accurate the solutions. This method is used in a wide range of subjects especially in problems in which determining an analytic solution would be too time-consuming (187).

To establish an MC model for a system, representative samples of the processes that usually occur within that system are mimicked. Due to the haphazard nature of some of the components of these processes, each event and outcome could possibly be unique. Probability density functions are employed to model the diverse stochastic processes within the greater system. To build a comprehensive system model, multiple instances of the process being modeled must be observed to capture enough data and effectively model a representative probabilistic distribution (188).

The mathematical algorithms underlying Monte Carlo methods are very complex, but nowadays many software tools enable physicists to use this method seamlessly and efficiently via intuitive user interfaces without requiring any special expertise (189).

4. Monte Carlo software:

4.1. MCNP:

MCNP is a well-known and widely used general-purpose Monte Carlo N–Particle code that can be used for neutron, photon, electron, or coupled neutron/photon/electron transport, including the capability to calculate eigenvalues for critical systems (190). It was first released in the mid-1970s for neutron and photon transport, and was enhanced over the years (191).

For neutrons transport simulations, all reactions given in a particular cross-section evaluation are accounted for. For photons, the code takes account of incoherent and coherent scattering, the possibility of fluorescent emission after photoelectric absorption, absorption in pair production with local emission of annihilation radiation, and bremsstrahlung.

The neutron energy regime is from 10^{-11} MeV to 20 MeV, and the photon and electron energy regimes are from 1 keV to 1000 MeV (191).

Its areas of application include, among others, medical physics, radiography, radiation protection and dosimetry, radiation shielding, nuclear oil well logging, decontamination and decommissioning (192).

4.2. EGS:

The EGS (Electron–Gamma–Shower) system of computer codes are a general-purpose package for the Monte Carlo simulation of the coupled transport of electrons and photons in an arbitrary geometry for particles with energies above a few keV up to several TeV. It is basically an analog Monte Carlo program. That is to say, each and every particle is followed until it reaches its final destiny, usually an energy limit (cutoff) or a discard boundary. Due to the statistical nature of the Monte Carlo method, the accuracy of the results will depend on the number of histories run (193).

The Latest version in the EGS codes is EGSnrc which is used to simulate particle transport for energies ranging from 1 keV to 10 GeV (194).

Some of the physics implemented in EGSnrc are:

- The radiation transport of electrons (+ or −) or photons can be simulated in any element, compound, or mixture.
- Both photons and charged particles are transported in steps of random length rather than in discrete steps.
- The dynamic range of charged particle kinetic energies goes from a few tens of keV up to a few hundred GeV.
- The dynamic range of photon energies lies between 1 keV and several hundred GeV (195).

4.3. FLUKA:

FLUKA is a multiparticle transport and interaction Monte Carlo code. It has a wide range of applications, in particle physics but also in accelerator design and shielding, dosimetry, radiation protection, hadrotherapy (196).

FLUKA is based on original and well tested microscopic models. Due to this "microscopic" approach to hadronic interaction modelling, each step is self–consistent and has solid physical bases. Performances are optimized comparing with particle production data at single interaction level. No tuning whatsoever is performed on "integral" data, such as calorimeter resolutions, thick target yields, etc. Therefore, final predictions are obtained with a minimal set of free parameters, fixed for all energies and target/projectile combinations. Results in complex cases as well as scaling laws and properties come forth naturally from the underlying physical models and the basic conservation laws are fulfilled a priori (197).

This software can simulate with high accuracy the interaction and propagation in matter of about 60 different particles, including photons and electrons from 100 eV–1 keV to thousands of TeV, neutrinos, muons of any energy, hadrons of energies up to 20 TeV and all the corresponding antiparticles, neutrons down to thermal energies and heavy ions. The program can also transport polarised photons and optical photons. Time evolution and tracking of emitted radiation from unstable residual nuclei can be performed on line (198).

4.4. PENELOPE:

PENELOPE is an acronym that stands for PENetration and Energy LOss of Positrons and Electrons (199).

The computer code system performs Monte Carlo simulation of coupled electron-photon transport in arbitrary materials for a wide energy range, from a few hundred eV to about 1 GeV. Photon transport is simulated by means of the standard, detailed simulation scheme. Electron and positron histories are generated on the basis of a mixed procedure, which combines detailed simulation of hard events with condensed simulation of soft interactions. A geometry package called PENGEOM permits the generation of random electron-photon showers in material systems consisting of homogeneous bodies limited by quadric surfaces, i.e., planes, spheres, cylinders, etc (200).

4.5. Geant4:

Geant4 is a toolkit for simulating the passage of particles through matter. It includes a complete range of functionality including tracking, geometry, physics models and hits. The physics processes offered cover a comprehensive range, including electromagnetic, hadronic and optical processes, a large set of long-lived particles, materials and elements, over a wide energy range starting, in some cases, from 250 eV and extending in others to the TeV energy range. It has been created exploiting software engineering and object-oriented technology and implemented in the C++ programming language. It has been used in applications in particle physics, nuclear physics, accelerator design, space engineering and medical physics (201).

5. Anthropomorphic computational phantoms:

Accurate radiation dosimetry is essential but also quite challenging for three reasons:

- There are many diverse exposure scenarios resulting in unique spatial and temporal relationships between the source and the human body.
- An exposure can involve multiple radiation types which are governed by rather different radiation physics principles including photons (and gamma rays), electrons, positrons, alpha particles, neutrons, and protons.
- The human body consists of three-dimensional (3D) inhomogeneous tissues of various geometric shapes and densities, leading to extremely complex radiation interaction patterns.

In order to calculate radiation dose in radiation protection, medical imaging or radiotherapy, it is necessary to use models of the human anatomy, those are called anthropomorphic computational phantoms. Depending on the complexity of these phantoms, three generations can be distinguished (202).

5.1. First-Generation Stylized Phantoms:

The first-generation computational phantoms were developed for the purpose of assessing organ doses from internally deposited radioactive materials for workers and patients. With the increase in the size and speed of computers, some progress occurred during the late 1950s and through the 1960s and eventually the efforts led to stylized anthropomorphic phantoms (203).

Fisher and Snyder at ORNL have reported in the 1960s the first attempts at developing a computational anthropomorphic phantom (204).

In 1969, Snyder and his colleagues reported the first heterogeneous phantom that became known as the ‘‘MIRD-5 Phantom’’ a name derived from the Medical Internal Radiation Dosimetry (MIRD) Committee of the Society of Nuclear Medicine which adopted the phantom (205).

Creating these phantoms is based on constructive solid geometry (CSG) method which allows the modeler to create a solid object using Boolean operators to combine very simple shapes called primitives. Examples of these primitives include cuboids, cylinders, prisms, pyramids, spheres, cones and ellipsoids surfaces that are easily described by quadric equations. CSG representations are easy to adopt and can yield good results when the objects are relatively simple in shape (206).

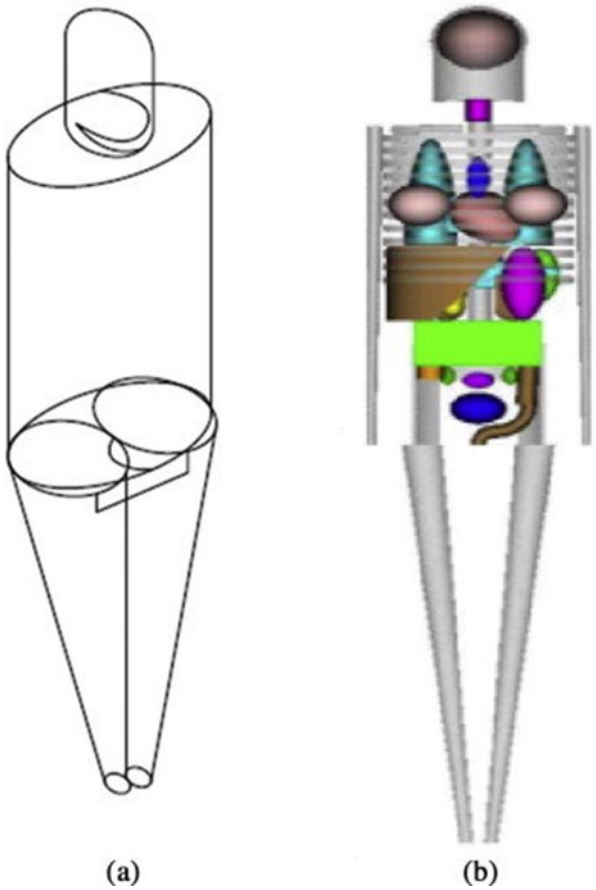

Figure 24 : *Stylized computational phantom (a) external view of male phantom (b) internal view of female phantom. (207)*

The original developers of these phantoms recognized the obvious shortcomings because human anatomy is too complex to be realistically modeled with a limited set of surface equations. Many anatomical details in these models were compromised that sometimes led to inaccurate results. Thus, the need arose to look for new ways to have more accurate results (203). This became possible only after the introduction of major tomographic medical imaging modalities such as CT and MRI (208).

5.2. Second-Generation Voxelized Phantoms:

Computational anthropomorphic phantom based on medical tomographic images where the anatomy is described by small three-dimensional volume elements (voxels) specifying the density and the atomic composition of the various organs and tissues of the human body (209).

In this era the medical communities took advantage of using the 3-D tomographic images to improve treatment planning and dose assessment, however, the task of developing well-defined standard human models faced some unique and intractable technical challenges:

- Whole-body models are needed, but medical images are often taken for a portion of the body (CT procedures expose the patients to intense X-rays, and MRI is time-consuming).
- A large number of internal organs/tissues have to be identified and segmented for organ dose calculations for systematic dose calculations, whereas, in radiotherapy, for example, only the tumor volume and adjacent regions need to be outlined.
- The image data size of a whole-body model can be potentially too big for a computer's memory to handle.
- A standardized patient model involves dose calculations for photons, electrons, neutrons, and protons, but the majority of the clinical procedures involve fewer types of radiation (210).

Four main phases should usually be followed for the development of a voxel model:

a) Acquisition of high-resolution CT or MRI data sets;
b) Classification and segmentation of the various tissues and organs through assignment of unique individual labels to each anatomical structure of interest according to the targeted application;
c) Identification of the type of biological tissue and organ and their elemental tissue compositions and mass densities using, for example, tissue characteristics from ICRU Report 46 (211) and ICRP Publication 89 (212);
d) Implementation of the computational model in a Monte Carlo package to simulate radiation transport and score quantities of interest for the task at hand (208).

Voxel phantoms have the following limitations:

- Surface contours of organs and tissues in voxel phantoms are primarily dependent on manual image segmentation.
- Some organs and tissues cannot easily be recognized even by experienced radiologists due to the limitations in image contrast (213).

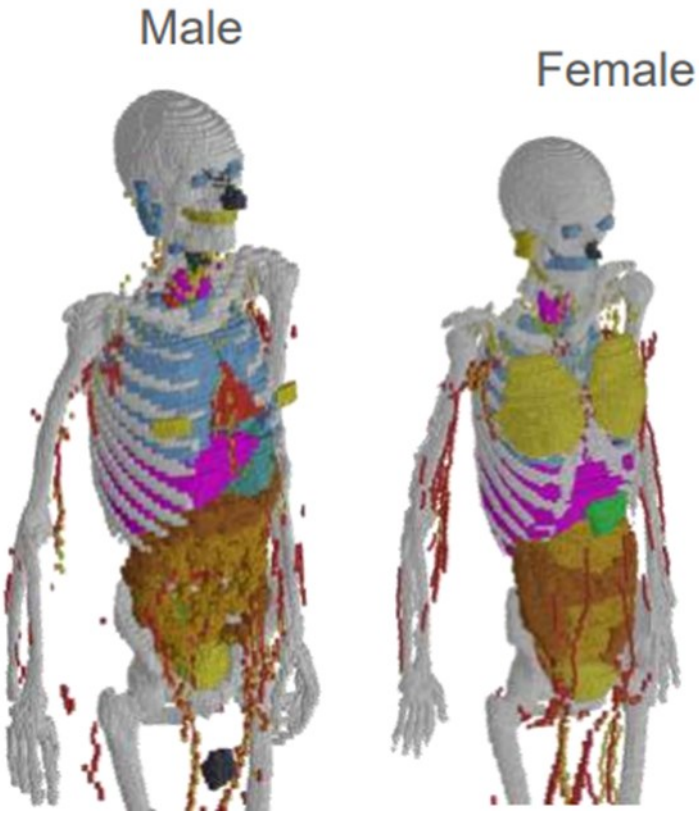

Figure 25 : *Voxelized phantoms (160).*

5.3. Third-Generation Hybrid Phantoms:

A hybrid approach to phantom construction incorporates the best features of both stylized and voxel phantoms. They retain both the anatomic realism of voxel phantoms and the flexibility of mathematical phantoms (214).

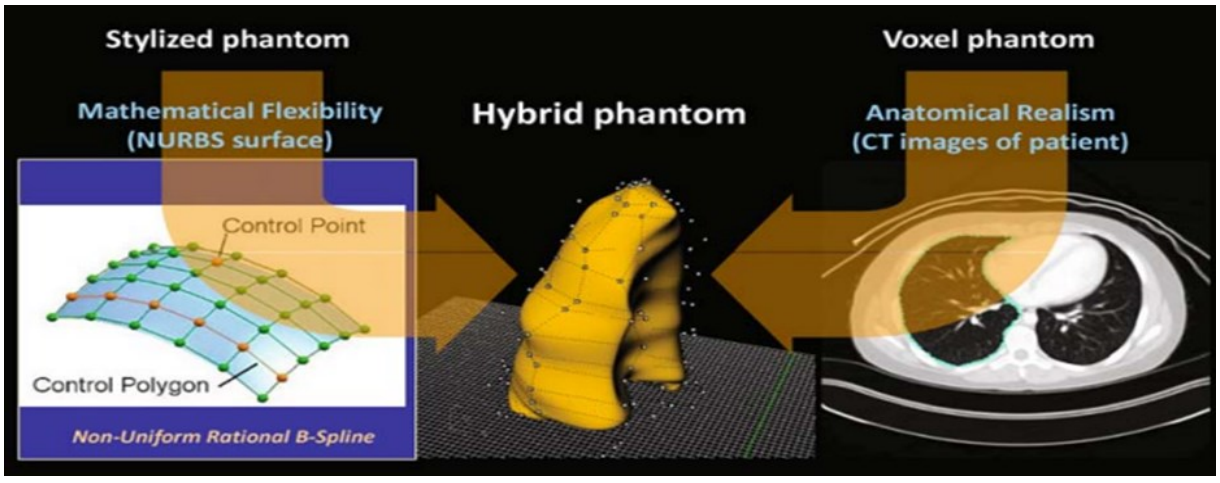

Figure 26 : *Construction of a hybrid phantom (215).*

Hybrid phantoms make use of non-uniform rational B-spline (NURBS) surfaces to describe the boundaries of both internal organs and exterior body surfaces (216).

Construction of a hybrid phantom is performed in four steps:

a) Transforming 2D images of human body to 3D polygon mesh model of exterior body and internal organs;
b) Creating NURBS surfaces;
c) Voxelization of NURBS surfaces;
d) Preparing the MCNP input file to simulate the creation and transportation of emitting particles through these boundary representation (BREP) structures (213).

Three advantageous features of hybrid phantoms:

- The ability to model underweight and overweight individuals during reconstruction of external or even internal exposures,
- The ability to reposition the arms and legs of the phantom to represent unique worker or patient-specific exposure postures
- The ability to extract individual organs or sets of organs from the whole-body phantom and voxelize those tissues at a significantly higher resolution than would be computationally permitted within a full-body phantom (217).

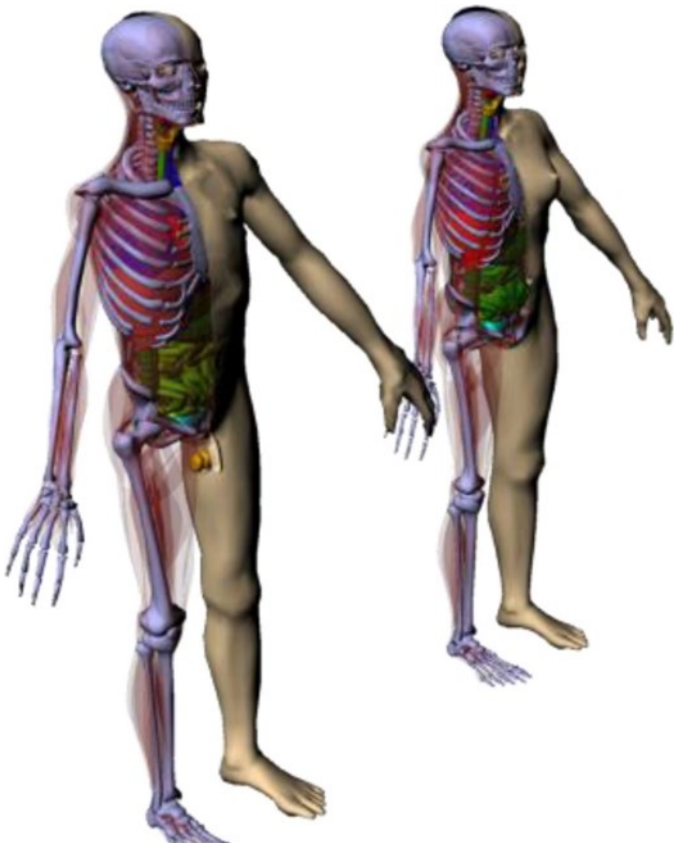

Figure 27 : *Hybrid phantoms. (203)*

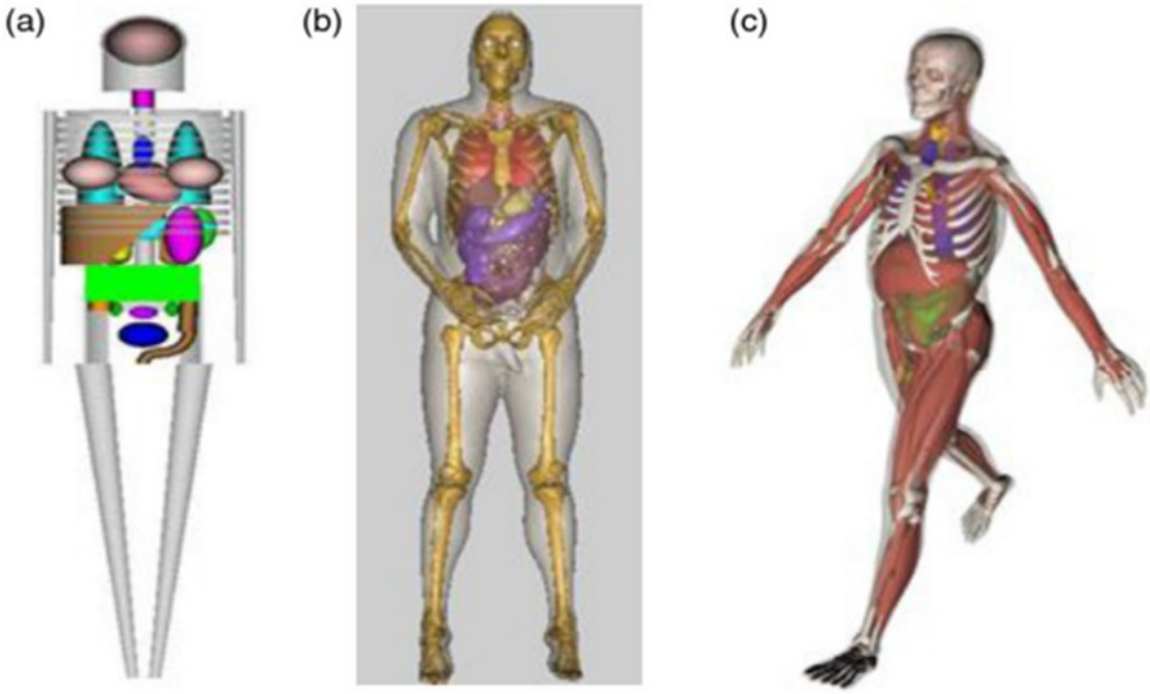

Figure 28 : *Three phantom generations; (a) stylized phantom; (b) voxel phantom (but displayed in smooth surfaces); (c) BREP phantom. (218)*

Part Two : Research Methodology

1. Problematic:

In recent years, a real revolution has profoundly changed the scope and outlook of nuclear medicine. This revolution is currently mainly concerned with cancer but will gradually be extended to other fields, including and not limited to cardiology and neurology.

These developments lead to particular radiation protection problems which must be considered for the optimum benefit of these diagnostic and therapeutic innovations.

Even if only one organ is exposed for exploration or treatment, different tissues may be irradiated. Therefore, it is essential to carry out dosimetric studies to ensure the radiation protection of the patient.

Since the internal dose is not measurable, its estimation is based on calculations taking into account experimental data and theoretical considerations.

Actually, one of the most common and widely used approaches for calculating internal doses in nuclear medicine has been developed by the Medical Internal Radiation Dose (MIRD) Committee (1999) and the Society of Nuclear Medicine Committee (SNM) and is commonly referred to as the MIRD formalism. The formalism of MIRD has been published in the form of pamphlets with associated publications (219,220).

These pamphlets propose a methodology for evaluating the dose absorbed by the organs of the human body, by tissue regions or by voxelated structures for diagnostic or therapeutic applications in nuclear medicine (221).

The effects induced by low doses of irradiation may differ from those observed during exposures to high doses of irradiation. The nature of these differences and their implications are still to be explored.

There is not a single form of a dose-response relationship for all cellular biological processes studied. Many efforts have been made to explore the relationships between radiation dose and effects on the biological processes involved in cancer. The various results obtained highlight a diversity of responses to the radiation dose according to the biological mechanism studied.

2. Aim of the study:

Modeling of the effects of low-energy ionizing radiation on different biological tissues in hyperthyroidism and thyroid cancer patients and comparison of our results with data acquired from experimental, clinical, and epidemiological studies.

3. Material and methods:

3.1. Epidemiological study:

a) Type, place, and period of the study:

It is a retrospective descriptive study that took place at the University Hospital Center of Tlemcen in the nuclear medicine department between the months of August 2021 and March 2022.

b) Study Population:

This study was conducted on a population of 542 patients with either hyperthyroidism or thyroid cancer to analyze some epidemiological (sex and age) and therapeutic (dose) parameters in each patient who received ^{131}I radiation therapy.

c) Inclusion criteria:

Included in our study were patients who received radioactive iodine therapy for hyperthyroidism and thyroid cancer whose ages range from 18 to 60 years old regardless of their sex and type of tumor during the study period.

d) Non-inclusion criteria:

Patients whose ages are less than 18 or more than 60 years old.

e) Ethical considerations:

Data collection was carried out with due regard for the anonymity of patients and the confidentiality of their information.

f) Data collection and conduction of the study:

All the information that was the subject of our analysis was collected from the data available in the register of the nuclear medicine department and the NUCLEUS software.

The study was conducted as follows:

For each subject, we identified:

Socio-demographic data:

- Age.
- Gender.

Clinical data:

- The prescribed dose.

g) Data Capture and Statistical Analysis:

The data were analyzed using Microsoft EXCEL 2019 software.

Results were expressed as a percentage for qualitative variables.

The tables and graphs are based on Microsoft EXCEL 2019 software.

3.2. Simulation:

a) Properties of the device and programs used for the simulation:

Processor: Intel® Core™ i7 CPU 860 @2.80GHz 2.79GHz.

Installed RAM: 8.00 GB.

System type: 64-bit operating system, ×64-based processor.

Ubuntu version 20.04.

TOPAS version 3.7.0 with a built-in Geant4 version 10.06.p03.

Stylized anthropomorphic phantom.

b) TOPAS MC:

TOPAS (222), launched in 2009, is a breakthrough software project that struck down a usability barrier for MC simulations that was limiting radiation therapy research.

TOPAS is a “user code” layered on top of Geant4. TOPAS includes the standard Geant4 toolkit, plus additional code to make Geant4 easier to control and to extend its functionality.

First developed for proton therapy simulations, TOPAS is arguably a gold standard for proton therapy MC simulations. TOPAS was next expanded to radiobiology (223,224). TOPAS has now become widely accepted in physics and biology, with 931 registered users at 342 institutions in 40 countries as of January 28, 2020. In addition, TOPAS has been licensed by several vendors of radiation therapy equipment and treatment planning software. TOPAS is part of the cadre of software tools supported by the National Cancer Institute program on Informatics Technology for Cancer Research with funding to support further development and sustainability (222).

Launching an application on TOPAS MC goes through many steps, the most important are the following:

1) Creating the material and the geometry.
2) Choosing the particle sources.
3) Creating the scorers.
4) Choosing the physics.
5) Visualization of the simulation in the Graphic User Interface.

3.2.1. Creating the Anthropomorphic phantom using TOPAS MC:

First of all, we start by resizing the world volume that will contain the phantom so that it is a $2 \times 2 \times 2\ m^3$ box, this would allow to increase the number of histories that can be launched.

Then the geometry that will serve as the human body (anthropomorphic phantom) must be created.

The phantom that was used in this study is based on an article written by Snyder et al. (205) and it was modified by Guatelli et al. (225)

Since the tissues defined in TOPAS MC do not resemble those that compose the human body, the first step should be defining the materials of each tissue of the various organs. In this simplified phantom only three types of tissue are needed: soft tissue, skeleton, and lung material.

In this example, the soft tissue material is composed of 16 elements with various proportions leading to an overall density of 1.04 g/cm^3.

```
sv:Ma/soft_tissue/Components = 16 "Hydrogen" "Carbon" "Nitrogen" "Oxygen"
"Sodium" "Magnesium" "Phosphorus" "Sulfur" "Chlorine" "Potassium" "Iron" "Zinc"
"Rubidium" "Strontium" "Zirconium" "Lead"
uv:Ma/soft_tissue/Fractions = 16 0.1047 0.2302 0.0234 0.6321
0.0013 0.00015 0.0024 0.0022 0.0014 0.0021 0.000063 0.000032
0.0000057 0.00000034 0.000008 0.00000016
d:Ma/soft_tissue/Density = 1.04 g/cm3
b:Ma/soft_tissue/NormalizeFractions = "True"
```

Figure 29 : *The algorithm for the soft tissue.*

The skeleton material is composed of 15 elements with various proportions and its overall density is 1.4862 g/cm^3.

```
sv:Ma/skeleton/Components = 15 "Hydrogen" "Carbon" "Nitrogen" "Oxygen" "Sodium"
"Magnesium" "Phosphorus" "Sulfur" "Chlorine" "Potassium" "Calcium" "Iron" "Zinc"
"Strontium" "Lead"
uv:Ma/skeleton/Fractions = 15 0.0704 0.2276 0.0387 0.4856 0.0032
0.0011 0.0694 0.0017 0.0014 0.0015 0.0991 0.00008 0.000048
0.000032 0.000011
d:Ma/skeleton/Density = 1.4862 g/cm3
b:Ma/skeleton/NormalizeFractions = "True"
```

Figure 30 : *The algorithm for the skeleton.*

As for the lung material, it is also composed of 16 elements with a total density of 0.2958 g/cm^3.

```
sv:Ma/lung_material/Components = 16 "Hydrogen" "Carbon" "Nitrogen" "Oxygen"
"Sodium" "Magnesium" "Phosphorus" "Sulfur" "Chlorine" "Potassium" "Calcium"
"Iron" "Zinc" "Rubidium" "Strontium" "Lead"
uv:Ma/lung_material/Fractions = 16 0.1021 0.1001 0.028 0.7596
0.0019 0.000074 0.00081 0.0023 0.0027 0.0020 0.00007
0.00037 0.000011 0.0000037 0.000000059 0.00000041
d:Ma/lung_material/Density = 0.2958 g/cm3
b:Ma/lung_material/NormalizeFractions = "True"
```

Figure 31 : *The algorithm for the lung material.*

Now the organs that will make up the anthropomorphic phantom can be created; some organs are formed by simple geometries that can be generated using TOPAS MC alone while others will need the use of Geant4 extensions.

Overall, the human phantom can be divided into 4 different volumes and each one of them is a mother volume to other daughter volumes that represent individual organs:

1) The head.
2) The trunk (including the right and left arms).
3) The right leg.
4) The left leg.

1) Head

The head volume is a parent volume for 4 other volumes that anatomically reside in this area; the skull, the brain, the upper spine and the thyroid.

The solutions for inequation 4.1 constitute the head of the phantom.

$$\left.\begin{array}{c}\left(\frac{x}{7}\right)^2+\left(\frac{y}{10}\right)^2 \leq 1 \\ 70 < z \leq 94\end{array}\right\} \qquad (\mathbf{4.1})$$

In order to achieve this geometry, the following code is to be inserted:

```
s:Ge/MIRDHead/Parent = "MIRD"
s:Ge/MIRDHead/Type = "MIRDHead"
s:Ge/MIRDHead/Material = "soft_tissue"
d:Ge/MIRDHead/ax = 7.0 cm
d:Ge/MIRDHead/by = 10.0 cm
d:Ge/MIRDHead/cz = 8.50 cm
d:Ge/MIRDHead/zcut1 = 0.0 cm
d:Ge/MIRDHead/zcut2 = 8.50 cm
d:Ge/MIRDHead/dx = 7.0 cm
d:Ge/MIRDHead/dy = 10.0 cm
d:Ge/MIRDHead/dz = 7.75 cm
d:Ge/MIRDHead/xx = 0.0 cm
d:Ge/MIRDHead/yy = 0.0 cm
d:Ge/MIRDHead/zz = 7.7500 cm
d:Ge/MIRDHead/TransX = 0. cm
d:Ge/MIRDHead/TransY = 0. cm
dc:Ge/MIRDHead/TransZ = 77.75 cm
d:Ge/MIRDHead/RotX = 180. deg
d:Ge/MIRDHead/RotY = 180. deg
s:Ge/MIRDHead/Color = "red"
s:Ge/MIRDHead/DrawingStyle = "FullWireFrame"
```

Figure 32 : *The algorithm for the head volume.*

The skull is defined as the volume between two nonconcentric ellipsoids and given mathematically by inequation 4.2:

$$\left.\begin{array}{c}\left(\frac{x}{6}\right)^2\left(\frac{y}{9}\right)^2\left(\frac{z-86.5}{6.5}\right)^2 \geq 1 \\ \left(\frac{x}{6.8}\right)^2\left(\frac{y}{9.8}\right)^2\left(\frac{z-85.5}{8.3}\right)^2 \leq 1\end{array}\right\} \qquad (\mathbf{4.2})$$

This volume is composed of the skeleton material and has a volume of 846.6 cm^3

The line of code that allows to create this volume is demonstrated in Figure 33.

```
s:Ge/MIRDSkull/Parent = "MIRDHead"
s:Ge/MIRDSkull/Type = "MIRDSkull"
s:Ge/MIRDSkull/Material = "skeleton"
d:Ge/MIRDSkull/ax_out = 6.8 cm
d:Ge/MIRDSkull/by_out = 9.8 cm
d:Ge/MIRDSkull/cz_out = 8.3 cm
d:Ge/MIRDSkull/ax_in = 6. cm
d:Ge/MIRDSkull/by_in = 9. cm
d:Ge/MIRDSkull/cz_in = 6.5 cm
d:Ge/MIRDSkull/xx = 0. cm
d:Ge/MIRDSkull/yy = 0. cm
d:Ge/MIRDSkull/zz = 1. cm
dc:Ge/MIRDSkull/TransX = 0. cm
dc:Ge/MIRDSkull/TransY = 0. cm
dc:Ge/MIRDSkull/TransZ = 7.75 cm
s:Ge/MIRDSkull/Color = "grey"
s:Ge/MIRDSkull/DrawingStyle = "Solid"
```

Figure 33 : *The algorithm for the skull volume.*

The brain is represented by an ellipsoid given by inequation 4.3; this volume is filled with the soft tissue material.

$$\left(\frac{x}{6}\right)^2 + \left(\frac{y}{9}\right)^2 + \left(\frac{z - 86.5}{6.5}\right)^2 \leq 1 \qquad (\mathbf{4.3})$$

The brain has a volume of 1.47 cm^3.

In TOPAS MC this geometry can be achieved by the following algorithm:

```
s:Ge/MIRDBrain/Parent = "MIRDHead"
s:Ge/MIRDBrain/Type = "G4Ellipsoid"
s:Ge/MIRDBrain/Material = "soft_tissue"
d:Ge/MIRDBrain/HLX = 6. cm
d:Ge/MIRDBrain/HLY = 9. cm
d:Ge/MIRDBrain/HLZ = 6.5 cm
d:Ge/MIRDBrain/TransX = 0. cm
d:Ge/MIRDBrain/TransY = 0. cm
d:Ge/MIRDBrain/TransZ = 8.75 cm
s:Ge/MIRDBrain/Color = "yellow"
s:Ge/MIRDBrain/DrawingStyle = "Solid"
```

Figure 34 : *The algorithm for the brain volume.*

The upper spine is a portion of the spine that resides in the head volume, it is an elliptical cylinder composed of the skeleton material, mathematically this volume is represented by inequation 4.4

$$\left.\begin{array}{c}\left(\frac{x}{2}\right)^2+\left(\frac{y-5.5}{2.5}\right)^2\leq 1\\ 70\leq z\leq 78.5\end{array}\right\} \quad (\mathbf{4.4})$$

The algorithm to create this volume is:

```
s:Ge/MIRDUpperSpine/Parent = "MIRDHead"
s:Ge/MIRDUpperSpine/Type = "MIRDUpperSpine"
s:Ge/MIRDUpperSpine/Material = "skeleton"
d:Ge/MIRDUpperSpine/dx = 2. cm
d:Ge/MIRDUpperSpine/dy = 2.5 cm
d:Ge/MIRDUpperSpine/dz = 4.25 cm
d:Ge/MIRDUpperSpine/xx = 20. cm
d:Ge/MIRDUpperSpine/yy = 10. cm
d:Ge/MIRDUpperSpine/zz = 5. cm
dc:Ge/MIRDUpperSpine/angle1 = -25. deg
d:Ge/MIRDUpperSpine/offsetX = 0. cm
d:Ge/MIRDUpperSpine/offsetY = -2.5 cm
d:Ge/MIRDUpperSpine/offsetZ = 5.5 cm
dc:Ge/MIRDUpperSpine/TransX = 0.0 cm
dc:Ge/MIRDUpperSpine/TransY = 5.5 cm
dc:Ge/MIRDUpperSpine/TransZ = -3.50 cm
s:Ge/MIRDUpperSpine/Color = "grey"
s:Ge/MIRDUpperSpine/DrawingStyle = "Solid"
```

Figure 35 : *the algorithm for the upper spine volume.*

The lobes of the thyroid lie between two concentric cylinders and are formed by a cutting surface; this volume is represented mathematically through the following inequations:

$$\left.\begin{array}{c}x^2+(y+6)^2\leq (2.2)^2\\ x^2+(y+6)^2\geq (1)^2\\ y+6\leq 0\\ 70\leq z\leq 75\end{array}\right\} \quad (\mathbf{4.5})$$

This organ has a volume of 19.89 cm^3 and it is filled with soft tissue material.

The following algorithm allows for the creation of this volume:

```
s:Ge/MIRDThyroid/Parent = "MIRDHead"
s:Ge/MIRDThyroid/Type = "MIRDThyroid"
s:Ge/MIRDThyroid/Material = "soft_tissue"
d:Ge/MIRDThyroid/z_out = 4.20 cm
d:Ge/MIRDThyroid/rmin = 0. cm
d:Ge/MIRDThyroid/rmax_out = 1.85 cm
d:Ge/MIRDThyroid/startphi = 0. deg
d:Ge/MIRDThyroid/deltaphi_out = 180. deg
d:Ge/MIRDThyroid/z_in = 4.50 cm
d:Ge/MIRDThyroid/rmax_in = 0.83 cm
d:Ge/MIRDThyroid/deltaphi_in = 360. deg
d:Ge/MIRDThyroid/xx = 3.72 cm
d:Ge/MIRDThyroid/yy = 3.72 cm
d:Ge/MIRDThyroid/zz = 20.00 cm
d:Ge/MIRDThyroid/angle1 = -50. deg
d:Ge/MIRDThyroid/angle2 = 50. deg
dc:Ge/MIRDThyroid/offsetX = 0.0 cm
dc:Ge/MIRDThyroid/offsetY = 0.0 cm
dc:Ge/MIRDThyroid/offsetZ = 4.20 cm
dc:Ge/MIRDThyroid/offsetZ1 = -5.40 cm
dc:Ge/MIRDThyroid/TransX = 0.0 cm
dc:Ge/MIRDThyroid/TransY = -3.91 cm
dc:Ge/MIRDThyroid/TransZ = -5.65 cm
dc:Ge/MIRDThyroid/RotX = 0. deg
dc:Ge/MIRDThyroid/RotY = 0. deg
dc:Ge/MIRDThyroid/RotZ = 180. deg
s:Ge/MIRDThyroid/Color = "orange"
s:Ge/MIRDThyroid/DrawingStyle = "Solid"
```

Figure 36 : *The algorithm for the thyroid volume.*

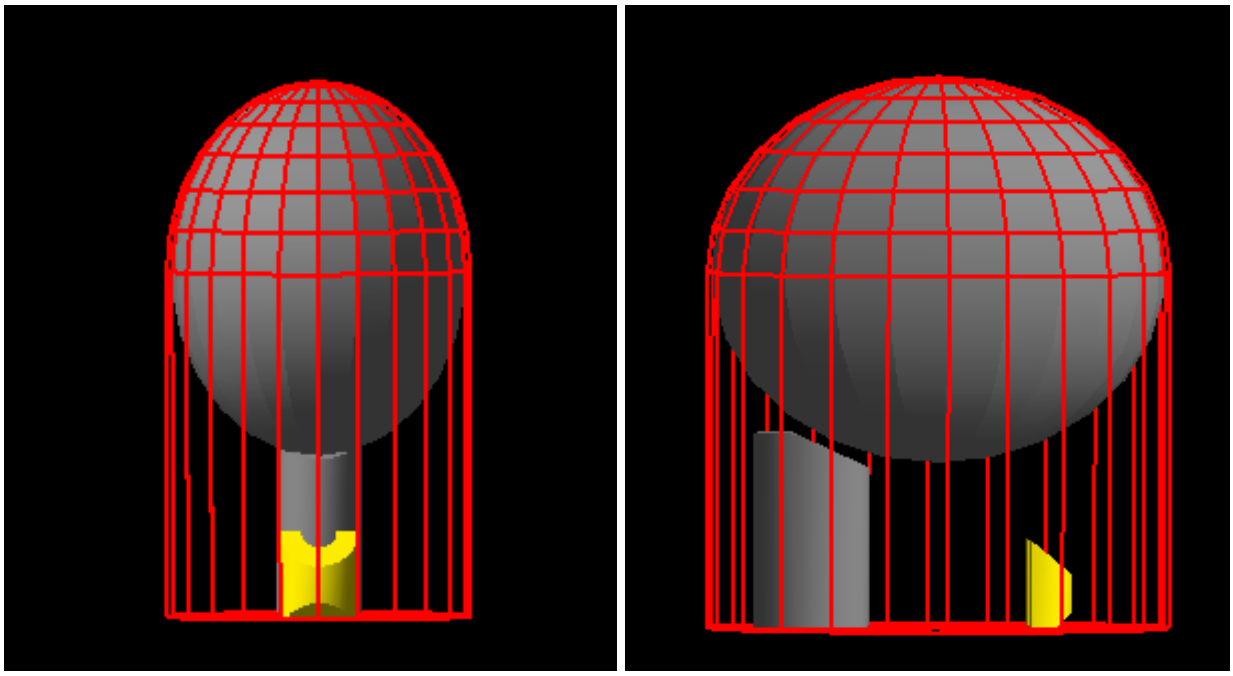

Figure 37: *TOPAS MC representation of the head volume and its constituents (red: head, yellow: thyroid, grey ellipsoid: skull and grey elliptical tube: upper spine).*

2) Trunk:

The trunk is represented by an elliptical cylinder, aside from the internal organs it also contains the arms and the hips, inequation 4.6 gives the mathematical representation of the trunk

$$\left.\begin{array}{l}\left(\frac{x}{10}\right)^2+\left(\frac{y}{20}\right)^2 \leq 1 \\ 0 \leq z \leq 70\end{array}\right\} \quad (\mathbf{4.6})$$

Figure 38 represents the line of code that creates the trunk in TOPAS MC

```
s:Ge/MIRDTrunk/Parent = "MIRD"
s:Ge/MIRDTrunk/Type = "G4EllipticalTube"
s:Ge/MIRDTrunk/Material = "soft_tissue"
d:Ge/MIRDTrunk/HLX = 20. cm
d:Ge/MIRDTrunk/HLY = 10. cm
d:Ge/MIRDTrunk/HLZ = 35. cm
d:Ge/MIRDTrunk/RotX = 180. deg
d:Ge/MIRDTrunk/RotY = 180. deg
d:Ge/MIRDTrunk/TransX = 0.0 cm
d:Ge/MIRDTrunk/TransY = 0.0 cm
d:Ge/MIRDTrunk/TransZ = 35. cm
s:Ge/MIRDTrunk/Color = "yellow"
s:Ge/MIRDTrunk/DrawingStyle = "FullWireFrame"
```

Figure 38 : *The algorithm for the trunk volume.*

The lungs are represented by half an ellipsoid each, with an anterior section removed, mathematically this volume is represented by inequation 4.7

$$\left.\begin{array}{l}\left(\frac{x-8.5}{5}\right)^2+\left(\frac{y}{7.5}\right)^2+\left(\frac{z-43.5}{24}\right)^2 \leq 1 \\ z \geq 43.5\end{array}\right\} \quad (\mathbf{4.7})$$

In TOPAS MC this volume is obtained by introducing the following lines of code:

```
s:Ge/MIRDLeftLung/Parent = "MIRDTrunk"
s:Ge/MIRDLeftLung/Type = "MIRDLung"
s:Ge/MIRDLeftLung/Material = "lung_material"
d:Ge/MIRDLeftLung/ax = 5. cm
d:Ge/MIRDLeftLung/by = 7.5 cm
d:Ge/MIRDLeftLung/cz = 24. cm
d:Ge/MIRDLeftLung/zcut1 = 0.0 cm
d:Ge/MIRDLeftLung/zcut2 = 24. cm
d:Ge/MIRDLeftLung/dx = 5.5 cm
d:Ge/MIRDLeftLung/dy = 8.5 cm
d:Ge/MIRDLeftLung/dz = 24. cm
d:Ge/MIRDLeftLung/offsetX = 0. cm
d:Ge/MIRDLeftLung/offsetY = 8.5 cm
d:Ge/MIRDLeftLung/offsetZ = 0. cm
d:Ge/MIRDLeftLung/offsetX1 = -6. cm
d:Ge/MIRDLeftLung/offsetY1 = 0.0 cm
d:Ge/MIRDLeftLung/offsetZ1 = 0.0 cm
dc:Ge/MIRDLeftLung/TransX = 8.50 cm
dc:Ge/MIRDLeftLung/TransY = 0.0 cm
dc:Ge/MIRDLeftLung/TransZ = 8.5 cm
s:Ge/MIRDLeftLung/Color = "blue"
s:Ge/MIRDLeftLung/DrawingStyle = "Solid"
```

Figure 39 : *The algorithm for the left lung volume.*

Creating the right lung is achieved by rotating the left lung volume around the z axis by 180°.

Both lungs are composed of soft tissue material and their volume is 3378 cm^3.

The inequations to create the heart are:

$$\left.\begin{array}{rl} x_1 = 0.6948(x+1) - 0.3237(y+3) - 0.6428(z-51) & \\ y_1 = 0.4226(x+1) - 0.9063(y+3) & \\ z_1 = 0.5826(x+1) - 0.2717(y+3) - 0.7660(z-51) & \\ \left(\frac{x_1}{8}\right)^2 + \left(\frac{y_1}{5}\right)^2 + \left(\frac{z_1}{5}\right)^2 \leq 1 & \\ x_1^2 + y_1^2 + z_1^2 \leq (5)^2 \quad if \quad x_1 < 0 & \\ \frac{x_1}{3} + \frac{z_1}{5} \geq -1 \quad if \quad x_1 < 0 & \end{array}\right\} \quad (\mathbf{4.8})$$

These complicated inequations can be solved easily using a computer and the resolution gives the shape of the heart of the phantom; the algorithm is represented in Figure 40

```
s:Ge/MIRDHeart/Parent = "MIRDTrunk"
s:Ge/MIRDHeart/Type = "MIRDHeart"
s:Ge/MIRDHeart/Material = "soft_tissue"
d:Ge/MIRDHeart/ax = 4.00 cm
d:Ge/MIRDHeart/by = 4.00 cm
d:Ge/MIRDHeart/cz = 7.00 cm
d:Ge/MIRDHeart/zcut1 = -7.00 cm
d:Ge/MIRDHeart/zcut2 = 0.0 cm
d:Ge/MIRDHeart/rmin = 0. cm
d:Ge/MIRDHeart/rmax = 3.99 cm
d:Ge/MIRDHeart/startphi = 0. deg
d:Ge/MIRDHeart/deltaphi = 360. deg
d:Ge/MIRDHeart/starttheta = 0. deg
d:Ge/MIRDHeart/deltatheta = 90. deg
d:Ge/MIRDHeart/TransX = 0.0 cm
d:Ge/MIRDHeart/TransY = -3.0 cm
d:Ge/MIRDHeart/TransZ = 15.32 cm
d:Ge/MIRDHeart/RotY = 25. deg
s:Ge/MIRDHeart/Color = "red"
s:Ge/MIRDHeart/DrawingStyle = "Solid"
```

Figure 40 : *The algorithm for the heart volume.*

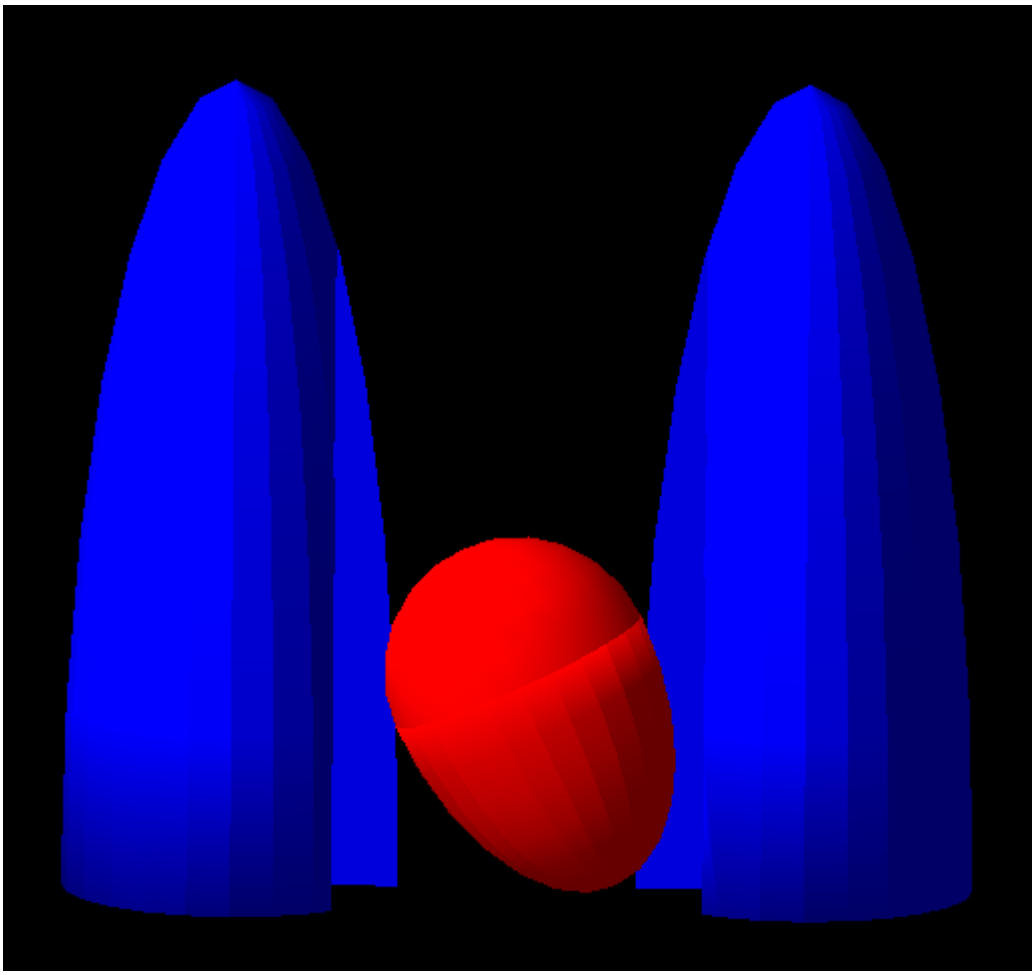

Figure 41 : *TOPAS MC representation of the heart and the lungs.*

The inequation to create the left kidney is:

$$\left.\begin{array}{l}\left(\frac{x-6}{4.5}\right)^2\left(\frac{y-6}{1.5}\right)^2\left(\frac{z-32.5}{5.5}\right)^2 \leq 1 \\ x \geq 3\end{array}\right\} \quad (\mathbf{4.9})$$

The right kidney is obtained by rotating the left kidney around the z axis by 180°.

Both kidneys are composed of soft tissue material and their volume is 311 cm^3.

The following lines of code are used to create the left kidney in TOPAS MC:

```
s:Ge/MIRDLeftKidney/Parent = "MIRDTrunk"
s:Ge/MIRDLeftKidney/Type = "MIRDKidney"
s:Ge/MIRDLeftKidney/Material = "soft_tissue"
d:Ge/MIRDLeftKidney/ax = 4.5 cm
d:Ge/MIRDLeftKidney/by = 1.5 cm
d:Ge/MIRDLeftKidney/cz = 5.5 cm
d:Ge/MIRDLeftKidney/xx = 6. cm
d:Ge/MIRDLeftKidney/yy = 12.00 cm
d:Ge/MIRDLeftKidney/zz = 12.00 cm
d:Ge/MIRDLeftKidney/offsetX = -6. cm
d:Ge/MIRDLeftKidney/offsetY = 0. cm
d:Ge/MIRDLeftKidney/offsetZ = 0. cm
dc:Ge/MIRDLeftKidney/TransX = 6. cm
dc:Ge/MIRDLeftKidney/TransY = 6. cm
dc:Ge/MIRDLeftKidney/TransZ = -2.50 cm
s:Ge/MIRDLeftKidney/Color = "green"
s:Ge/MIRDLeftKidney/DrawingStyle = "Solid"
```

Figure 42 : *The algorithm for the left kidney volume.*

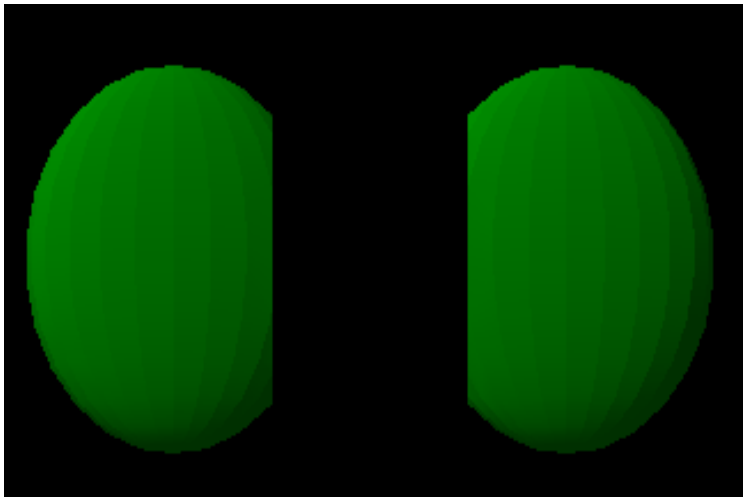

Figure 43 : *TOPAS MC representation of the left and right kidney.*

The liver is defined by an elliptical cylinder cut by a plan, mathematically it is represented by inequation 4.10

$$\left.\begin{array}{l} \left(\frac{x}{16.5}\right)^2 + \left(\frac{y}{8}\right)^2 \leq 1 \\ \frac{x}{35} + \frac{y}{45} - \frac{z}{43} \leq -1 \\ 27 \leq z \leq 43 \end{array}\right\} \quad (\mathbf{4.10})$$

The liver is composed of soft tissue material and it has a volume of 1833 cm^3.

Figure 44 represents the algorithm to create this volume in TOPAS MC:

```
s:Ge/MIRDLiver/Parent = "MIRDTrunk"
s:Ge/MIRDLiver/Type = "MIRDLiver"
s:Ge/MIRDLiver/Material = "soft_tissue"
d:Ge/MIRDLiver/dx = 14.19 cm
d:Ge/MIRDLiver/dy = 7.84 cm
d:Ge/MIRDLiver/dz = 7.21 cm
d:Ge/MIRDLiver/xx = 20.00 cm
d:Ge/MIRDLiver/yy = 50.00 cm
d:Ge/MIRDLiver/zz = 50.00 cm
dc:Ge/MIRDLiver/angle1 = 32. deg
dc:Ge/MIRDLiver/angle2 = 40.9 deg
dc:Ge/MIRDLiver/angle3 = 180. deg
d:Ge/MIRDLiver/offsetX = 10.00 cm
d:Ge/MIRDLiver/offsetY = 0.0 cm
d:Ge/MIRDLiver/offsetZ = 0.0 cm
dc:Ge/MIRDLiver/TransX = 0.0 cm
dc:Ge/MIRDLiver/TransY = 0.0 cm
dc:Ge/MIRDLiver/TransZ = 0.0 cm
dc:Ge/MIRDLiver/RotX = 180.0 deg
s:Ge/MIRDLiver/Color = "orange"
s:Ge/MIRDLiver/DrawingStyle = "Solid"
```

Figure 44 : *The algorithm for the liver volume.*

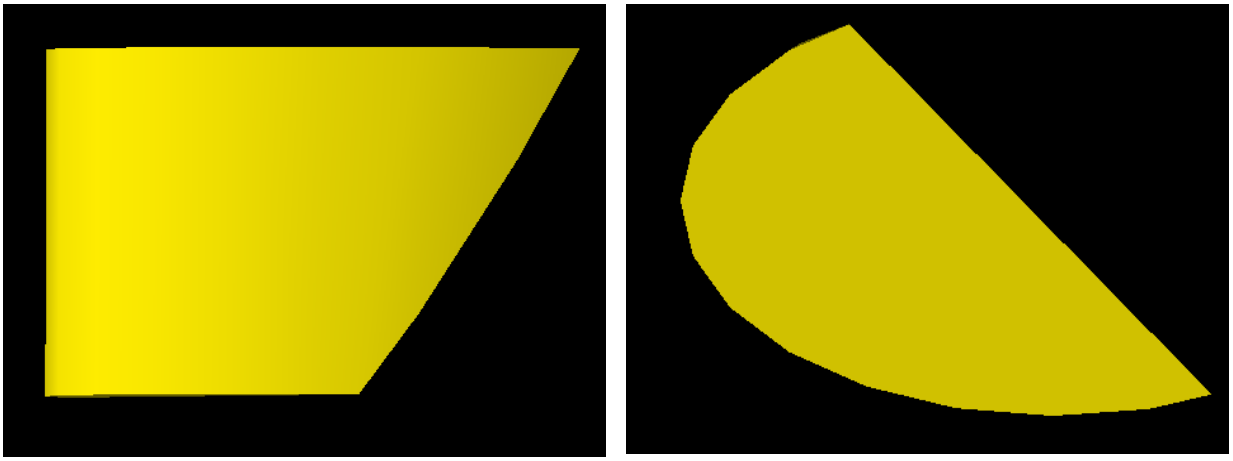

Figure 45 : *TOPAS MC representation of the liver volume (left: front view, right: top view).*

The stomach is an ellipsoid, its inequation is:

$$\left(\frac{x-8}{4}\right)^2\left(\frac{y+4}{3}\right)^2\left(\frac{z-35}{8}\right)^2 \leq 1 \quad (\mathbf{4.11})$$

It is made of soft tissue material.

The following algorithm is used to obtain this volume:

```
s:Ge/MIRDStomach/Parent = "MIRDTrunk"
s:Ge/MIRDStomach/Type = "G4Ellipsoid"
s:Ge/MIRDStomach/Material = "soft_tissue"
d:Ge/MIRDStomach/HLX = 4.5 cm
d:Ge/MIRDStomach/HLY = 3. cm
d:Ge/MIRDStomach/HLZ = 8. cm
dc:Ge/MIRDStomach/ZTop = 8. cm
dc:Ge/MIRDStomach/ZBottom = -8. cm
dc:Ge/MIRDStomach/TransX = 8.0 cm
dc:Ge/MIRDStomach/TransY = -4.0 cm
dc:Ge/MIRDStomach/TransZ = 0.0 cm
s:Ge/MIRDStomach/Color = "orange"
s:Ge/MIRDStomach/DrawingStyle = "Solid"
```

Figure 46 : *The algorithm of the stomach volume.*

The stomach's cavity, which is an improvement made by Guatelli et al. is also an ellipsoid that is defined mathematically by the following inequation:

$$\left(\frac{x-8}{3.387}\right)^2 + \left(\frac{y+4}{2.387}\right)^2 + \left(\frac{z-35}{7.387}\right)^2 \leq 1 \quad (\mathbf{4.12})$$

It is composed of air.

```
s:Ge/MIRDCavity/Parent = "MIRDStomach"
s:Ge/MIRDCavity/Type = "G4Ellipsoid"
s:Ge/MIRDCavity/Material = "G4_AIR"
d:Ge/MIRDCavity/HLX = 3.387 cm
d:Ge/MIRDCavity/HLY = 2.387 cm
d:Ge/MIRDCavity/HLZ = 7.387 cm
dc:Ge/MIRDCavity/ZTop = 7.387 cm
dc:Ge/MIRDCavity/ZBottom = -7.387 cm
dc:Ge/MIRDCavity/TransX = 0.0 cm
dc:Ge/MIRDCavity/TransY = 0.0 cm
dc:Ge/MIRDCavity/TransZ = 0.0 cm
s:Ge/MIRDCavity/DrawingStyle = "Solid"
```

Figure 47 : *the algorithm to create the stomach's cavity volume.*

Figure 48: *TOPAS MC representation of the stomach volume (yellow) and the stomach's cavity (white).*

The pancreas is half an ellipsoid with a section removed, it is defined by the following inequations:

$$\left.\begin{array}{c} \left(\frac{x}{15}\right)^2 + y^2 + \leq \left(\frac{z-37}{3}\right)^2 \leq 1 \\ x \geq 0 \\ z \geq 37 \quad if \quad x > 3 \end{array}\right\} \quad (\mathbf{4.13})$$

It is filled with the soft tissue material and it has a volume of 61.07 cm^3.

Figure 49 represents the lines of code that allow to create the volume of the pancreas.

```
s:Ge/MIRDPancreas/Parent = "MIRDTrunk"
s:Ge/MIRDPancreas/Type = "MIRDPancreas"
s:Ge/MIRDPancreas/Material = "soft_tissue"
d:Ge/MIRDPancreas/ax = 3. cm
d:Ge/MIRDPancreas/by = 1. cm
d:Ge/MIRDPancreas/cz = 15. cm
d:Ge/MIRDPancreas/zcut1 = -15. cm
d:Ge/MIRDPancreas/zcut2 = 0.0 cm
d:Ge/MIRDPancreas/xx = 6. cm
d:Ge/MIRDPancreas/yy = 2. cm
d:Ge/MIRDPancreas/zz = 12. cm
d:Ge/MIRDPancreas/offsetX = -3. cm
d:Ge/MIRDPancreas/offsetY = 0.0 cm
d:Ge/MIRDPancreas/offsetZ = -9. cm
dc:Ge/MIRDPancreas/TransX = 0.0 cm
dc:Ge/MIRDPancreas/TransY = 0.0 cm
dc:Ge/MIRDPancreas/TransZ = 2. cm
dc:Ge/MIRDPancreas/RotY = 90. deg
s:Ge/MIRDPancreas/Color = "purple"
s:Ge/MIRDPancreas/DrawingStyle = "Solid"
```

Figure 49 : *The algorithm for the pancreas volume.*

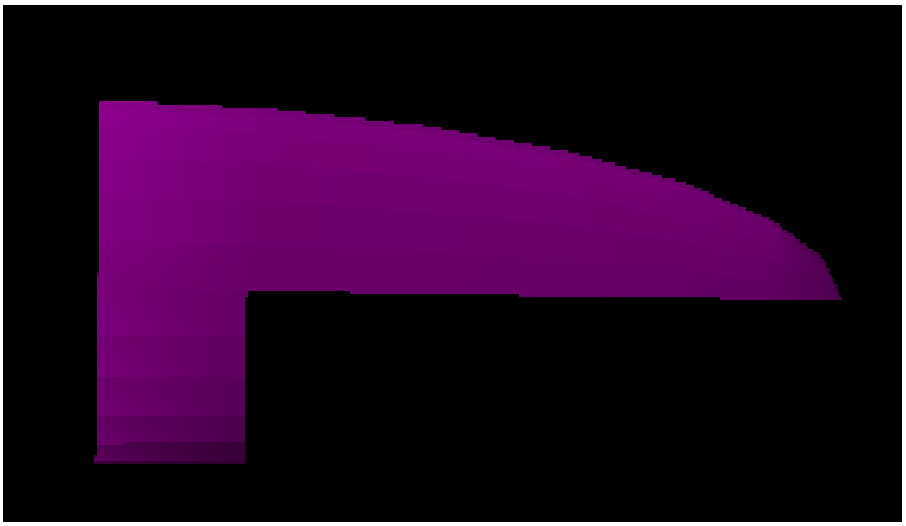

Figure 50 : *TOPAS MC representation of the pancreas volume.*

The spleen is represented by a simple ellipsoid given by inequation 4.14

$$\left(\frac{x-11}{3.5}\right)^2+\left(\frac{y-3}{2}\right)^2+\left(\frac{z-37}{6}\right)^2\leq 1 \quad (\mathbf{4.14})$$

It has a volume of 175.93 cm^3 and it entirely composed of soft tissue.

To represent it in TOPAS MC, the following algorithm is needed.

```
s:Ge/MIRDSpleen/Parent = "MIRDTrunk"
s:Ge/MIRDSpleen/Type = "G4Ellipsoid"
s:Ge/MIRDSpleen/Material = "soft_tissue"
d:Ge/MIRDSpleen/HLX = 3.5 cm
d:Ge/MIRDSpleen/HLY = 2. cm
d:Ge/MIRDSpleen/HLZ = 6. cm
d:Ge/MIRDSpleen/TransX = 11. cm
d:Ge/MIRDSpleen/TransY = 3. cm
d:Ge/MIRDSpleen/TransZ = 2. cm
s:Ge/MIRDSpleen/Color = "green"
s:Ge/MIRDSpleen/DrawingStyle = "Solid"
```

Figure 51 : *The algorithm of the spleen volume.*

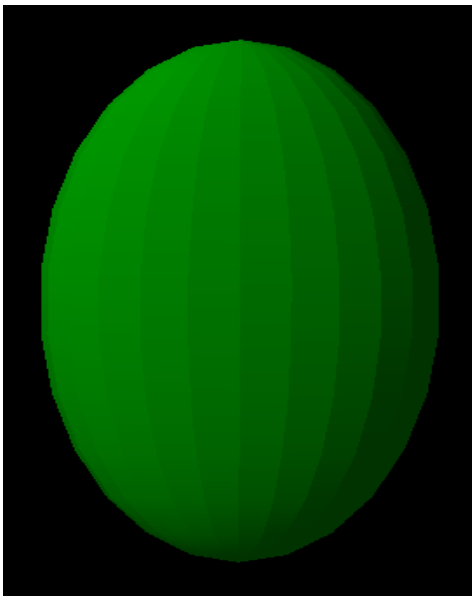

Figure 52 : *TOPAS MC representation of the spleen volume.*

The thymus is also represented as an ellipsoid that is given by inequation 4.15

$$\left(\frac{x\ +\ 2}{3}\right)^2 + \left(\frac{y\ +\ 6}{0.5}\right)^2 + \left(\frac{z\ -\ 60.5}{4}\right)^2 \leq\ 1 \quad (\mathbf{4.15})$$

It has a volume of 25.13 cm^3 and it is composed of soft tissue.

```
s:Ge/MIRDThymus/Parent = "MIRDTrunk"
s:Ge/MIRDThymus/Type = "G4Ellipsoid"
s:Ge/MIRDThymus/Material = "soft_tissue"
d:Ge/MIRDThymus/HLX = 3. cm
d:Ge/MIRDThymus/HLY = 0.5 cm
d:Ge/MIRDThymus/HLZ = 4. cm
d:Ge/MIRDThymus/TransX = 2. cm
d:Ge/MIRDThymus/TransY = -6. cm
d:Ge/MIRDThymus/TransZ = 25.5 cm
s:Ge/MIRDThymus/Color = "orange"
s:Ge/MIRDThymus/DrawingStyle = "Solid"
```

Figure 53 : *The algorithm of the thymus volume.*

The small intestine is represented by inequation 4.16

$$\left.\begin{array}{c} x^2\ +(y\ +\ 3.8)^2\ \leq (11.3)^2 \\ -7\ \leq\ y \leq\ 3 \\ 17\ \leq\ z \leq\ 27 \end{array}\right\} \quad (\mathbf{4.16})$$

It has a volume of 1.696 cm^3 and it is composed of soft tissue.

Figure 54 represents the line of code that creates the small intestine

```
s:Ge/MIRDSmallIntestine/Parent = "MIRDTrunk"
s:Ge/MIRDSmallIntestine/Type = "MIRDSmallIntestine"
s:Ge/MIRDSmallIntestine/Material = "soft_tissue"
d:Ge/MIRDSmallIntestine/boxX = 11. cm
d:Ge/MIRDSmallIntestine/boxY = 3.53 cm
d:Ge/MIRDSmallIntestine/boxZ = 5. cm
d:Ge/MIRDSmallIntestine/tubsRmin = 0.0 cm
d:Ge/MIRDSmallIntestine/tubsRmax = 11. cm
d:Ge/MIRDSmallIntestine/tubsZ = 5. cm
d:Ge/MIRDSmallIntestine/tubsSphi = 0. degree
d:Ge/MIRDSmallIntestine/tubsDphi = 360. degree
d:Ge/MIRDSmallIntestine/xx = 0. cm
d:Ge/MIRDSmallIntestine/yy = -1.33 cm
d:Ge/MIRDSmallIntestine/zz = 0. cm
d:Ge/MIRDSmallIntestine/xx1 = 0. cm
d:Ge/MIRDSmallIntestine/yy1 = 0.8 cm
d:Ge/MIRDSmallIntestine/zz1 = 0. cm
d:Ge/MIRDSmallIntestine/xx2 = -8.0 cm
d:Ge/MIRDSmallIntestine/yy2 = 0.0 cm
d:Ge/MIRDSmallIntestine/zz2 = 6.275 cm
d:Ge/MIRDSmallIntestine/xx3 = -16.72 cm
d:Ge/MIRDSmallIntestine/yy3 = 0.0 cm
d:Ge/MIRDSmallIntestine/zz3 = -2.865 cm
d:Ge/MIRDSmallIntestine/xx4 = 8.0 cm
d:Ge/MIRDSmallIntestine/yy4 = -0.3 cm
d:Ge/MIRDSmallIntestine/zz4 = -2.775 cm
d:Ge/MIRDSmallIntestine/dx = 2.50 cm
d:Ge/MIRDSmallIntestine/dy = 2.50 cm
d:Ge/MIRDSmallIntestine/dz = 4.775 cm
d:Ge/MIRDSmallIntestine/dx1 = 2.50 cm
d:Ge/MIRDSmallIntestine/dy1 = 1.50 cm
d:Ge/MIRDSmallIntestine/dz1 = 10.50 cm
d:Ge/MIRDSmallIntestine/dx2 = 1.88 cm
d:Ge/MIRDSmallIntestine/dy2 = 2.13 cm
d:Ge/MIRDSmallIntestine/dz2 = 7.64 cm
dc:Ge/MIRDSmallIntestine/angle1 = 90. deg
dc:Ge/MIRDSmallIntestine/angle2 = 90. deg
dc:Ge/MIRDSmallIntestine/angle3 = 180. deg
dc:Ge/MIRDSmallIntestine/angle4 = 180. deg
dc:Ge/MIRDSmallIntestine/TransX = 0. cm
dc:Ge/MIRDSmallIntestine/TransY = -2.66 cm
dc:Ge/MIRDSmallIntestine/TransZ = -13. cm
dc:Ge/MIRDSmallIntestine/RotX = 0. deg
dc:Ge/MIRDSmallIntestine/RotY = 0. deg
dc:Ge/MIRDSmallIntestine/RotZ = 180. deg
s:Ge/MIRDSmallIntestine/Color = "orange"
s:Ge/MIRDSmallIntestine/DrawingStyle = "Solid"
```

Figure 54 : *The algorithm for the small intestine volume.*

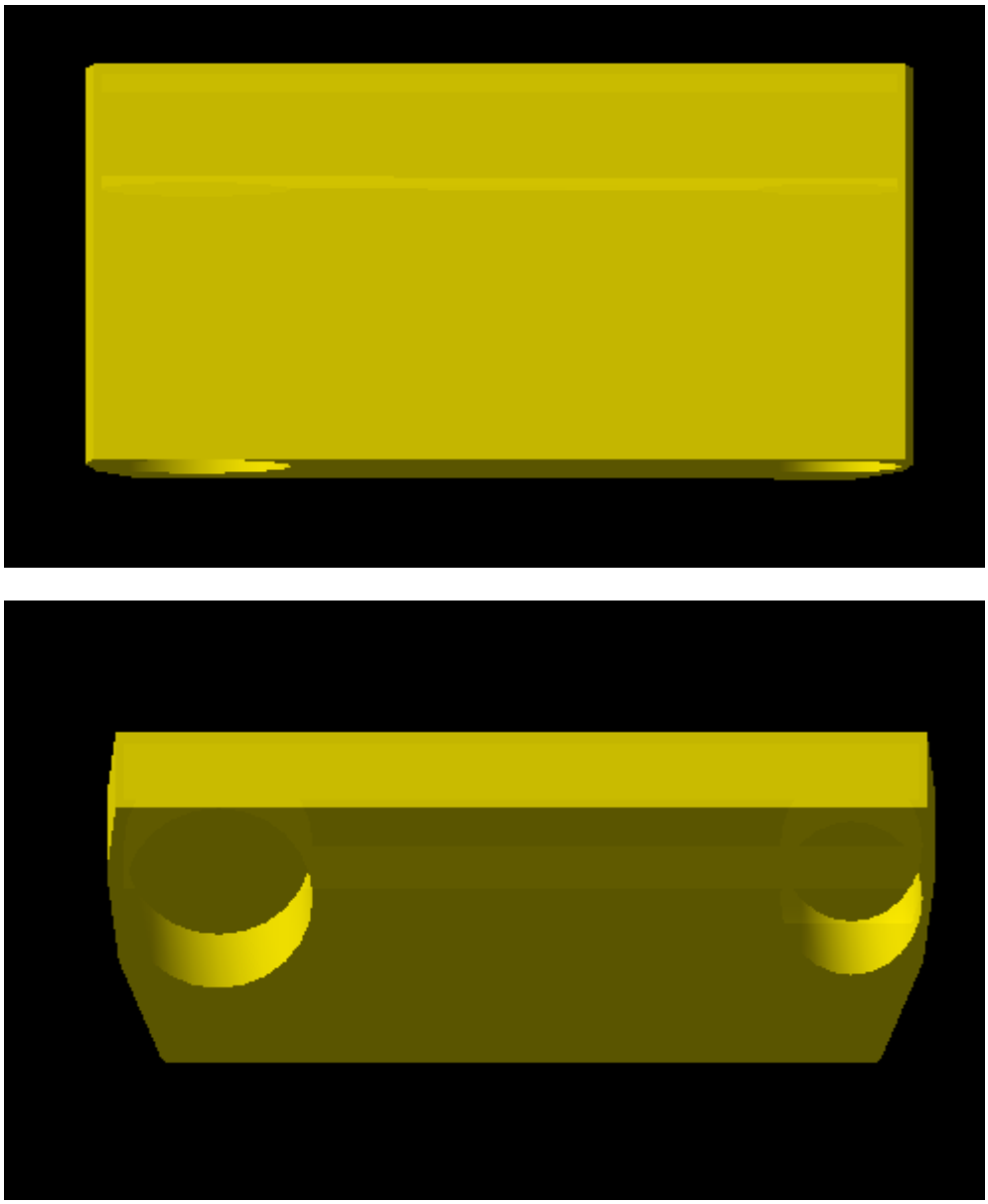

Figure 55 : *TOPAS MC representation of the small intestine volume (up: front view, down: bottom view).*

The urinary bladder is represented by an ellipsoid which is defined by the following inequation:

$$\left(\frac{x}{6}\right)^2 + \left(\frac{y + 4.5}{4.5}\right)^2 + \left(\frac{z - 8}{4.5}\right)^2 \leq 1 \quad (\mathbf{4.17})$$

It is considered moderately full and its volume is 508.94 cm^3.

In order to get this volume in TOPAS MC the following algorithm is needed:

```
s:Ge/MIRDUrinaryBladder/Parent = "MIRDTrunk"
s:Ge/MIRDUrinaryBladder/Type = "MIRDUrinaryBladder"
s:Ge/MIRDUrinaryBladder/Material = "soft_tissue"
d:Ge/MIRDUrinaryBladder/ax = 4.958 cm
d:Ge/MIRDUrinaryBladder/by = 3.458 cm
d:Ge/MIRDUrinaryBladder/cz = 3.458 cm
d:Ge/MIRDUrinaryBladder/dx = 4.706 cm
d:Ge/MIRDUrinaryBladder/dy = 3.206 cm
d:Ge/MIRDUrinaryBladder/dz = 3.206 cm
dc:Ge/MIRDUrinaryBladder/TransX = 0.0 cm
dc:Ge/MIRDUrinaryBladder/TransY = -4.5 cm
dc:Ge/MIRDUrinaryBladder/TransZ = -27. cm
s:Ge/MIRDUrinaryBladder/Color = "green"
s:Ge/MIRDUrinaryBladder/DrawingStyle = "Solid"
```

Figure 56 : *The algorithm for the urinary bladder volume.*

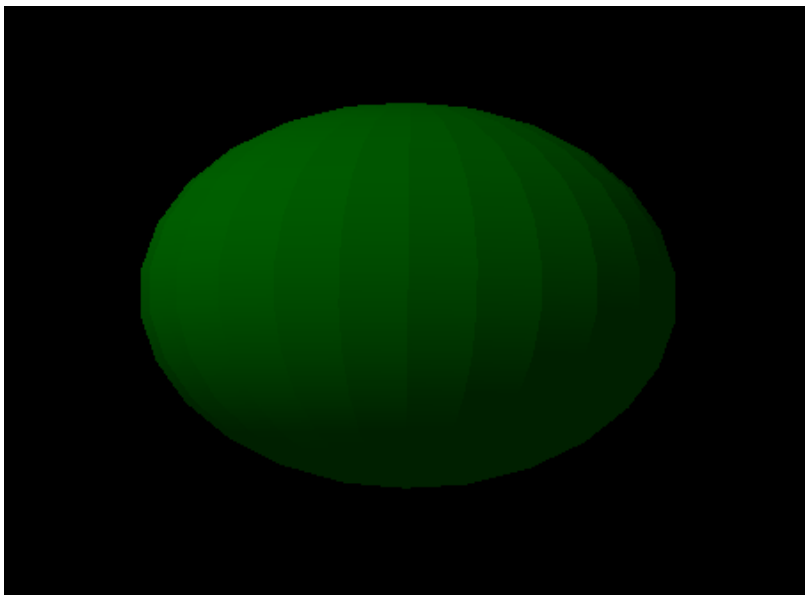

Figure 57 : *TOPAS MC representation of the urinary bladder volume.*

3) Left and right legs:

The legs were created based on the improved version of the phantom made by Guatelli et al. since their phantom has separate legs whereas the original phantom has just one truncated elliptical cone that is supposed to represent both legs.

Each leg is represented by a cone and the following algorithm allows the creation of the left leg.

```
s:Ge/MIRDLeftLeg/Parent = "MIRD"
s:Ge/MIRDLeftLeg/Type = "G4Cons"
s:Ge/MIRDLeftLeg/Material = "soft_tissue"
d:Ge/MIRDLeftLeg/RMin1 = 0. cm
d:Ge/MIRDLeftLeg/RMax1 = 2.0 cm
d:Ge/MIRDLeftLeg/RMin2 = 0. cm
d:Ge/MIRDLeftLeg/RMax2 = 10. cm
d:Ge/MIRDLeftLeg/HL = 40.0 cm
d:Ge/MIRDLeftLeg/SPhi = 0. deg
d:Ge/MIRDLeftLeg/DPhi = 360. deg
d:Ge/MIRDLeftLeg/TransX = 10. cm
d:Ge/MIRDLeftLeg/TransY = 0. cm
d:Ge/MIRDLeftLeg/TransZ = -40. cm
d:Ge/MIRDLeftLeg/RotX = 180. deg
d:Ge/MIRDLeftLeg/RotY = 180. deg
s:Ge/MIRDLeftLeg/Color = "yellow"
s:Ge/MIRDLeftLeg/DrawingStyle = "Solid"
```

Figure 58 : *The algorithm for the left leg.*

Each leg contains a cone made of skeleton material to represent leg bone; this is achieved by inserting the following algorithm.

```
s:Ge/MIRDLeftLegBone/Parent = "MIRDLeftLeg"
s:Ge/MIRDLeftLegBone/Type = "G4Cons"
s:Ge/MIRDLeftLegBone/Material = "skeleton"
d:Ge/MIRDLeftLegBone/RMin1 = 0.0 cm
d:Ge/MIRDLeftLegBone/RMin2 = 0.0 cm
d:Ge/MIRDLeftLegBone/RMax1 = 1. cm
d:Ge/MIRDLeftLegBone/RMax2 = 3.5 cm
d:Ge/MIRDLeftLegBone/SPhi = 0. deg
d:Ge/MIRDLeftLegBone/DPhi = 360. deg
d:Ge/MIRDLeftLegBone/HL = 39.9 cm
d:Ge/MIRDLeftLegBone/TransX = 0.0 cm
d:Ge/MIRDLeftLegBone/TransY = 0.0 cm
d:Ge/MIRDLeftLegBone/TransZ = 0.1 cm
s:Ge/MIRDLeftLegBone/Color = "grey"
s:Ge/MIRDLeftLegBone/DrawingStyle = "Solid"
```

Figure 59 : *The algorithm for the left leg bone.*

More on the improvements made by Guatelli's team, they have decided to create two separate sex-based phantoms rather than the hermaphrodite phantom created by Snyder's team that already contains testicles, ovaries and a uterus.

The female anthropomorphic phantom differs from the male anthropomorphic phantom in five organs that are sex-specific to it: a uterus, two ovaries, located inside the trunk, and two breasts located outside of the trunk.

The ovaries are represented by ellipsoids, inequation 4.18 defines the left ovary

$$(x - 6)^2 + \left(\frac{y}{0.5}\right)^2 + \left(\frac{z - 15}{2}\right)^2 \leq 1 \quad (\mathbf{4.18})$$

It is composed of soft tissue and it has a volume of 4.19 cm^3.

In order to get the right ovary, a rotation of 180° around the z axis is needed.

In TOPAS MC this volume is easily obtained by inserting the following line of code:

```
s:Ge/MIRDLeftOvary/Parent = "MIRDTrunk"
s:Ge/MIRDLeftOvary/Type = "G4Ellipsoid"
s:Ge/MIRDLeftOvary/Material = "soft_tissue"
d:Ge/MIRDLeftOvary/HLX = 1. cm
d:Ge/MIRDLeftOvary/HLY = 0.5 cm
d:Ge/MIRDLeftOvary/HLZ = 2. cm
d:Ge/MIRDLeftOvary/TransX = -6. cm
d:Ge/MIRDLeftOvary/TransY = 0.5 cm
d:Ge/MIRDLeftOvary/TransZ = -20. cm
s:Ge/MIRDLeftOvary/Color = "purple"
s:Ge/MIRDLeftOvary/DrawingStyle = "Solid"
```

Figure 60 : *The algorithm for the left ovary volume.*

The uterus is also an ellipsoid but it is cut by a plan, inequation 4.19 gives its mathematical representation

$$\left.\begin{array}{c}\left(\frac{x}{2.5}\right)^2\left(\frac{y+2}{5}\right)^2\left(\frac{z-14}{1.5}\right)^2 \leq 1 \\ y \geq -4.5\end{array}\right\} \quad (\mathbf{4.19})$$

It is considered to be entirely composed of soft tissue material and it has an overall volume of 66.27 cm^3.

Figure 61 represent the code that creates the uterus in TOPAS MC.

```
s:Ge/MIRDUterus/Parent = "MIRDTrunk"
s:Ge/MIRDUterus/Type = "G4Ellipsoid"
s:Ge/MIRDUterus/Material = "soft_tissue"
d:Ge/MIRDUterus/HLX = 2.5 cm
d:Ge/MIRDUterus/HLY = 1.5 cm
d:Ge/MIRDUterus/HLZ = 5.0 cm
d:Ge/MIRDUterus/ZTop = 2.5 cm
d:Ge/MIRDUterus/ZBottom = -5. cm
d:Ge/MIRDUterus/RotX = 90. deg
d:Ge/MIRDUterus/TransX = 0. cm
d:Ge/MIRDUterus/TransY = 2. cm
d:Ge/MIRDUterus/TransZ = -21. cm
s:Ge/MIRDUterus/Color = "purple"
s:Ge/MIRDUterus/DrawingStyle = "Solid"
```

Figure 61 : *The algorithm for the uterus volume.*

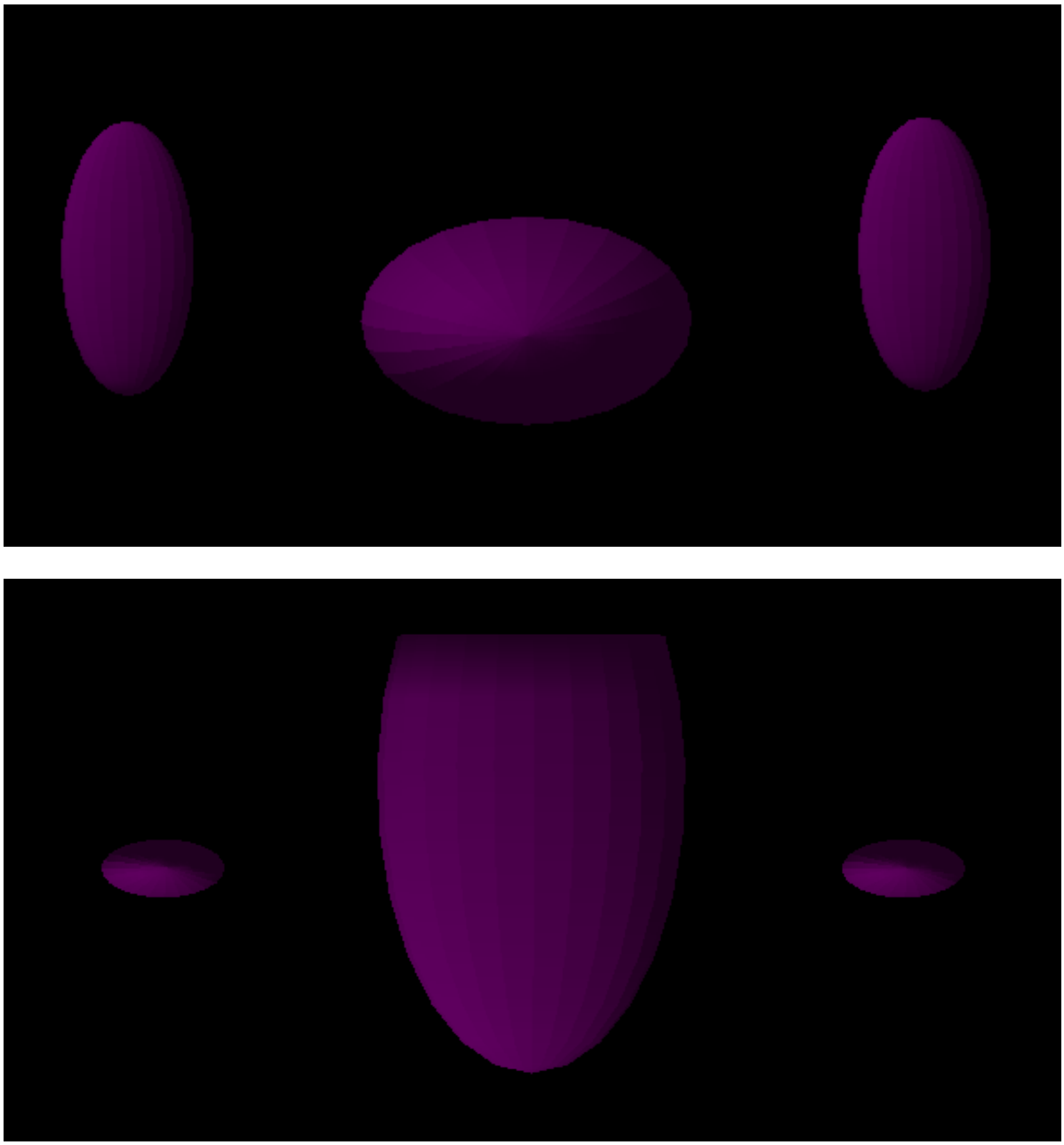

Figure 62 : *TOPAS MC representation of the uterus and the two ovaries' volumes (up: front view; down: upper view).*

The breasts are an improvement implemented by Guatelli's team, they don't have the trunk as a mother volume since they are located outside of it, they are made of soft tissue material.

The line of code that creates the left breast in TOPAS MC is shown in figure 63, getting the right breast simply needs a rotation by 180° around the z axis.

```
s:Ge/MIRDLeftBreast/Parent = "MIRD"
s:Ge/MIRDLeftBreast/Type = "MIRDBreast"
s:Ge/MIRDLeftBreast/Material = "soft_tissue"
d:Ge/MIRDLeftBreast/ax = 4.95 cm
d:Ge/MIRDLeftBreast/by = 4.35 cm
d:Ge/MIRDLeftBreast/cz = 4.15 cm
d:Ge/MIRDLeftBreast/dx = 20. cm
d:Ge/MIRDLeftBreast/dy = 10. cm
d:Ge/MIRDLeftBreast/dz = 35. cm
d:Ge/MIRDLeftBreast/angle1 = 90. deg
d:Ge/MIRDLeftBreast/offsetX = -10. cm
d:Ge/MIRDLeftBreast/offsetY = 0.0 cm
d:Ge/MIRDLeftBreast/offsetZ = -8.66 cm
dc:Ge/MIRDLeftBreast/RotX = 90. deg
dc:Ge/MIRDLeftBreast/RotY = 0. deg
dc:Ge/MIRDLeftBreast/RotZ = 16. deg
dc:Ge/MIRDLeftBreast/TransX = 10.0 cm
dc:Ge/MIRDLeftBreast/TransY = 9.1 cm
dc:Ge/MIRDLeftBreast/TransZ = 52.0 cm
s:Ge/MIRDLeftBreast/Color = "magenta"
s:Ge/MIRDLeftBreast/DrawingStyle = "Solid"
```

Figure 63 : *The algorithm for the left breast.*

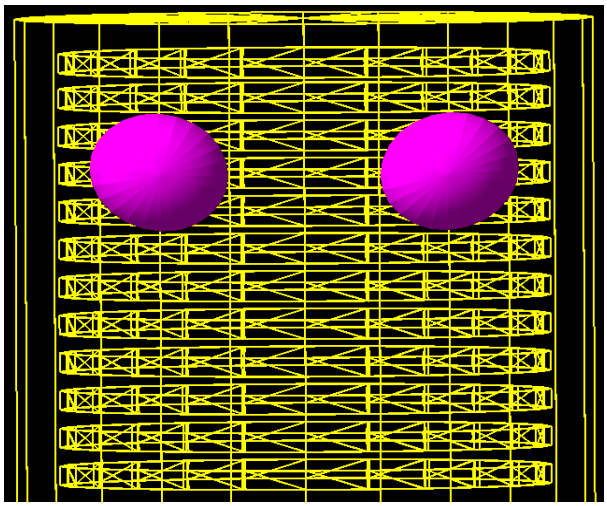

Figure 64 : *TOPAS MC representation of the breasts and rib cage volumes.*

As for the male anthropomorphic phantom, its specific organs are the male genitalia and two testes.

The same as for the breast, the male genitalia was an improvement implemented by Guatelli's team, it is made of soft tissue material and located under the trunk in a space on top of both legs in order to simulate the real anatomy of a male.

Figure 65 represents the line of code that creates this organ.

```
s:Ge/MIRDMaleGenitalia/Parent = "MIRD"
s:Ge/MIRDMaleGenitalia/Type = "MIRDMaleGenitalia"
s:Ge/MIRDMaleGenitalia/Material = "soft_tissue"
d:Ge/MIRDMaleGenitalia/pDz = 2.4 cm
d:Ge/MIRDMaleGenitalia/pTheta = 0. deg
d:Ge/MIRDMaleGenitalia/pPhi = 0. deg
d:Ge/MIRDMaleGenitalia/pDy1 = 4.76 cm
d:Ge/MIRDMaleGenitalia/pDx1 = 9.52 cm
d:Ge/MIRDMaleGenitalia/pDx2 = 9.52 cm
d:Ge/MIRDMaleGenitalia/pAlp1 = 0. deg
d:Ge/MIRDMaleGenitalia/pDy2 = 5. cm
d:Ge/MIRDMaleGenitalia/pDx3 = 10. cm
d:Ge/MIRDMaleGenitalia/pDx4 = 10. cm
d:Ge/MIRDMaleGenitalia/pAlp2 = 0. deg
d:Ge/MIRDMaleGenitalia/rmin1 = 0. cm
d:Ge/MIRDMaleGenitalia/rmin2 = 0. cm
d:Ge/MIRDMaleGenitalia/dz = 5. cm
d:Ge/MIRDMaleGenitalia/rmax1 = 9.51 cm
d:Ge/MIRDMaleGenitalia/rmax2 = 10.01 cm
d:Ge/MIRDMaleGenitalia/startphi = 0. deg
d:Ge/MIRDMaleGenitalia/deltaphi = 360. deg
d:Ge/MIRDMaleGenitalia/offsetX = 20.00 cm
d:Ge/MIRDMaleGenitalia/offsetY = 0.0 cm
d:Ge/MIRDMaleGenitalia/offsetZ = 0.0 cm
d:Ge/MIRDMaleGenitalia/offsetX1 = -10.00 cm
d:Ge/MIRDMaleGenitalia/offsetY1 = -5.0 cm
d:Ge/MIRDMaleGenitalia/offsetZ1 = 0.0 cm
dc:Ge/MIRDMaleGenitalia/TransX = 0.0 cm
dc:Ge/MIRDMaleGenitalia/TransY = 5.0 cm
dc:Ge/MIRDMaleGenitalia/TransZ = -2.4 cm
s:Ge/MIRDMaleGenitalia/Color = "yellow"
s:Ge/MIRDMaleGenitalia/DrawingStyle = "Solid"
```

Figure 65 : *The algorithm for the male genitalia.*

The testicles are represented by two ellipsoids made of soft tissue material; each one has a volume of 18.79 cm^3.

The left testicle is given by inequation 4.20

$$\left(\frac{x - 1.3}{1.3}\right)^2 + \left(\frac{y + 2.2}{1.5}\right)^2 + \left(\frac{z + 2.3}{2.3}\right)^2 \leq 1 \quad (\mathbf{4.20})$$

To represent it in TOPAS MC the following code is needed:

```
s:Ge/MIRDLeftTeste/Parent = "MIRDMaleGenitalia"
s:Ge/MIRDLeftTeste/Type = "G4Ellipsoid"
s:Ge/MIRDLeftTeste/Material = "soft_tissue"
d:Ge/MIRDLeftTeste/HLX = 1.3 cm
d:Ge/MIRDLeftTeste/HLY = 1.5 cm
d:Ge/MIRDLeftTeste/HLZ = 2.3 cm
d:Ge/MIRDLeftTeste/TransX = -1.4 cm
d:Ge/MIRDLeftTeste/TransY = 3. cm
d:Ge/MIRDLeftTeste/TransZ = 0. cm
s:Ge/MIRDLeftTeste/Color = "yellow"
s:Ge/MIRDLeftTeste/DrawingStyle = "Solid"
```

Figure 66 : *The algorithm for the left testicle volume.*

3.2.2. Particle sources

After defining the geometry, we proceeded to define the particle sources, in our case study the radioactive element is ^{131}I which emits beta and gamma particles with each disintegration, since TOPAS MC is not equipped with libraries that contain the probabilities for each transition of each radioisotopes, those probabilities should be considered as inputs for the user, that is why choosing the iodine spectrum is the first step, this choice is based on the literature and for this simulation we agreed on the following spectrum:

ENERGY (KEV)	PROBABILITY (%)
606.3	89.4
333.8	7.2
247.9	2.13
303.9	0.643
806.9	0.386
629.7	0.06

Table 3 : *^{131}I β^- Transitions (226).*

ENERGY (KEV)	PROBABILITY (%)
364.490	83.1
636.990	7.15
284.305	6.45
80.1854	6.63
722.909	1.794
503.004	0.3571

Table 4 : *^{131}I γ Transitions (226).*

Defining a source volume in TOPAS MC is simple, first of all, we start by defining which type of source we are going to work with depending on the situation being simulated; when it comes to ingested radioisotopes in general and iodine in particular we consider that they are uniformly distributed in the source organ, as a result we choose the volumetric source type because it is the most suitable for an ingested iodine capsule, this choice stays relevant even when the substance passes on to other organs.

Then, the volume in which our particles disintegrate must be chosen depending on the procedure that is being simulated, so in the case of ^{131}I-Na capsule the first step in its absorption is the stomach, and protocol for iodine radiotherapy dictates that this capsule should be taken on an empty stomach, so, in order to achieve a realistic setting the cavity of the stomach was created filled with air and it is only natural that this cavity will be chosen as the first source of radiation.

Figure 67 represents the algorithm that allows for the disintegration of the ^{131}I in the stomach's cavity.

```
s:So/MySource_Beta_Stomach_Cavity/Type = "Volumetric"
s:So/MySource_Beta_Stomach_Cavity/ActiveMaterial = "G4_AIR"
s:So/MySource_Beta_Stomach_Cavity/Component = "MIRDCavity"
s:So/MySource_Beta_Stomach_Cavity/BeamParticle = "e-"
s:So/MySource_Beta_Stomach_Cavity/BeamEnergySpectrumType = "Continuous"
dv:So/MySource_Beta_Stomach_Cavity/BeamEnergySpectrumValues = 6 606.3
333.8 247.9 303.9 806.9 629.7 keV
uv:So/MySource_Beta_Stomach_Cavity/BeamEnergySpectrumWeights = 6 0.89562107414
0.0721305563 0.0213386229 0.0064416594 0.00386699926 0.00060108796
ic:So/MySource_Beta_Stomach_Cavity/NumberOfHistoriesInRun = 100000000

s:So/MySource_Gamma_Stomach_Cavity/Type = "Volumetric"
s:So/MySource_Gamma_Stomach_Cavity/ActiveMaterial = "G4_AIR"
s:So/MySource_Gamma_Stomach_Cavity/Component = "MIRDCavity"
s:So/MySource_Gamma_Stomach_Cavity/BeamParticle = "gamma"
s:So/MySource_Gamma_Stomach_Cavity/BeamEnergySpectrumType = "Discrete"
dv:So/MySource_Gamma_Stomach_Cavity/BeamEnergySpectrumValues = 6 364.490
636.990 284.305 80.1854 722.909 503.004 keV
uv:So/MySource_Gamma_Stomach_Cavity/BeamEnergySpectrumWeights = 6 0.78781960732
0.06778471952 0.06114845327 0.06285492173 0.01700780235 0.00338544382
ic:So/MySource_Gamma_Stomach_Cavity/NumberOfHistoriesInRun = 100000000
```

Figure 67 : *The algorithm for the stomach's cavity as a source.*

Since iodine is absorbed in the small intestine, this organ should be considered as the second source while accounting for the number of nuclei that has already disintegrated in the stomach.

The algorithm is identical to that used in the stomach's cavity seeing that all the parameters stay the same, only two parameters should be changed: the active material and the component.

Figure 68 represents the line of code that will launch the disintegration of ^{131}I in the intestine.

```
s:So/MySource_Beta_Small_Intestine/Type = "Volumetric"
s:So/MySource_Beta_Small_Intestine/ActiveMaterial = "soft_tissue"
s:So/MySource_Beta_Small_Intestine/Component = "MIRDSmallIntestine"
s:So/MySource_Beta_Small_Intestine/BeamParticle = "e-"
s:So/MySource_Beta_Small_Intestine/BeamEnergySpectrumType = "Continuous"
dv:So/MySource_Beta_Small_Intestine/BeamEnergySpectrumValues = 6 606.3
333.8 247.9 303.9 806.9 629.7 keV
uv:So/MySource_Beta_Small_Intestine/BeamEnergySpectrumWeights = 6 0.89562107414
0.0721305563 0.0213386229 0.0064416594 0.00386699926 0.00060108796
ic:So/MySource_Beta_Small_Intestine/NumberOfHistoriesInRun = 100000000

s:So/MySource_Gamma_Small_Intestine/Type = "Volumetric"
s:So/MySource_Gamma_Small_Intestine/ActiveMaterial = "soft_tissue"
s:So/MySource_Gamma_Small_Intestine/Component = "MIRDSmallIntestine"
s:So/MySource_Gamma_Small_Intestine/BeamParticle = "gamma"
s:So/MySource_Gamma_Small_Intestine/BeamEnergySpectrumType = "Discrete"
dv:So/MySource_Gamma_Small_Intestine/BeamEnergySpectrumValues = 6 364.490
636.990 284.305 80.1854 722.909 503.004 keV
uv:So/MySource_Gamma_Small_Intestine/BeamEnergySpectrumWeights = 6 0.78781960732
0.06778471952 0.06114845327 0.06285492173 0.01700780235 0.00338544382
ic:So/MySource_Gamma_Small_Intestine/NumberOfHistoriesInRun = 100000000
```

Figure 68 : *The algorithm for the small intestine as a source.*

After its absorption, iodine is quickly transported to the thyroid where it is going to exercise its main action of radiotherapy, so this organ is selected as the third source of disintegration.

Since the thyroid and the small intestine are made up of the same material, the algorithms are almost similar, the only change that should be made is that of the component.

Figure 69 represents the algorithm that allows for disintegrations of iodine in the thyroid.

```
s:So/MySource_Beta_Thyroid/Type = "Volumetric"
s:So/MySource_Beta_Thyroid/ActiveMaterial = "soft_tissue"
s:So/MySource_Beta_Thyroid/Component = "MIRDThyroid"
s:So/MySource_Beta_Thyroid/BeamParticle = "e-"
s:So/MySource_Beta_Thyroid/BeamEnergySpectrumType = "Continuous"
dv:So/MySource_Beta_Thyroid/BeamEnergySpectrumValues = 6 606.3
333.8 247.9 303.9 806.9 629.7 keV
uv:So/MySource_Beta_Thyroid/BeamEnergySpectrumWeights = 6 0.89562107414
0.0721305563 0.0213386229 0.0064416594 0.00386699926 0.00060108796
ic:So/MySource_Beta_Thyroid/NumberOfHistoriesInRun = 100000000

s:So/MySource_Gamma_Thyroid/Type = "Volumetric"
s:So/MySource_Gamma_Thyroid/ActiveMaterial = "soft_tissue"
s:So/MySource_Gamma_Thyroid/Component = "MIRDThyroid"
s:So/MySource_Gamma_Thyroid/BeamParticle = "gamma"
s:So/MySource_Gamma_Thyroid/BeamEnergySpectrumType = "Discrete"
dv:So/MySource_Gamma_Thyroid/BeamEnergySpectrumValues = 6 364.490
636.990 284.305 80.1854 722.909 503.004 keV
uv:So/MySource_Gamma_Thyroid/BeamEnergySpectrumWeights = 6 0.78781960732
0.06778471952 0.06114845327 0.06285492173 0.01700780235 0.00338544382
ic:So/MySource_Gamma_Thyroid/NumberOfHistoriesInRun = 100000000
```

Figure 69 : *The algorithm for the thyroid as a source.*

Now to the elimination phase, iodine is eliminated through urine, that is to say, it must go through the kidneys and the urinary bladder, these three organs represent excellent candidates to be considered as sources.

In the case of the kidneys figure 70 shows the code used to set both of them as a source.

As for the urinary bladder figure 71 represents the algorithm used to set it as a source.

```
s:So/MySource_Beta_RightKidney/Type = "Volumetric"
s:So/MySource_Beta_RightKidney/ActiveMaterial = "soft_tissue"
s:So/MySource_Beta_RightKidney/Component = "MIRDRightKidney"
s:So/MySource_Beta_RightKidney/BeamParticle = "e-"
s:So/MySource_Beta_RightKidney/BeamEnergySpectrumType = "Continuous"
dv:So/MySource_Beta_RightKidney/BeamEnergySpectrumValues = 6 606.3
333.8 247.9 303.9 806.9 629.7 keV
uv:So/MySource_Beta_RightKidney/BeamEnergySpectrumWeights = 6 0.89562107414
0.0721305563 0.0213386229 0.0064416594 0.00386699926 0.00060108796
ic:So/MySource_Beta_RightKidney/NumberOfHistoriesInRun = 1000000

s:So/MySource_Gamma_RightKidney/Type = "Volumetric"
s:So/MySource_Gamma_RightKidney/ActiveMaterial = "soft_tissue"
s:So/MySource_Gamma_RightKidney/Component = "MIRDRightKidney"
s:So/MySource_Gamma_RightKidney/BeamParticle = "gamma"
s:So/MySource_Gamma_RightKidney/BeamEnergySpectrumType = "Discrete"
dv:So/MySource_Gamma_RightKidney/BeamEnergySpectrumValues = 6 364.490
636.990 284.305 80.1854 722.909 503.004 keV
uv:So/MySource_Gamma_RightKidney/BeamEnergySpectrumWeights = 6 0.78781960732
0.06778471952 0.06114845327 0.06285492173 0.01700780235 0.00338544382
ic:So/MySource_Gamma_RightKidney/NumberOfHistoriesInRun = 1000000

s:So/MySource_Beta_LeftKidney/Type = "Volumetric"
s:So/MySource_Beta_LeftKidney/ActiveMaterial = "soft_tissue"
s:So/MySource_Beta_LeftKidney/Component = "MIRDLeftKidney"
s:So/MySource_Beta_LeftKidney/BeamParticle = "e-"
s:So/MySource_Beta_LeftKidney/BeamEnergySpectrumType = "Continuous"
dv:So/MySource_Beta_LeftKidney/BeamEnergySpectrumValues = 6 606.3
333.8 247.9 303.9 806.9 629.7 keV
uv:So/MySource_Beta_LeftKidney/BeamEnergySpectrumWeights = 6 0.89562107414
0.0721305563 0.0213386229 0.0064416594 0.00386699926 0.00060108796
ic:So/MySource_Beta_LeftKidney/NumberOfHistoriesInRun = 100000000

s:So/MySource_Gamma_LeftKidney/Type = "Volumetric"
s:So/MySource_Gamma_LeftKidney/ActiveMaterial = "soft_tissue"
s:So/MySource_Gamma_LeftKidney/Component = "MIRDLeftKidney"
s:So/MySource_Gamma_LeftKidney/BeamParticle = "gamma"
s:So/MySource_Gamma_LeftKidney/BeamEnergySpectrumType = "Discrete"
dv:So/MySource_Gamma_LeftKidney/BeamEnergySpectrumValues = 6 364.490
636.990 284.305 80.1854 722.909 503.004 keV
uv:So/MySource_Gamma_LeftKidney/BeamEnergySpectrumWeights = 6 0.78781960732
0.06778471952 0.06114845327 0.06285492173 0.01700780235 0.00338544382
ic:So/MySource_Gamma_LeftKidney/NumberOfHistoriesInRun = 100000000
```

Figure 70 : *The algorithm for the right and left kidneys as a source.*

```
s:So/MySource_Beta_UrinaryBladder/Type = "Volumetric"
s:So/MySource_Beta_UrinaryBladder/ActiveMaterial = "soft_tissue"
s:So/MySource_Beta_UrinaryBladder/Component = "MIRDUrinaryBladder"
s:So/MySource_Beta_UrinaryBladder/BeamParticle = "e-"
s:So/MySource_Beta_UrinaryBladder/BeamEnergySpectrumType = "Continuous"
dv:So/MySource_Beta_UrinaryBladder/BeamEnergySpectrumValues = 6 606.3
333.8 247.9 303.9 806.9 629.7 keV
uv:So/MySource_Beta_UrinaryBladder/BeamEnergySpectrumWeights = 6 0.89562107414
0.0721305563 0.0213386229 0.0064416594 0.00386699926 0.00060108796
ic:So/MySource_Beta_UrinaryBladder/NumberOfHistoriesInRun = 100000000

s:So/MySource_Gamma_UrinaryBladder/Type = "Volumetric"
s:So/MySource_Gamma_UrinaryBladder/ActiveMaterial = "soft_tissue"
s:So/MySource_Gamma_UrinaryBladder/Component = "MIRDUrinaryBladder"
s:So/MySource_Gamma_UrinaryBladder/BeamParticle = "gamma"
s:So/MySource_Gamma_UrinaryBladder/BeamEnergySpectrumType = "Discrete"
dv:So/MySource_Gamma_UrinaryBladder/BeamEnergySpectrumValues = 6 364.490
636.990 284.305 80.1854 722.909 503.004 keV
uv:So/MySource_Gamma_UrinaryBladder/BeamEnergySpectrumWeights = 6 0.78781960732
0.06778471952 0.06114845327 0.06285492173 0.01700780235 0.00338544382
ic:So/MySource_Gamma_UrinaryBladder/NumberOfHistoriesInRun = 100000000
```

Figure 71 : *The algorithm for the urinary bladder as a source.*

3.2.3. Scoring

After ordering the program to simulate ^{131}I disintegration it has to find one or multiple volumes in which it is going to score the data, we can choose as much volume scorers as we need and we can also precise what we want to score, in our case study we have chosen 20 scorers, those are represented by the volumes of the stomach, the small intestine, the thyroid, the heart, the left and right kidneys, the urinary bladder, the left and right lungs, the breasts, the uterus and the ovaries among others. The data that must be scored is the energy deposited in those volume and also the absorbed dose.

Figure 72 represents the algorithm in which we declare the stomach as a scorer and we precise the absorbed dose as the data being scored.

```
s:Sc/StomachScorer/Quantity = "DoseToMedium"
s:Sc/StomachScorer/Component = "MIRDStomach"
b:Sc/StomachScorer/OutputToConsole = "True"
s:Sc/StomachScorer/IfOutputFileAlreadyExists = "Overwrite"
```

Figure 72 : *The algorithm for the stomach as a scorer for absorbed dose.*

For every other volume scorer, it is simply defined by changing its name and setting the component parameter to the desired volume: MIRDLeftKidney, MIRDThyroid….

3.2.4. Physics

It is important to note that TOPAS MC has its own physics processes libraries that handle all the physical phenomena that take place when ^{131}I disintegrates, in other words, it is going to perform all of the radiation interactions with matter as seen in chapter 2 and this depending on the tissue and the energy previously defined.

3.2.5. The TOPAS Graphical User Interface

This interface would allow the visualization of the geometry as well as its manipulation and adjustment, in order to run more histories we decided to run the program in batch system without using the GUI.

After we have set all the conditions and parameters we launched the program for 10^7 histories, TOPAS MC ran for more than 3H and each source was run separately for both male and female phantoms, for hyperthyroidism and cancer.

4. Results

4.1. Epidemiology results:

a) Distribution by pathology:

Hyperthyroidism	Thyroid cancer	Total
74	468	542

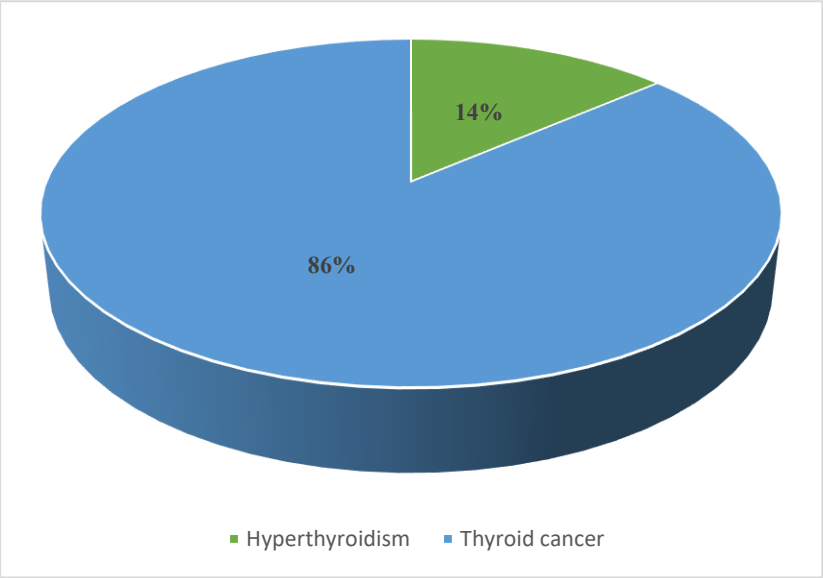

Figure 73 : *Pie of pathology distribution.*

Out of the 542 patients who meet the set criteria 86% undergo ^{131}I radioactive therapy for thyroid cancer while 14% are being treated for hyperthyroidism.

b) Hyperthyroidism:

1) Sex distribution:

Female	**Male**	**Total**
47	27	74

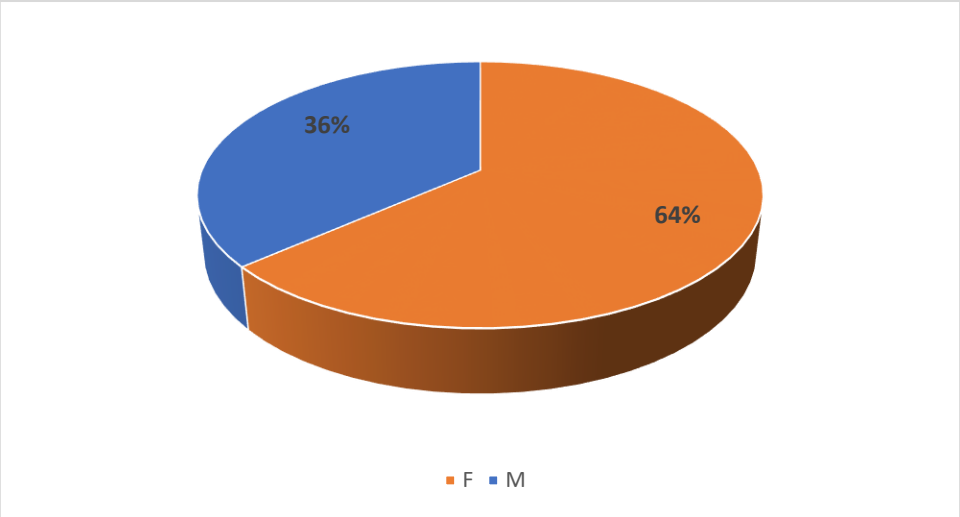

Figure 74 : *Pie of sex distribution for hyperthyroidism.*

The female sex is predominant compared to the male sex with a percentage of 64% for women and 36% for men; the sex ratio is 1.78 in favor of women.

2) Age distribution:

- Females:

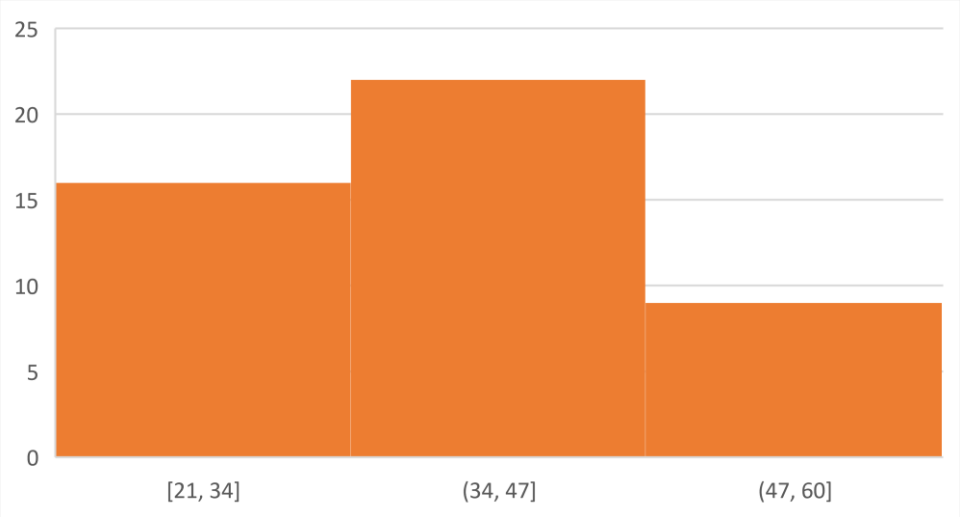

Figure 75 : *Chart of female age distribution for hyperthyroidism.*

For females, the mean age was 40.5 years with a spike in frequency in the age group]34-47] or 46.80% of women. The minimum age was 21 and the maximum age was 60.

- Males:

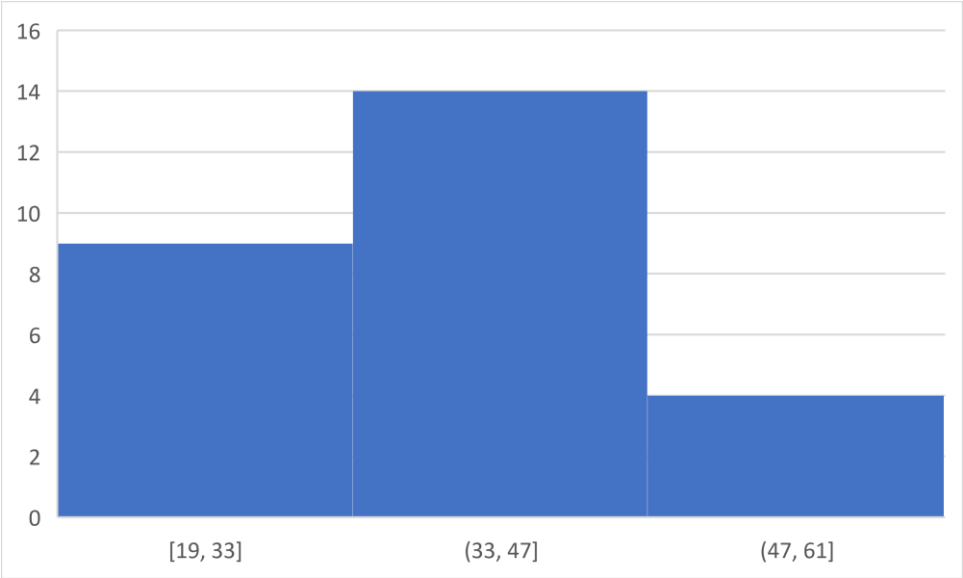

Figure 76 : *Chart of male age distribution for hyperthyroidism.*

For males, the average age was 39.5 years with a spike in frequency in the]33-47] age group or 51.85% of men. The minimum age was 19 and the maximum age was 60.

3) Dose distribution:

- Female:

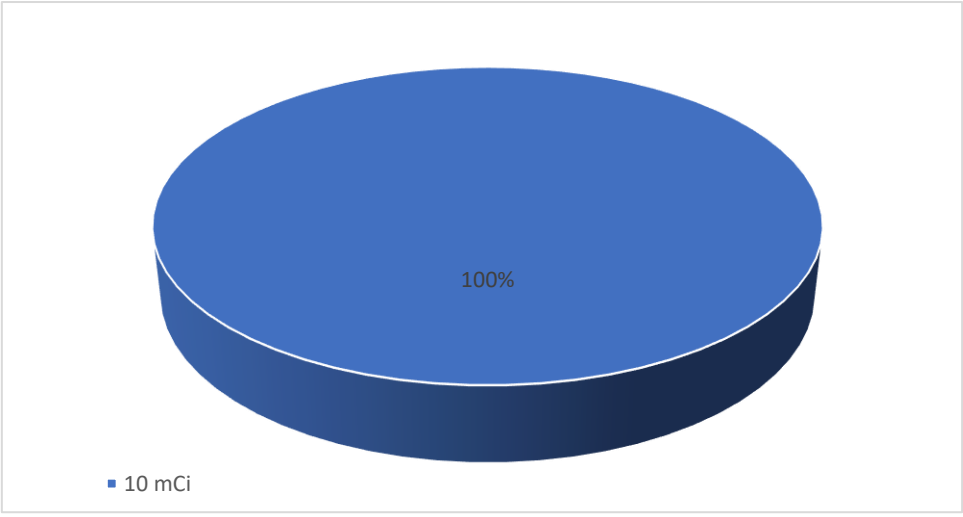

Figure 77 : *Pie of female dose distribution in hyperthyroidism.*

100% of females treated with radioactive thyroid for hyperthyroidism at the University Hospital Center of Tlemcen have received a dose of 10 mCi.

- Male:

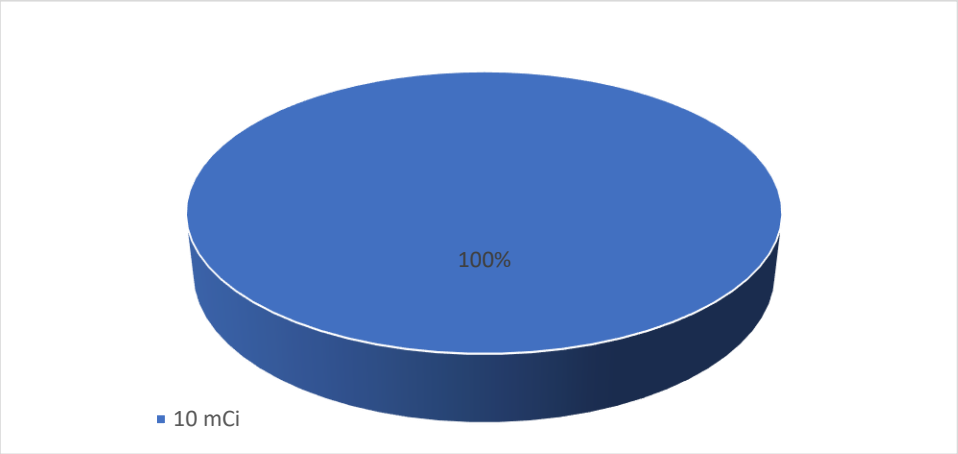

Figure 78 : *Pie of male dose distribution in hyperthyroidism.*

All the males that have undergone radioactive iodine therapy for hyperthyroidism at the University Hospital Center of Tlemcen have received a 10 mCi dose.

c) Thyroid cancer

1) Sex distribution:

Female	Male	Total
407	61	468

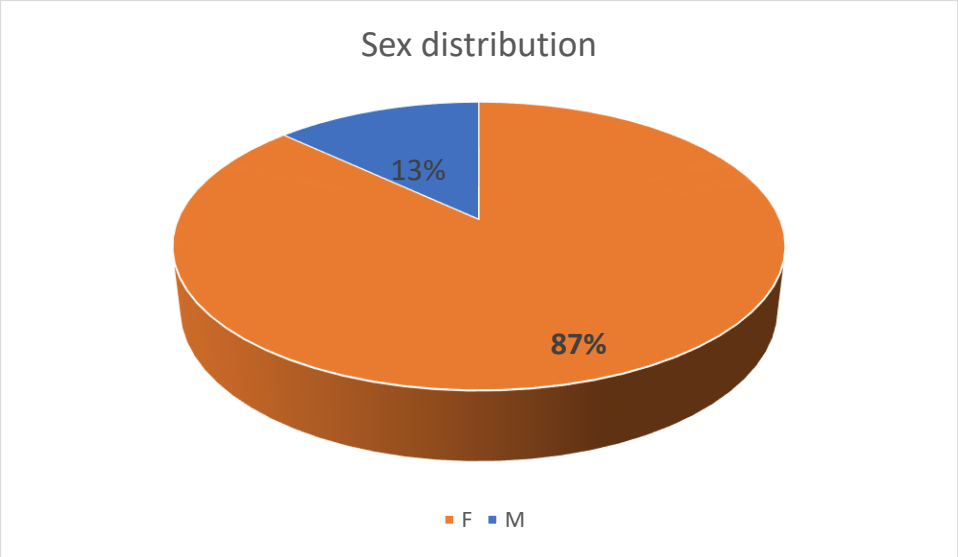

Figure 79 : *Pie of sex distribution for thyroid cancer.*

The female sex is predominant compared to the male sex with a percentage of 87% for women and 13% for men; with a sex ratio of 6.69 in favor of women.

2) Age distribution:

- Females:

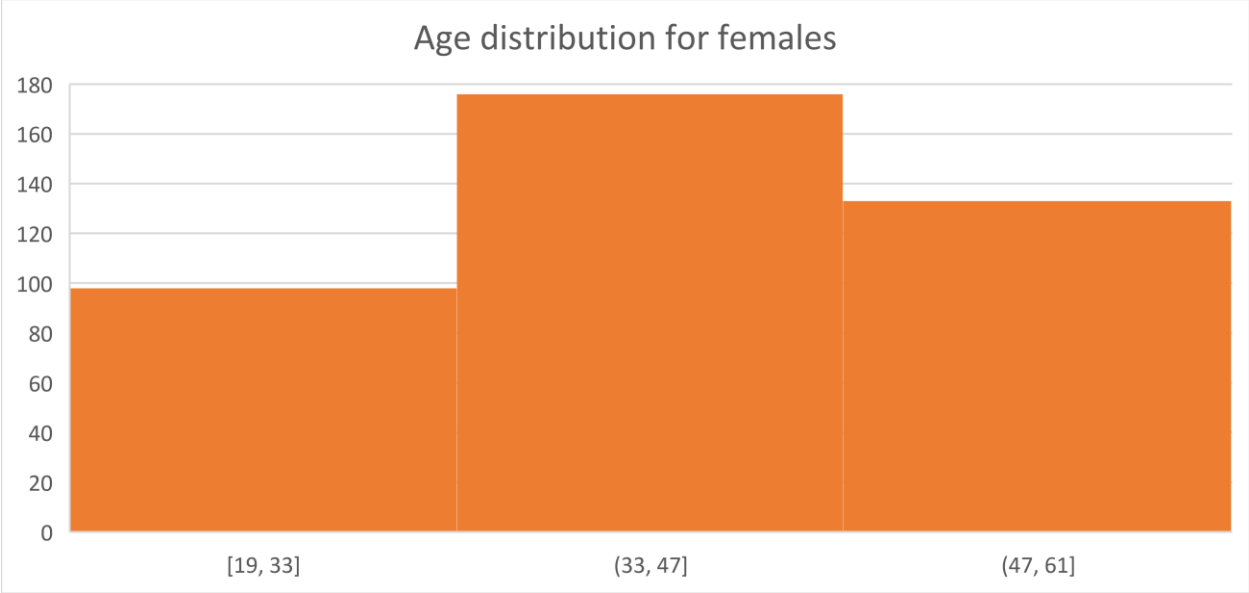

Figure 80 : *Chart of female age distribution for thyroid cancer.*

For females, the mean age was 39.5 years with a spike in frequency in the age group]33-47] or 43.24% of women. The minimum age was 19 and the maximum age was 60.

- Males:

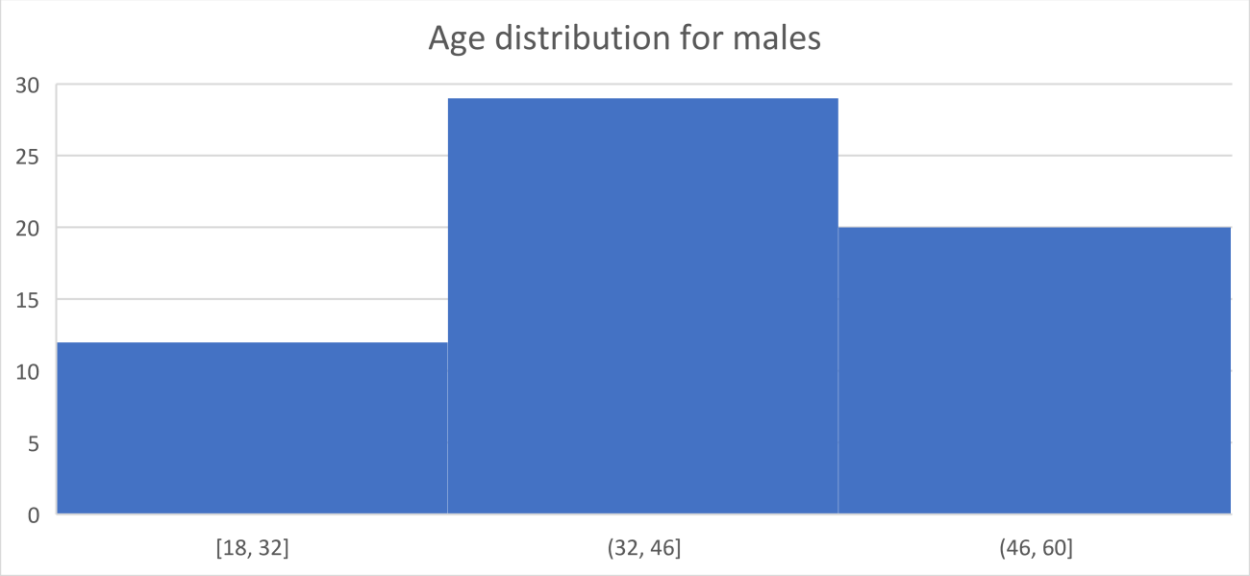

Figure 81 : *Chart of male age distribution for thyroid cancer.*

For males, the average age was 39 years with a spike in frequency in the]32-46] age group or 47.54% of men. The minimum age was 18 and the maximum age was 60.

3) Dose distribution:
   - Female:

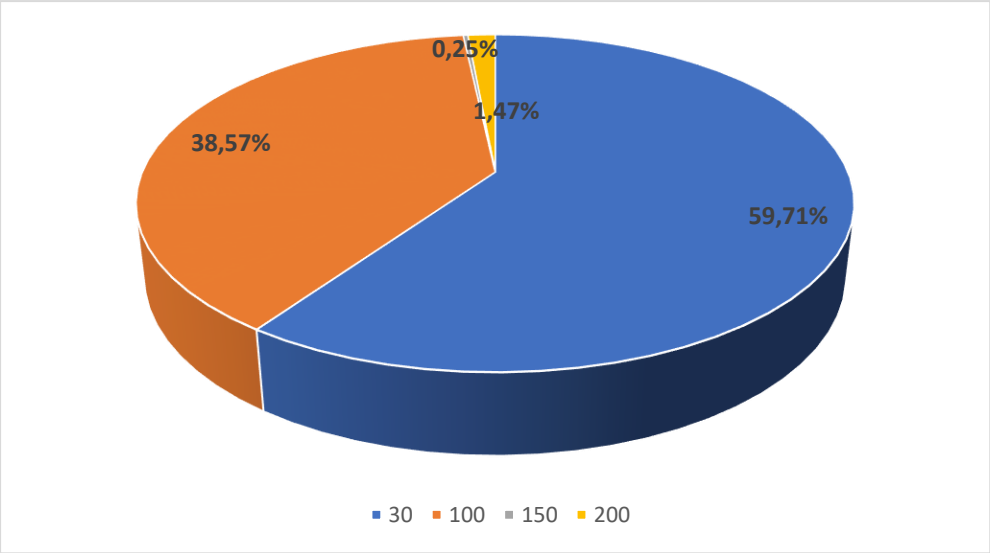

Figure 82 : *Pie of female dose distribution in thyroid cancer.*

59.17% of females treated with radioactive thyroid for hyperthyroidism at the University Hospital Center of Tlemcen have received a dose of 30 mCi, while 38.57% of patients have received a 100 mCi dose, a rare number of patients have been prescribed a dose of 200 mCi or 150 mCi with percentages of 1.47% and 0.25% respectively.

- Male:

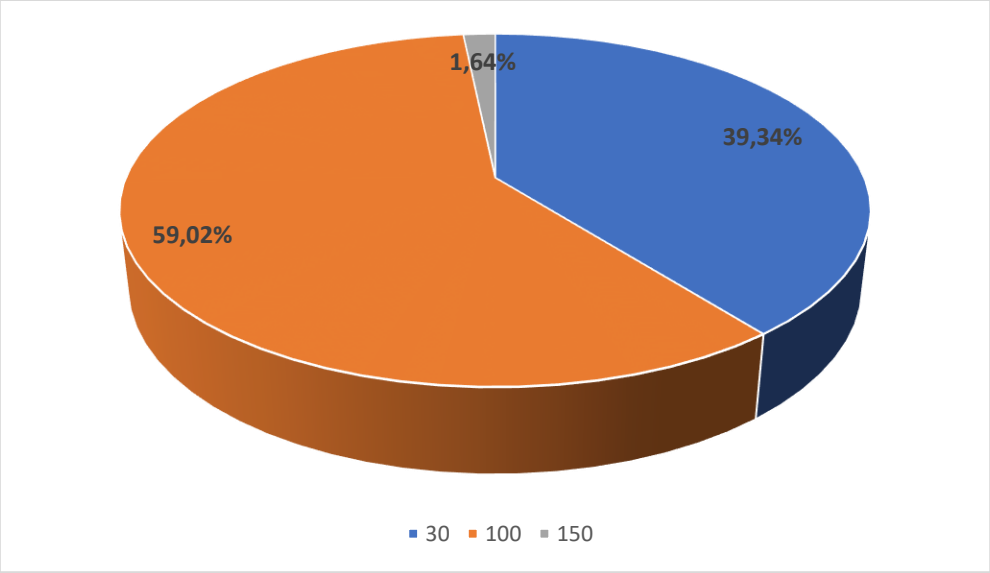

Figure 83 : *Pie of male dose distribution in thyroid cancer.*

A shift in prescription is noted in the male group, the most prescribed dose is 100 mCi at a percentage of 59.02%, while the 30 mCi dose is prescribed to 39.34% of patients and a small number of patients (1.64%) get prescribed the 150 mCi dose.

4.2. Simulation results

4.2.1. Hyperthyroidism:

a) Source: Stomach's cavity.

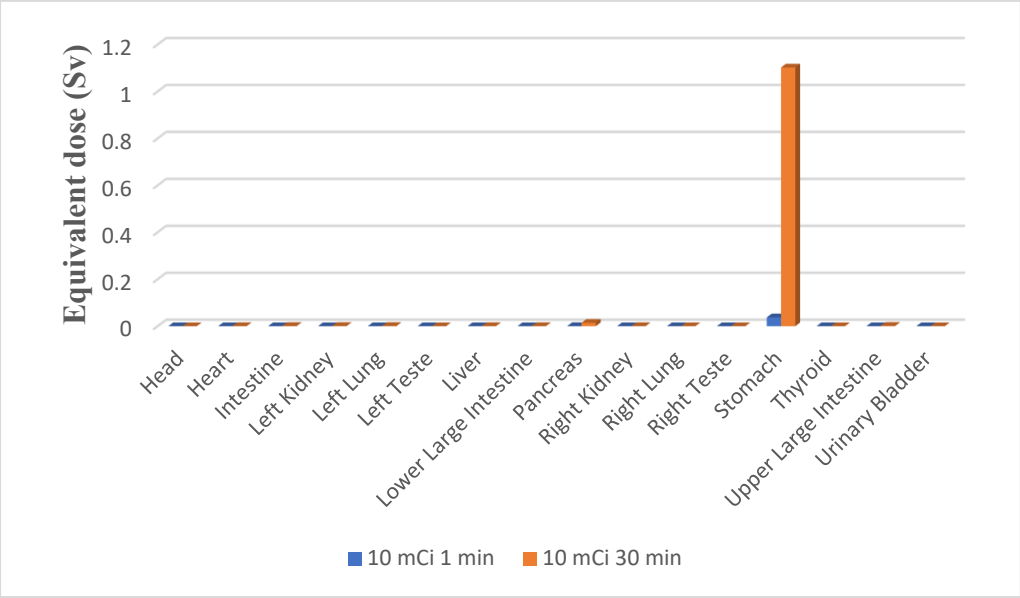

Figure 84 : *Equivalent dose at 1 and 30 min for a male afflicted with hyperthyroidism.*

1 min after ingestion of NaI capsule, the equivalent dose to the stomach is approximately 0.04 Sv, whereas after 30 min residence in the stomach, this organ absorbed an equivalent dose of 1.10 Sv

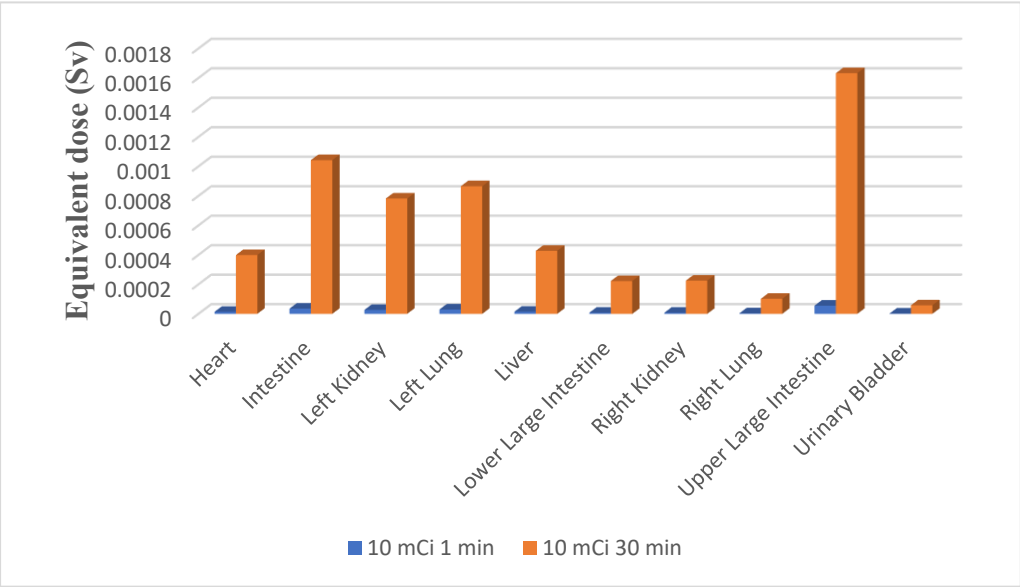

Figure 85 : *Equivalent dose at 1 and 30 min for a male afflicted with hyperthyroidism (HT<1.8E-03 Sv).*

The upper large intestine is the third most irradiated organ after the stomach, the second one being the pancreas, its equivalent doses at 1 and 30 min residence time in the stomach are 5.55E-05 Sv and 1.63E-03 Sv respectively.

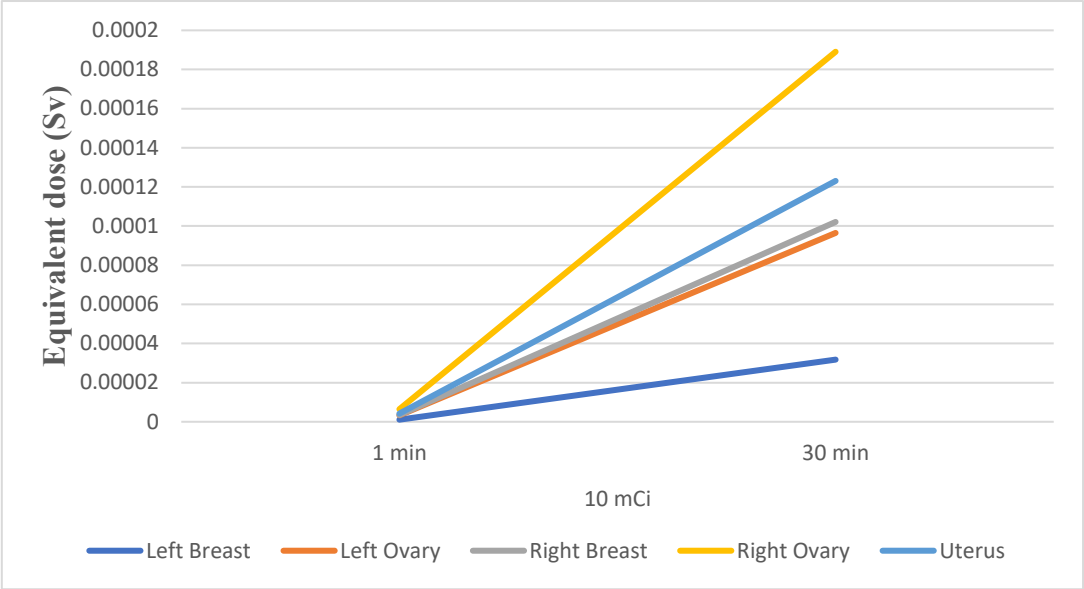

Figure 86 : *Equivalent dose after 1 and 30 min for a female afflicted with hyperthyroidism (sex-specific organs).*

Regarding the female specific organs, the right ovary is the most irradiated among them, its equivalent doses at 1 and 30 min are 6.44E-06 Sv and 1.89E-04 Sv respectively.

b) Source: small intestine.

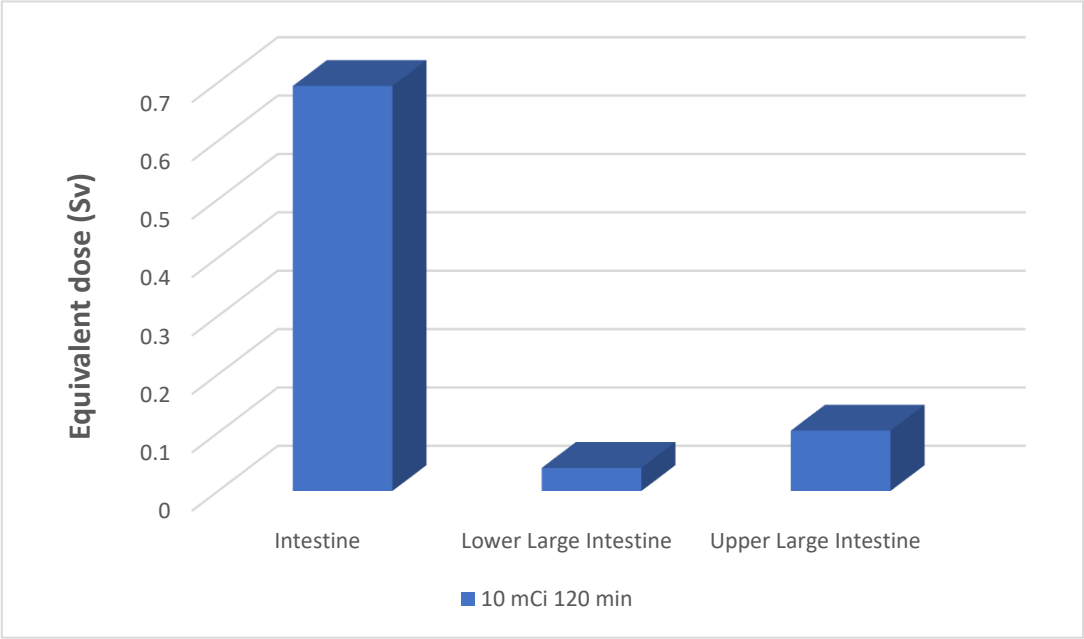

Figure 87 : *Equivalent dose after 90 min residence in the small intestine for a male afflicted with hyperthyroidism.*

After 90 min residence in the small intestine the equivalent dose received by this organ is 0.69 Sv, the upper large intestine and the lower large intestine have received an equivalent dose of 0.10 Sv and 0.04 Sv respectively.

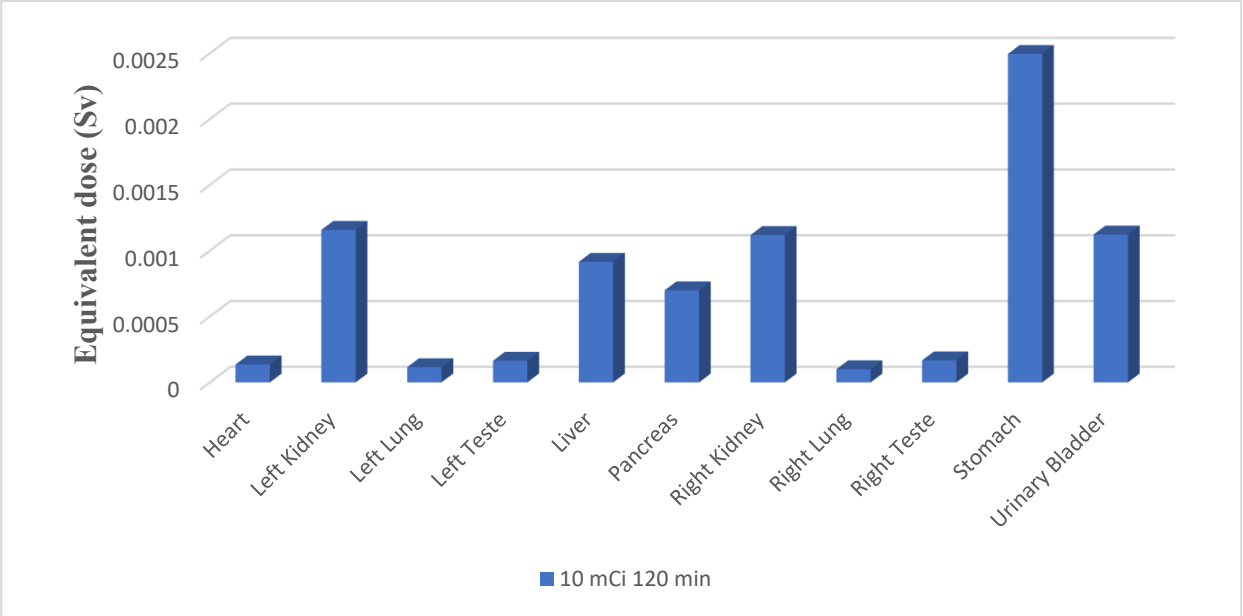

Figure 88 : *Equivalent dose after 90 min residence in the small intestine for a male afflicted with hyperthyroidism (H_T<2.5E-03 Sv).*

At the same time, the stomach has received an equivalent dose of 2.49E-03 Sv, while the left kidney, the right kidney and the urinary bladder have received approximately the same equivalent dose of 1.15E-03 Sv.

Figure 89 : *Equivalent dose after 90 min residence in small intestine for a female afflicted with hyperthyroidism (sex-specific organs).*

In regard to the female specific organs the right ovary is still the most irradiated organ among them with an equivalent dose of 2.34E-02 Sv, while the left ovary is a close second absorbing an equivalent dose of 2.15E-02 Sv.

c) Source: thyroid.

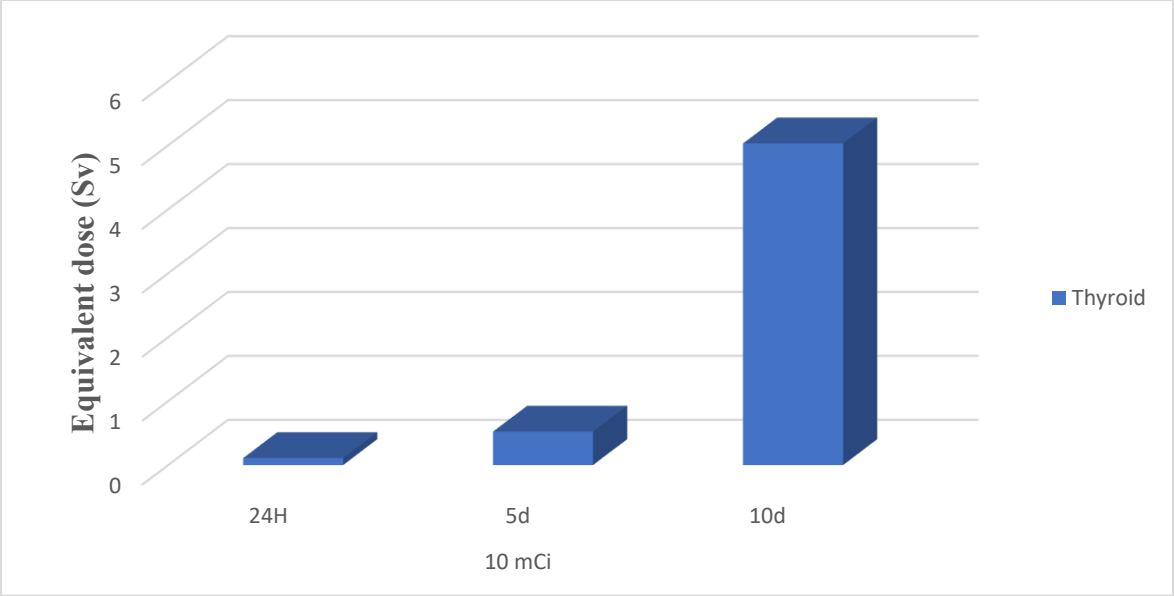

Figure 90 : *Equivalent dose to the thyroid after 24H, 5 and 10 days residence in the thyroid for a male afflicted with hyperthyroidism.*

In the case of hyperthyroidism, 25% of the absorbed ^{131}I is fixed by the thyroid, the self-absorbed equivalent dose by this organ is 0.11, 0.53 and 5.03 Sv at 24H, 5d and 10d respectively.

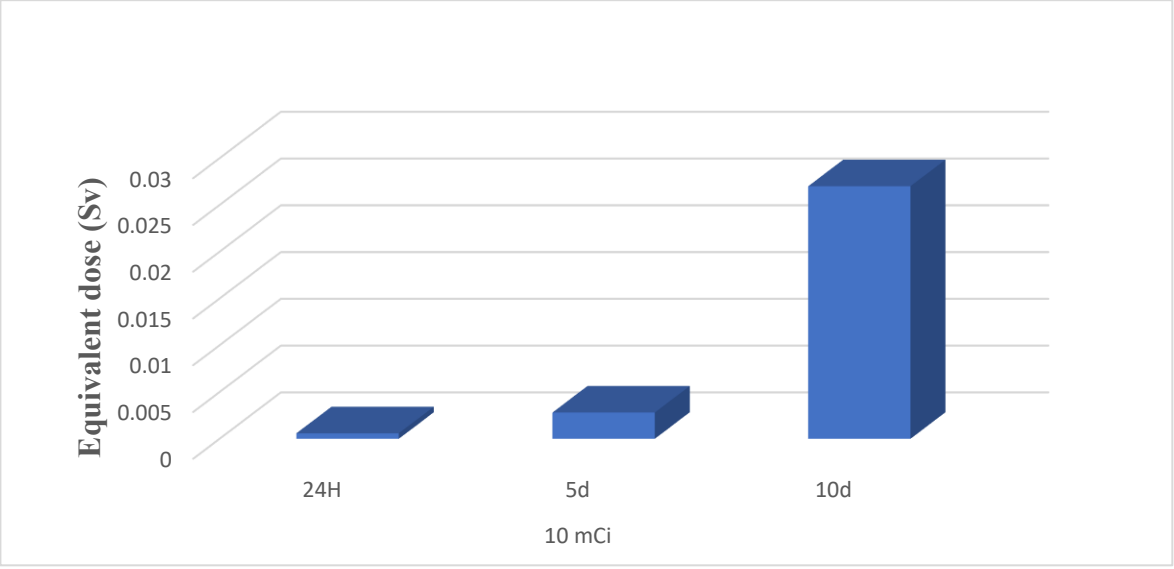

Figure 91 : *Equivalent dose to the head after 24H, 5 and 10 days residence in the thyroid for a male afflicted with hyperthyroidism.*

The head is the second organ in importance in regards to the equivalent dose, it registers 5.86E-04, 2.80E-03 and 2.70E-02 Sv at 24H, 5d and 10d respectively.

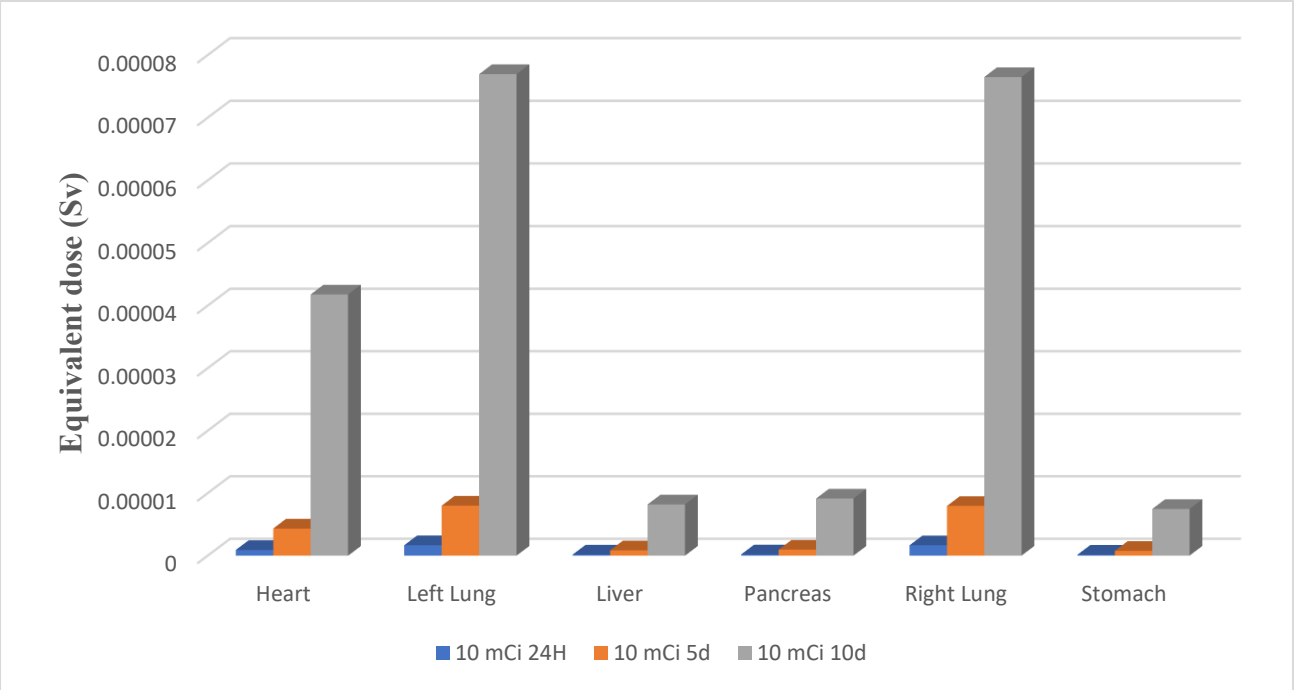

Figure 92 : *Equivalent dose after 24H, 5 and 10 days residence in the thyroid for a male afflicted with hyperthyroidism (H_T<0.8E-04 Sv)*

The cardiothoracic organs come third in importance, with the left and right lung absorbing approximatively the same equivalent dose of 1.67E-06, 7.99E-06 and 7.69E-05 Sv at 24H, 5d and 10d respectively. The heart also receives a significant equivalent dose of 9.07E-07, 4.34E-06 and 4.17E-05 Sv at 24H, 5d and 10d respectively.

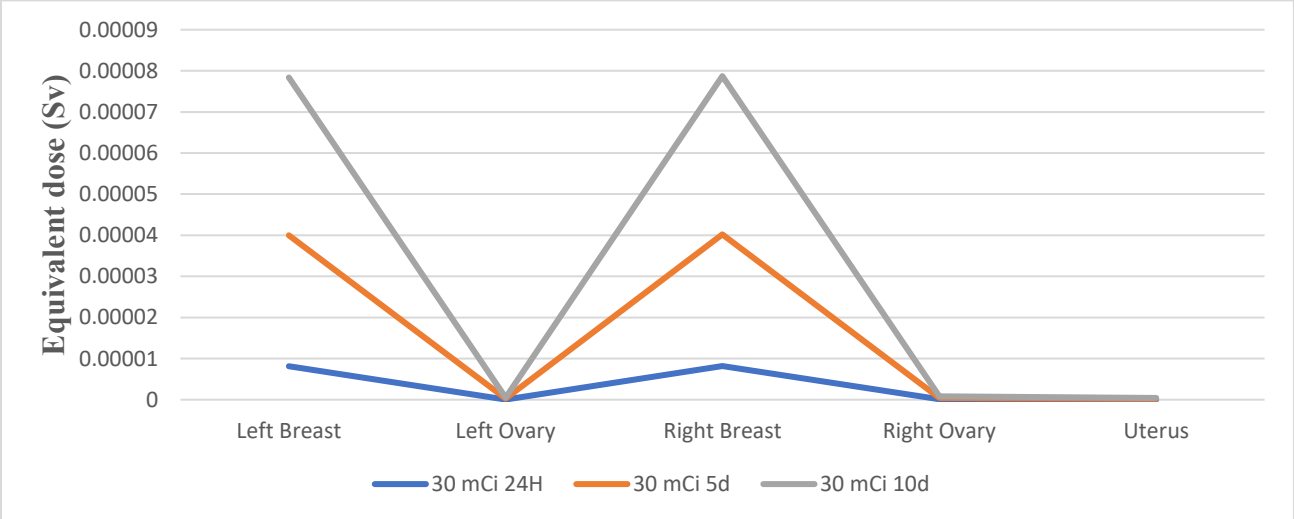

Figure 93 : *Equivalent dose after 24H, 5 and 10 days residence in the thyroid for a female afflicted with hyperthyroidism (sex-specific organs).*

For the female phantom, the third place is reserved, by a small margin, to the left and right breasts who absorb an equivalent dose of 8.18E-06, 4.02E-05 and 7.87E-05 Sv at 24H, 5d and 10d respectively.

d) Source: kidneys.

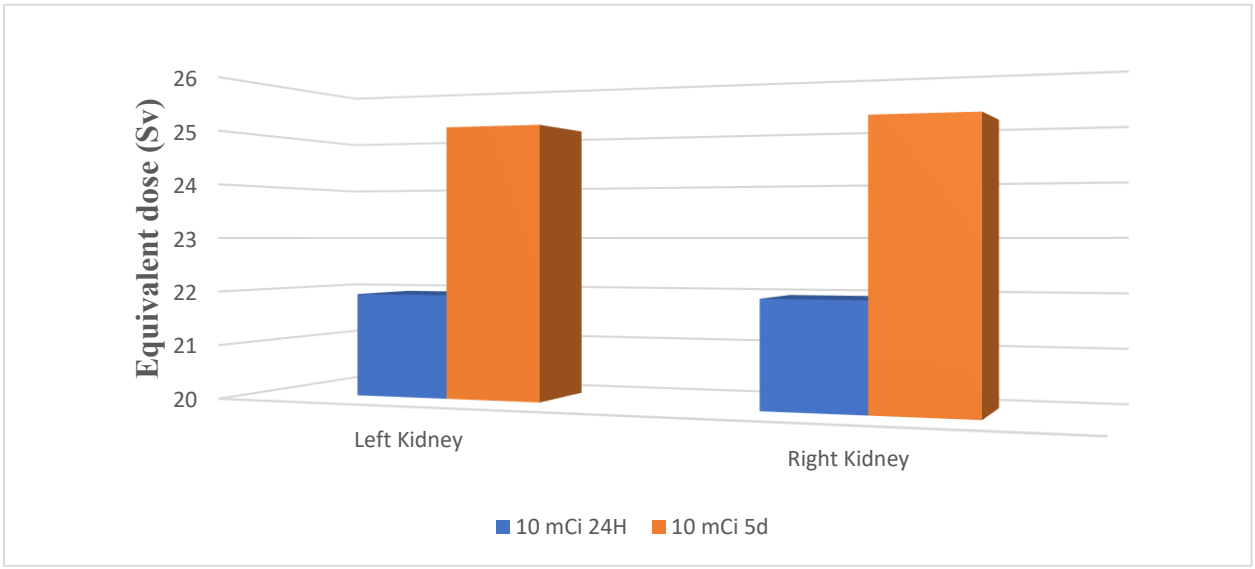

Figure 94 : *Equivalent dose to the kidneys after 24H and 5 days residence in the kidneys for a male afflicted with hyperthyroidism.*

In hyperthyroidism 75% of the absorbed ^{131}I will be eliminated without passing through the thyroid, this yields an important equivalent dose of about 21.9 and 25 Sv at 24H and 5d respectively in both kidneys.

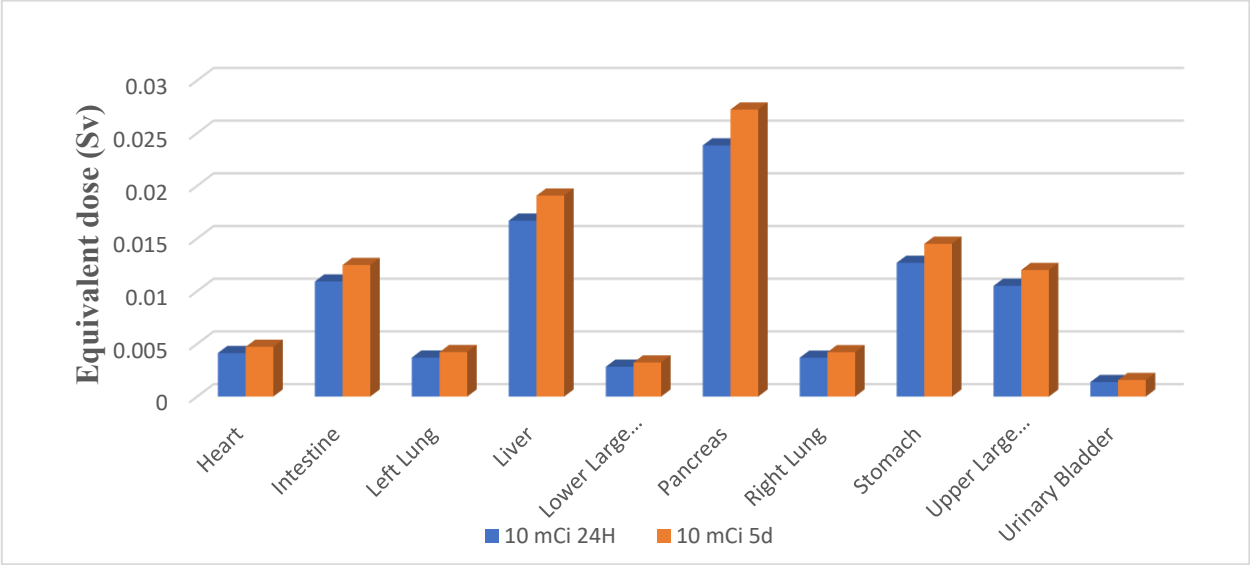

Figure 95 : *Equivalent dose after 24H and 5 days residence in the kidneys for a male afflicted with hyperthyroidism (H_T<0.3E-01 Sv).*

Among the organs of the abdomen, it's the pancreas that receives the most important equivalent dose which is 2.38E-02 and 2.72E-02 Sv at 24H and 5d respectively, as for the stomach it receives an equivalent dose of 1.26E-02 and 1.45E-02 Sv at 24H and 5d respectively.

Figure 96 : *Equivalent dose after 24H and 5 days residence in the kidneys for a female afflicted with hyperthyroidism (sex-specific organs).*

The female specific organs that were irradiated the most in the elimination phase are: the right ovary with an equivalent dose of 4.11E-03 and 4.70E-03 Sv at 24H and 5d respectively; the uterus follows suit as it presents an equivalent dose of 3.94E-03 and 4.50E-03 Sv at 24H and 5d respectively; the right ovary absorbs an equivalent dose of 3.83E-03 and 4.38E-03 Sv at 24H and 5d respectively, and finally the left and right breasts showed approximately the same equivalent dose of 7.25E-04 and 8.29E-04 Sv at 24H and 5d respectively.

e) Source: urinary bladder

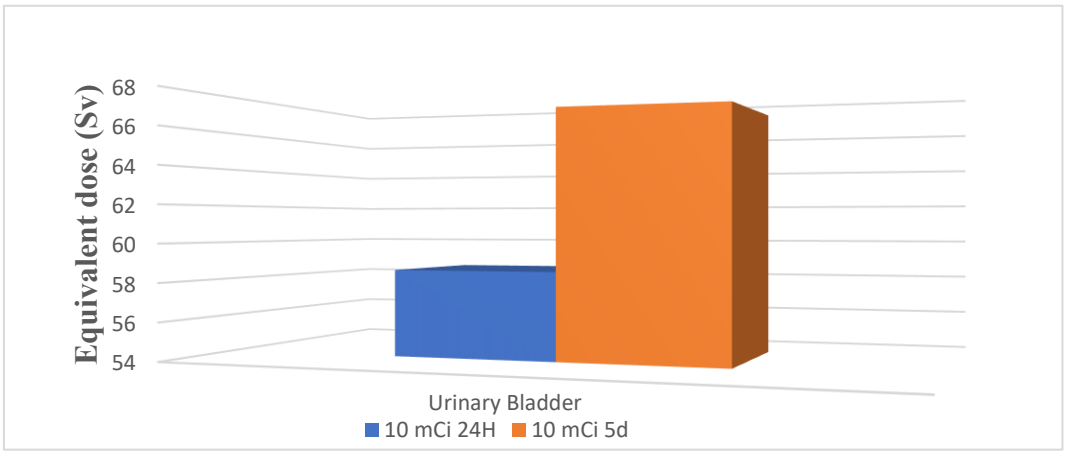

Figure 97 : *Equivalent dose to the urinary bladder after 24H and 5 days residence in the urinary bladder for a male afflicted with hyperthyroidism.*

The self-absorbed equivalent dose in the urinary bladder is 58.6 and 66.9 Sv at 24H and 5d respectively.

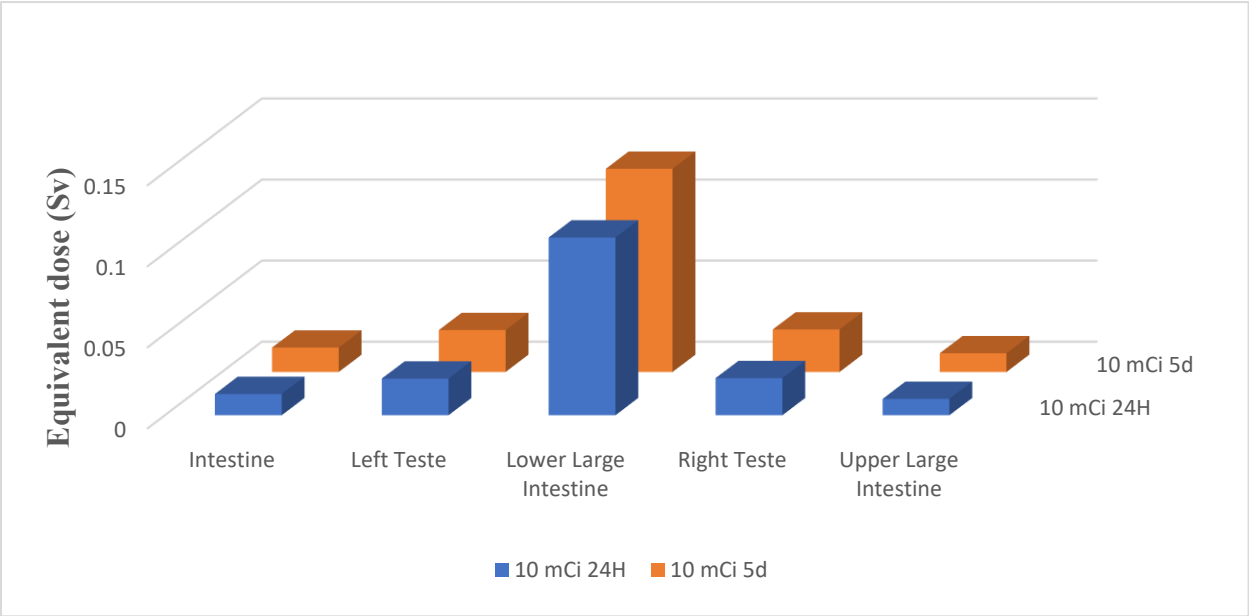

Figure 98 : *Equivalent dose after 24H and 5 days residence in the urinary bladder for a male afflicted with hyperthyroidism (H_T<1.4E-01 Sv)*

Other than the lower large intestine which absorbs and equivalent dose of 0.10 and 0.12 Sv at 24H and 5d respectively, the left and right testes absorb an important equivalent dose in regards to the rest of the organs, it is 2.29E-02 and 2.62E-02 Sv at 24H and 5d respectively.

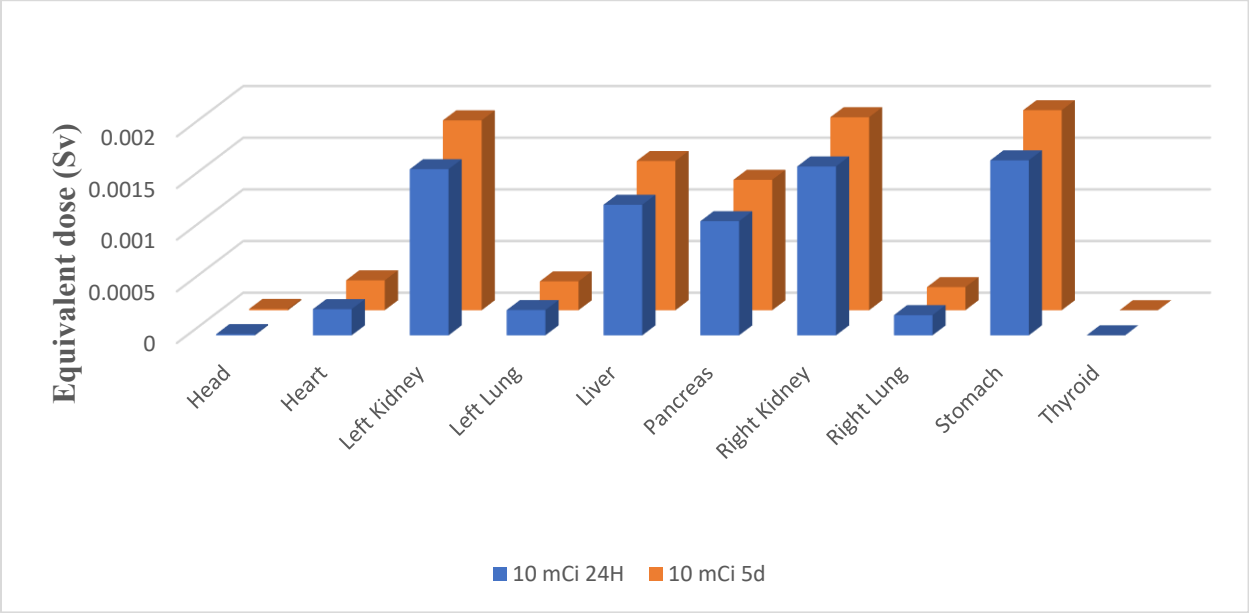

Figure 99 : *Equivalent dose after 24H and 5 days residence in the urinary bladder for a male afflicted with hyperthyroidism (H_T<0.2E-02 Sv)*

The stomach, the left and the right kidneys receive approximately the same equivalent dose which is 1.69E-03 and 1.93E-03 at 24H and 5d respectively, while the liver receives an equivalent dose of 1.26E-03 and 1.44E-03 at 24H and 5d respectively.

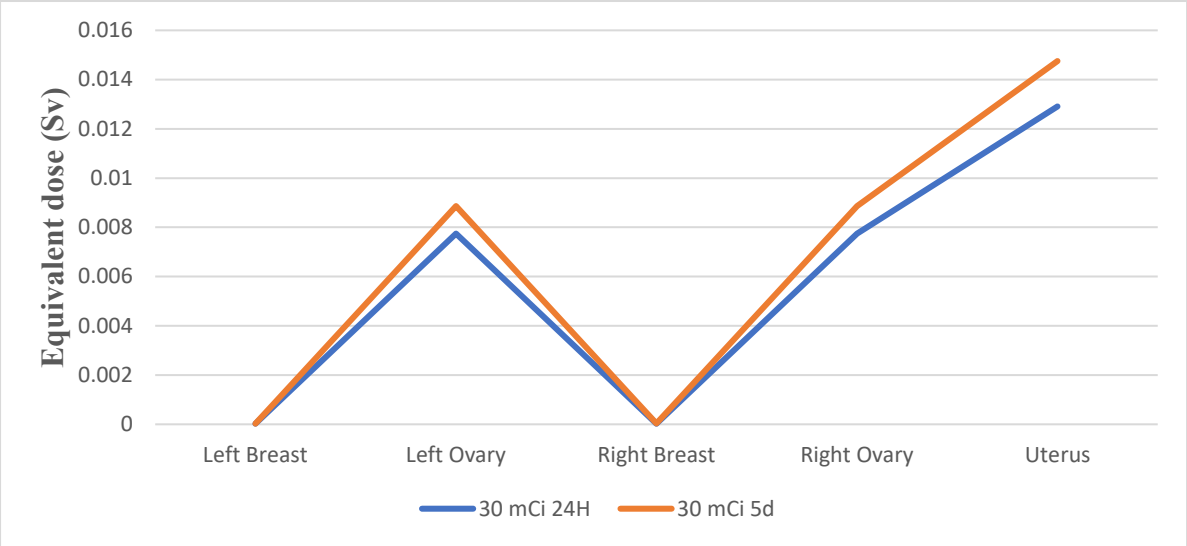

Figure 100 : *Equivalent dose after 24H and 5 days residence in the urinary bladder for a female afflicted with hyperthyroidism (sex-specific organs)*

When ^{131}I resides in the urinary bladder the uterus is the most affected organ by radiation among the female specific organs, it absorbs an equivalent dose of 1.29E-02 and 1.48E-02 Sv at 24H and 5d respectively; the two ovaries receive the same dose, that of 7.75E-03 and 8.85E-03 Sv at 24H and 5d respectively.

- Cumulative equivalent doses 2H after the ingestion of the capsule:

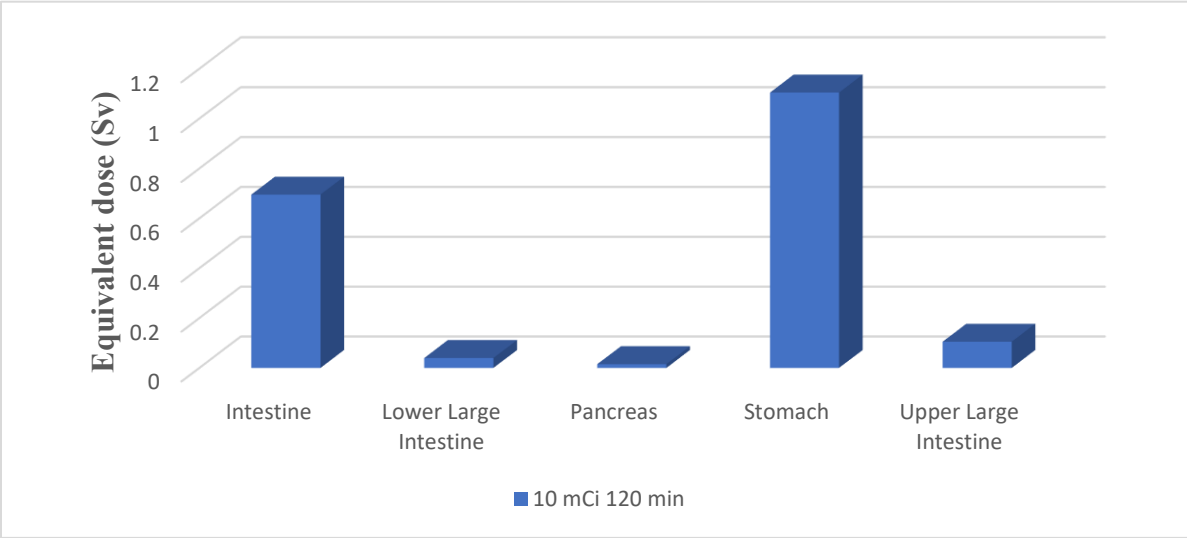

Figure 101 : *Equivalent dose 2H after the ingestion of NaI capsule for a male afflicted with hyperthyroidism*

2 hours after the ingestion of the ^{131}I capsule, the stomach is the most irradiated organ receiving an equivalent dose of 1.10 Sv, the intestine follows suit and stands at an equivalent dose of 0.69 Sv.

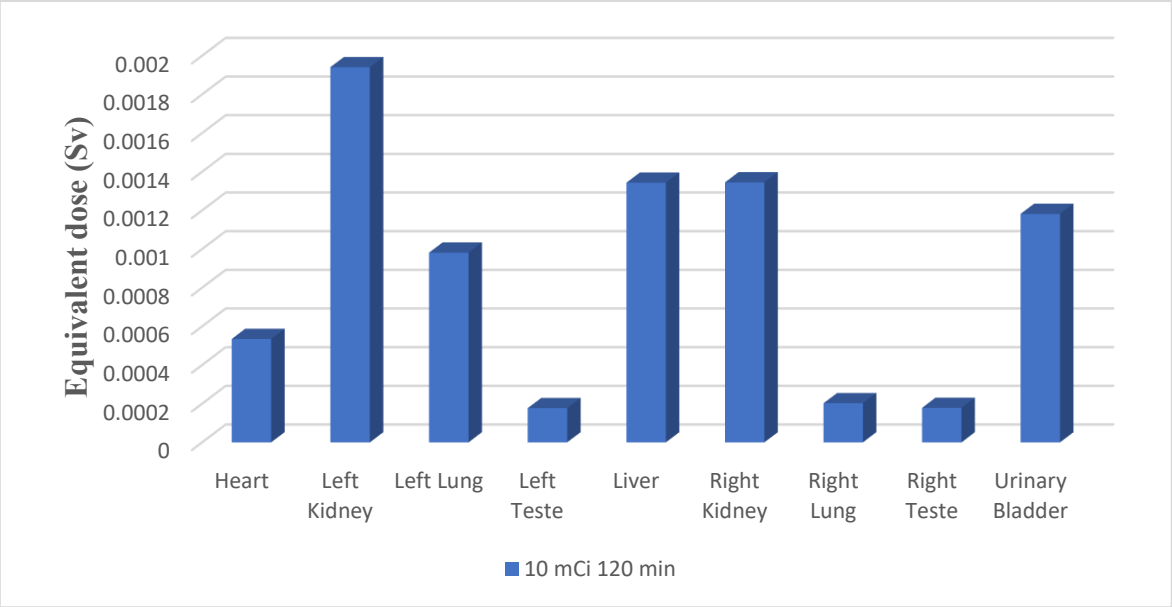

Figure 102 *: Equivalent dose 2H after ingestion of capsule for a male afflicted with hyperthyroidism (H_T<0.2E-02 Sv).*

The equivalent dose for the left kidney is 1.94E-03 Sv, whereas that of the liver and the right kidney is of 1.34E-03 Sv.

- Cumulative equivalent doses 24H after the ingestion of the capsule:

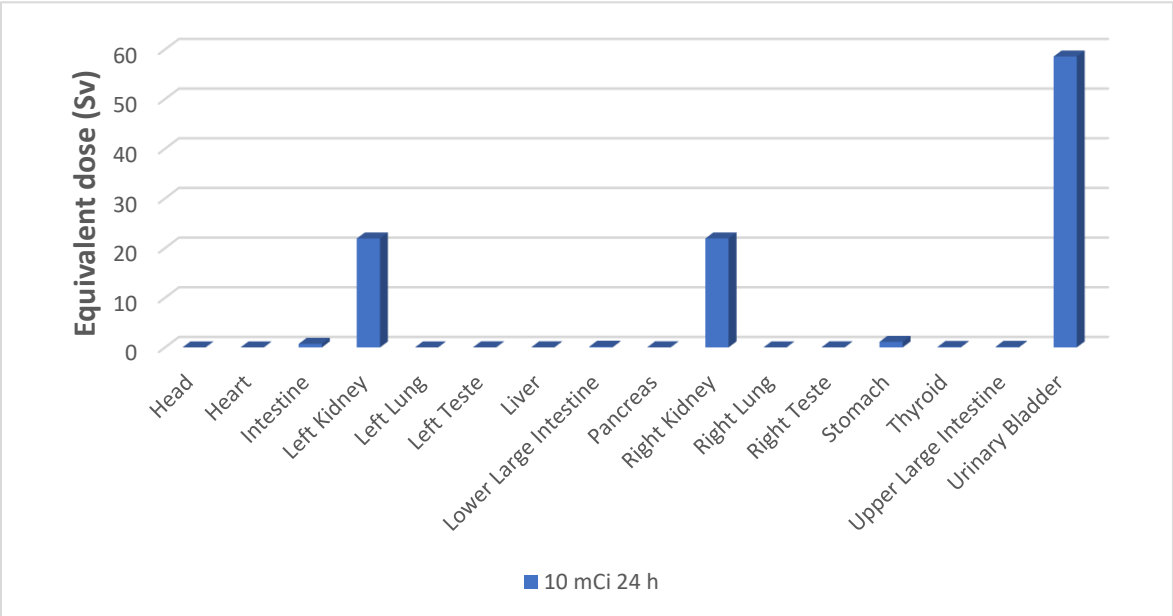

Figure 103 : *Equivalent dose 24H after ingestion of capsule for male afflicted with hyperthyroidism.*

In 24H time the most affected organs from the radiation are the urinary bladder, the left and right kidneys.

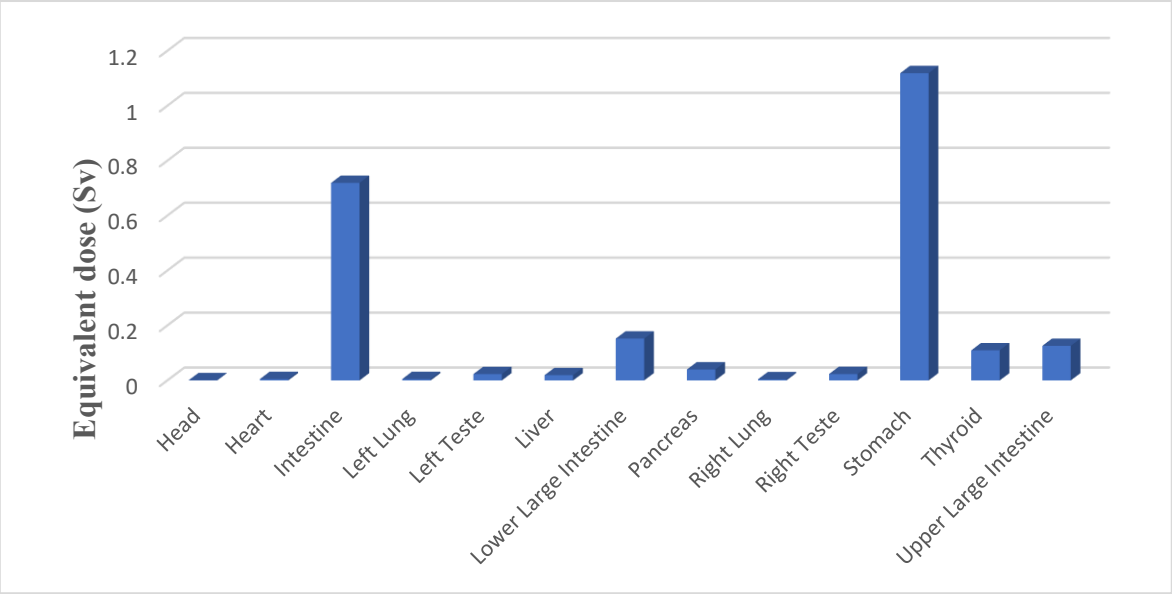

Figure 104 : *Equivalent dose 24H after ingestion of capsule for male afflicted with hyperthyroidism (H_T<1.2 Sv).*

The stomach and the intestine are also very affected during the first 24H after the ingestion of ^{131}I.

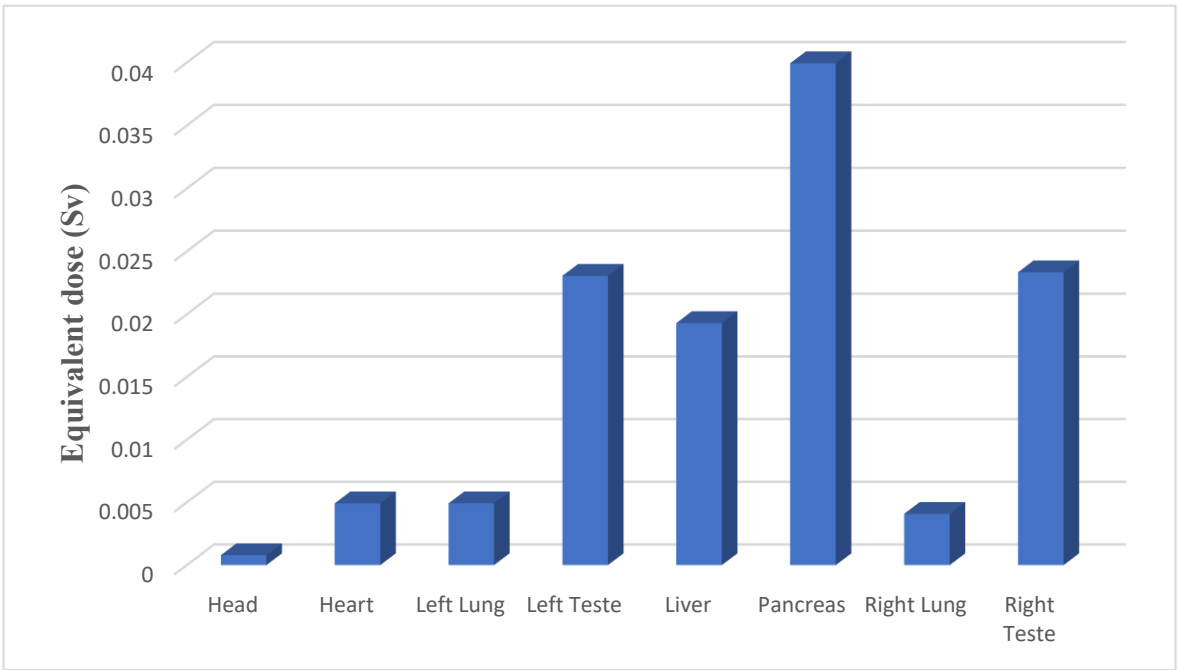

Figure 105 : *Equivalent dose 24H after ingestion of capsule for male afflicted with hyperthyroidism (H_T<0.04 Sv).*

In 24H time the pancreas has an equivalent dose of 3.99E-02 Sv, the right and left testes have an equivalent dose of 2.33E-02 Sv.

- Cumulative equivalent doses 5 days after the ingestion of the capsule

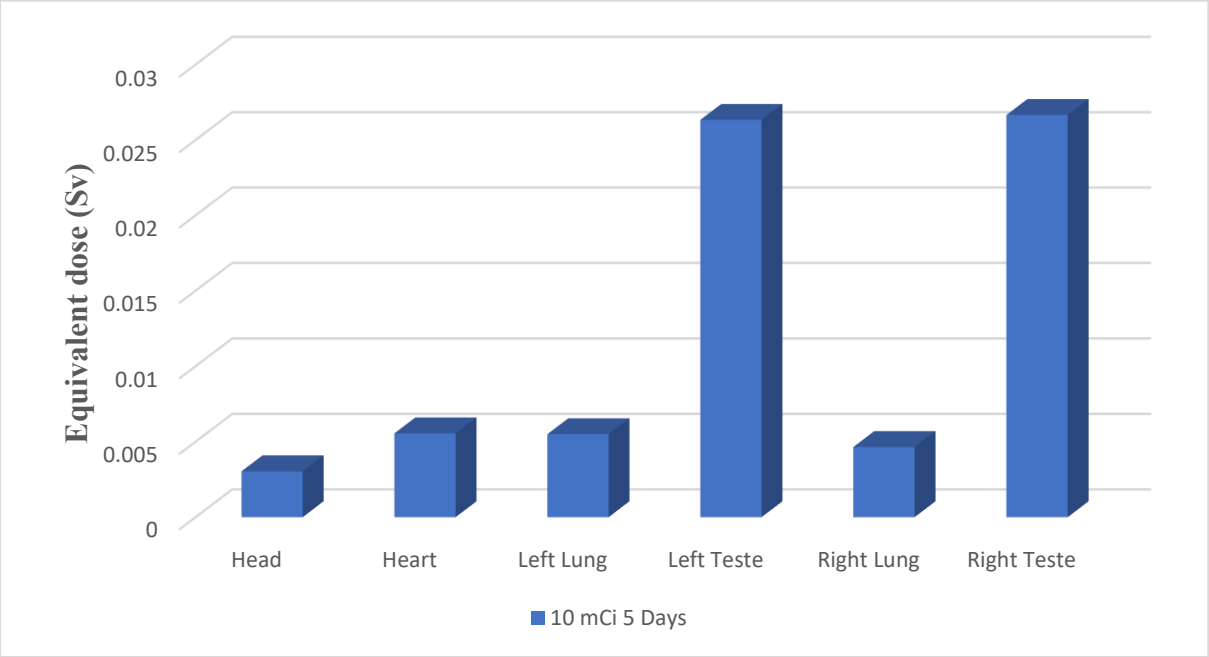

Figure 106 : *Equivalent dose 5d after ingestion of capsule for male afflicted with hyperthyroidism (H_T<0.3E-1 Sv).*

In 5 days time the testes absorb an equivalent dose of 2.66E-02 Sv.

4.2.2. Thyroid cancer:

- Source: stomach's cavity.

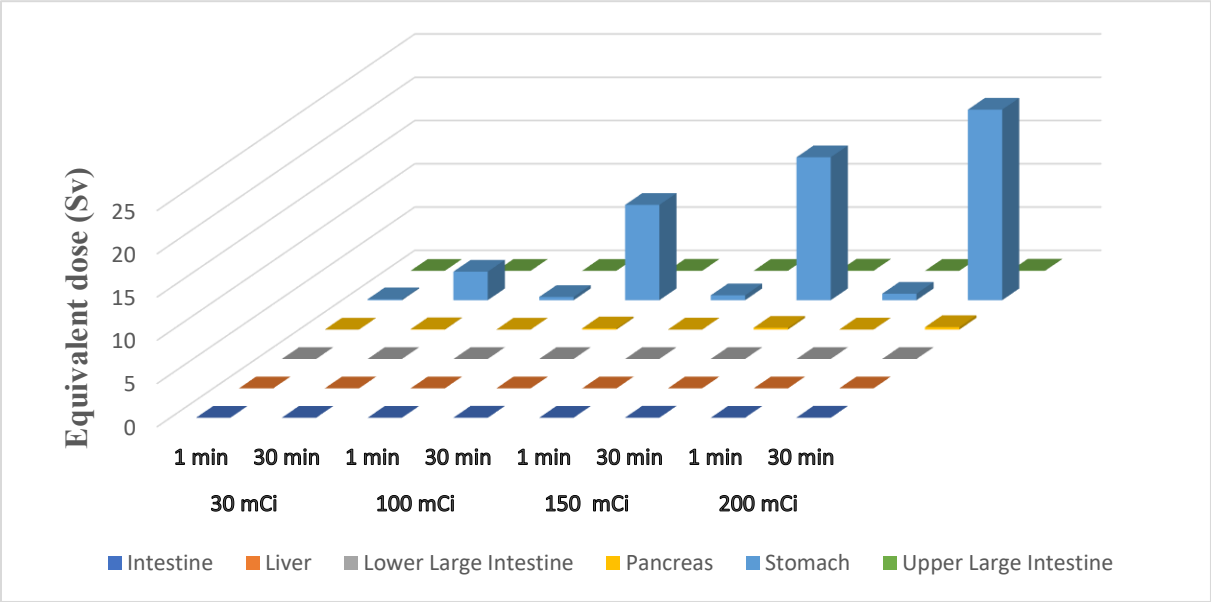

Figure 107 : *Equivalent dose at 1 and 30 min for a male afflicted with thyroid cancer.*

1 min after the ingestion of the NaI capsule, the equivalent doses to the stomach are 0.11, 0.37, 0.56 and 0.75 Sv at 30, 100, 150 and 200 mCi respectively, whereas after 30 min residence time in the stomach, this organ absorbs an equivalent dose of 3.30, 11.02, 16.52 and 22.03 Sv at 30, 100, 150 and 200 mCi respectively.

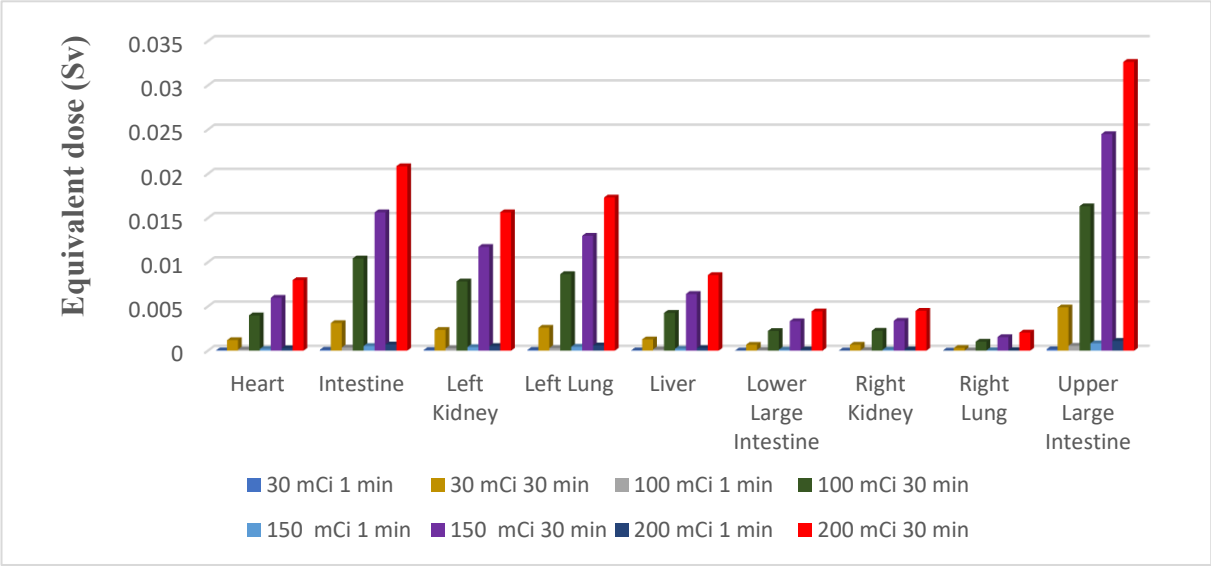

Figure 108 : *Equivalent dose at 1 and 30 min for a male afflicted with thyroid cancer (H_T<0.35E-01 Sv)*

The upper large intestine absorbed an equivalent dose of 1.11E-03 Sv 1 min after receiving an activity of 200 mCi whereas 30 min of the same exposure results in an equivalent dose of 3.26E-02 Sv.

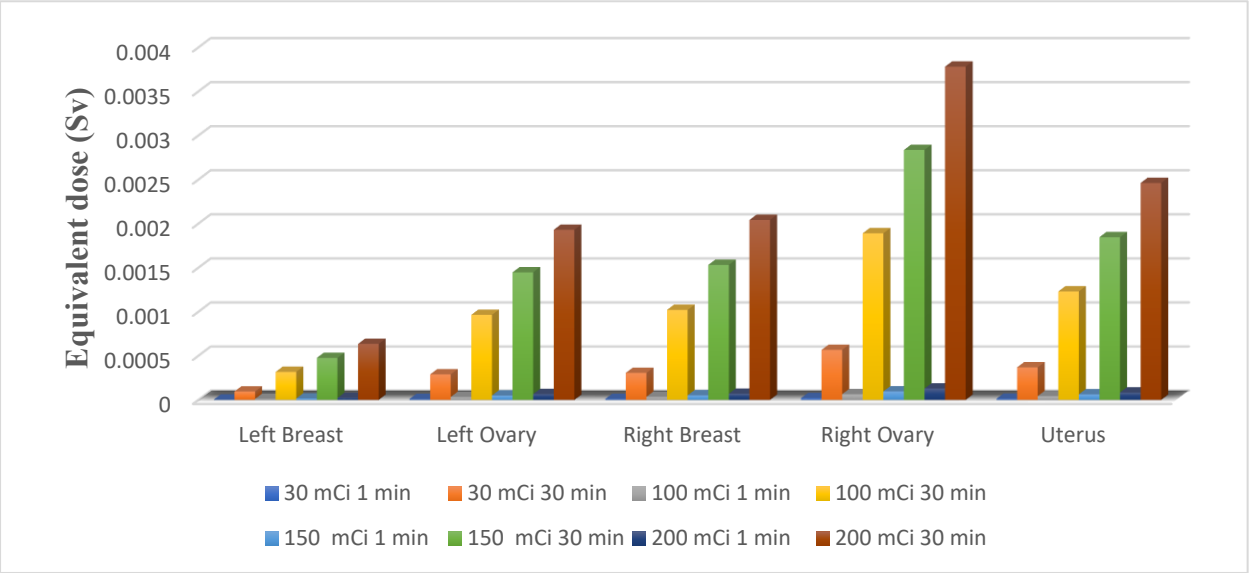

Figure 109 : *Equivalent dose at 1 and 30 min for a female afflicted with thyroid cancer (sex-specific organs).*

Among the female specific organs, the right ovary received the highest equivalent dose, 3.78E-03 Sv from 30 min of 200 mCi exposure, the equivalent dose to the uterus is slightly higher than that of the right breast and the left ovary.

- Source: small intestine

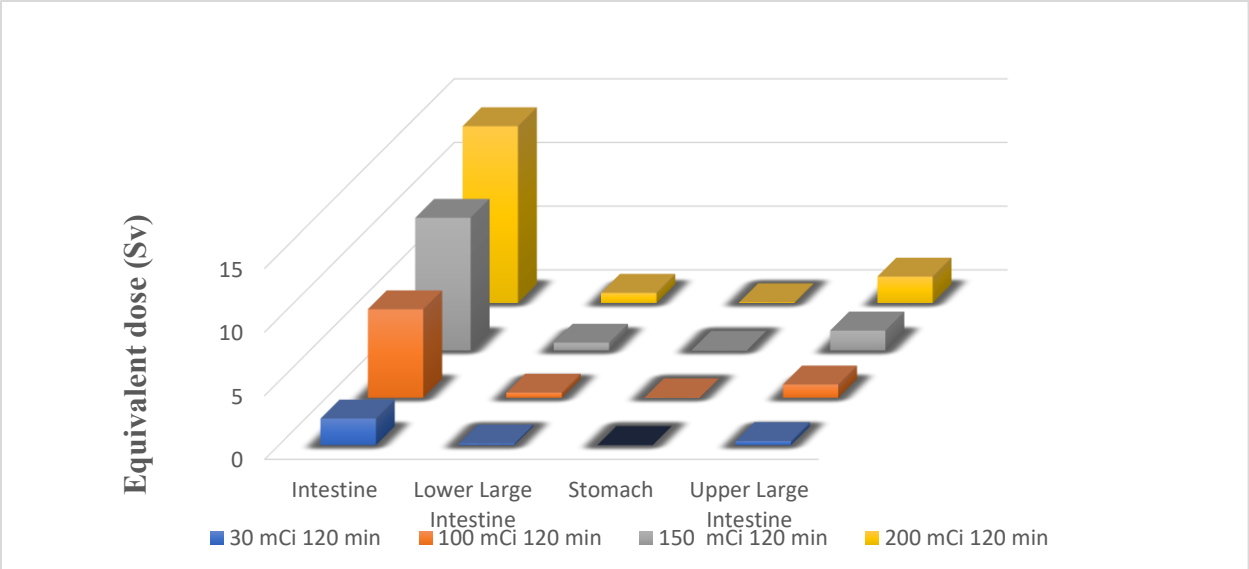

Figure 110 : *Equivalent dose after 90 min residence in the small intestine for a male afflicted with thyroid cancer.*

After 90 min residence of ^{131}I in the intestine, the equivalent dose absorbed from a 200 mCi exposure is 13.88 Sv, the upper large intestine receives 2.07 Sv from the same exposure.

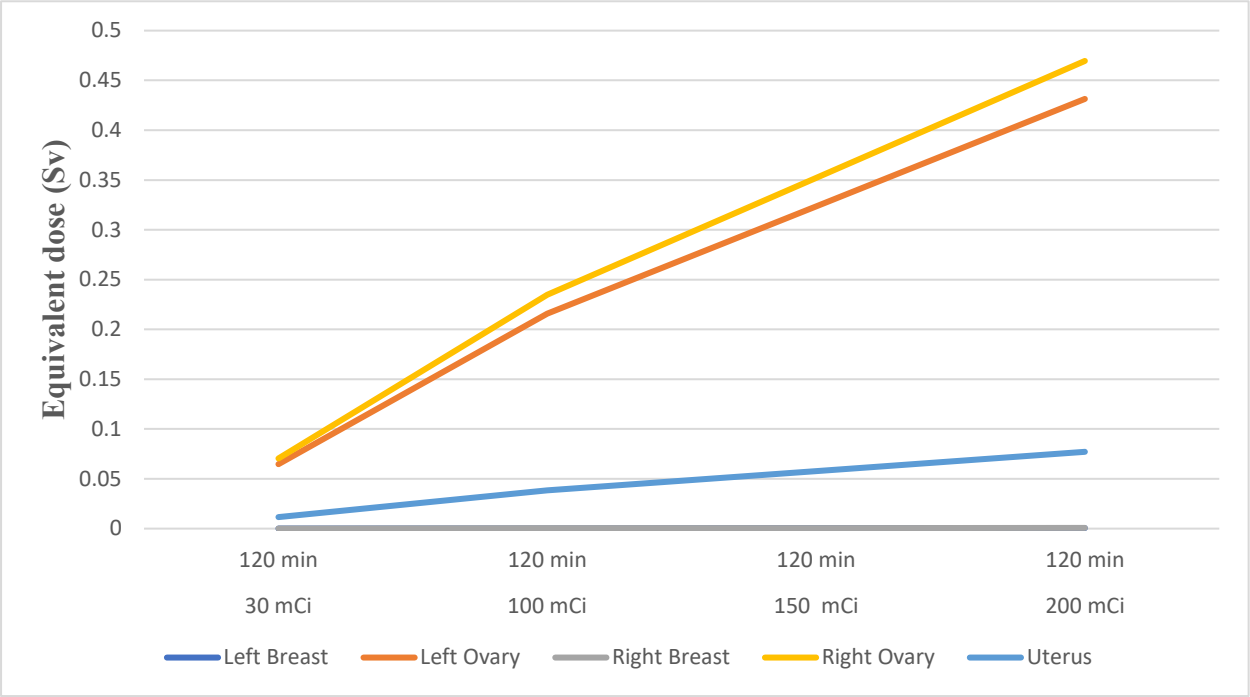

Figure 111 : *Equivalent dose after 90 min residence in the small intestine for a female afflicted with thyroid cancer (sex-specific organs).*

In the female phantom 90 min residence in the intestine would result in the right ovary as the highest irradiated female-specific organ, 0.47 Sv from 200 mCi exposure.

- Source: thyroid

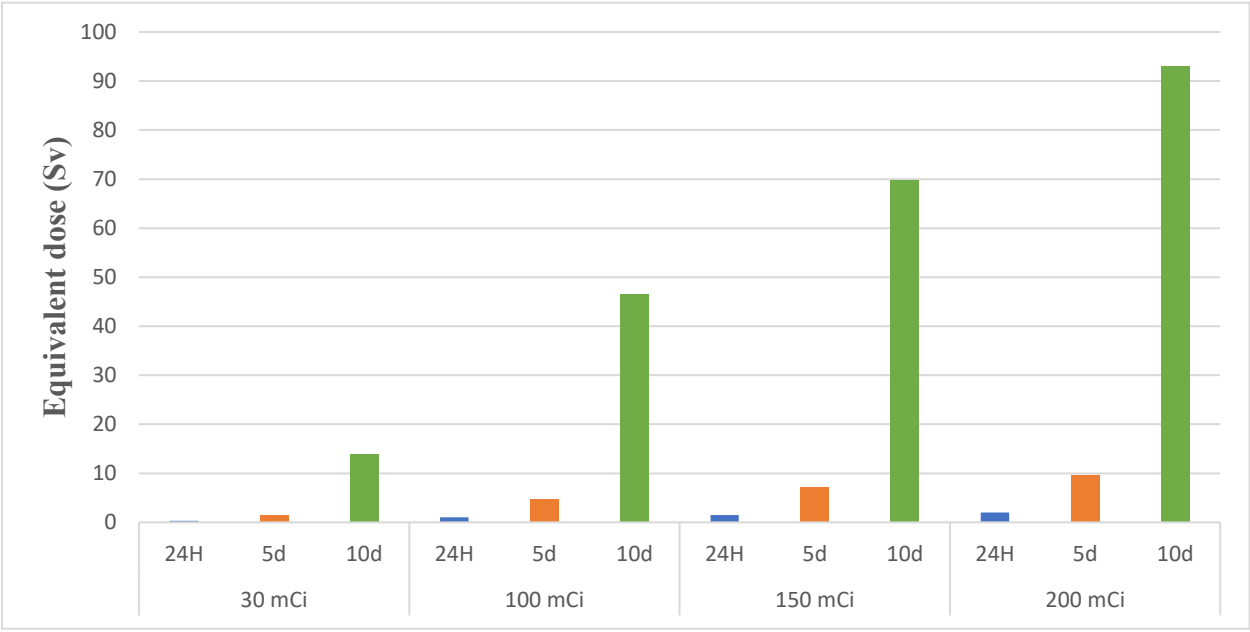

Figure 112 : *Equivalent dose to the thyroid after 24H, 5 and 10 days residence in the thyroid for a male afflicted with thyroid cancer*

The self-absorbed equivalent doses in the thyroid from a 200 mCi exposure are 2.02, 9.67 and 93.01 Sv at 24H, 5d and 10d respectively.

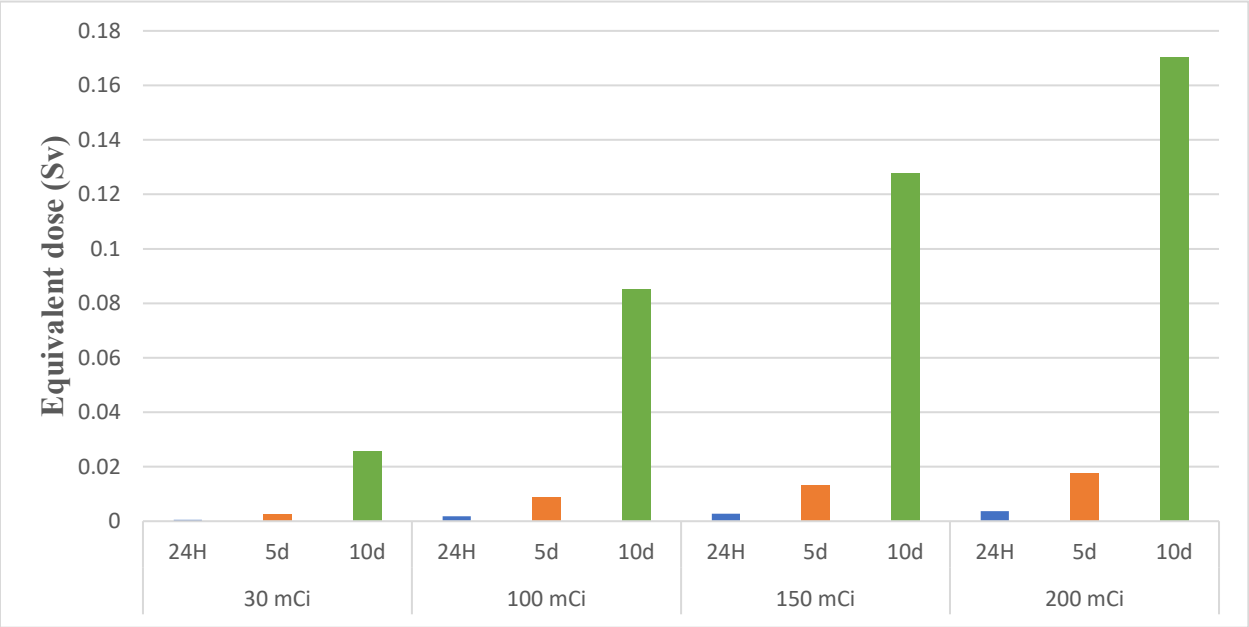

Figure 113 : *Equivalent dose to the head after 24H, 5 and 10 days residence in the thyroid for a male afflicted with thyroid cancer.*

The cross-absorbed doses in the head from a 200 mCi exposure are 3.70E-03, 1.77E-02 and 0.17 Sv at 24H, 5d and 10d respectively.

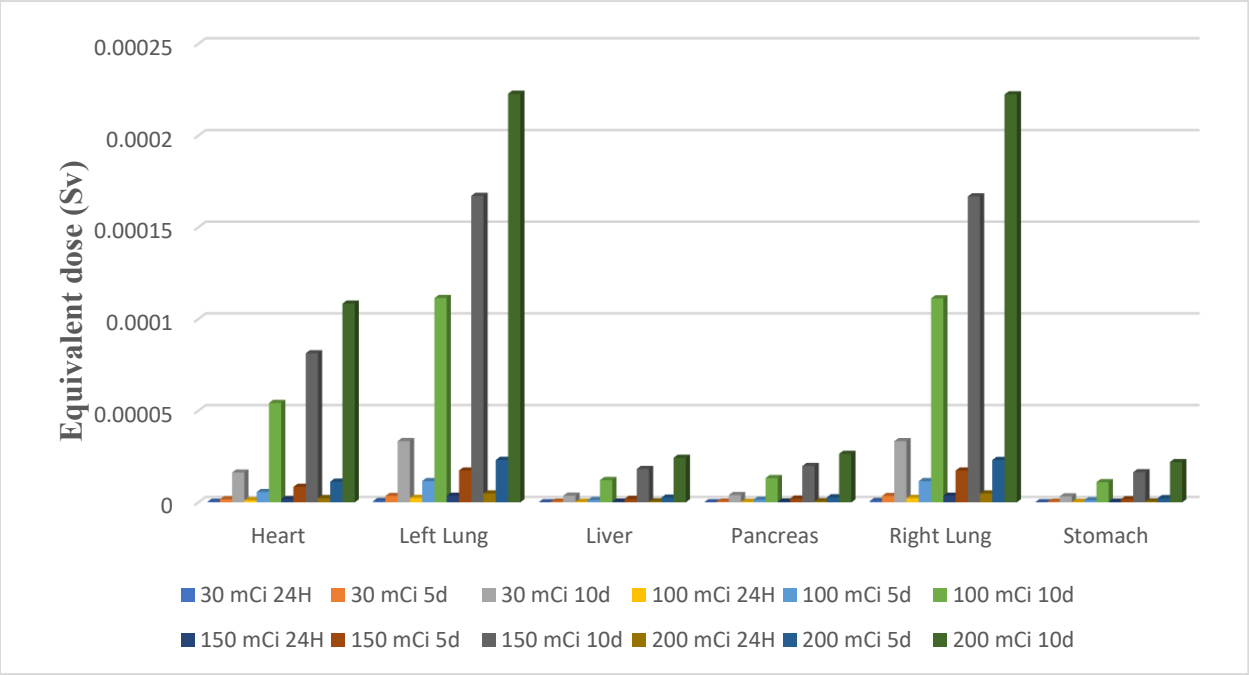

Figure 114 : *Equivalent dose after 24H, 5 and 10 days residence in the thyroid for a male afflicted with thyroid cancer (H_T<2.5E-04 Sv).*

The cardiothoracic organs are the most exposed organs from the trunk, the left and right lung have similar equivalent doses from 200 mCi exposure which are: 4.83E-06, 2.31E-05 and 0.22E-03 Sv at 24H, 5d and 10d respectively.

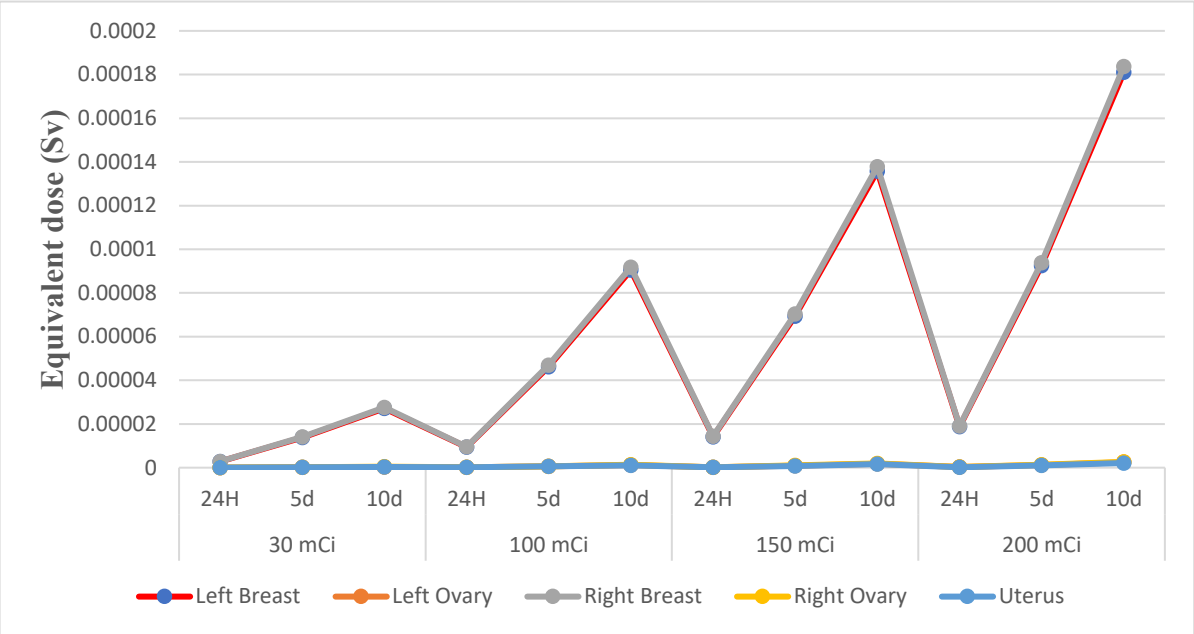

Figure 115 : *Equivalent dose after 24H, 5 and 10 days residence in the thyroid for a female afflicted with thyroid cancer (sex-specific organs)*

The right and left breasts are the most exposed female-specific organs, after 10 days exposure to a 200 mCi ^{131}I source, the equivalent dose in these two is 1.83E-04 Sv.

- Source: kidneys.

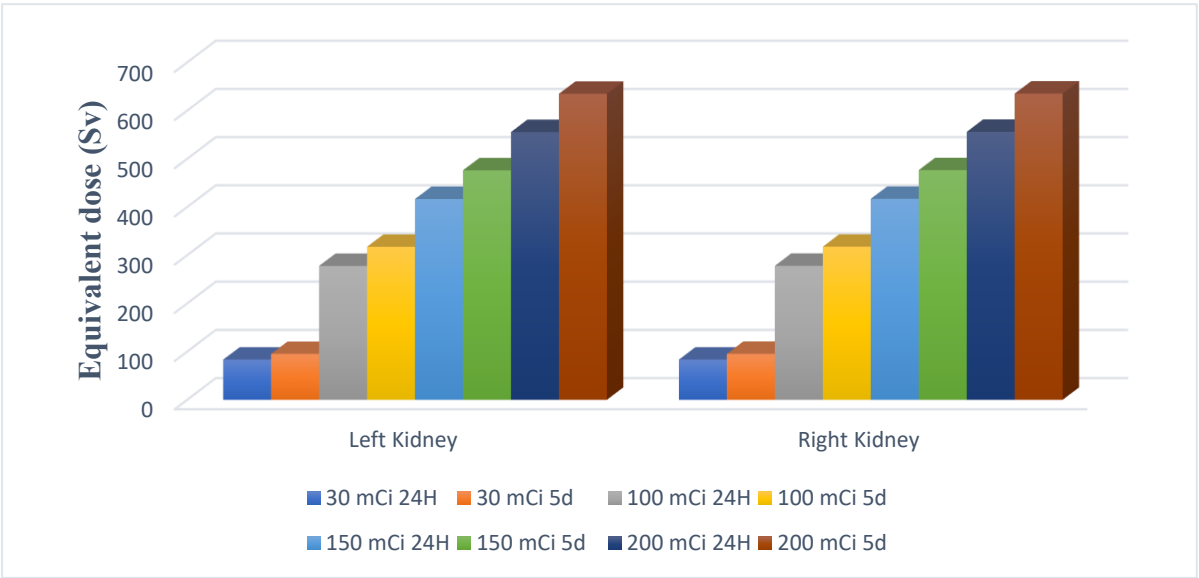

Figure 116 : *Equivalent dose in kidneys after 24H and 5 days residence in the kidneys for a male afflicted with thyroid cancer*

The self-absorbed equivalent dose to both kidneys is similar, it is 95.30 Sv 5 days from an exposure to 30 mCi and 635 Sv 5 days after an exposure to 200 mCi.

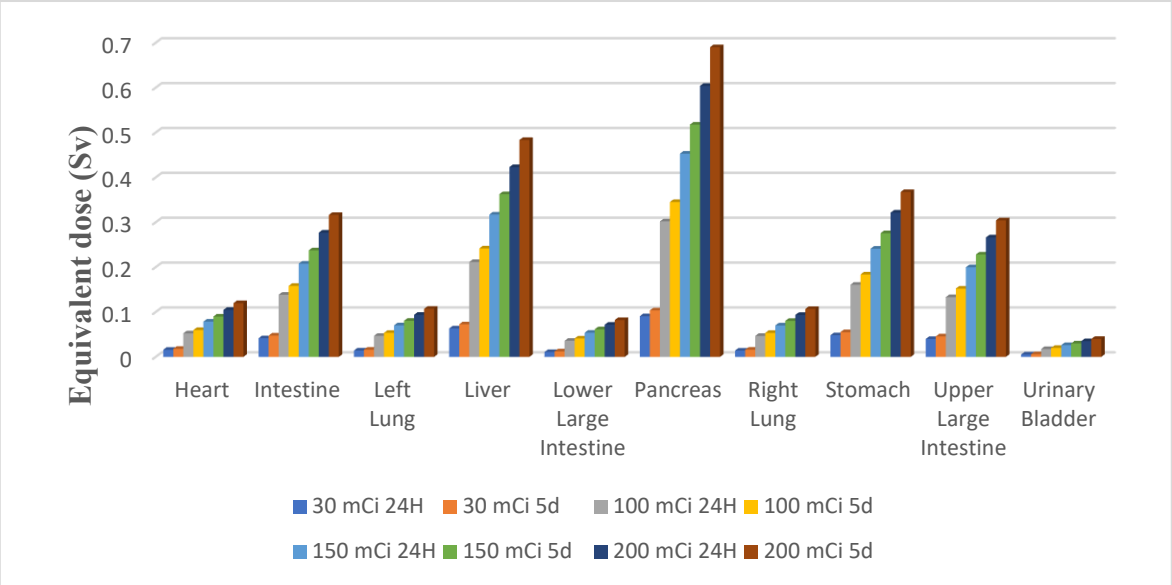

Figure 117 : *Equivalent dose after 24H and 5 days residence in the kidneys for a male afflicted with thyroid cancer (H_T<0.7 Sv).*

Among the organs located in the trunk, the pancreas is the most exposed with an equivalent dose of 0.69 Sv after 5 days of exposure to a 200 mCi source.

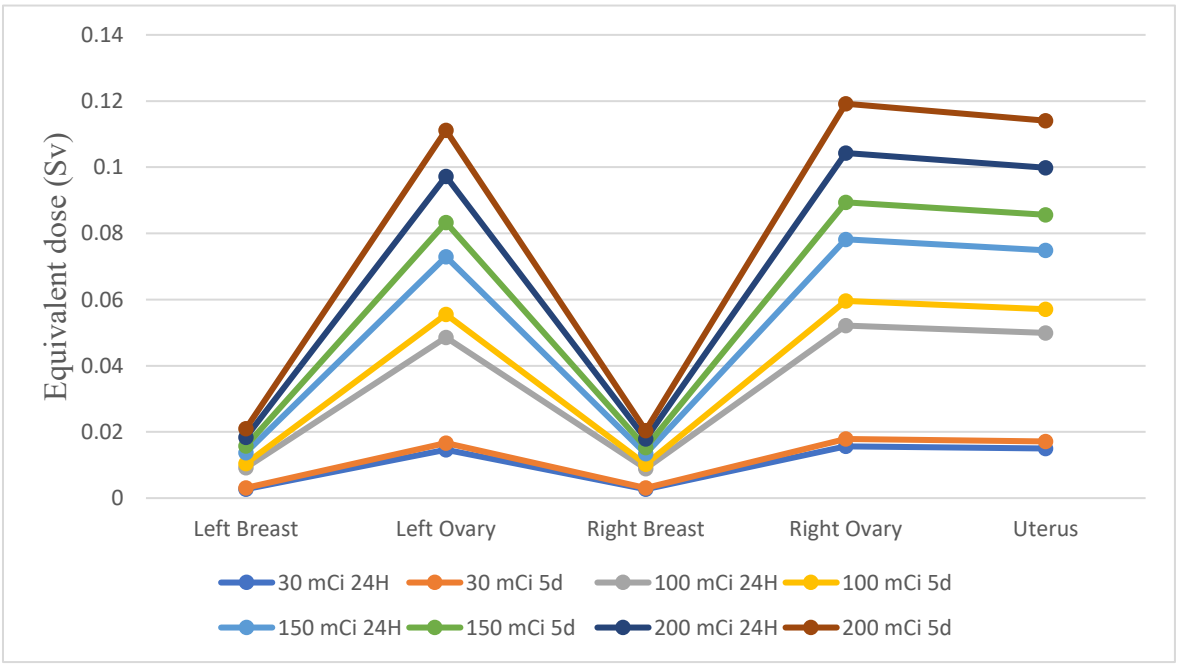

Figure 118 : *Equivalent dose after 24H and 5 days residence in the kidneys for a female afflicted with thyroid cancer (sex-specific organs)*

From the female-specific organs the right ovary, the uterus and the left ovary are the most exposed to radiation, be it for a low or a high dose, for 24H or 5 days.

- Source: urinary bladder

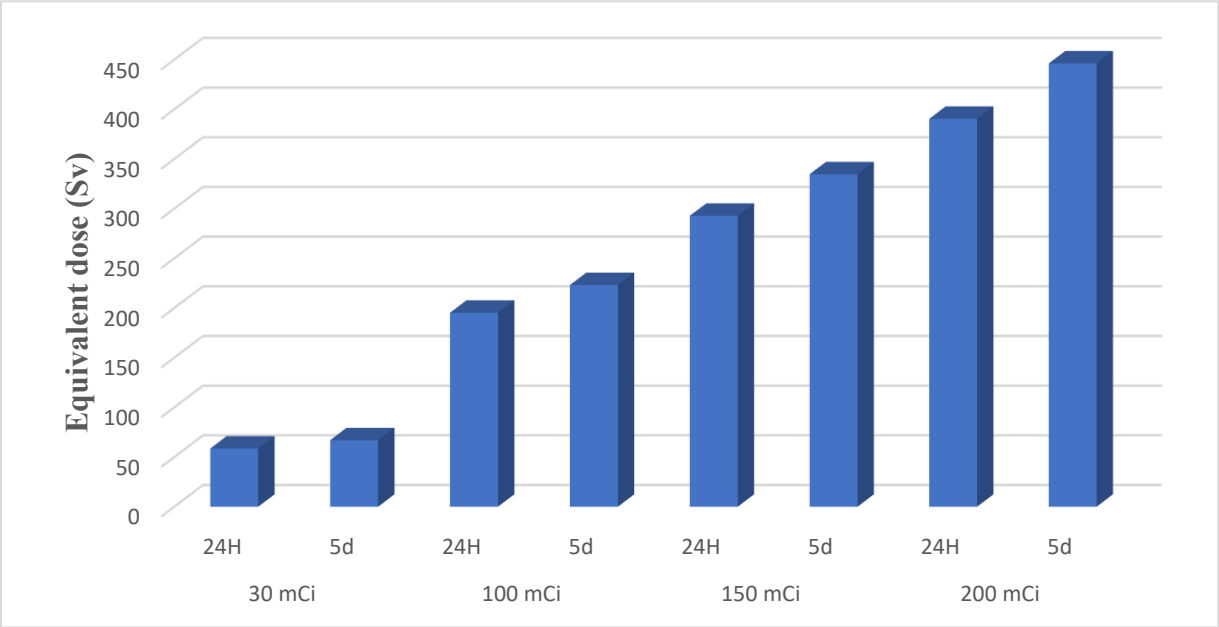

Figure 119 : *Equivalent dose to the urinary bladder after 24H and 5 days residence in the urinary bladder for a male afflicted with thyroid cancer*

The self-absorbed equivalent dose to the urinary bladder from a 200 mCi exposure at 24H and 5d is 390 Sv and 446 Sv respectively.

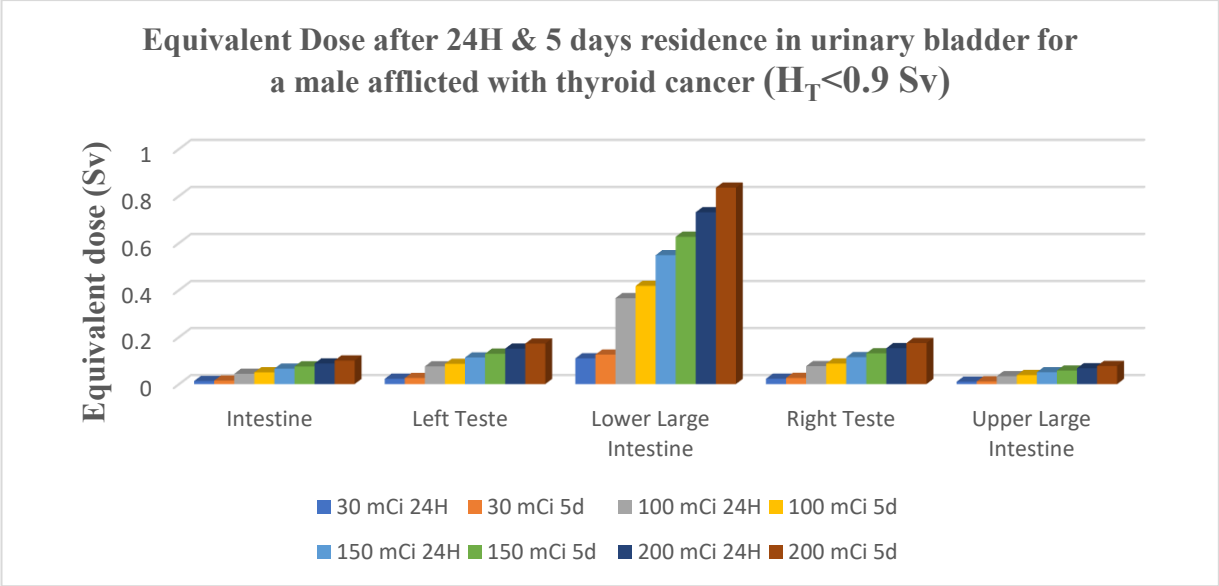

Figure 120 : *Equivalent dose after 24H and 5 days residence in the urinary bladder for a male afflicted with thyroid cancer (H_T<0.9 Sv).*

When ^{131}I is concentrated in the urinary bladder, aside from the self-absorbed dose, the most irradiated organ is the lower larger intestine.

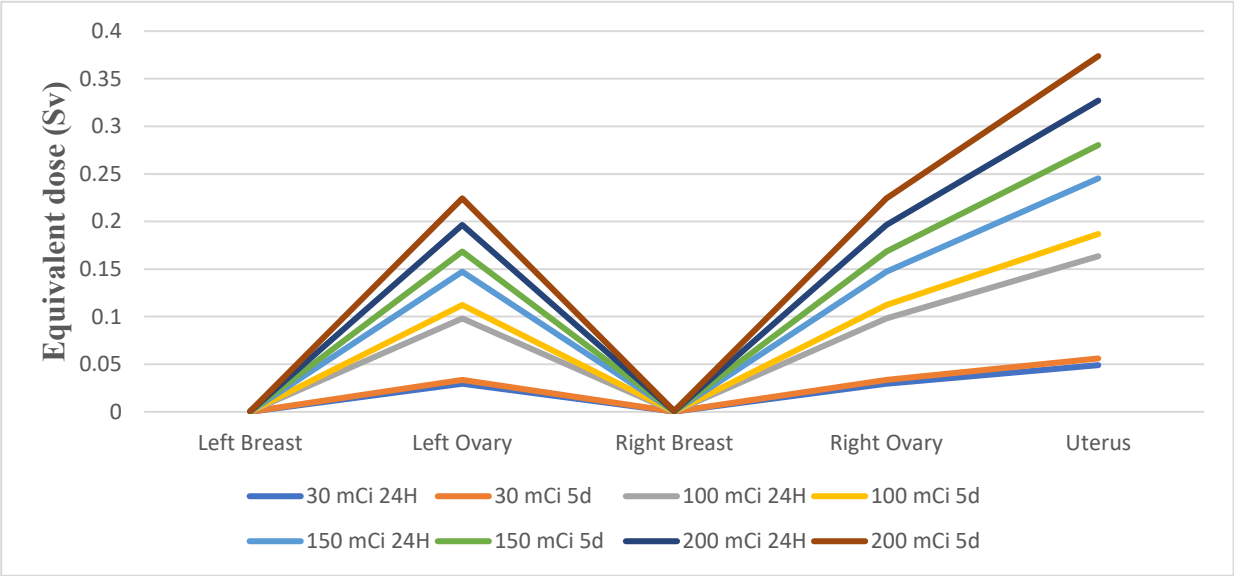

Figure 121 : *Equivalent dose after 24H and 5 days residence in the urinary bladder for a female afflicted with thyroid cancer (sex-specific organs)*

Regardless of the administered activity, the uterus is the most exposed organ followed by the two ovaries.

- Cumulative equivalent doses 2H after the ingestion of the capsule:

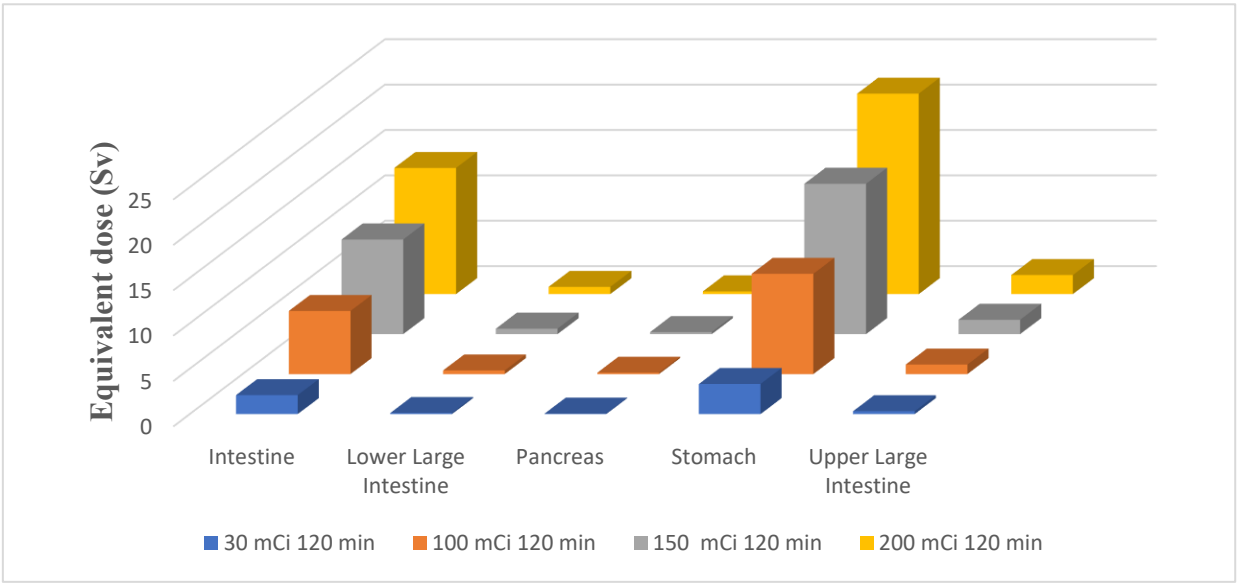

Figure 122 : *Equivalent dose 2H after the ingestion of the capsule for a male afflicted with thyroid cancer.*

Even after 2H after the ingestion of ^{131}I capsule the stomach is still the most irradiated organ.

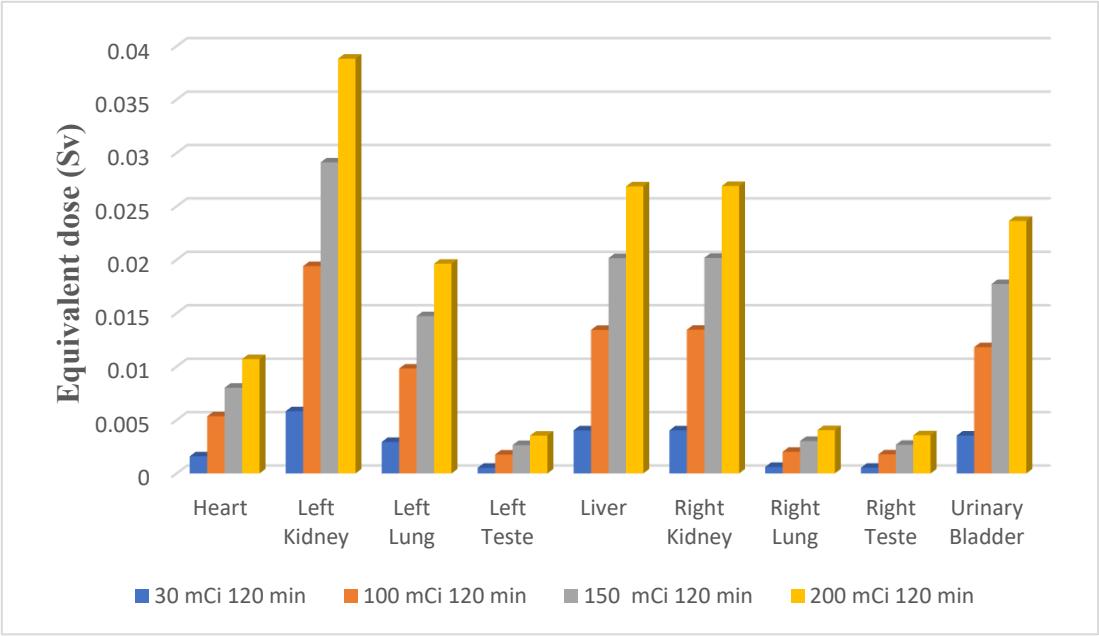

Figure 123 : *Equivalent dose 2H after ingestion of the capsule for a male afflicted with thyroid cancer (H_T<0.4E-01 Sv).*

In 2 hours, the left kidney is more irradiated than the right; the latter along with the liver, the urinary bladder and the left lung have approximately the same equivalent dose.

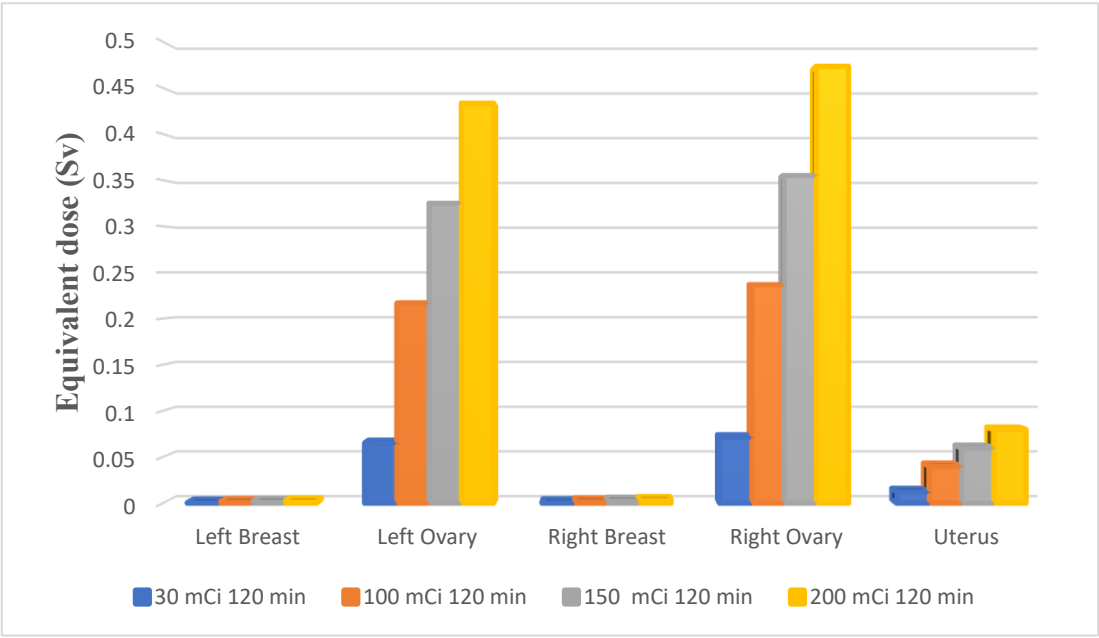

Figure 124 : *Equivalent dose 2H after ingestion of the capsule for a female afflicted with thyroid cancer (sex-specific organs).*

The right and left ovary present approximately the same equivalent dose of 0.47 Sv in 2 hours' time after an exposure to 200 mCi of ^{131}I.

- Cumulative equivalent doses 24H after the ingestion of the capsule:

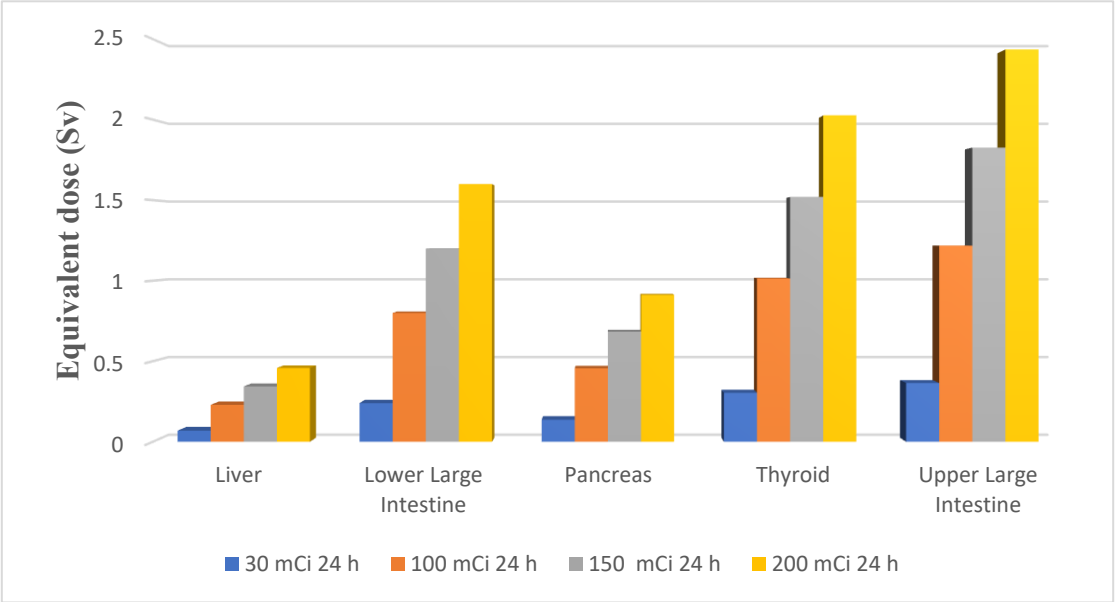

Figure 125 : *Equivalent dose 24H after ingestion of capsule for male afflicted with thyroid cancer (H_T<2.5 Sv).*

Ingesting a capsule of 200 mCi activity results in an equivalent dose to the upper large intestine of 2.44 Sv and to the pancreas of 0.91 Sv.

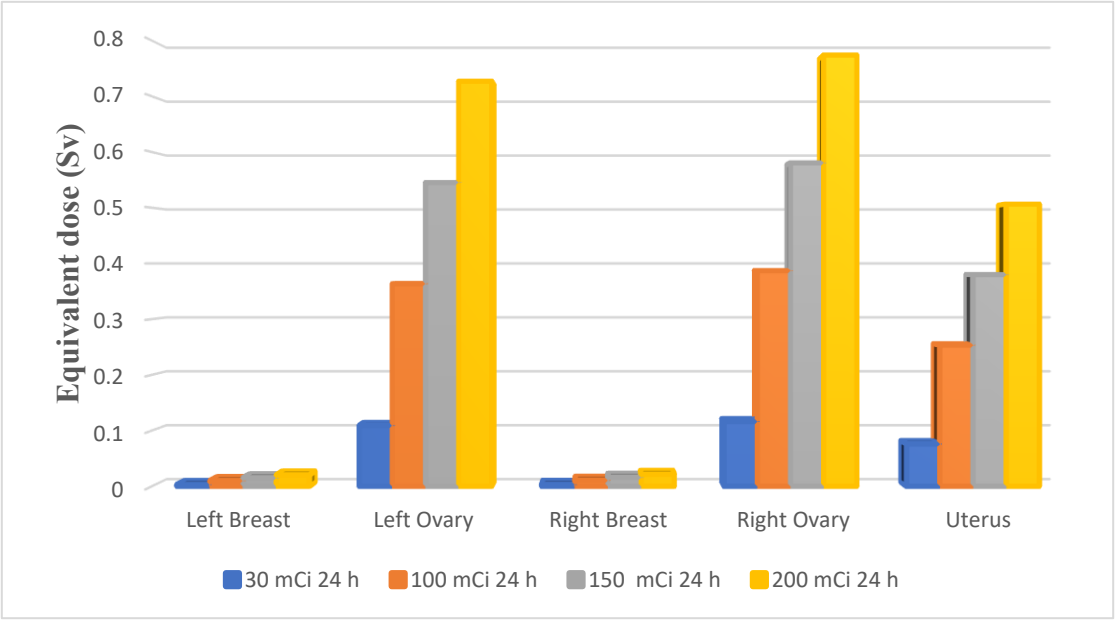

Figure 126 : *Equivalent dose 24H after ingestion of capsule for a female afflicted with thyroid cancer (sex-specific organs).*

Regarding the female-specific organs the left and right ovary have an equivalent dose of 0.72 and 0.77 Sv respectively when irradiated with a source of 200 mCi, the uterus on the other hand receives an equivalent dose of 0.5 Sv in the same conditions.

- Cumulative equivalent doses 5 days after the ingestion of the capsule:

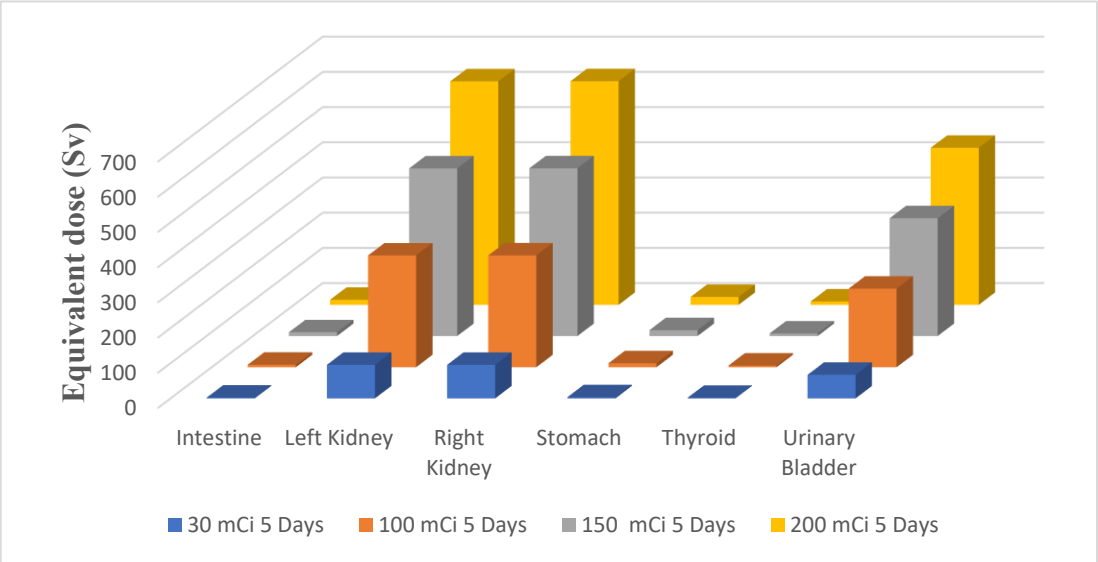

Figure 127 : *Equivalent dose 5d after ingestion of the capsule for male afflicted with thyroid cancer.*

In thyroid cancer treatment 95% of the administered ^{131}I is eliminated directly, so 5 days after the ingestion of the capsule it is apparent that the most exposed organs are the two kidneys followed by the urinary bladder.

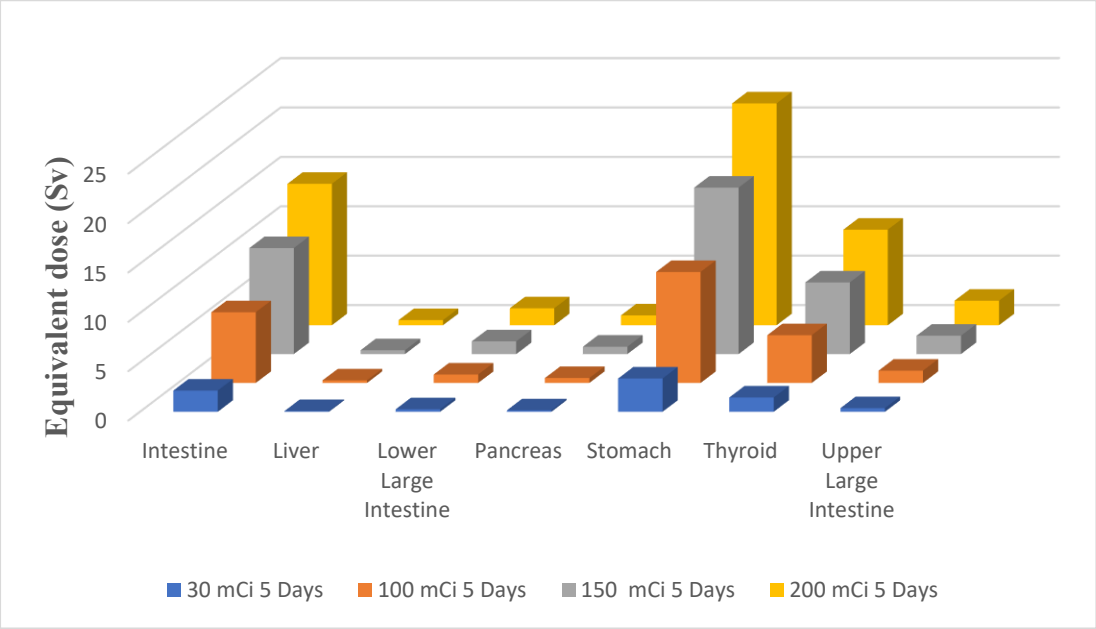

Figure 128 : *Equivalent dose 5d after ingestion of the capsule for male afflicted with thyroid cancer (H_T<25 Sv).*

The cumulative equivalent dose in the stomach in 5 days is 22.46 Sv from an activity of 200 mCi, the intestine receives an equivalent dose of 14.32 Sv from the same activity while the thyroid is exposed to an equivalent dose of 9.67 Sv in similar conditions.

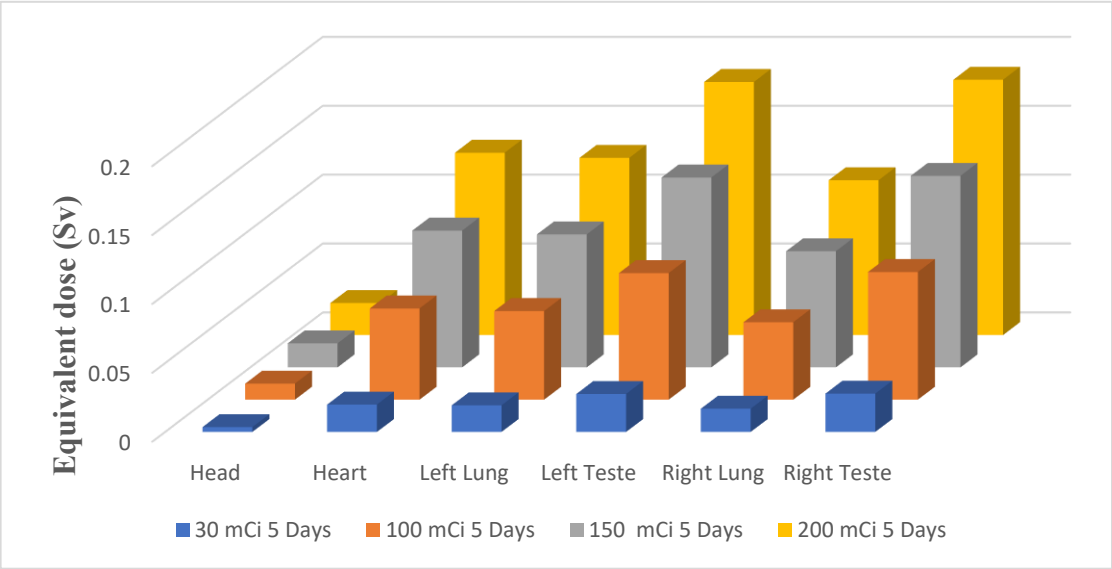

Figure 129 : *Equivalent dose 5d after ingestion of the capsule for male afflicted with thyroid cancer (H_T<0.2 Sv).*

The testes are also highly exposed in 5 days (H_T= 0.18 Sv; 120 mCi) along with the heart (H_T= 0.13 Sv; 120 mCi) and lungs (H_T= 0.12 Sv; 120 mCi).

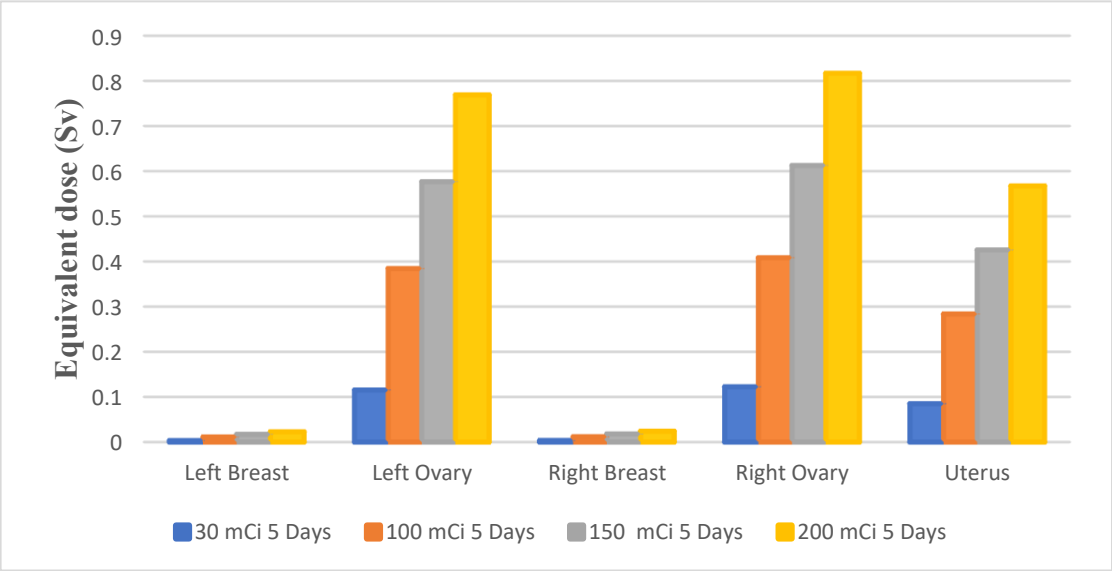

Figure 130 : *Equivalent dose 5d after ingestion of the capsule for a female afflicted with thyroid cancer (sex-specific organs).*

The 5 days exposure to an ingested capsule of 200 mCi of ^{131}I results in an equivalent dose to the ovaries of around 0.8 Sv and an equivalent dose of 0.57 Sv to the uterus.

4.2.3. Comparison between hyperthyroidism and thyroid cancer:

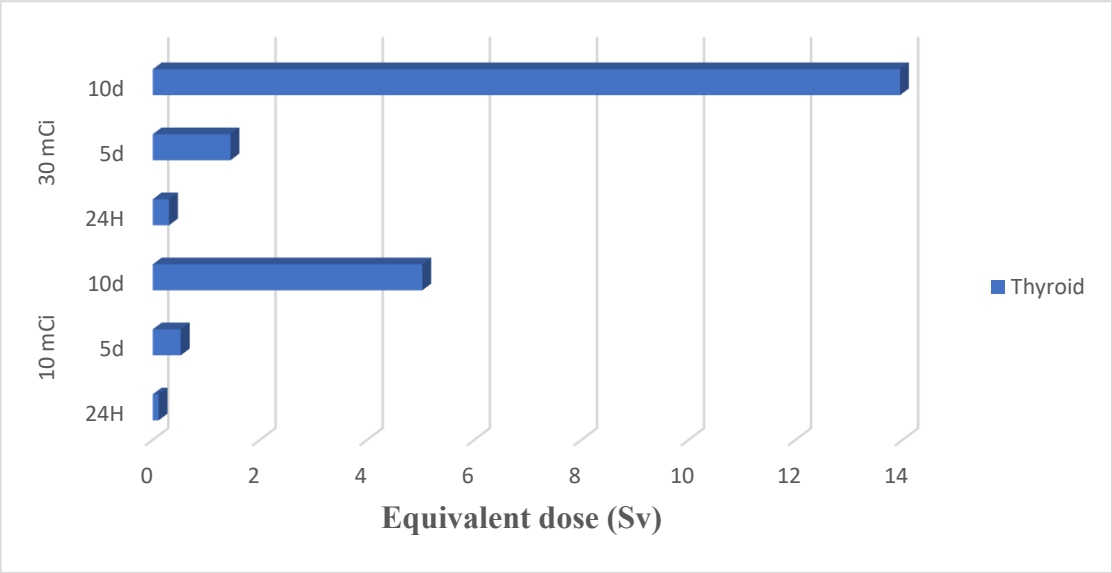

Figure 131 : *A comparison between equivalent dose in the thyroid in male after 24H, 5 and 10 days residence in thyroid*

Between hyperthyroidism (10 mCi) and thyroid cancer (30 mCi; the smallest prescribed dose) the biggest equivalent dose is that of 30 mCi which in 10d is 13.95 Sv yet in the case of 10 mCi it is 5.03 Sv.

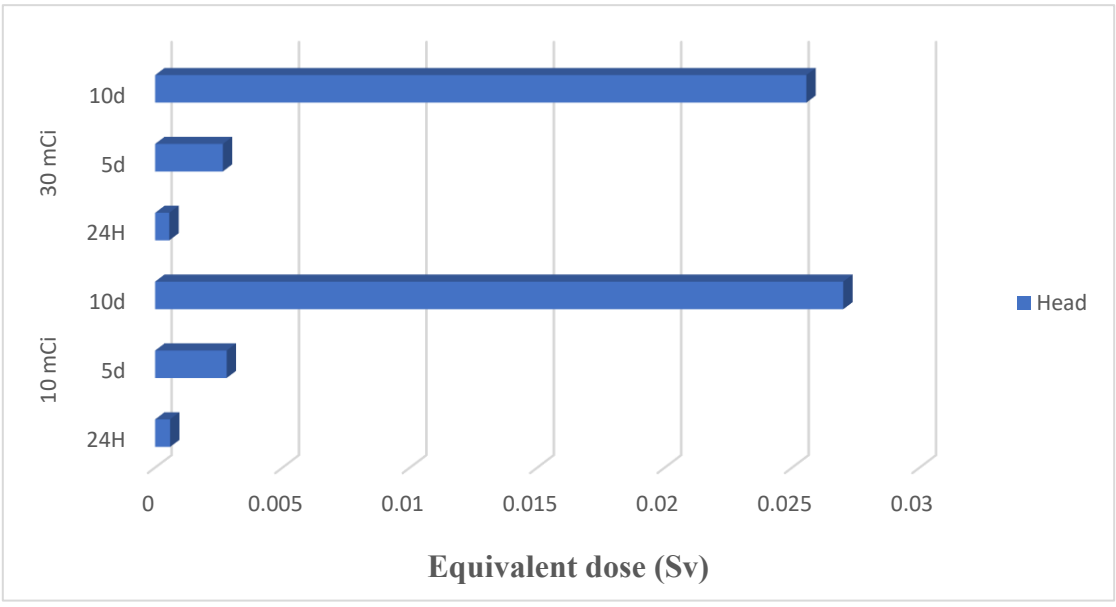

Figure 132 : *A comparison between equivalent dose in the head in male after 24H, 5 and 10 days residence in thyroid*

Interestingly, the equivalent dose to the head from hyperthyroidism's treatment; even though of smaller activity; is higher than that in the thyroid cancer's treatment, the value in 10d is respectively 2.70E-02 Sv and 2.55E-02 Sv.

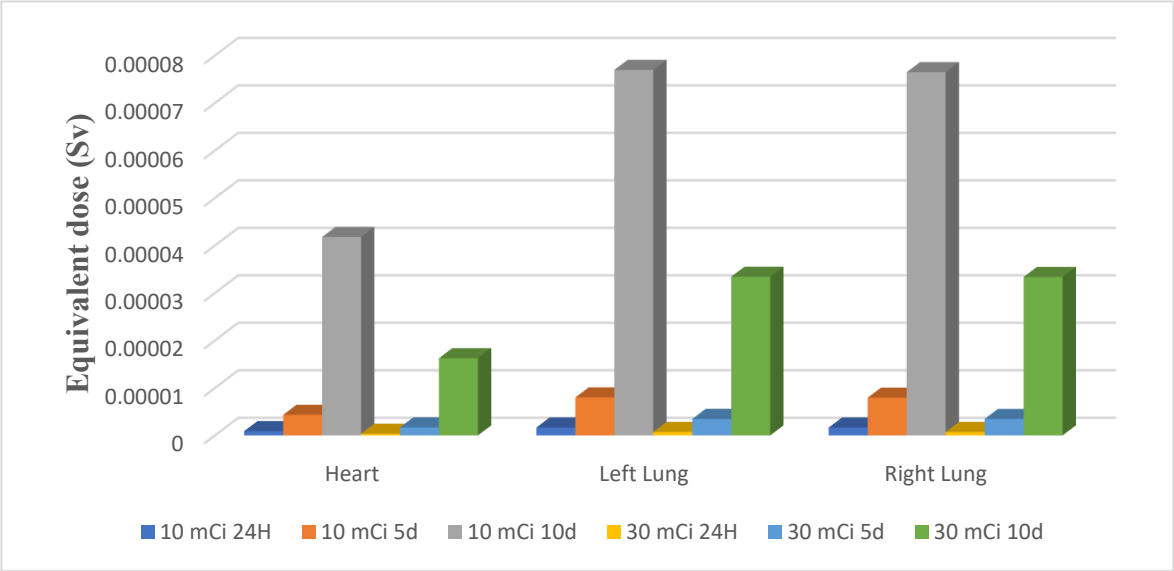

Figure 133 : *A comparison between equivalent dose in the heart, left & right lung in a male after 24H, 5 and 10 days residence in thyroid.*

The equivalent dose to the lungs is more than 2 times higher in hyperthyroidism than in thyroid cancer (7.70E-05/3.34E-05; 10d), a similar result is found in the heart where the equivalent dose is 2.5 higher in hyperthyroidism (4.18E-05/1.63E-05; 10d).

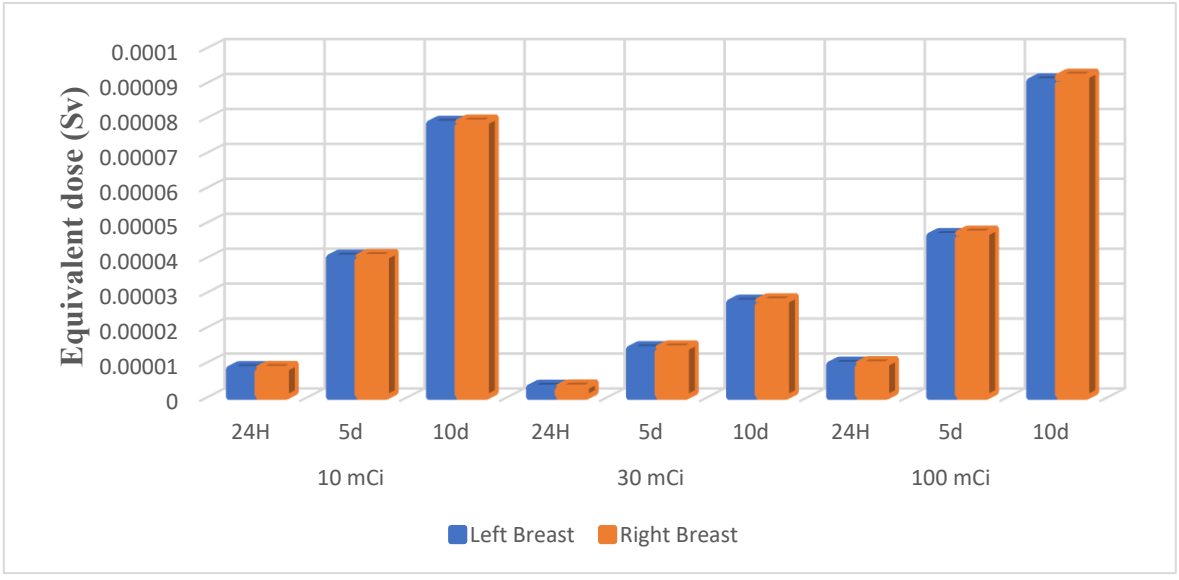

Figure 134 : *A comparison between equivalent dose in the left & right lung in a female after 24H, 5 and 10 days residence in thyroid*

In 10 days' time, the equivalent dose to the breasts is 7.87E-05 Sv when treating for hyperthyroidism, 2.75E-05 Sv from 30 mCi exposure and 9.18E-05 Sv from 100 mCi exposure, in thyroid cancer treatment; it becomes clear that the equivalent dose in 10 mCi in this scenario is 2.86 times higher than 30 mCi and 1.16 times lower than 100 mCi.

5. Discussion

a) socio-demographic description

Within the 8 months of our study, 542 patients were prescribed radioiodine therapy in the department of nuclear medicine in the University Hospital Center of Tlemcen; 86% of them were diagnosed with thyroid cancer while the remaining 14% with hyperthyroidism.

In our study, out of the 74 patients afflicted with hyperthyroidism, 47 (63.51%) were females and 27 (36.49%) were males, the F/M sex ratio was 1.74, these results are consistent with a study carried out from 1965 to 1968 in Nagano Prefecture Japan by Rukio Furihata and Masao Makiuchi (227) where 47 cases were diagnosed with hyperthyroidism; from which 12 were males (25.53%) and 35 (74.47%) were females with a F/M sex ratio of 2.91, a similar outcome was found in a study conducted by Zdraveska et al. (228) for 5 years in which 329 patients took part; 234 were females and 95 were males, the F/M sex ratio was 2.5; the results confirm a female predominance in hyperthyroidism.

All of the 74 patients treated for hyperthyroidism in the University Hospital Center of Tlemcen were prescribed a dose of 10 mCi, whereas another study shows a variety of doses indicated in the treatment of hyperthyroidism, Zdraveska et al. (228) have directed a study on 30 patients who were treated with radioiodine for hyperthyroidism; 34% have been prescribed a dose of 30 mCi, and 30% a dose of 10 mCi while the rest got prescribed doses varying from 5 to 35 mCi.

Out of the remaining 468 patients; 407 were females with a F/M sex ratio of 6.69; just like with hyperthyroidism it is clear that there is a female predominance in patients afflicted with thyroid cancer, this female predominance is a constant epidemiological feature found in most of the conducted studies, in particular, an epidemiological study carried out by Guidoum et al (229) in two wilayas of northern eastern Algeria where a F/M sex ratio of 6.1 was found in Guelma whereas El Taref registered a sex ratio of 12.7 in favor of females; another study conducted in Gabon (230) have shown practically comparable results; from 131 patients suffering from thyroid cancer 93.12% were female, i.e. a F/M sex ratio of 13.5; some fascinating results have been deduced from the study of Benouis et al. (94) which was conducted on 1376 cases of thyroid cancer over three years; 94.75% of patients were women with a sex ratio of 18.08.

These findings can be explained by the fact that thyroid cancer's growth is thought to be promoted by high estrogen levels, Manole et al. (231) have confirmed and extended this theory since their RT-PCR and Western Blot analysis have shown high expression of ER mRNA in thyroid cancer patients.

The mean age in males is 39 ± 9.291 years whereas in females it is 39.5 ± 10.371 years those results differ from the results of Guidoum et al (229) which were 45.4 ± 16.3 years and 42.6 ± 14.6 years in males and females respectively, as well as results of Bendouida et al (232) which showed an age average of 45.60 ± 15.71 years in patients, these differences could be interpreted by the criteria we imposed in our case study in which we did not include any patient whose age is less than 18 or more than 60 years old.

Our results show a peak for the group of]34-47] for females and]32-46] for males of 43.24% and 47.54% respectively similar results were found in Benouis et al. (94) study which presented a peak for the group]40-60] of 45.88%.

59.17% of females and 59.02% of males are treated with a dose of 30 mCi while 38.57% of females and 39.34% of males have been prescribed a dose of 100 mCi, the rest of the females 1.47% and 0.25% have been treated with 200 mCi and 150 mCi respectively; the predominance of these prescribed doses (30 mCi and 100 mCi) is observed in the study of Yusuke Iizuka et al. (222) in which their patients have undergone iodine radiation therapy for thyroid cancer and the used doses were 30 mCi (57.14%) and 100 mCi (40.33%) while the rest of the patients (2.53%) have been prescribed a dose of 80 mCi.

b) Results analysis

Equivalent dose estimations were performed for all activities used in radioiodine therapy for thyroid cancer and hyperthyroidism treatment in the nuclear medicine department in the University Hospital Center of Tlemcen, the lowest of which is the dose used in the treatment of hyperthyroidism i.e., 10 mCi, while the maximum dose used for thyroid cancer therapy is 200 mCi, regardless of the choice being empirical or based on dosimetry-guided techniques, the ATA 2009 guidelines and the European 2006 consensus report suggest that clinicians can choose between the low dose and the high dose (233,234). The National Comprehensive Cancer Network guidelines recommend using 30 to 100 mCi radioiodine in cases of papillary, follicular, or Hurthle cell carcinoma ≥ 1 cm in diameter, with nodal or distant metastases or with aggressive histology when there is suspected or proven thyroid bed uptake in total body radioiodine scan after thyroidectomy (235).

Equivalent dose estimations were done for most organs (target organs), these doses may result from radioactive decay occurring in other regions called source regions thus the equivalent dose in a given organ is typically the sum of contributions from various sources including the self-absorbed dose. Five source organs are included in the calculation of the equivalent dose representing five important stops in the pharmacokinetics' profile of iodine hence the urgent need for some information in dose calculation including the fractional long-term retention of the radionuclide, turnover of the radiopharmaceutical and its metabolites, fractional gastrointestinal absorption values since it is administered orally, distribution of radioisotope within different organs and its excretion pathways.

When we compare our results with ICRP pamphlet N° 11, we observe some differences which are due to various reasons:

- The first possible reason is the model used for simulation, since some modifications were made in the tissues' density and composition which would infer a change in organ mass and therefore a significant change in absorbed dose besides some of the geometries were slightly changed to turn the hermaphrodite phantom into separate male and female phantoms.
- The second reason is the spectrum used for simulation which is different from the one used for MIRD calculations, due to the unavailability of the spectrum used by MIRD, our choice landed on the ^{131}I spectrum given by the table of radionuclides (226).
- We also made the assumption that iodine's distribution in an organ is homogenous which is not really the case, for example in the case of thyroid, iodine is concentrated in

the colloid, therefore a volumetric source is not accurate but it is the closest to represent the distribution of radioiodine in the source organs.

- Another reason would be the total number of histories during the simulation which in our case was 10^7.

The values of effective doses for stomach and other organs such as intestine, upper and lower large intestine, liver, lungs, kidneys, and urinary bladder are presented in figures number 85, 86, 108 and 109, while the effective dose for breasts, ovaries and the uterus are presented in figure number 87 and 110.

In these figures are given the compared values for 1 minute and 30 minutes in the case of hyperthyroidism as well as thyroid cancer. In both cases the highest received equivalent dose is to the stomach, being the source of emission, this organ receives the total dose generated by β-decay, the highest stomach doses were expected concerning the β-γ nature of ^{131}I decay. The β particles and secondary electrons created through interaction of γ-rays deposit their energies in short path-lengths. These energy depositions result in absorbed doses to the stomach in which the radionuclide is localized and to organs in its vicinity (236). γ-decay can penetrate through the stomach wall and deposit its energy in the adjacent organs, the first one being the pancreas, due to its close proximity, followed by the large intestine, the intestine, left lung and left kidney. The right ovary, even though it gets exposed to a smaller dose from that of the abdominal organs it is still much more affected than the rest of the female specific organs.

In figures 88, 89 and 111 is shown the comparison of equivalent dose in intestine and abdominal organs after 90 min residence in small intestine, logically the highest equivalent dose is that of the intestine, given that it receives a self-absorbed dose, the second most affected organ is the large intestine followed by the stomach, kidneys and urinary bladder, these organs only receive a cross-dose due to the penetration of γ-rays through the intestinal wall. It is clear in figures 90 and 112 that both the ovaries and the uterus receive an equivalent dose much higher than that of the large intestine making them the second most affected organ in females in this stage of ingestion. This is in concordance with the fact that women may have transient ovarian failure. The increase in frequency of miscarriage during the year preceding conception has led to the recommendation of postponing conception until one year after treatment with ^{131}I.(235)

Needless to say, figures 91 and 113 prove that the thyroid is the most exposed organ when iodine reaches this organ, hence its use in hyperthyroidism and thyroid carcinoma, interestingly enough the human head is the second most irradiated organ in this stage as seen in figures 92 and 114 this can in a way explain why salivary glands are affected in radioiodine treatment, these findings are in accordance with the fact that radioactive iodine therapy can be associated with significant sequelae. Short-term complications occur in 10–30% of patients and include radiation thyroiditis, painless neck edema, sialadenitis and tumor hemorrhage or edema (235).These acute side effects are usually mild and resolve rapidly.

Figure 93 and 115 shows that heart and lungs are more affected than the rest of the body; nonetheless, that dose is less when the iodine was in the stomach or the intestine, the cause of which could be that there were more nuclei in the capsule at the absorption phase or even the fact that the bones with their higher density constitutes an obstacle to γ-rays coming from the thyroid something that is not an issue for the radiation coming from the stomach and the intestine since there's only soft tissue that separates them from the cardiothoracic organs.

Figures 94 and 116 demonstrates the equivalent dose absorbed in female-specific organs, contrary to previous sources, when iodine reaches the thyroid the most irradiated female organ becomes the breast while the dose received by the ovaries and uterus is very low.

Figures 95, 96, 117 and 118 represent equivalent dose in various time stamps while iodine is being eliminated through the kidneys, the two kidneys receive a self-absorbed dose and register the highest equivalent dose in the elimination phase which is understandable since 75% or 95%, depending on the thyroid's uptake, of the iodine that is absorbed through the intestine gets eliminated directly with no fixation in the thyroid, this is the most important reason why we can observe a higher equivalent dose in kidneys over the thyroid; other affected organs are the pancreas; liver; intestine and the stomach.

Because of their proximity to the kidneys, the ovaries and the uterus receive a higher equivalent dose than the breast, approximately 9 times higher, this is represented in figures 97 and 119.

Figures 98, 99 and 120 and 121 represent the equivalent dose in the urinary bladder which is the last stop for the radioiodine, due to its self-absorbed dose the urinary bladder is the most irradiated organ in this phase, the large intestine and testes are affected with a considerable dose as well. As for the female specific-organs figures 101 and 122 explicitly show that the uterus is the most exposed organ.

Figures 104, 105 and 128 shows that in 24H after being treated with radioiodine, the urinary bladder is the most affected organ even more than the thyroid which is supposed to be the main target for this therapy, the kidneys also receive a very high equivalent dose followed by the stomach, intestine and large intestine.

Figure 133 show that a dose of 10 mCi in hyperthyroidism is bound to produce a higher equivalent dose in the head than that of 30 mCi; the same thing can be deduced from figure 134 which shows how a 10 mCi dose leaves an equivalent dose in the lungs and heart more important than that of 30 mCi; an observation that holds true in the case of the breasts in the female population, as shown in figure 135, a 10 mCi capsule gives an absorbed dose higher than that of 30 mCi and close to that of 100 mCi. In thyroid cancer therapy and due to ablation of the thyroid the uptake in the thyroid may be very small, and in these cases the absorbed dose due to iodide taken up in the stomach may be of more interest this holds true for the kidneys and the urinary bladder as well.

c) Interpretation with epidemiological and clinical elements:

Actually, health effects are neither a concern to the patients, nor to the physicians because of the overall effect in treating tumors. Although there may be a risk of getting secondary cancers over many decades, this therapy is generally preferred over the certainty of dying from thyroid cancer. But in the latest years our findings are that thyroid cancer occurs at very young population

There are many epidemiological studies that reports that it appears to be no risk of cancer from radioiodine therapy (237). There are factors in the studies that might have an effect on the results:

- The short period of following patients

- The absorbed dose calculations were based upon the model, usually ICRP Publication 53, and not the individual biokinetics data.
- The age limit for radioiodine treatment is lowered. (238)

In another study (239), an elevated risk for stomach, kidney and brain cancer was seen. The risk for stomach cancer increased with dose although it was not statistically significant.

d) Limits of the study:

We encountered several problems in finding good biokinetic information from measurements on man. In general, published data are scarce, especially with regard to quantitative measurements. The clinician is often only interested in the initial distribution and metabolism of a test substance, whereas for dosimetry calculations, long-term retention is of prime importance.

On another hand, this simulation is supposed to cover a 10 day interval during which a lot of physiological process are bound to happen; mainly food digestion, defecation, urination and perspiration all would affect the contents of the volumes that are considered hollow and empty; there was not a clear and well-described method to take these factors into consideration.

Several hours were spent in simulating 10^7 histories in only one source, attempting to simulate 10^8 histories would result in days of processing data, while 10^9 histories would take weeks to give results; this process would have to be repeated for all the source organs for the two sexes and for both hyperthyroidism and thyroid cancer; this could take-up months of simulation not taking into account all the variables that could stop the process and result in restarting it all over again; this time constraint is basically due to the small processing power of the utilized PC.

6. Conclusion

The introduction of radioactive isotopes in diagnosis and treatment has improved and revolutionized patient care, however, as optimal and safe as it is believed to be, it is still radioactivity, delivered to the human body from a radionuclide either internally or from an external source. Fearing that things would get out of hand, the implementation of standardized protocols, activity calibration, and purity control became an integral part of these procedures and a must-know for all practitioners involved in this line of work, especially radiopharmacists; these health professionals ought to be well versed in pharmacology to develop patient-specific pharmacokinetic models for radiopharmaceuticals which behavior differs immensely from other drugs due to their disintegration through time, hence the data derived from their stable isotopes would lack accuracy.

^{131}I is one of the safest, most tolerable radionuclides and it is used for the treatment of hyperthyroidism and thyroid cancer, its effectiveness has been proven over the years, however, fear of the unknown is a constant voice ricocheting in the minds of health professionals “How to objectify and quantify this safety?”

Internal dosimetry has come up with mathematical models and complex computer programs to assess the absorbed dose received due to radiotherapy and environmental exposure to radiation, unlike external dosimetry that can be measured, internal dosimetry must be calculated, in this study TOPAS MC was used to determine the effective dose to several internal organs.

Our investigations have confirmed, yet again, the predominance of females afflicted with thyroid disease, something that is in accordance with published literature, furthermore, more intensive study has allowed the estimation of equivalent dose in various critical organs; our findings show that the most exposed organ depends on the considered phase from the pharmacokinetics profile, in the gastrointestinal phase the stomach receive an excessive equivalent dose followed by the colon and the small intestine, the distribution phase explicitly shows that the thyroid is the most exposed organ, something that explains the use of ^{131}I in the treatment of thyroid’s afflictions, an interesting result was the high dose received by the head which parallel the clinical studies that prove an exposition of the salivary glands after radioiodine therapy; in the elimination phase the kidneys and the urinary bladder become the most exposed organ to radiation, this dose depends intimately on the thyroid’s uptake of radioiodine; on another note the ovaries, breasts and uterus have received considerable doses after exposition to ^{131}I; interestingly, simulation results after 5 days have shown that the kidneys and urinary ladder receiver higher equivalent doses than those absorbed by the thyroid which is expected seeing that most of the absorbed activity is directly eliminated.

In order to build on this work and optimize the results some key points have to be addressed:

- Creating a detailed yet simplified compartmental pharmacokinetic model for ^{131}I that takes into account the basic pharmacokinetic data as well as long-time retention in each organ is of utmost priority, this model should also consider the state of the gastrointestinal tract and the urinary bladder at each interval, adjustments should be made accordingly to simulate the state of the digestive and urinary system in real time.

CONCLUSION

- Switching to a cluster computer would allow to process more data efficiently and in a limited time frame, this would allow also for increasing the number of launched histories in the simulation to improve the accuracy of the results.
- Efforts should be made to collect data in order to create a North African or Algerian stylized phantom representative of the studied population, there are bound to be differences in height, weight, or organs' volumes and masses between a Caucasian and a North African population, hence results would obviously differ.
- Yearly updates are made in TOPAS MC, whenever it will become possible, upgrading to a more anatomically realistic phantom would also improve results, second generation phantoms, even though less flexible than the one used in this study, would give more accurate results.

REFERENCES

1. Isselt JWH Van, Becquerel H, Curie M, Hevesy G De, Cassen B, The HA. The philosophy of science : a history of radioiodine and nuclear medicine. 2010;3.
2. De Jong SA. Thyroid Cancer: A Comprehensive Guide to Clinical Management. 2nd editio. Vol. 124, Archives of Pathology & Laboratory Medicine. Humana Press; 2000. 117 p.
3. Murray GR. Note on the Treatment of Myxoedema by Hypodermic Injections of an Extract of the Thyroid Gland of a Sheep. Br Med J. 1891 Oct;2(1606):796–7.
4. MacKenzie HW. A case of myxoedema treated with great benefit by feeding with fresh thyroid glands. Br Med J. 1892;2(940):1–2.
5. FOX EL. A case of myxoedema treated by taking extract of thyroid by the mouth. Br Med J. 1892;2:941.
6. Baumann E. Ueber das normale Vorkommen von Jod im Thierkörper.(I. Mittheilung). 1896;
7. Kelly FC. Iodine in Medicine and Pharmacy Since its Discovery-1811-1961. Proc R Soc Med [Internet]. 1961 Oct;54(10):831–6. Available from: https://pubmed.ncbi.nlm.nih.gov/19994130
8. Thompson WO, Thompson PK, Braily AG, Cohen AC. Prolonged treatment of exophthalmic goiter by iodine alone. Arch Intern Med [Internet]. 1930 Apr 1;45(4):481–502. Available from: https://doi.org/10.1001/archinte.1930.00140100003001
9. Starr P, Walcott HP, Segall HN, Means JH. The effect of iodine in exophthalmic goiter. Arch Intern Med. 1924;34(3):355–64.
10. Abraham G. The history of iodine in medicine. Part I: From discovery to essentiality. Orig Internist. 2006;13(1):37.
11. Iodine (WHO Food Additives Series 24) [Internet]. [cited 2022 Jan 27]. Available from: https://inchem.org/documents/jecfa/jecmono/v024je11.htm
12. Underwood EJ. Trace elements in human and animal nutrition. New York, USA, Academic Press, Inc.; 1971. 281 p.
13. FAO; WHO. Trace elements in human nutrition and health World Health Organization. World Heal Organ [Internet]. 1996;1–343. Available from: https://apps.who.int/iris/handle/10665/37931
14. Koutras, D.A., Matolinovic, J. and Vought R. Endemic goitre and endemic cretinism. Iodine Nutrition in Health and Disease. Ecol iodine (eds JB Stanbury BS Hetzel). 1985;(Wiley Eastern Limited, New Delhi):185–195.
15. Fish LH, Schwartz HL, Cavanaugh J, Steffes MW, Bantle JP, Oppenheimer JH. Replacement dose, metabolism, and bioavailability of levothyroxine in the treatment of hypothyroidism. N Engl J Med. 1987;316(13):764–70.
16. Hays MT. Localization of human thyroxine absorption. 1991;1(3):241–8.

17. Fisher DA, Oddie TH, Epperson D. Effect of increased dietary iodide on thyroid accumulation and secretion in euthyroid Arkansas subjects. J Clin Endocrinol Metab [Internet]. 1965 Dec 1 [cited 2022 Jan 27];25(12):1580–90. Available from: https://academic.oup.com/jcem/article/25/12/1580/2717651

18. Cuddihy RG. Thyroidal iodine-131 uptake, turnover and blocking in adults and adolescents. Health Phys. 1966;12(8):1021–6.

19. Oliner L, Kohlenbrener RM, Fields T, Kunstadter RH, Goldstein DR. Thyroid function studies in children: normal values for thyroidal I131 uptake and PBI131 levels up to the age of 18. J Clin Endocrinol Metab. 1957;17(1):61–75.

20. Van Dilla MA, Fulwyler MJ. Thyroid metabolism in children and adults using very small (nanocurie) doses of iodine125 and iodine131. In: Biology of Radioiodine. Elsevier; 1964. p. 245–51.

21. Keating F.R. Jr AA. The metabolism of iodine in man as disclosed with the use of radioiodine. Recent Prog Horm Res. 1949;(4):429–481.

22. Morrison RT, Birkbeck JA, Evans TC, Routh JI. Radioiodine uptake studies in newborn infants. J Nucl Med. 1963;4.

23. Ogborn RE, Waggener RE, VanHove E. Radioactive-iodine concentration in thyroid glands of newborn infants. Pediatrics. 1960;26(5):771–6.

24. Nicola JP, Basquin C, Portulano C, Reyna-Neyra A, Paroder M, Carrasco N. The Na+/I− symporter mediates active iodide uptake in the intestine. Am J Physiol - Cell Physiol [Internet]. 2009 Apr [cited 2022 Jan 27];296(4):C654. Available from: /pmc/articles/PMC2670652/

25. Cavalieri RR. Iodine metabolism and thyroid physiology: current concepts. Thyroid. 1997 Apr;7(2):177–81.

26. Hays MT. Estimation of total body iodine content in normal young men. Thyroid. 2001;11(7):671–5.

27. Wolff J. Transport of iodide and other anions in the thyroid gland. Physiol Rev. 1964 Jan;44:45–90.

28. Sternthal E, Lipworth L, Stanley B, Abreau C, Fang SL, Braverman LE. Suppression of thyroid radioiodine uptake by various doses of stable iodide. N Engl J Med. 1980 Nov;303(19):1083–8.

29. Brown-Grant K. Extrathyroidal iodide concentrating mechanisms. Physiol Rev. 1961;41(1):189–213.

30. DeLange FM, Ermans AM. Iodine deficiency. In: Werner and Ingbar's The thyroid: a fundamental and clinical text (Eds: Braverman, L.E. & Utiger R.D). Philadelphia, PA: Lippincott-Raven; 1996. 296–316 p.

31. Saller B, Fink H, Mann K. Kinetics of acute and chronic iodine excess. Exp Clin Endocrinol diabetes. 1998;106(S 03):S34–8.

32. Kramer GH, Hauck BM, Chamberlain MJ. Biological half-life of iodine in adults with intact thyroid function and in athyreotic persons. Radiat Prot Dosimetry.

2002;102(2):129–35.

33. Braverman LE, Kopp P, Utiger RD. Thyroid hormone synthesis: thyroid iodine metabolism. In: Werner and Ingbar's the thyroid: a fundamental and clinical text. Lippincott, Williams & Wilkins; 2005. p. 52–76.

34. Engler D, Burger AG. The deiodination of the iodothyronines and of their derivatives in man. Endocr Rev. 1984;5(2):151–84.

35. Visser TJ. Importance of deiodination and conjugation in the hepatic metabolism of thyroid hormone. Thyroid Gland. 1990;255–83.

36. Peeters RP, Visser TJ. Metabolism of Thyroid Hormone. New Compr Biochem [Internet]. 2017 Jan 1 [cited 2022 Jan 27];18:81–103. Available from: https://www.ncbi.nlm.nih.gov/books/NBK285545/

37. Robbins J. Factors altering thyroid hormone metabolism. Environ Heal Perspect. 1981;38:65–70.

38. Brown-Grant K. The iodide concentrating mechanism of the mammary gland. J Physiol [Internet]. 1957 [cited 2022 Jan 27];135(3):644–54. Available from: https://www.ncbi.nlm.nih.gov/pmc/articles/PMC1358939/

39. Berry MJ, Banu L, Larsen PR. Type I iodothyronine deiodinase is a selenocysteine-containing enzyme. Nature. 1991;349(6308):438–40.

40. Braverman LE, Ingbar SH, Sterling K. Conversion of thyroxine (T4) to triiodothyronine (T3) in athyreotic human subjects. J Clin Invest. 1970;49(5):855–64.

41. Green WL, Ingbar SH. The peripheral metabolism of tri-and tetraiodothyroacetic acids in man. J Clin Endocrinol Metab. 1961;21(12):1548–65.

42. Young Jr WF. Human liver tyrosylsulfotransferase. Gastroenterology. 1990;99(4):1072–8.

43. Risher J, Keith LS. Iodine and inorganic iodides: human health aspects. World Health Organization; 2009.

44. Hedrick WR, DiSimone RN, Keen RL. Radiation dosimetry from breast milk excretion of iodine-123. J Nucl Med. 1987;28(4):544–5.

45. Langer P, Moravec R, Ohradka B, Földes O. Iodothyronines in human bile. Endocrinol Exp. 1988;22(1):35–9.

46. Speller E, Brodribb W. Breastfeeding and thyroid disease: A literature review, breastfeeding review 20(2). 2012;41–7.

47. Smyth PPA, Duntas LH. Iodine uptake and loss-can frequent strenuous exercise induce iodine deficiency? Horm Metab Res [Internet]. 2005 Sep [cited 2022 Jan 27];37(9):555–8. Available from: https://pubmed.ncbi.nlm.nih.gov/16175493/

48. Bakheet SMB, Hammami MM, Hemidan A, Powe JE, Bajaafar F. Radioiodine secretion in tears. J Nucl Med. 1998;39(8 SUPPL.):1452–4.

49. Mani RS. Reactor-produced radionuclides. In: Radionuclides Production. CRC

Press; 2019. p. 1–46.

50. Coenen HH, Mertens J, Mazière B. Radioionidation reactions for pharmaceuticals: compendium for effective synthesis strategies. Springer Science & Business Media; 2006.

51. Fonslet J, Koziorowski J. Dry distillation of radioiodine from TeO2 targets. Appl Sci. 2013;3(4):675–83.

52. Iodine, Radioactive - Toxicity Summary [Internet]. [cited 2022 Jan 26]. Available from: https://webwiser.nlm.nih.gov/substance?substanceId=414&identifier=Iodine, Radioactive&identifierType=name&menuItemId=69&catId=79

53. Al-jubeh W, Shaheen A, Zalloum O. Radioiodine I-131 for diagnosing and treatment of thyroid diseases. Comun Pers. 2012;(June 2012).

54. World Nuclear Association. Radioisotopes in Medicine | Nuclear Medicine [Internet]. World Nuclear Association. 2011 [cited 2022 Jan 26]. Available from: https://world-nuclear.org/information-library/non-power-nuclear-applications/radioisotopes-research/radioisotopes-in-medicine.aspx

55. Biersack H-J, Freeman LM. Clinical nuclear medicine. 2007. 287–290 p.

56. Allahabadia A, Franklyn JA. Iodine, Radioactive. 2004;

57. Sanders TP, Kuhl DE. Technetium pertechnetate as a thyroid scanning agent. Radiology. 1968;91(1):23–6.

58. Kassis AI. Therapeutic radionuclides: biophysical and radiobiologic principles. In: Seminars in nuclear medicine. Elsevier; 2008. p. 358–66.

59. Abrahamson S. Adverse reproductive outcomes in families of atomic veterans: The feasibility of epidemiologic studies. Radiat Res. 1995;144(2):248.

60. Nuclear Radiation and the Thyroid | American Thyroid Association [Internet]. [cited 2022 Jan 26]. Available from: https://www.thyroid.org/nuclear-radiation-thyroid/

61. Keating FR, Power MH, Berkson J, Haines SF. The urinary excretion of radioiodine in various thyroid states. J Clin Invest. 1947;26(6):1138–51.

62. Kaiho T. Iodine made simple. Taylor & Francis Group. 2017. 104–105 p.

63. Leaper DJ, Durani P. Topical antimicrobial therapy of chronic wounds healing by secondary intention using iodine products. Int Wound J. 2008;5(2):361–8.

64. Gottardi W, Block SS. Disinfection, sterilization and preservation. Lea Febiger Philadelphia. 1991;152–65.

65. Miles M. Goitre, cretinism and iodine in South Asia: historical perspectives on a continuing scourge. Med Hist. 1998;42(1):47–67.

66. Lugol JGA. Mémoire sur l'emploi de l'iode dans les maladies scrofuleuses: lu à l'Académie Royale des Sciences dans la séance du 22 juin 1829. J.-B. Baillière; 1831.

67. Sibbald R, Leaper D, Queen D. Iodine made easy. Wounds Int. 2011;2(2):1–6.

68. Kaiho T. Iodine chemistry and applications. John Wiley & Sons, Ltd; 2014.

69. Santos JAR, Christoforou A, Trieu K, McKenzie BL, Downs S, Billot L, et al. Iodine fortification of foods and condiments, other than salt, for preventing iodine deficiency disorders. Cochrane Database Syst Rev. 2019;(2).

70. Ahmad SI. Thyroid disorders & therapy. Syed KI, Shamim A, editors. Vol. 1. 2016. 3–4 p.

71. Thyroid anatomy: overview, structure, fascia and ligament [Internet]. [cited 2022 Jan 28]. Available from: https://reference.medscape.com/article/835535-overview

72. Anatomie du corps thyroïde - EM consulte [Internet]. [cited 2022 Jan 30]. Available from: https://www.em-consulte.com/article/10416/anatomie-du-corps-thyroide

73. The thyroid gland - location - blood supply - teachmeanatomy [Internet]. [cited 2022 Jan 28]. Available from: https://teachmeanatomy.info/neck/viscera/thyroid-gland/

74. Dillon MJ. Berne & Levy Physiology. Vol. 18, European Journal of Clinical Pharmacology. 1980. 105–108 p.

75. Khan YS, Farhana A. Histology, thyroid gland. StatPearls [Internet]. 2021 Dec 8 [cited 2022 Jan 28]; Available from: https://www.ncbi.nlm.nih.gov/books/NBK551659/

76. Glandular tissue: The histology guide [Internet]. [cited 2022 Jan 30]. Available from: https://www.histology.leeds.ac.uk/glandular/thyroid.php

77. JE H. Guyton and Hall textbook of medical physiology. Vol. 107, Philadelphia, PA: Saunders Elsevier. 2011. 907–909 p.

78. Nyström E, Berg GEB, Jansson SKG, Torring O, Valdemarsson S V. Thyroid disease in adults. Springer Science & Business Media; 2010.

79. Organization WH. Vitamin and mineral requirements in human nutrition. World Health Organization; 2004.

80. Pesce L, Kopp P. Iodide transport: implications for health and disease. Int J Pediatr Endocrinol [Internet]. 2014;2014(1):8. Available from: https://doi.org/10.1186/1687-9856-2014-8

81. Bizhanova A, Kopp P. Minireview: The sodium-iodide symporter NIS and pendrin in iodide homeostasis of the thyroid. Endocrinology [Internet]. 2009/02/05. 2009 Mar;150(3):1084–90. Available from: https://pubmed.ncbi.nlm.nih.gov/19196800

82. Eskandari S, Loo DDF, Dai G, Levy O, Wright EM, Carrasco N. Thyroid Na+/I- symporter. Mechanism, stoichiometry, and specificity. J Biol Chem. 1997;272(43):27230–8.

83. Dohán O, De la Vieja A, Paroder V, Riedel C, Artani M, Reed M, et al. The sodium/iodide Symporter (NIS): characterization, regulation, and medical significance. Endocr Rev. 2003 Feb;24(1):48–77.

84. Taurog A, Dorris ML, Doerge DR. Mechanism of simultaneous iodination and coupling catalyzed by thyroid peroxidase. Arch Biochem Biophys. 1996 Jun;330(1):24–32.

85. Friesema ECH, Ganguly S, Abdalla A, Manning Fox JE, Halestrap AP, Visser TJ. Identification of monocarboxylate transporter 8 as a specific thyroid hormone transporter. J Biol Chem. 2003 Oct;278(41):40128–35.

86. Hennemann G, Docter R, Visser TJ, Postema PT, Krenning EP. Thyroxine plus low-dose, slow-release triiodothyronine replacement in hypothyroidism: proof of principle. Thyroid. 2004 Apr;14(4):271–5.

87. Pilo A, Iervasi G, Vitek F, Ferdeghini M, Cazzuola F, Bianchi R. Thyroidal and peripheral production of 3,5,3'-triiodothyronine in humans by multicompartmental analysis. Am J Physiol. 1990 Apr;258(4 Pt 1):E715-26.

88. De Leo S, Lee SY, Braverman LE. Hyperthyroidism. Lancet (London, England) [Internet]. 2016/03/30. 2016 Aug 27;388(10047):906–18. Available from: https://pubmed.ncbi.nlm.nih.gov/27038492

89. Hyperthyroidism: Primary Versus Secondary - LabCE.com, Laboratory Continuing Education [Internet]. [cited 2022 Jan 28]. Available from: https://www.labce.com/spg864464_hyperthyroidism_primary_versus_secondary.aspx

90. Fox T, Brooke A, Vaidya B. Endocrinology. Woolven S, Pattullo K, editors. London: JP Medical Ltd.; 2015.

91. Halenka M, Fryšák Z. Atlas of thyroid ultrasonography. Atlas of Thyroid Ultrasonography. 2017.

92. Novodvorsky P, Allahabadia A. Thyrotoxicosis. Medicine (Baltimore). 2017;45(8):510–6.

93. Thyroid Cancer: Introduction | Cancer.Net [Internet]. [cited 2022 Jan 28]. Available from: https://www.cancer.net/cancer-types/thyroid-cancer/introduction

94. Benouis A, Bekkouche Z, Merad MS, Loudjedi L, Khelil H, Berber N. Thyroid Cancer in Western Algeria: Histopathological and Epidemiological Study. J Cancer Ther. 2017;08(07):672–82.

95. H.-J. Biersack ; F. Grünwald. Thyroid cancer. Springer; 2005.

96. Summary of product characteristics for sodium iodide (I131) capsules T 37-7400 MBq, hard capsule. :1–17.

97. I-131 Sodium Iodide [Internet]. [cited 2022 Jan 29]. Available from: https://www.oncidiumfoundation.org/2019/11/30/131i-sodium-iodide/?sfw=pass1643458171

98. Saha GB. Fundamentals of Nuclear Pharmacy. Sixth. Fundamentals of Nuclear Pharmacy. Taylor and Francis Boca Raton, London, New York; 2017. 127–128 p.

99. Committee for Medicinal Products for Human Use. Guideline on core SmPC and Package Leaflet for sodium iodide (131 I) for therapeutic use. 2016;44(October

2016). Available from: https://www.ema.europa.eu/en/core-smpc-package-leaflet-sodium-iodide-131-i-therapeutic-use

100. Haghighatafshar M, Banani A, Zeinali-Rafsanjani B, Etemadi Z, Ghaedian T. Impact of the amount of liquid intake on the dose rate of patients treated with radioiodine. Indian J Nucl Med [Internet]. 2018;33(1):10–3. Available from: https://pubmed.ncbi.nlm.nih.gov/29430108

101. Sodium Iodide I 131 - FDA prescribing information, side effects and uses [Internet]. [cited 2022 Jan 29]. Available from: https://www.drugs.com/pro/sodium-iodide-i-131.html

102. I-131 Sodium Iodide Theracap [Internet]. [cited 2022 Jan 29]. Available from: https://www.oncidiumfoundation.org/2019/11/30/131i-sodium-iodide/

103. Rousset B, Dupuy C, Miot F, Dumont J. Chapter 2 Thyroid Hormone Synthesis And Secretion. Endotext [Internet]. 2015 Sep 2 [cited 2022 Jan 27]; Available from: https://www.ncbi.nlm.nih.gov/books/NBK285550/

104. Publique BDED, Médicaments DES. Base de données publique des médicaments. 2014;ci:9–11.

105. Nuclear Medicine - Advancing Nuclear Medicine Through Innovation - NCBI Bookshelf [Internet]. [cited 2022 Feb 3]. Available from: https://www.ncbi.nlm.nih.gov/books/NBK11471/

106. Stabin MG, Flux GD. Internal dosimetry as a tool for radiation protection of the patient in nuclear medicine. Biomed Imaging Interv J. 2007;3(2).

107. L'Annunziata MF. Radioactivity. Elsevier Gezondheidszorg; 2007. 1–1 p.

108. Introduction to Radioactivity | Definition, Examples, Diagrams [Internet]. [cited 2022 Jan 31]. Available from: https://www.toppr.com/ask/en-my/content/concept/introduction-to-radioactivity-210547/

109. Natural and artificial radioactivity [Internet]. [cited 2022 Jan 31]. Available from: http://www.chm.bris.ac.uk/webprojects2002/sidell/NAT&ART.htm

110. Nuclear Technology Education Consortium [Internet]. [cited 2022 Jan 31]. Available from: http://www.ntec.ac.uk/Phys/content/s8.html

111. La décroissance radioactive — Site des ressources d'ACCES pour enseigner les Sciences de la Vie et de la Terre [Internet]. [cited 2022 Jan 31]. Available from: http://acces.ens-lyon.fr/acces/thematiques/limites/Temps/datation-isotopique/comprendre/la-decroissance-radioactive

112. Britannica, The Editors of Encyclopaedia. "half-life". Encyclopedia Britannica, 7 Feb. 2020, https://www.britannica.com/science/half-life-radioactivity. Accessed 7 May 2022.

113. WHO. Radiopharmaceuticals methods of analysis. 2008;

114. Radioactivity : Radioactive Half-life [Internet]. [cited 2022 Jan 31]. Available from: https://www.radioactivity.eu.com/site/pages/Radioactive_Half_life.htm

115. Biological Half-life [Internet]. [cited 2022 Jan 31]. Available from: http://hyperphysics.phy-astr.gsu.edu/hbase/Nuclear/biohalf.html

116. Radioactive Decay Laws, Half-life, The Physical Half-life. [cited 2022 Jan 31]; Available from: https://www.mn.uio.no/fysikk/english/services/knowledge/radiation-and-health/chap03.pdf

117. Effective Half-life | NRC.gov [Internet]. [cited 2022 Jan 31]. Available from: https://www.nrc.gov/reading-rm/basic-ref/glossary/effective-half-life.html

118. Stabin MG. Radiation protection and dosimetry. Radiation Protection and Dosimetry. 2007. 207–209 p.

119. Radiation Basics | US EPA [Internet]. [cited 2022 Jan 31]. Available from: https://www.epa.gov/radiation/radiation-basics

120. Podgorsak EB. Biological and Medical Physics, Biomedical Engineering: Radiation Physics for Medical Physicist. 2013. 204–310 p.

121. Types of Radiation [MOE] [Internet]. [cited 2022 May 9]. Available from: https://www.env.go.jp/en/chemi/rhm/basic-info/1st/01-03-02.html

122. Magill J, Galy J. Radioactivity-Radionuclides-Radiation: Including the Universal Nuclide Chart on CD-ROM. Springer; 2005. 62–64 p.

123. Choppin G, Liljenzin J-O, Rydberg J. Radiochemistry and nuclear chemistry. Butterworth-Heinemann; 2002. 61 p.

124. Alpha decay - Energy Education [Internet]. [cited 2022 Feb 1]. Available from: https://energyeducation.ca/encyclopedia/Alpha_decay

125. Prūsis I, Prūsis P. About Beta Decay. 2019;(March):1–4.

126. Welsh JS. Beta decay in science and medicine. Am J Clin Oncol. 2007 Aug;30(4):437–9.

127. Walker J, Halliday D, Resnick R. Fundamentals of Physics Halliday & resnick 10ed. Wiley. 2014. 1293 p.

128. Martin BR. Physics - Nuclear and Particle. Nuclear and Particle Physics. 2006. 62 p.

129. Nondestructive Evaluation Physics : X-Ray [Internet]. [cited 2022 Feb 1]. Available from: https://www.nde-ed.org/Physics/X-Ray/gamma.xhtml

130. Stark, Glenn. “gamma ray”. Encyclopedia Britannica, 22 Oct. 2021, https://www.britannica.com/science/gamma-ray. Accessed 7 May 2022.

131. Photoelectric Effect – The Physics Hypertextbook [Internet]. [cited 2022 Feb 1]. Available from: https://physics.info/photoelectric/

132. Tabakov S, Milano F, Strand S-E, Lewis C, Sprawls P, editors. Encyclopaedia of medical physics volume I and II. 2013. 555 p.

133. Photoelectric Effect | Chemistry for Non-Majors [Internet]. [cited 2022 Feb 1].

Available from: https://courses.lumenlearning.com/cheminter/chapter/photoelectric-effect/

134. Nilsson B, Brahme A. Interaction of ionizing radiation with matter. 2014;

135. Mahuvava C, Du Plessis FCP. Monte Carlo evaluation of the dose perturbation effect of hip prostheses for megavoltage photon radiotherapy. Phys Medica Eur J Med Phys. 2015;31:10.

136. The Compton Effect or Compton Scattering in Physics [Internet]. [cited 2022 Feb 1]. Available from: https://www.thoughtco.com/the-compton-effect-in-physics-2699350

137. Parks; James Edgar. The compton effect- Compton scattering and gamma ray spectroscopy. 2015;

138. Compton Scattering | Definition & Formula | nuclear-power.com [Internet]. [cited 2022 Feb 1]. Available from: https://www.nuclear-power.com/nuclear-power/reactor-physics/interaction-radiation-matter/interaction-gamma-radiation-matter/compton-scattering/

139. Compton Effect - Engineering Physics Class [Internet]. [cited 2022 May 9]. Available from: https://sites.google.com/site/puenggphysics/home/unit-iv/compton-effect

140. Pedroso de Lima JJ. Nuclear Medicine Physics. Taylor & Francis Group; 2011. 443 p.

141. Turner JE. Interaction of ionizing radiation with matter. Health Phys. 2005;88(6):38.

142. da Cruz Roque RJ. X-ray imaging using 100μm thick Gas Electron Multipliers operating in Kr-CO2 mixtures. University of Coimbra; 2018. p. 13.

143. Krumeich F. Properties of Electrons, their Interactions with Matter. ETH Zurich [Internet]. 2015;(1):1–24. Available from: www.microscopy.ethz.ch

144. Types of Electron Interactions - OzRadOnc [Internet]. [cited 2022 Feb 1]. Available from: http://ozradonc.wikidot.com/physics:electron-interactions-types

145. Manual RC. Biological effects of radiation. Phys Today. 1956;9(7):34–5.

146. Desouky O, Ding N, Zhou G. Targeted and non-targeted effects of ionizing radiation. J Radiat Res Appl Sci [Internet]. 2015;8(2):247–54. Available from: http://dx.doi.org/10.1016/j.jrras.2015.03.003

147. Deterministic Effects and Stochastic Effects [MOE] [Internet]. [cited 2022 Feb 1]. Available from: https://www.env.go.jp/en/chemi/rhm/basic-info/1st/03-01-04.html

148. Deterministic vs. Stochastic Effects: What Are the Differences? [Internet]. [cited 2022 Feb 1]. Available from: https://versantphysics.com/2021/04/21/deterministic-vs-stochastic-effects/

149. Stochastic Effects | NRC.gov [Internet]. [cited 2022 Feb 1]. Available from: https://www.nrc.gov/reading-rm/basic-ref/glossary/stochastic-effects.html

150. Choudhary S. Deterministic and Stochastic Effects of Radiation. Cancer Ther Oncol Int J. 2018;12(2):1–2.

151. What is Dosimetry and Why is it Important for Cancer Treatment? [Internet]. [cited 2022 Feb 1]. Available from: http://www-naweb.iaea.org/na/news-na/na-what-is-dosimetry.html

152. External Dosimetry | Argonne National Laboratory [Internet]. [cited 2022 Feb 1]. Available from: https://www.anl.gov/external-dosimetry

153. What is External Dosimetry - Definition [Internet]. [cited 2022 Feb 1]. Available from: https://www.radiation-dosimetry.org/what-is-external-dosimetry-definition/

154. Personal dosimeter - PM1610B / PM1610B-01 Series - POLIMASTER - gamma / X-ray / radiation [Internet]. [cited 2022 May 9]. Available from: https://www.directindustry.com/prod/polimaster/product-23674-1633807.html

155. Clements BW, Casani JAP. Disasters and Public Health: Planning and Response: Second Edition. Disasters and Public Health: Planning and Response: Second Edition. 2016. 1–501 p.

156. Ziad I, John M, Douglas Z. Clinical arrhythmology and electrophysiology: a companion to Braunwald's heart disease. Third edit. Clinical Arrhythmology. 2011. 1062 p.

157. Cherry S, Sorenson J, Phelps M. Physics in Nuclear Medicine. 4th ed. Philadelphia, PA; 2012.

158. C.White S, J.Pharoah M. Oral radiography Principles and Interpretation. 7th editio. Mosby; 2014. 15 p.

159. Brahme A. Comprehensive biomedical physics. Newnes; 2014.

160. Radiobiology and Radiation Safety | Radiology Key [Internet]. [cited 2022 May 9]. Available from: https://radiologykey.com/radiobiology-and-radiation-safety/

161. Radiation doses - Canadian Nuclear Safety Commission [Internet]. [cited 2022 Feb 1]. Available from: http://nuclearsafety.gc.ca/eng/resources/radiation/introduction-to-radiation/radiation-doses.cfm

162. Mortiningsih. ICRP 103. Qual Res Psychol. 2006;0(2):47–54.

163. Vano E, Frija G, Loose R, Paulo G, Efstathopoulos E, Granata C, et al. Dosimetric quantities and effective dose in medical imaging: a summary for medical doctors. Insights Imaging [Internet]. 2021;12(1). Available from: https://doi.org/10.1186/s13244-021-01041-2

164. van der Aart J, Hallett WA, Rabiner EA, Passchier J, Comley RA. Radiation dose estimates for carbon-11-labelled PET tracers. Nucl Med Biol. 2012;39(2):305–14.

165. Calculation of Equivalent Dose and Effective Dose [MOE] [Internet]. [cited 2022 May 9]. Available from: https://www.env.go.jp/en/chemi/rhm/basic-info/1st/02-03-06.html

166. Road LP, Vic Y, Parade U, Nsw M, Box PO. Guide to calculation of ' cumulative

equivalent dose ’ for the purpose of applying ionising radiation factors contained in Statements of Principles determined under Part XIA of the Veterans ’ Entitlements Act 1986 (Cth). 2017;8.

167. Lerch H, Jigalin A. Nuclear medicine: Medical technology research. NuklearMedizin. 2005;44(6):267–71.

168. Dokholyan N V, Noel J, Onuchic J. Radiation Physics for Medical Physicists by Ervin B. Podgorsak 2nd Edition 2010 [Internet]. Computational Modeling of Biological Systems. 2012. 31–54 p. Available from: http://dx.doi.org/10.1007/978-1-4614-2146-7_2

169. Loke KSH, Padhy AK, Ng DCE, Goh ASW, Divgi C. Dosimetric considerations in radioimmunotherapy and systemic radionuclide therapies: a review. World J Nucl Med. 2011;10(2):122.

170. Smith EM. General considerations in calculation of the absorbed dose of radiopharmaceuticals used in nuclear medicine. In: Medical radionuclides: radiation dose and effects Proceedings of a symposium held at the Oak Ridge Associated Universities Oak Ridge: United States Atomic Energy Commission. 1970. p. 17–27.

171. Eckerman KF. Dosimetric methodology of ICRP. Oak Ridge Natl Lab [Internet]. Available from: http://www.iaea.org/inis/collection/NCLCollectionStore/_Public/27/019/27019191.pdf

172. Christensen R. The Dosimetry of Ionizing Radiation, Volume 1 edited by Kenneth R. Kase, Bengt E. Bjärngard, and F. H. Attix . Med Phys. 1987;14(3):426–7.

173. Hobbie RK, Roth BJ. Intermediate physics for medicine and biology. 4th Editio. 2007. 489–490 p.

174. Albandar H. Basic Modes of Radioactive Decay. Use of Gamma Radiation Techniques in Peaceful Applications [Internet]. 2019 Aug 26; Available from: https://www.intechopen.com/books/use-of-gamma-radiation-techniques-in-peaceful-applications/basic-modes-of-radioactive-decay.

175. Britannica, The Editors of Encyclopaedia. “decay constant”. Encyclopedia Britannica, 8 Sep. 2020, https://www.britannica.com/science/decay-constant. Accessed 8 May 2022.

176. Russell K. Hobbie BJR. Intermediate Physics for Medicine and Biology. Fourth Edi. 2016. 1–23 p.

177. Hamby DM. Radiation Dosimetry, Instrumentation and Methods, 2nd Edition. Health Physics. 2001. 470 p.

178. Sjögreen Gleisner K. Dosimetry and dosimetric tools in radionuclide therapy, including results from a European survey.

179. Bolch WE, Eckerman KF, Sgouros G, Thomas SR. MIRD pamphlet no. 21: a generalized schema for radiopharmaceutical dosimetry—standardization of nomenclature. J Nucl Med. 2009;50(3):477–84.

180. Izzaty RE, Astuti B, Cholimah N. Specific absorbed fractions of energy at various ages from internal photon sources. Angew Chemie Int Ed 6(11), 951–952. 1967;5–24.

181. Amato E, Lizio D, Baldari S. Applications of the monte carlo method in medical physics. Med Phys. 2013;(March 2013):105–13.

182. Harrison RL. Introduction to Monte Carlo simulation. AIP Conf Proc. 2009;1204:17–21.

183. Raychaudhuri S. Introduction to monte carlo simulation. 2008;91–100.

184. What is Monte Carlo Simulation? | IBM [Internet]. [cited 2022 Feb 15]. Available from: https://www.ibm.com/cloud/learn/monte-carlo-simulation

185. Metropolis N, Ulam S. The monte carlo method. J Am Stat Assoc. 1949;44(247):335–41.

186. Maria A. Monte Carlo Simulation in Radionuclide Therapy Dosimetry. Biomed J Sci Tech Res. 2019;15(1):11102–7.

187. Britannica, The Editors of Encyclopaedia. “Monte Carlo method”. Encyclopedia Britannica, 10 Jan. 2022, https://www.britannica.com/science/Monte-Carlo-method. Accessed 9 May 2022.

188. Mavaddat N, Ahderom S, Tiporlini V, Alameh K. Simulation of biomedical signals and images using Monte Carlo methods for training of deep learning networks [Internet]. Deep Learning Techniques for Biomedical and Health Informatics. Elsevier Inc.; 2020. 213–236 p. Available from: http://dx.doi.org/10.1016/B978-0-12-819061-6.00009-4

189. Monte Carlo Simulation | Analytica [Internet]. [cited 2022 Feb 15]. Available from: https://analytica.com/technology/monte-carlo-simulation-software/

190. Briesmeister JF. MCNPTM – A General Monte Carlo N-Particle Transport Code. Los Alamos Natl Lab. 2000;(March):790.

191. Brown FB, Barrett RF, Booth TE, Bull JS, Cox LJ, Forster RA, et al. Los Alamos Title: MCNP Version 5. 2002;836. Available from: https://mcnp.lanl.gov/pdf_files/la-ur-02-3199.pdf

192. Los Alamos National Laboratory: MCNP Home Page [Internet]. [cited 2022 Feb 15]. Available from: https://laws.lanl.gov/vhosts/mcnp.lanl.gov/

193. Nelson W, Namito Y. The EGS4 Code System: Solution of gamma-ray and electron transport problems. Supercomput Nucl Appl Mito City (Japan), 12-16 Mar 1990. 1990;1990(February).

194. Kawrakow I. Accurate condensed history Monte Carlo simulation of electron transport. I. EGSnrc, the new EGS4 version. Med Phys. 2000;27(3):485–98.

195. Kawrakow I, Rogers DWO. The EGSnrc Code System : Monte Carlo Simulation of Electron and Photon Transport. System. 2003;2001–3.

196. Battistoni G, Cerutti F, Fassò A, Ferrari A, Muraro S, Ranft J, et al. The FLUKA

code: Description and benchmarking. AIP Conf Proc. 2007;896(1):31–49.

197. Fasso' A, Ferrari A, Roesler S, Sala PR, Ballarini F, Ottolenghi A, et al. The physics models of FLUKA: status and recent development. 2003;(1232). Available from: http://arxiv.org/abs/hep-ph/0306267

198. Ferrari A, Sala PR, Fasso A, Ranft J. Fluka: a multi-particle transport code (Program version 2021). 2021;(May):1–498.

199. Dunn WL, Shultis JK. The Basis of Monte Carlo. Exploring Monte Carlo Methods. 2012. 21–46 p.

200. Salvat F, Fernández-Vera J, Sempau J. PENELOPE-2008: A Code System for Monte Carlo Simulation of Electron and Photon Transport. 2009;(November):324.

201. Agostinelli S, Allison J, Amako K al, Apostolakis J, Araujo H, Arce P, et al. GEANT4—a simulation toolkit. Nucl instruments methods Phys Res Sect A Accel Spectrometers, Detect Assoc Equip. 2003;506(3):250–303.

202. Xu XG;, Eckerman KF. Handbook of Anatomical Models for Radiation Dosimetry. 2009.

203. Xu XG. An exponential growth of computational phantom research in radiation protection, imaging, and radiotherapy: a review of the fifty-year history. Phys Med Biol. 2014;59(18):R233.

204. Fisher Jr HL, Snyder WS. Distribution of dose in the body from a source of gamma rays distributed uniformly in an organ. In: Proceedings of the First International Congress of Radiation Protection. Elsevier; 1968. p. 1473–86.

205. Snyder WS, Ford MR, Warner GG, Fisher Jr HL. Estimates of absorbed fractions for monoenergetic photon sources uniformly distributed in various organs of a heterogeneous phantom. Oak Ridge National Lab., Tenn.; 1969.

206. Foley JD, Van FD, Van Dam A, Feiner SK, Hughes JF, Hughes J. Computer graphics: principles and practice. Vol. 12110. Addison-Wesley Professional; 1996.

207. Taleb B, Khadour A, Bitar A. Reconstruction of head-to-knee voxel model for Syrian adult male of average height and weight. Egypt J Radiol Nucl Med. 2015;46(2):491–7.

208. Zaidi H, Tsui BMW. Review of computational anthropomorphic anatomical and physiological models. Proc IEEE. 2009;97(12):1938–53.

209. Voxel phantom - ICRPaedia [Internet]. [cited 2022 Feb 17]. Available from: http://icrpaedia.org/Voxel_phantom

210. Zaidi H, Xie GX. Computational anthropomorphic models of the human anatomy: The path to realistic Monte Carlo modeling in radiological sciences. Annu Rev Biomed Eng. 2007;9:471–500.

211. International Commission on Radiation Units and Measurements MD (United States) B. Photon, electron, proton and neutron interaction data for body tissues [Internet]. United States; Available from: http://inis.iaea.org/search/search.aspx?orig_q=RN:23082971

212. Valentin J. Basic anatomical and physiological data for use in radiological protection: reference values: ICRP Publication 89. Ann ICRP. 2002;32(3–4):1–277.

213. Hoseinian Azghadi E, Rafat Motavalli L, Miri Hakimabad H. Hybrid Phantom Applications to Nuclear Medicine. J Biomed Phys Eng. 2012;2(1).

214. Lee C, Lodwick D, Williams JL, Bolch WE. Hybrid computational phantoms of the 15-year male and female adolescent: Applications to CT organ dosimetry for patients of variable morphometry. Med Phys. 2008;35(6):2366–82.

215. Bolch W, Lee C, Wayson M, Johnson P. Hybrid computational phantoms for medical dose reconstruction. Radiat Environ Biophys. 2010;49(2):21.

216. Piegl L. On NURBS: a survey. IEEE Comput Graph Appl. 1991;11(01):55–71.

217. Hurtado JL, Lee C, Lodwick D, Goede T, Williams JL, Bolch WE. Hybrid computational phantoms representing the reference adult male and adult female: Construction and applications for retrospective dosimetry. Health Phys. 2012;102(3):292–304.

218. Borbinha JC. Organ Dose Estimates in Thorax CT: Voxel Phantom Organ Matching With Individual Patient Anatomy. 2017.

219. Howell RW, Wessels BW, Loevinger R, Committee M. The MIRD perspective 1999. J Nucl Med. 1999;40(1):3S-10S.

220. Snyder WS. " S" absorbed dose per unit cumulated activity for selected radionuclides and organs. MIRD Pam no 11. 1975;

221. Hadid L. Optimisation de la radioprotection en médecine nucléaire: De la dosimétrie de référence à la dosimétrie personnalisée. Paris 7; 2011.

222. Perl J, Shin J, Schümann J, Faddegon B, Paganetti H. TOPAS: an innovative proton Monte Carlo platform for research and clinical applications. Med Phys. 2012;39(11):6818–37.

223. Ramos-Méndez J, Perl J, Schuemann J, Shin J, Paganetti H, Faddegon B. A framework for implementation of organ effect models in TOPAS with benchmarks extended to proton therapy. Phys Med Biol. 2015;60(13):5037.

224. Polster L, Schuemann J, Rinaldi I, Burigo L, McNamara AL, Stewart RD, et al. Extension of TOPAS for the simulation of proton radiation effects considering molecular and cellular endpoints. Phys Med Biol. 2015;60(13):5053.

225. Guatelli S, Mascialino B, Pia MG, Pokorski W. Geant4 anthropomorphic phantoms. IEEE Nucl Sci Symp Conf Rec. 2006;3:1359–62.

226. Bé M-M, Chisté V, Dulieu C, Kellett MA, Mougeot X, Arinc A, et al. Table of Radionuclides [Internet]. Vol. 8, Monographie BIPM-5. Pavillon de Breteuil, F-92310 Sèvres, France: Bureau International des Poids et Mesures; 2016. Available from: http://www.bipm.org/utils/common/pdf/monographieRI/Monographie_BIPM-5_Tables_Vol8.pdf

227. Maruchi N, Furihata R, Makiuchi M. Epidemiological studies on hyperthyroidism.

Endocrinol Jpn. 1969;16(6):665–72.

228. Zdraveska Kochovska M. Effective dose estimation and risk assessment in patients treated with iodine 131I using Monte Carlo simulation. Универзитет у Новом Саду. 2014;

229. Guidoum M, Kherfi-Kadi H, Benharkat-Boughaba O, Djemaa-Bendjazia A, Keghouche S, Abedi-Ardekani B, et al. Patterns of benign and malignant lesions of the thyroid in two wilayahs of Northeastern Algeria. J Cancer Epidemiol. 2015;2015.

230. Ntyonga-Pono MP, Nguizi-Ogoula S, Mabika-Mabika B, Adegnka-Ayola A, Mougougou A, Minko-Mi-Etoua D. LES TUMEURS THYROIDIENNES OPERES AU GABON Données anatomo-pathologiques et épidémiologiques A propos de 131 cas. Med Afr Noire. 1998;45(6):409–11.

231. Manole D, Schildknecht B, Gosnell B, Adams E, Derwahl M. Estrogen promotes growth of human thyroid tumor cells by different molecular mechanisms. J Clin Endocrinol Metab. 2001;86(3):1072–7.

232. Bendouida AF, Moulessehoul S, Harir N, Rih A, Diaf M, Belhandouze L. Epidemiology, diagnosis and treatement of thyroid cancer in Western Algeria (Sidi bel Abbes region). J Africain du Cancer / African J Cancer [Internet]. 2015;7(4):213–7. Available from: https://doi.org/10.1007/s12558-015-0405-6

233. Association BT. Guidelines for the management of thyroid cancer. In Royal College of Physicians; 2007.

234. Pacini F, Schlumberger M, Dralle H, Elisei R, Smit JWA, Wiersinga W. European consensus for the management of patients with differentiated thyroid carcinoma of the follicular epithelium. Eur J Endocrinol. 2006;154(6):787–803.

235. Carballo M, Quiros RM. To treat or not to treat: the role of adjuvant radioiodine therapy in thyroid cancer patients. J Oncol. 2012;2012.

236. Jokic VS, Kocovska MZ. New technique for effective dose estimation using Monte Carlo simulation for the patients undergoing radioiodine therapy. Measurement. 2013;46(1):795–802.

237. Franklyn JA, Maisonneuve P, Sheppard M, Betteridge J, Boyle P. Cancer incidence and mortality after radioiodine treatment for hyperthyroidism: a population-based cohort study. Lancet. 1999;353(9170):2111–5.

238. Wartofsky L, Glinoer D, Solomon B, Lagasse R. Differences and similarities in the treatment of diffuse goiter in Europe and the United States. Exp Clin Endocrinol Diabetes. 1991;97(02/03):243–51.

239. Holm LE, Hall P, Wiklund K, Lundell G, Berg G, Bjelkengren G, et al. Cancer risk after iodine-131 therapy for hyperthyroidism. J Natl Cancer Inst. 1991;83(15):1072–7.

Abstract

By 1946, ^{131}I has become one of the first radioisotopes used in radiotherapy for the treatment of benign thyroid disease as well as thyroid cancer, ever since, its application has grown exponentially; while many alternatives have shown up over the years, ^{131}I is still considered the gold standard and for good reason.

As safe as it may be considered, radioiodine therapy is still radioactivity being delivered to biological tissue and since it is delivered orally many organs other than the original target will be exposed to unnecessary radiation, hence the importance of internal dosimetry in this practice.

The aim is to estimate the equivalent dose in non-target organs in the treatment of patients afflicted with hyperthyroidism and thyroid cancer using Monte Carlo simulation applied through TOPAS toolkit on a stylized anthropomorphic phantom, interesting results came to light; apart from the thyroid, numerous organs have registered high equivalent doses, the stomach was the most exposed organ in the gastrointestinal phase; while the kidneys and urinary bladder showed elevated doses in the elimination phase surpassing that of the thyroid in the first days following treatment, breasts and ovaries were not exempt of the radiation since they too have absorbed a considerable amount in the 10 days after the ingestion of the NaI capsule.

For the purpose of radiation protection and optimum outcomes for radionuclide radiotherapy, implementing internal dosimetry in the plan of treatment to exact a paradigm shift from fixed dose to patient-specific dose is worthwhile in providing patients with a better quality of care while minimizing the probability of carcinogenesis and chromosomic aberrations.

Keywords: equivalent dose; hyperthyroidism; internal dosimetry; Monte Carlo; radioactive iodine 131; stylized anthropomorphic phantom; thyroid cancer; TOPAS.

ملخص

بحلول عام 1946، أصبح اليود المشع 131 (^{131}I) أحد أول النظائر المشعة المستعملة في العلاج الإشعاعي لمعالجة أمراض الغدة الدرقية الحميدة فضلا عن سرطان الغدة الدرقية، و منذ ذلك الحين، ازداد إستعماله زيادة كبيرة؛ فبالرغم من ظهورالعديد من البدائل على مر السنين، إلا أن اليود المشع 131 لا يزال يعتبر معيار الذهب وهذا لأسباب وجيهة.

بقدر ما يعتبر آمنا، يبقى العلاج باليود المشع عبارة عن إشعاع تتعرض إليه الأنسجة البيولوجية وبما أنه يسلم شفويا، فإن العديد من الأعضاء بخلاف العضو المستهدف الأساسي ستتعرض لإشعاعات غير ضرورية، ومن ثم فإن قياس الجرعات الداخلية في هذه الممارسة ذو أهمية بالغة.

والهدف من ذلك هو تقدير الجرعة المكافئة في الأعضاء غير المستهدفة في علاج المرضى المصابين بفرط نشاط الغدة الدرقية وسرطان الغدة الدرقية باستخدام محاكاة مونتي كارلو التي تطبق من خلال مجموعة أدوات توباس على فانتوم بشري مبسط، وقد ظهرت نتائج مثيرة للاهتمام إلى الضوء؛ وإلى جانب الغدة الدرقية، سجلت عدة أعضاء جرعات مكافئة عالية، وكانت المعدة أكثر الأعضاء تعرضا في مرحلة الهضم؛ في حين أظهرت الكلى والمثانة جرعات مرتفعة في مرحلة الإطراح البولي متجاوزة جرعة الغدة الدرقية في الأيام الأولى التي تلي العلاج، لم ينفذ الثديين والمبيضين من الإشعاع لأنهما أظهرا امتصاص كمية كبيرة في العشرأيام التي تلت شرب كبسولة اليود المشع.

بغرض الحماية من الإشعاع وللحصول على نتائج مثلى للعلاج الإشعاعي بالنويات المشعة، إن القيام بقياس الجرعات الداخلية و إدراجها في خطة العلاج بهدف تحويل البروتوكول من الجرعة الثابتة إلى الجرعة الخاصة بالمريض مفيد في تزويد المرضى بجودة رعاية أفضل مع تقليل إحتمال الإصابة بالسرطان و كذا التحورات في الصبغيات.

الكلمات المفتاحية: الجرعة المكافئة ؛ اليود المشع 131 ؛ توباس ؛ سرطان الغدة الدرقية ؛ فانتوم بشري مبسط ؛ فرط نشاط الغدة الدرقية ؛ قياس الجرعات الداخلية ؛ مونتي كارلو.

Résumé

En 1946, ^{131}I est devenu l'un des premiers radio-isotopes utilisés en radiothérapie pour le traitement des maladies bénignes de la thyroïde ainsi que le cancer thyroïdien, depuis, son application a augmenté de façon exponentielle ; Alors que de nombreuses alternatives ont fait leur apparition au fil des années, ^{131}I est toujours considéré comme l'étalon-or et ceci pour une bonne raison.

Aussi sûr que cela puisse être, La thérapie par l'iode radioactif reste toujours une radioactivité transmise aux tissus biologiques et, comme elle est administrée par voie orale, de nombreux organes autres que la cible initiale seront exposés inutilement à des rayonnements, d'où l'importance de la dosimétrie interne dans cette pratique.

L'objectif est d'estimer la dose équivalente dans les organes non cibles dans le traitement des patients atteints d'hyperthyroïdie et de cancer thyroïdien à l'aide de la simulation de Monte Carlo appliquée par la boîte à outils TOPAS sur un fantôme anthropomorphique de première génération, des résultats intéressants ont été mis en évidence; en dehors de la thyroïde, de nombreux organes ont enregistré des doses équivalentes élevées, l'estomac était l'organe le plus exposé dans la phase gastro-intestinale; alors que les reins et la vessie ont montré des doses élevées dans la phase d'élimination dépassant celle de la thyroïde dans les premiers jours suivant le traitement; les seins et les ovaires n'ont pas été exemptés de la radiation puisqu'ils en ont absorbé une quantité considérable dans les 10 jours suivant l'ingestion de la capsule de NaI.

Aux fins de la radioprotection et d'obtenir des résultats optimaux pour la radiothérapie par radionucléides, mettre en œuvre la dosimétrie interne dans le plan de traitement pour imposer un changement de paradigme de la dose fixe vers une dose spécifique au patient est indispensable pour fournir aux patients des soins de meilleure qualité tout en minimisant la probabilité de cancérogenèse et d'aberrations chromosomiques.

Mots clés : cancer de la thyroïde, dose équivalente, dosimétrie interne, fantôme anthropomorphique de première génération, hyperthyroïdie, iode radioactif 131, Monte Carlo, TOPAS.